Development and Evaluation of Lipo-polymeric Nano-carriers Containing MicroRNA-34a and Docetaxel for the Treatment of Breast Cancer

THESIS

Submitted in partial fulfillment
of the requirements for the degree of
DOCTOR OF PHILOSOPHY

by

SAURABH SHARMA
2015PHXF0415P

Under the Supervision of
Dr. DEEPAK CHITKARA

BIRLA INSTITUTE OF TECHNOLOGY AND SCIENCE
PILANI, RAJASTHAN
2020

CERTIFICATE

This is to certify that the thesis entitled **"Development and Evaluation of Lipo-polymeric Nano-carriers Containing MicroRNA-34a and Docetaxel for the Treatment of Breast Cancer"** submitted by **Mr. Saurabh Sharma,** ID No. **2015PHXF0415P** for the award of Ph.D. Degree of the Institute, embodies the original work done by him under my supervision.

Supervisor

Dr. DEEPAK CHITKARA
Assistant Professor
Department of Pharmacy
BITS-Pilani, Pilani Campus

Date:
Place:

CHAPTER 1

INTRODUCTION

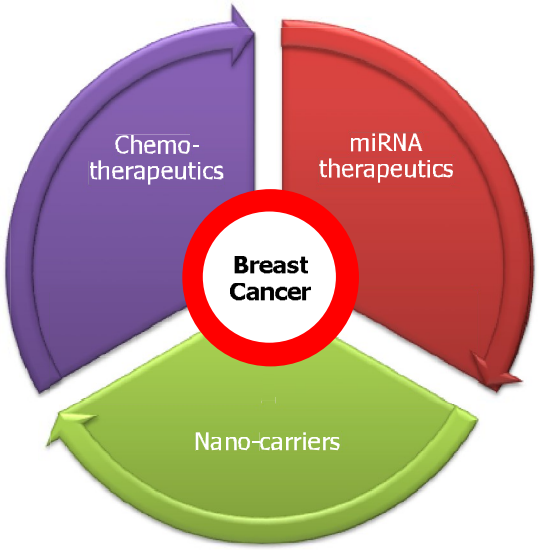

- Breast Cancer
- Triple-Negative Breast cancer (TNBC)
- Chemotherapy for TNBC
- Docetaxel formulations
- miRNA therapeutics
- Folate receptor targeting in cancer
- Outline of current research work
- Objectives of the research work

1.1. Breast cancer

Cancer is a group of diseases involving the uncontrolled cellular proliferation [1] wherein these rapidly growing cells demonstrates six hallmarks, i.e., 1) sustained and proliferative signaling mechanism, 2) cell death resistance, 3) growth suppressor evasion, 4) invasion and metastasis activation, 5) angiogenesis induction, and 6) enabling of replicative immortality [1, 2]. There are more than a hundred types of cancers identified to date that are classified based upon the tissues from where they originated. The most common cancers include lung cancer (incidence 11.6 % and mortality 18.4%), breast cancer (incidence 11.6 % and mortality 6.6%), colorectal cancer (incidence 10.2 % and mortality 9.2 %), prostate cancer (incidence 7.1 % and mortality 3.5 %), stomach cancer (incidence 5.7 % and mortality 8.2 %) and liver cancer (incidence 4.7 % and mortality 8.2 %) [3]. Among these, breast cancer is the second most common cancer [4] and as per WHO, the total number of breast cancer cases will reach 27.78 million by 2040.

Breast cancer originates from the malignant cells within the inner lining of the milk ducts (tiny tubes that carry the milk from the lobules to the nipple) or glands (lobules, milk-producing gland) or less frequently in the stromal tissues (fatty tissue and connective tissue surrounding the ducts and lobules, blood vessels, and lymphatic vessels) [5]. The diagnostic screening of breast cancer was performed by mammography either before symptoms appear or after lump formation [6]. After cancer detection, the fine or large needle biopsy was performed for microscopic observations of cancer. Treatment strategies and prognosis of breast cancer are based upon the severity and its spreadness. Two major cancer staging systems have been adopted for statistical and descriptive analysis of tumor registry data. These are the American Joint Committee on Cancer staging system and the Surveillance, Epidemiology, and End Results (SEER) summary staging system. The system is further subdivided into two principal groups, i.e., i) anatomic and ii) prognostic [7]. The anatomic

group is based on the extent of cancer, which includes tumor size (T), lymph node status (N), and distant metastasis (M) [8]. On the other side, the prognostic group is based on the presence/absence of estrogen receptors (ER), progesterone receptors (PR), human epidermal growth factor receptor 2 (HER2, a growth-promoting protein) and/or the number of copies of the HER2 gene (HER2+/HER2-), and grade (reflecting how closely cancer's microscopic appearance looks like normal breast tissue) [9-11]. As per the SEER staging system the breast cancer is classified into four subtypes, including i) In-situ (Ductal carcinoma-in-situ and Lobular carcinoma in-situ) ii) invasive cancer, iii) molecular and, iv) histological subtypes [12].

Among these, the histological subtype is based upon the size, morphology and cancer cell arrangement. There are stages/grading of breast tumors that were classified based on a numerical scale from 0-4, indicating the tumor severity, size and aggressive behavior [13]. In stage 0, the cells are abnormal and confined to the milk lobes. In this stage the tumor is non-spreadable and tumor size < 2 cm. In stage I, the cancer is localized and is further subdivided into IA and IB. In stage IA, tumor measures up to 2 cm and is without lymph node involvement, while stage IB is invasive wherein no tumor is present in the breast, but the cancer cells have formed into clusters of 0.2 – 2 mm in diameter and may also be present in the lymph nodes. Stage II is also subdivided into two parts, i.e., IIA and IIB, wherein in IIA, there is the absence of a tumor in the breast region but is present in the axillary or sentinel lymph node as compared IIB. Also, in stage IIB, the tumor size is larger than 5 cm. In Stage III, also known as locally advanced cancer, the tumor size is more than 5 cm and cancer cells invade in the axillary lymph nodes or attached to each other or spread to the breastbone, nearest lymph node and the chest wall. It is subdivided into three parts, i.e., IIIA, IIIB and IIIC. In stage IIIA, there is an absence of a tumor in the breast and showed the presence of 4-5 axillary or sentinel lymph node. In stage IIIB, it cannot be identified based on the size of

the tumor but involves up to 9 axillary or sentinel lymph nodes. In this stage, the inflammation, redness, warmness, swelling of the breast skin occur. In stage IIIC, more than ten axillary or sentinel lymph nodes are involved and lymph node locations are above and below the clavicle. In stage IV, the tumor is spread to various body organs/tissues such as lungs, liver, brain and bones [13].

1.2. Triple-Negative Breast cancer (TNBC)

The molecular subtypes of cancer are based upon the receptor expression of ER, PR, and HER2. There are four major molecular subtypes, i.e., i) Luminal A (HR^+/HER^-), ii) Luminal B (HR^+/HER^+), iii) Basal-like (HR^-/HER^-) and iv) HER-2 (HR^-/HER^+) enriched [14]. The classification is based on the expression of estrogen receptor (ER), progesterone receptors (PR), human epidermal growth factor receptor-2 (HER2) and the treatment options are decided accordingly. If either of ER or PR is present on the surface of breast cancer cells, it is classified as the hormone receptor-positive (HR^+) [15, 16]. This type of tumor grows slowly than hormone receptor-negative and is mainly treated with hormonal therapies using drugs such as tamoxifen (Novadex®) [17]. Also, higher copies of the HER2 gene lead to the overexpression of HER2 protein within breast cancer cells and are thus known as HER2 positive breast cancer. This type of cancer is mainly treated with drugs targeting HER2 protein. If breast cancer cells are ER-positive, PR-positive, and HER 2 positive, then they are known as the triple-positive, while the absence of these receptors makes them TNBC. In TNBC, the cancer cells grow and spread more quickly than most other types of breast cancer [18].

The identification of TNBC is assessed by immunohistochemistry (IHC) or fluorescence in-situ hybridization (gene amplification) analysis and if the patient's IHC samples were found to be ER-/PR-/and HER2-, it could be classified as TNBC [19]. Owing

to the distinct metastatic nature, high aggressiveness, unique molecular profiling, poor prognosis and lack of targeted therapy as compared to other subtypes of breast cancer, TNBC is very difficult to treat [19]. It is nonresponsive to hormonal therapy or any therapy that targets ER, PR and HER2 receptors and resembles that of basal cell line cancers that are highly aggressive tumors. On the basis of the molecular heterogeneity, TNBC was further sub-classified into six subtypes, i.e., Basal like1, Basal like2, Mesenchymal (M), Mesenchymal stem line, Immunomodulatory and Luminal androgen receptor based tumor [20].

TNBC is heterogeneous in nature; therefore, investigation of genetic profiling and molecular biomarkers are necessary for the selection of the treatment. Its treatment includes a combination of surgery, radiotherapy and chemotherapy. As per the American Cancer Society reports, there is a grade/tumor stage-wise treatment of TNBC. In stage I to stage III, mastectomy or lumpectomy needs to be performed after checking the characteristic of lymph nodes. If the tumor size is very large and/ or cancerous cells are found in the lymph node, then a combination of chemotherapy, radiotherapy and surgery is preferred. In the case of Stage IV grade TNBC, the first and most important treatment is chemotherapy [21]; however, there is a poor prognosis in the treatment of TNBC due to a very limited number of targeted therapies.

1.3. Chemotherapy for TNBC

In contrast to other types of breast cancer, chemotherapy is the only viable option effective for TNBC. Systemic chemotherapeutics such as taxanes (PTX and DTX), anthracyclines, cisplatin, gemcitabine, capecitabine, trastuzumab or bevacizumab alone or in combination are given before the surgery to reduce the tumor size. Further, chemoadjuvant could be given after surgery as well. Among various chemotherapeutic agents, taxanes such

as paclitaxel and docetaxel play an important role in TNBC treatment. Paclitaxel is obtained from the bark of Taxus brevifolia [22], while docetaxel is a semi-synthetic derivative of paclitaxel [23]. These taxanes bind to the β-tubulin, promote microtubule stabilization and arrest the cell cycle in the G2M phase. Microtubules are associated with shape maintenance, interphase functions, signal transmission, and intracellular transport. Taxane's act on N-terminal amino acids of the β-tubulin subunit and disrupts the balance within the microtubule network with the interference of cell division, leading to cell death [23, 24]. As compared to PTX, DTX showed a difference in microtubule polymerization pattern, higher intracellular concentration, longer retention and increased upregulation of thymidine phosphorylase. Apart from these advantages, DTX exhibited better *in vitro*/*in vivo* anticancer activity, greater induction apoptosis *via* enhancing BCL-2 phosphorylation activity. Also, DTX showed a linear pharmacokinetic (PK) profile and lower dose schedule dependency as compared to PTX [25]. Paclitaxel has ester of acetate on C-10 position, while DTX contains a hydroxyl group at C-10 position, which enhances the solubility of docetaxel as compared to paclitaxel [26, 27]. Docetaxel having a 3° butyl carbamate ester (-COO-) with a phenylpropionate side chain at C-13 position and an oxetane ring at C-4 and C-5 position. All these properties reflect the better therapeutic efficacy of DTX over PTX. Table 1.1 mention the physicochemical and pharmacokinetic properties of DTX (https://pubchem.ncbi.nlm.nih.gov/compound/Docetaxel).

1.4. Docetaxel formulations

According to the biopharmaceutical classification system, DTX belongs to Class IV showing low solubility and low permeability; thus, it could not be given *via* oral route. Further, its limited aqueous solubility (0.274 mg/L at 25°C) causes a major hurdle in formulation development for the parenteral route. To enhance the solubility, a surfactant

Table 1.1. Physicochemical and pharmacokinetic properties of DTX

Physicochemical property	**Reported value**
Molecular formula	$C_{43}H_{53}NO_{14}$
Molecular weight	807.87 g/mol
Melting point	232°C
Aqueous solubility	0.274 mg/L at 25°C
Log P	2.83
Appearance	White crystalline powder
Pharmacokinetic property	**Reported value**
Pharmacokinetic pattern	Linear up to 115 mg/m^2
Steady-state volume of distribution	~74 liters/m^2
Elimination half-life	
Two-compartment	~12 h
Three-compartment	~13 h
Plasma protein binding	>90%
Systemic clearance	~300 ml/min/m2

(tween 80) and an organic cosolvent (ethyl alcohol) are added in the conventional formulations of DTX (Taxotere®, Duopafei® and Docefrenz®). These marketed formulations are the intravenous solution for injection wherein each vial contains 20 mg/mL or 40 mg/mL of DTX [28]. According to the world health organization, Taxotere® comes under an essential medicine list, but due to a higher concentration of tween 80 and ethanol, it suffers from severe adverse effects such as hypersensitivity reactions, accumulated fluid retention, nausea and mouth sores [29]. Further, the conventional formulations of DTX are associated with side effects due to non-specific delivery to normal tissues. The reversible and long-term toxicity is observed due to the low therapeutic index and high frequency of drug administration. Apart from this, DTX is a substrate for P-glycoprotein, which could lead to the development of drug resistance [30]. Thus there is a need to develop nanomedicines for effective and safe delivery of DTX that could overcome the limitations of conventional formulations and improve the therapeutic outcome.

1.4.1. Nano-carriers for the delivery of DTX

Nanocarriers provide several advantages over the conventional formulations, including protection of the drug from degradation, sustained and controlled release, escape from the reticuloendothelial system (RES), reduced toxicity, higher accumulation in the tumors, higher intracellular uptake and better efficacy [31]. These nanocarriers harness the advantage of enhanced permeation and retention (EPR) effect of the tumors and could release the drug inside the tumor cells, thereby improving the efficacy of the chemotherapeutic agent. Further, efflux pumps present in chemoresistant cancers may be overcome by these nanocarriers and thus providing improved efficacy in the resistant cancers. For DTX delivery, several nanoformulation has been reported, including polymeric nanoparticles (PNs), lipid-based nanoemulsions (NEs), liposomes (LPs), solid lipid nanoparticles (SLNs), micelles, polymer-drug conjugates (PDCs), dendrimers (DN), and inorganic nanoparticles (INPs). Some of DTX formulations have also reached the clinical stage, as shown in Table 1.2 [32].

1.4.1.1. Liposomes

These are spherical vesicles composed of bilayer lipid membrane consisting of phospholipids and cholesterol that could entrap both the hydrophobic and hydrophilic drug molecules. Vakili-Ghartavol et al. have optimized the conditions for loading DTX in liposomes using a remote loading method wherein a size of 115 nm with PDI <0.2 and higher drug encapsulation efficiency was observed (34-67%). Further, the drug release was better controlled in these liposomes with a better biodistribution in the tumors with a significantly delay tumor growth [33]. Li et al. have prepared DTX loaded folate-poly (PEG-cyanoacrylate-co-cholesteryl cyanoacrylate) (FA-PEG-PCHL)-modified freeze-dried

liposomes that showed better cytotoxicity in MCF-7 and A-549 cells as compared to the non-targeted formulation and free drug.

Table 1.2. Docetaxel nanoformulations in clinical trials

Name	Composition	Company	Status	Indications
BIND-014	PSMA targeted PEG-PLGA nanoparticles	BIND Therapeutics	Phase II	Solid tumors
PNP-DTX	Polymeric nanoparticles	Samyang Pharmceuticals	Phase I	Solid tumors
CRLX301	Polymeric nanoparticles DTX conjugate	Cerulean Pharma	Phase II	Refractory solid tumors
Cripec-DTX	Polymeric nanoparticles	Cristal Therapeutics	Phase I	Solid tumors
NKTR-105	PEG-DTX conjugates	Nektar Therapeutics	Phase I	Solid tumors, ovarian cancer
LE-DT	DTX Liposomes	NeoPharm, Inc	Phase II	Advanced solid tumor
ATI-1123	Liposomes	Azaya Therapeutics	Phase I	Advanced solid tumor
ANX-514	Injectable DTX emulsion	ADVENTRX Pharmaceuticals	Phase I	Locally advanced or metastatic breast cancer, non-small cell lung cancer, hormone refractory metastatic prostate cancer.
Dendrimer-DTX	Dendrimers	Sylvania Platinum Ltd	Phase I/II	Advanced cancer
DEP-docetaxel	Dendrimers	Starpharma	Phase II	Advanced cancer
ABI-008	Albumin-bound docetaxel	Abraxis BioScience	Phase I/II, preclinical studies	Metastatic breast cancer, hormone-refractory prostate cancer
ModraDoc006	Solid dispersion	Modra Pharmaceuticals	Phase II	Metastatic prostate cancer

Also, a higher intracellular uptake and apoptosis was observed with the folate targeted liposomes. Further, in the pharmacokinetic study, the area under the plasma concentration-time of folate targeted liposomes was significantly higher as compared to the non-targeted formulation and free drug [34]. In another study, DTX has been loaded into pH-sensitive liposomes containing RGD on the surface to enable dual targeting. These liposomes demonstrated the faster release of DTX at pH 5.0 than pH 7.4, longer blood circulation in rats and higher tumor inhibition [35]. Yoon et al. also demonstrated that RIPL peptide targeted liposomes containing DTX have higher antitumor efficacy as compared to the DTX solution [36]. In another study, vitamin-E TPGS coated liposomes were prepared by a thin-film dispersion that showed a particle size of 140 nm and high encapsulation efficiency of 99%. These liposomes demonstrated a significant improvement in the cytotoxicity and uptake in MCF-7 and resistant MCF-7/ADR cells [37]. Two liposomal formulations of DTX are under phase 1 clinical trial, i.e., docetaxel loaded liposomes (LE-DT) [38] developed by NeoPharma Inc. (Waukegan, Illinois, USA) [39] and docetaxel containing protein stabilizing liposome (PSL™) (ATI-1123) developed by Azaya Therapeutics (San Antanio, Texas, US). LE-DT is a lyophilized liposomal powder prepared by a thin-film hydration method and consists of cholesterol, Dioleoyl-sn-glycero-3-phosphocholine, tetramyristoyl cardiolipin, and alpha-tocopheryl acid succinate [38]. The drawback associated with liposomes is low encapsulation efficacy, rapid leakage of drug and stability issues [40].

1.4.1.2. Lipid-based nanoemulsions

These are thermodynamically stable, colloidal nanoparticles that are composed of two immiscible liquids in a single-phase stabilized by surfactant and co-surfactant. A study by Yadav and Gupta demonstrated that folate targeted solid fat nanoemulsion of tristearin and soya phosphatidylcholine showed lower cytotoxicity with improved cellular uptake in HeLa

cells. In another study, Akhtartavan et al. used ethyl oleate, tween 80 and PEG 600 for preparing the DTX loaded self-nano emulsifying drug delivery system that showed an IC50 of 0.98 µg/ml in MCF-7 cells which was significantly lower than the free DTX. Afzal et al. have prepared albumin anchored DTX lipid nanoemulsion wherein albumin was coupled with sterylamine containing lipid nanoemulsion that showed a particle size of approximately 452 nm with an encapsulation efficiency of 99%, improved in vitro cytotoxicity in HeLa and MCF-7 cells and improved antitumor activity [41]. Gaoe et al. prepared DTX nanoemulsions of 72.3 nm size that showed an encapsulation efficiency of 93.1 %. These nanoemulsions showed similar in vitro cytotoxicity in U87 cells and bEnd.3 cells with a reduced in vivo toxicity as compared to Taxotere® [42]. The presence of surfactant may cause adverse effects, thus, a surfactant-free injectable nanoemulsion (ANX-514) is developed by ADVENTRX Pharmaceuticals Inc. (San Diego, California, USA)[42]. It is tween-80/ethanol free formulation used to reduce the adverse effect due to Taxotere®. ANX-514 tested on MDA-MB-435 human breast, hepatoma and S180 murine sarcoma tumor models at 10 mg/kg dosing cycle showed equivalent tumor reduction activity as compared to Taxotere® [42].

1.4.1.3. Solid-lipid nanoparticles

These are colloidal nanocarrier composed of surfactant stabilized solid lipid (solid at room and body temperature), emulsifier and water. Various advantages that SLNs offer include easy scale up with low production cost, protection from particle aggregation, higher drug entrapment and sustained release from lipid matrix [43] [44]. Da Rocha et al. prepared 128 nm sized SLNs of Compritrol ATO 888 as a lipid matrix with a DTX entrapment efficiency of 86% [45]. These DTX loaded SLNs showed 100 times lower IC50 in 4T1 cells as compared to free DTX with a concomitant improved in vivo efficacy in 4T1 tumor-bearing mice. Lee et al. have prepared hyaluronic acid-coated DTX loaded SLNs using stearic acid,

hexadecyltrimethylammonium bromide , soy phosphatidylcholine that showed a particle size of 224.3 nm. These SLNs showed higher uptake and cytotoxicity in MCF-7/ADR cells [46]. Limitations associated with SLNs include drug degradation during processing, larger particle size and polydispersity, co-existence of numerous colloidal forms and drug expulsion from lipid matrix. To overcome these issues, nanostructured lipid carriers have been proposed. Mathur et al. prepared the DTX loaded NLCs of 154.1 nm size with an encapsulation efficiency of 86.12 %. Further, these NLCs were stable in the gastrointestinal conditions, i.e., at pH-1.2, pH-4.5, pH-6.8, and pH-7.4. In vitro cytotoxicity assay revealed a reduction in IC50 of DTX in NCI-H46 cells when given in the form of NLCs as compared to the free DTX [47].

1.4.1.4. Polymer-drug conjugates

Over the few years, polymer-drug conjugates (PDCs) have been a remarkable contribution in nanocarrier mediated drug delivery for cancer treatment. In this system, drugs could be grafted on the polymers *via* an amide or ester linkage that could increase the solubility of the hydrophobic drug, enhance RES escape, sustained drug release profile, better pharmacokinetic profile, and enhanced tumor targeting via EPR effect. Liu et al. have conjugated DTX to mPEG of 2 KDa molecular weight *via* an ester linkage. These conjugates self assembles to form 100 nm-sized micelles with a critical micelle concentration of 0.88 mg/ml. *In vivo* assessment of these conjugates showed a 1.8 fold higher AUC and 2.5 fold higher maximal tolerated dose (MTD) as compared to Taxotere® [48]. In another study, Guo et al. conjugated DTX to mPEG-PLGA polymer *via* disulfide bond to obtain a reduction sensitive DTX conjugated polymeric micelles of 112.3 nm size. These micelles were more cytotoxic to MCF-7 and B16F10 cells as compared to free DTX [49]. Zhang et al. also showed that redox-sensitive DTX conjugated micelles prepared using methoxy poly(ethylene

glycol)-poly(γ-benzyl l-glutamate) polymer have low CMC, nanometric size with narrow polydispersity and improved cytotoxicity and uptake in MCF-7/ADR and A549 cells [50]. NKTR-105 is a pegylated docetaxel conjugate developed by Nektar Therapeutics under Phase I trial for the treatment of solid tumors. Ersnsting et al. developed a docetaxel conjugate known as Cellax™; composed of acetylated CMC, PEG and docetaxel. Cellax™ showed the enhanced pharmacokinetic profile, effective tumor biodistribution and enhanced efficacy in tumor model with low toxicity [51].

1.4.1.5. Polymeric nanoparticles

Rafiei and Haddadi have used Poly(lactic acid-co-glycolic acid) (PLGA) as a biocompatible, biodegradable and non-toxic polymer for preparing DTX loaded nanoparticles using an emulsion-solvent evaporation method for sustained drug delivery [52]. For achieving targeting, Jose et used transferrin conjugated PLGA for the fabrication of the DTX loaded nanoparticles that showed an IC50 of 4.392 μM/mL in MCF-7 cells as compared to 6.24 and 7.097 for non-targeted nanoparticles and free DTX, respectively [53]. In another report, authors had developed spherical DTX-loaded PEG-PLGA polymeric nanoparticles modified with NGR (NGR–NP-DTX) with a size of 148 nm that demonstrated higher uptake in CD13-overexpressed tumor cells (HT-1080 cell line) with enhanced in vitro cytotoxicity and in vivo tumor suppression [54]. In another attempt, Chen et al. improved the antitumor efficacy of DTX by delivering it as aptamer-anchored nanoparticles (DTX-apt-NPs). These DTX-apt-NPs were prepared by the solvent diffusion technique exhibited particle size of 93.6 nm, high encapsulation (97.62%) and showed significantly improved cellular uptake with enhanced in vitro antitumor action employing clathrin-dependent endocytic uptake mechanism [55]. Further pharmacokinetics of DTX was significantly improved with prolonged therapeutic plasma levels up to 48-72 h when delivered as pegylated

poly(anhydride) nanoparticles composed of a copolymer of methyl vinyl ether, maleic anhydride (Gantrez® AN) and poly(ethylene glycol) (PEG2000 or PEG6000) [56]. In another research work, to overcome the problem of chemo-resistance against DTX in TNBC, authors had developed DTX loaded PGMA-PAA-nanoparticles and surface functionalized with EN1-iPeps engineered with RGD sequences for tumor-specific targeting. These targeted system demonstrated enhanced cytotoxicity and apoptosis in cancer cells with negligible effect on normal/healthy cells serving as a safe and effective therapeutic strategy in treating chemoresistant TNBC [57]. Further, sustained release of DTX was achieved after encapsulating it into polyhydroxybutyrate-*co*-hydroxyvalerate nanoparticles with enhanced cytotoxicity in MCF-7 cell line [58]. BIND-014 is a polymeric nanoparticle in phase II clinical trial for the treatment of solid tumors [59]. It is composed of PEG_{5k}-PLA_{16K} (97.5.5%) and ACUPA-PEG_{5k}-PLA_{16K} (2.5%) polymer which is functionalized with prostate-specific antigen small molecule (S,S-2-[3-[5-amino-1-carboxypentyl]-ureido]-pentanedioic acid (PSMA; ACUPA). Thee nanoparticles are of 100 nm size and contain 10% w/w of docetaxel for active targeted drug delivery [60].

1.5. miRNA therapeutics

In 1993, Ambros's research group discovered *lin-4* as the first microRNA (miRNA) in a nematode, Caenorhabditis elegans [61]. Now there are more than 2500 mature miRNAs reported to be expressed in the cells. These miRNAs are small, non-coding RNAs of 20-25 nucleotide sequences that are involved in several cellular functions, including cell proliferation, maintenance, differentiation and apoptosis. miRNAs do not convey genetic information; rather, miRNAs indirectly controls the translation of coding mRNA and thereby, regulating the expression of the specific gene. It is believed that miRNAs are responsible for regulating around more than one-third of all human genes post-transcriptionally. Moreover,

alteration in endogenous miRNA expression has also shown in a significant number of pathophysiological conditions such as cancer, suggesting the involvement of miRNA in disoriented cellular functions like stemness, malignant transformation, resistance, etc [62].

miRNAs usually binds to the 3'UTR region of the target mRNA sequence and responsible for either down-regulating translation to target protein or degradation of targeted mRNA. The extent of RNAi silencing activity completely depends upon complementary miRNA and mRNA sequences. If the miRNA sequence completely compliments the target mRNA, in such a case, target mRNA is marked for sequential enzymatic degradation. On the other hand, if the target mRNA sequences partially mismatches, then the function of the target gene is inhibited that primarily inhibits the ribosomal access to the target mRNA and further inhibiting the steps required to synthesize the desired protein

1.5.1. Biosynthesis of miRNAs

The biosynthesis of miRNAs involves several steps with two major locations in the cellular compartment, i.e., i) nucleus and ii) cytoplasm [64]. In the nucleus, the pri-miRNA and pre-miRNA are synthesized and pre-miRNA is then transported to the cytoplasm and its further processing with RNA induced silencing complex (RISC) finally leads to the gene silencing (figure 1.1). The process starts within the nucleus with the transcription of a 3' polyadenylated and 5' capped primary transcript miRNA (pri-miRNA) by RNase polymerase II /III. The pri-miRNA is almost 1 kb and have a stem and loop like segment. The pri-miRNA transcription from miRNA gene is governed by proteins; for example, p53 protein is involved in miRNA-34a cluster, MYC for miRNA-17 cluster and MYOD1 for miRNA-1 cluster, ZEB1, ZEB2 for miRNA-200 cluster and MYC for miRNA-15 a cluster. Apart from this, histone protein alterations and methylation of DNA is also involved in miRNA gene regulation. The cleavage of pri-miRNA is initiated by type III RNase DROSHA and DGCR8

(DiGeorge syndrome critical region 8 gene, RNA binding protein) known as microprocessor complex. After processing, pri-miRNA is converted into 70 nucleotide stem-loop structure named hairpin-like precursor miRNA (known as pre-miRNA). Both protein DROSHA and DGCR8 are only found in humans, while plant cells used DICER for miRNA processing [65]. Up to this step, the process is accomplished within the nucleus, following which precursor miRNA is transported to the cytoplasm in the next step where it is further processed with the help of some surface protein/transporter complex named as Ran/GTP/Exportin 5. The translocation of pre-miRNA from the nucleus to the cytoplasm is governed by the presence of exportin-5 (XPO5) and RanGTP (GTP binding nuclear protein) [66].

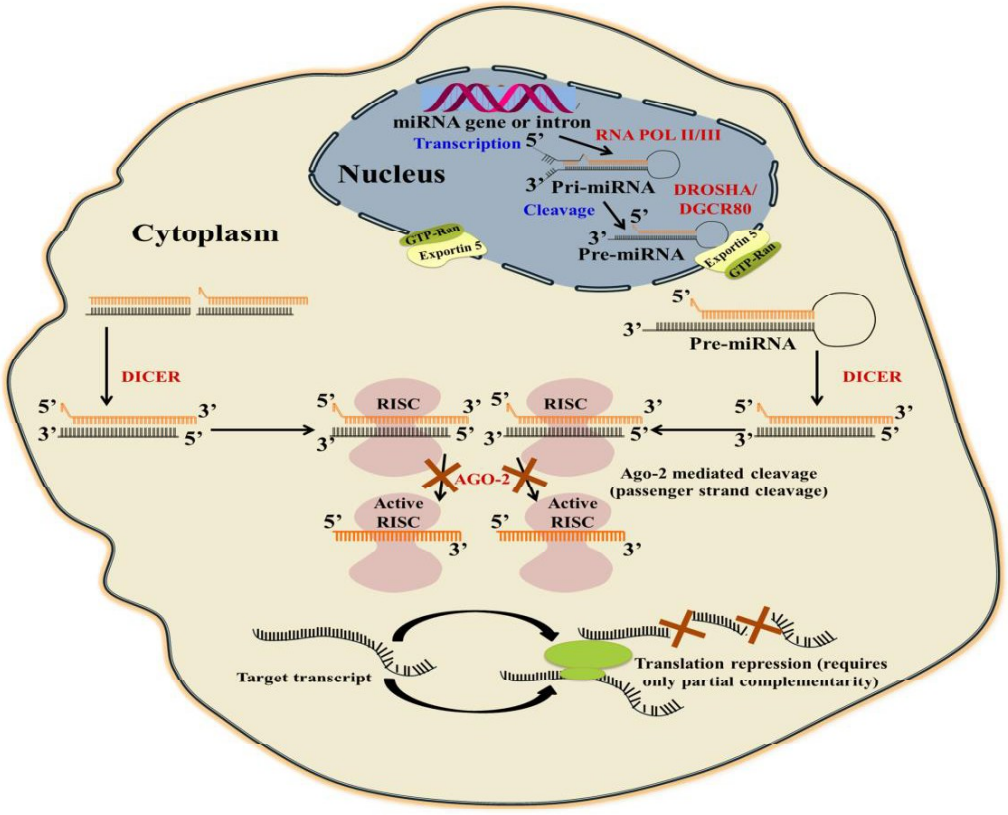

Figure 1.1. miRNA biosynthesis and its mechanism of action

It is facilitated by the formation of a nuclear pore complex involving hydrolysis of GTP followed by the transfer of pre-miRNA into the cytosol. Here, Exportin-5 and RanGTP together form a baseball like structure whose positively charge inner face interacts with the stem of pre-miRNA and its tunnel-like structure on the lower side interacts with the 3' overhang (2nt long) of pre-miRNA. In the cytoplasm, Dicer (2000 KDa) enzyme, RNase-III type endonuclease, cleaves the terminal loop resulting in double-stranded miRNA. It contains C- terminal tandem and N-terminal helicase domain where the C-terminal act as a catalytic center and N-terminal for identifying the pre-miRNA for Dicer interaction [67]. The 5' phosphorylated end of pre-miRNA binds to the Dicer and cleaves into a small miRNA sequence. This sequence interacts with the Argonaute protein, resulting in the separation of two strands, one is the passenger strand and the other is the guide strand [68]. The passenger strand is discarded, whereas mature miRNA guide strand associates with other cofactor GW182 and forms an effector complex known as RISC. This miRNA-RISC complex binds at partially complementary sites of the target 3′ overhang untranslated region (UTR) of mRNA inducing translation repression via destabilizing the mRNA or binds with the complementary site of target mRNAs resulting into mRNA degradation (gene silencing) [69].

1.5.2. Cancer stem cells and miRNAs

CSCs are small sub-population in cancer cells that have been shown to play a role in chemo-resistance, metastasis, invasion and cancer relapse/ re-occurrence. There are several reports suggesting the association of CSCs pathway with drug resistance and the resulting failure of effective taxane therapy. Currently, several studies are going on the CSCs and their major pathways associated with cancer development and progression. These CSCs related pathways and functions are known to be governed by the specific miRNAs. These miRNAs are also known as master regulators responsible for self-renewal and differentiation of cancer

stem cells and their abnormal expression in various types of cancer. miRNA profiling of human breast cancer tissues has provided several aberrantly expressed miRNAs in human breast cancer, including miR-34a known as a master tumor suppressor miRNA. miR-34a has been shown to inhibit cancer regulating mechanisms by interfering with their genes such as CDK4 and CDK6 (cell cycle progression), BCL2, BAX and BCLXL (apoptosis), JAG1 and NOTCH1 (metastasis**)** [70]. Literature evidence suggests the potential microRNA therapeutics in cancer treatment. The impaired regulation of miRNA was found in poorly differentiated tumors such as TNBC and metastatic breast cancer [71]. These miRNAs could be upregulated and participate in carcinogenesis (known as oncomiRs) or are downregulated (such as tumor suppressor miRNAs) that play a role in inhibiting cancer progression with direct or indirect inhibition of proto-oncogene expression [72].

1.5.3. miRNA-34a: as a master tumor suppressor

miRNA-34a (miR-34a) plays an important role in cancer therapy, as it acts as a master tumor suppressor. The miR-34 consisted of 3 family members, viz. miR-34a, miR-34b, and miR-34c. miR-34a is also being associated with the modulation of cancer stem cells in various cancer, including breast cancer, prostate cancer, pancreatic cancer and glioblastoma [73]. In triple-negative breast cancer, miR-34a showed pro-apoptotic functions inducing p53 induced apoptosis [74]. miR-34a is involved in the regulation of various genes, including TP53, NOTCH1, SIRT1, etc. Literature evidence suggested the role of miR-34a in chemo-resistance, cancer progression, metastasis and invasion. Li et al. studied the miR-34a expression and its relation to chemo-resistance in cell-based experiments and in a cohort of 113 breast cancer samples [7]. Downregulation of miR-34a in multidrug-resistant breast cancer cells as compared to non-resistant breast cancer was observed. Further, lower miR-34a expression was correlated with the overall survival rate and disease-free survival. The

transfection of miR-34a mimic in resistance cancer cells reduced the multidrug resistance via altering the expression of various genes such as BCL-2, NOTCH-1 and CCND (cell cycle protein, EGFR mediated G1 phase and S phase transition)[75]. Further, a lower expression of miR-34a was observed in MCF7/ADR cells due to the p53 mutation [76]. After treatment with p53RNAi, there was a lowering of the expression of primary miR-34a and mature miR-34a. Further, it was observed that the cancer stem cell (CSC) proliferation was reduced with an increase in the sensitivity to doxorubicin and reduced tumor suppression in nude mice by ectopic expression of miR-34a [76]. In another study by Li et al., it was shown that miR-34a targets a protein known as tumor protein D52 (TPD52), which is a small hydrophilic polypeptide involved in migration, invasion and proliferation of breast cancer cells [74]. The data showed that reduced miR-34a expression resulted in the activation of TPD52 and TGF-β-N-cadherin pathway that further activates the epithelial-mesenchymal transition (EMT) and enhances the proliferation and migration of breast cancer cells. Enhancing the miR-34a levels reduced breast cancer by inhibiting cell migration and proliferation upon reduction in the TPD52 level.

1.5.4. Combination of miRNAs with chemotherapeutics

A combination of miRNA with anticancer drugs could improve the therapeutic outcome in cancer. The combination therapy suppresses the angiogenesis of tumor, alter the EMT transition, down-regulate the antiapoptotic BCL-2 like proteins, participate in autophagy mechanism and reduce the expression of drug efflux transporter proteins. Several studies had reported improvement in the efficacy of paclitaxel, docetaxel, gemcitabine and doxorubicin when combined with miR-34a. Ren et al. have used poly(amidoamine) dendrimers for co-delivery of antisense miR-21 (as-miR-21) and 5-Fluorouracil. The co-delivery of as-miR-21 significantly improved the cytotoxicity and dramatically increased the apoptosis of U251 cells, while the migration ability of the tumor cells was decreased [77].

Table 1.3. Co-delivery of miRNA and small molecules

S. No.	Formulation	Polymer	Application
1.	Core-Shell Nanoparticles of miRNA-34a and docetaxel	Amine modified Bovine serum albumin	Metastatic breast cancer
2.	miRNA-34a and paclitaxel solid lipid nanoparticles	Dimethyldioctadecylammonium bromide (DDAB), GMS, Cholesterol	Synergistic therapy lung caner
3.	HA-CS/miRNA-34a Doxorubicin nanoparticles	Hyaluronic acid (HA)-chitosan (CS)	Triple negative breast cancer
4.	Gemcitabine conjugated miRNA-205 complexed Micelles	Gemcitabine conjugated cationic polymer	Pancreatic cancer, gemcitabine resistant MIA PaCa-2^R cells
5.	Doxorubicin and miiRNA-542-3p nanoparticles	Hyaluronic acid (HA)-covalently grafted PEI-PLGA	Triple negative breast cancer
6.	Doxorubicin (Dox)/P-gp-siRNA complexed mesoporous nanoparticles	Mesoporous Silica NPs and PEI-PEG	MDR breast cancer
7.	iMSNs ICG loaded siPlk1 and miR-200c complexed nanoparticles	PC/DSPE-mPEG/DSPE-PEG-DBCO and Amine-functionalized MSNs	iRGD Peptide receptor mediated Triple negative breast cancer
8.	miRNa-34a/MDR-1-siRNA/doxorubicin self-assembled Nanoparticles	(i) Hyaluronan (HA) shell as CD44-targeting ligand, (ii) hydrophobic 5β-cholanic acid inner core, (iii) phosphate receptor Zn(II)-dipicolylamine (DPA/Zn); (iv) calcium phosphate	Ovarin cancer
9.	Co-delivery of miR-200c and docetaxel gelatinases-stimuli nanoparticles	Gelatinases-stimuli poly(ethylene glycol)-peptide-poly(ε-caprolactone)	Inhibit Cancer stem cells (CSCs) or non CSC and synergistic effect
10.	Antisense-miR-21-Orlistat polymeric Nanoparticles	PLGA-PEG	Triple-negative breast cancer

miR-205 and gemcitabine, a small hydrophilic molecule, were co-delivered using cationic polymers wherein gemcitabine was chemically conjugated to the polymer chain [78]. Core-shell nano-carriers coated by cationic albumin has been previously reported to co-deliver miR-34a and DTX with improved *in vitro* performance and significantly inhibited tumor growth and metastasis in 4T1 tumor-bearing mice model [79]. Further, Sanjun et al. reported cationic solid lipid nanoparticles loaded with miR-34a and paclitaxel (PTX) that exhibited enhanced efficacy in treating murine B16F10-$CD44^{+}$ melanoma metastasized to the lungs [80]. Qin et al., verified the synergetic effects of co-delivered miR-200c and docetaxel using gelatinases-stimuli nanoparticles on the inhibition of CSCs with resultant enhancement in the cytotoxicity and in vivo tumor suppression due to decrease in the level of class III beta-tubulin and regression of EMT [81].

1.5.5. Delivery of miRNA therapeutics

Although miRNA therapeutics offer a unique strategy to improve the treatment outcome in cancer, however several challenges in its *in vivo* delivery limit its clinical translation. These includes:

- Rapid clearance *via* renal excretion
- Degradation by nucleases in plasma
- Innate immune response resulting in unwanted toxicity
- Hydrophilic nature, high molecular weight, and negative charge
- Endo/lysosomal degradation
- Off-target effects

In order to overcome these hurdles, an effective delivery carrier is required that efficiently complexes with the miRNA, show high transfection efficiency followed by a successful endosomal escape to release miRNA into the cytoplasm. Further, it should be

stable and have low toxicity. Both viral and non-viral vectors have been utilized for gene delivery applications. Although viral vectors provide high transfection efficiency, however safety concerns such as immunogenicity, mutagenesis, etc, limit their clinical potential. In contrast to viral vectors, non-viral vectors demonstrate higher biocompatibility, lesser immunogenicity, protection of payload against proteolytic enzyme and plasma components, scalable and amenable to modifications in the backbone that could help in tailoring the properties of the delivery carrier such as complexation behavior, uptake, transfection and endosomal escape. Additionally, combination delivery could be achieved using non-viral vectors wherein another chemotherapeutic agent could be loaded simultaneously in the carrier [82]. Several non-viral vectors have been reported for gene delivery application that includes lipid-based systems (lipoplexes, cationic SLNs), polymeric systems (polyplexes, polymeric nanoparticles, micelleplexes), inorganic nanoparticles, dendriplexes, etc.

1.5.5.1. Lipid-based systems

Liposomes are spherical lipid bilayered vesicles ranging from 50-1000 nm in diameter, capable of encapsulating hydrophilic molecule payload within an aqueous domain or hydrophobic lipid molecules within the lipid bilayer. They are biocompatible, biodegradable, non-immunogenic in nature, making them a suitable candidate for the hydrophilic payload delivery system. Liposomes can be processed with ease to manipulate size, charge and lamellar composition to reduce toxicity, improve bioavailability, pharmacokinetics and accumulation at the target site. miRNAs and other genetic material are electrostatically complexed with cationic lipid such as N, N-trimethylammonium chloride (DOTMA), dimethyl dioctadecyl ammonium bromide (DDAB), 1,3-Di-Oleoyloxy- 2-(6-Carboxy-spermyl)-propylamide (DOSPER) and 1,2-dioleoyl-3-trimethylammo¬nium propane (DOTAP) to form lipoplexes. To date, lipoplexes are widely used and explored as a

nanocarrier for delivering genetic material to the target site [83]. Mirna Therapeutics Inc. and Marina biotech developed NOV340 technology (SMARTICLES) for delivering miR-34a mimics. Liposomal preparation consists of amphoteric lipid exhibiting cationic charge at low pH and neutral or anionic at pH 7 or higher. Complexation of the miRNA with the lipids is facilitated at acidic pH while in the body fluids, wherein the pH is from 7 to 7.5, the liposomes become slightly anionic inhibiting interaction with the negatively charged cell membrane. In tumor tissue, at low pH, liposomes acquire the cationic charge, interact with the cell membrane and deliver the miR-34a mimics [84].

Yan et al., designed miRNA silencing slug gene and loaded them into a peptide-functionalized liposome that exhibits round shape with a particle size of around 120 nm. Functionalized miRNA liposomal preparation demonstrated efficient cellular uptake by TNBC cells in vitro, resulting in the silencing of slug gene and protein. In vivo treatment with modified miRNA liposomes exerted a remarkable anticancerous effect with nearly complete inhibition of tumor growth [85]. Sharma et al., developed stearylamine based cationic liposomal preparation carrying miR-191 inhibitor for the treatment of breast cancer. miRNA Liposomal formulation showed particle size ranging from 70-100 nm with a spherical morphology demonstrating improved cellular uptake, transfection efficiency, apoptotic cell death and tumoral growth inhibition in MCF-7 and ZR-75-1 breast cancer cells. In addition to that, anti-miR-191 loaded lipoplexes also remarkedly increase the chemosensitivity to anticancer drugs in the free form [86]. Shi et al., co-delivered PTX and miR-34a using cationic solid lipid nanoparticles**.** The SLNs showed smaller particle size, sustained release and better efficacy to the target tumor tissue as compared to miRNA-34a or paclitaxel alone [80]. Antonellis et al. developed stable nucleic acid lipid particles (SNALPs) carrying miR-199b-5p with particle size ranging from 190 nm to 260 nm having a narrow PDI,

demonstrated impairment in cell proliferation and protein expression in various cancerous cell lines [87].

1.5.5.2. Polymeric nanocarriers

1.5.5.2.1. Cationic polymers

The cationic polymers could efficiently complex with the miRNAs by electrostatic interactions [88]. The most commonly used cationic polymer for gene delivery includes poly(ethylene imines), PEI, which is chemically composed of a secondary amino group with one ethylene spacer and is commercially available in a linear and branched form with varying molecular weights. The positive charge generated from the cationic functionality (amino group) is responsible for complexation with nucleic acids *via* electrostatic interaction. Increasing the number and density of amines group in cationic polymer results in an increase in net positive charge that could enhance the complexation efficiency. PEI has weak-base buffering action because of proton accepting behavior responsible for reducing nuclease activity along with protecting nucleic acid from endo-lysosomal degradation pathway as a result of the "proton sponge effect". PEI-miRNA complexes, when administered systemically, could result in significant suppression of tumors compared to controls, suggesting these nanocarriers as a promising approach for miRNA therapeutics for the treatment of cancer [89]. In the previous research work, PEI has been successfully employed *in-vitro* for delivering miR-145 to metastatic breast cancer cells [90] and *in vivo* xenograft colon cancer models [91]. Even though PEI based nanocarrier exhibited efficient miRNA complexation with improved delivery capabilities, but exert several disadvantages due to the cytotoxicity associated with the presence of high positive charge and their non-biodegradable nature thus limiting their potential application use [92]. There are various reports available wherein cationic polymers like PEI, branched PEI, PAMAM have shown

surface charge-dependent cell cytotoxicity [93]. Successful designing of gene delivery carrier needs an optimum balance between cationic charge that helps in gene complexation and transfection along with the presence of suitable functionality in a polymer structure that provides the endosomal escape to successfully release the gene into the cytoplasm. Attempts have been made to reduce toxicity and improve biodistribution of such type of cationic nanocarriers by surface modification using PEG [94]. Zhang et al. had delivered miR-145 to prostate cancer used using branched PEI-PEG nanoparticles [95].

Putnam et al. synthesized a poly-l-lysine-grafted-imidazole acetic acid for effective gene transfer with lower cytotoxicity [96]. In this report, it was shown that the balance between cationic amines with endosomal escaping moieties leads to efficient gene transfer with lower cytotoxicity. Cholesterol is one of the components of the cell membrane layer, so it's incorporation in the structure of the polymeric carrier could help in improving biocompatibility and cellular uptake of the nanocarrier. Chen et al. reported cholesterol grafted bio-reducible polyamidoamine for the delivery of siRNA [97]. The study data concluded the impact of cholesterol grafting on the rPAA backbone leads to a stable siRNA nano-complex with higher transfection ability and endosomal escape. Kim et al. reported the role of cholesterol in effective gene delivery by providing "protein corona," effect, i.e., resistance to serum degradation, enhanced the transfection efficiency and lower cytotoxicity than other cationic lipids.

To overcome the problems of toxicity and biodegradability associated with cationic PEI based nanoparticles, amphiphilic biodegradable polymers, including polyesters and polycarbonates, have been explored for gene-based therapeutics. Polyesters (PLGA and PCL) have been used for delivering nucleic acids and offers advantages such as biocompatibility and biodegradability [98, 99]. By altering the ratio of lactic and glycolic acid, the degradation rate can be modulated, ranging from months to years. However, miRNA complexation with

PLGA nanoparticles exerts the challenge of low encapsulation efficiencies that could be overcome by incorporating cationic compounds along with PLGA [100]. For instance, the complexation of miRNAs on the surface of PLGA nanoparticles could be improved by coating with protamine sulfate (PS) [98]. In another report Wang et al., co-delivered doxorubicin (DOX) and miR-542-3p in TNBC cells using PLGA-PEI nanoparticles [101]. Further PLGA-PEI nanoparticles were covalently grafted with hyaluronic acid for specifically targeting breast cancer cells, thereby enhancing *in vitro* cytotoxicity.

1.5.5.2.2. Amphiphilic copolymer for gene delivery application

The nanotechnology-based platform has gained more research attention for delivering the low molecular weight chemotherapeutics molecule with oligonucleotide such as miRNA/siRNA. Among all the polymeric nanoformulation, micelleplexes possesses special advantage for co-delivery of small molecule and miRNA. Wherein, the core is composed of the hydrophobic component that can load small hydrophobic molecule and cationic outer shell can be used to electrostatically complexed the negative charged hydrophilic miRNA; providing major benefits in altering EMT transition, reducing chemoresistance, induced apoptotic pathway and autophagic response, and inhibiting tumor angiogenesis etc. Such nanocarriers are self-assembled, thermodynamically stable and elicit smaller particle sizes (less than 200 nm). There are several reports published in which micelleplexes can be deployed to the targeted site *viz.* passively targeting the cancer cell with an EPR effect. In a research published by Mittal et al., copolymers consisting of pegylated polycarbonate polymer with cationic functionality was utilized for co-delivery of gemcitabine and miRNA 205 for pancreatic tumor [101]. In this study, the polymeric micelles nanoformulation was developed by film hydration method, exhibited smaller particle size, narrow PDI and greater stability. The micelles showed longer stability in the serum/ biological system with an

effective reduction in tumor weight and volume in the tumor xenograft model. In another study, Kumar et al. synthesized copolymer mPEG-b-PCC-g-DC-g-TEPA and developed micelleplexes co-delivering small molecule hedgehog inhibitor and miRNA for treatment of pancreatic cancer. The obtained micelleplexes were used to efficiently load hydrophobic molecule and miR-let7b at a low N/P ratio, smaller particle size of less than 100 nm and showed good serum stability [102]. However, such combinational treatment using the micellar nanocarrier system led to effective pancreatic tumor suppression in *in vivo* tumor mice model. Zhu et al. prepared the MMP-2 siRNA and paclitaxel loaded micelleplexes for the treatment of prostate cancer using a cationic polymeric system [103]. These block polymer formed smaller particle size, stable micelles with low CMC and demonstrated good transfection efficiency as well as predominant accumulation in the tumoral tissue. Zeng et al., developed a micelels of PEG-PLL-PLLeu polymers for delivery of docetaxel and Bcl-2-siRNA wherein hydrophobic PLLeu was used to entrap the small hydrophobic molecule into its core while and PLL cationic shell allowed to electrostatically complex with siRNA. These micelleplexes showed a particle size of around 100 nm, demonstrating superior *in vitro* and *in vivo* tumour suppression [104]. In another study, Qian et al., designed and synthesized star-shaped PLA-b-PDMAEMA copolymer with variable molecular architecture. PLA-PDMAEMA copolymer micelles were prepared using the solvent evaporation method, wherein, micelles with smaller particle size, possessed low CMC and the net surface positive charge was obtained. The micellar copolymer exhibited 2.5 times higher transfection efficiency than PEI, which was further used to co-deliver DOX and miR-21 inhibitor into the cancer cells demonstrating good anti-proliferative efficiency and tumor stasis in vitro and in vivo [105]. Sun et al., designed and synthesized biodegradable triblock poly(ethylene glycol)-b-poly(ε-caprolactone)-b-poly(2-aminoethyl ethylene phosphate) copolymer for breast cancer. Micellar preparation was made using the solvent evaporation method resulting in a

mean particle size of 50 nm co-delivering PTX and PLK1-siRNA exhibited effective tumoral cell uptake and induce synergistic suppression in tumor xenograft mice model [106].

1.5.5.2.3. Dendriplexes

The word dendrimer primarily originated from a Greek word "dendron" meaning tree and "meros" meaning part. Dendrimers are known to possess three dimensional, nano-sized, hyperbranched architecture, which is characterized by a unique well-defined symmetrical molecular structure. This branched structure was initially discovered by Fritz Vogtle in 1978 and later on, several other research groups like Donald Tomalia, George R. Newkome entered into a deeper phase of exploring the concept of hyperbranched dendrimers [107]. Dendrimers are composed of mainly three parts: a) a small initiator core, b) interior layer (generations) of the same units diverging out from the core and c) exterior functional group attached to the outermost layer. Furthermore, end groups (functional groups on the periphery) can also be tailored to obtain the desired alterations in their physiochemical and biological properties like shape, size, solubility, rigidity and viscosity, etc. They are considered as a potential non-viral carrier system, as they significantly alter the biocompatibility, binding efficiency, transfection efficiency, biodistribution and internalization into the tumoral cells [108].

A wide range of dendrimers has been designed, synthesized and studied up to date, but the most widely used cationic dendrimers for the delivery of miRNA include Polyadmidoamine (PAMAM), Polypropylenimine (PPI), Poly-L-Lysine (PLL), carbosilane, peptide and phosphorus dendrimers, etc [109]. In a study, Mei et al. conjugated 5-Fluorouracil to PAMAM dendrimer and later on, it was complexed with antisense miR-21. These dendriplexes exhibited lower particle size that significantly increased the cellular uptake from 3.5% to 54.5%, resulting in improved cell migration, chemosensitivity and reduced migration in MCF-7 cells in vitro [110]. Furthermore, Mei et al., co-delivered taxol

and miR-21 inhibitor using PAMAM dendrimers. In vitro analysis exhibited significant enhancement in transfection efficiency and reduced cell viability leading to the sensitization of breast cancer MCF-7 cells to taxol *via* inhibiting the AKT pathway [111]. In another study, Song et al. developed core-shell tecto PAMAM dendrimer (CSTDs) for co-delivery of miR-21 inhibitor and DOX to the cancer cells. Electrostatically complexed genetic material loaded hydrophobic molecule to dendrimer exhibited effective transfection efficiency that resulted in enhanced cancer therapy in vitro [112]. Ren et al., co-delivered miR-21 inhibitor with taxol using PAMAM in cancer cells demonstrating a substantial reduction in IC50 value and cell invasiveness with improved chemosensitivity, apoptosis and anti-proliferative effect *in vitro* [113].

1.5.5.2.4. Inorganic nanoparticles

Inorganic materials including iron oxides, calcium phosphate, silica and gold are reported to be used for constructing nano-based carrier for drug or gene delivery and offers advantages such as biocompatibility, modulable size and morphology [98]. The magnetic nanoparticles are combined with cationic compounds for achieving high miRNA complexation [98]. Streptavidin-coated magnetite nanoparticles had been modified using biotin-bound miR-335/PEI complexes for delivering miRNA to human mesenchymal stem cells [98]. Silica and mesoporous silica-based nanoparticles (MSPs) possess high biocompatibility and stability, thus grabbed attention for therapeutic applications. MSPs have been explored for co-delivery of Temozolomide (TMZ) and anti-miR-221 to treat drug-resistant glioma cells [98]. Tivnan et al. developed silica nanoparticles for delivering miR-34a for the treatment of neuroblastoma [98]. Calcium phosphate (CaP) nanoparticles offer numerous advantages, including lower cost, non-toxicity, manufacturability , and bioresorption and have been widely used as carriers for gene delivery for 40 years. DNA-

CaP nanoparticles get degraded rapidly in the mild acidic condition of the lysosome, leading to burst release in the cytosol [114]. However, CaP has poor interaction with miRNAs because of low spatial charge density that can be improved by incorporation of PEI. Gold nanoparticles (Au-NPs) are surface-functionalized with amino or thiol groups for miRNA complexation and offers advantages including biocompatibility, ease of surface functionalization, tunable size and shape with excellent intracellular uptake [115]. miRNA complexation onto Au-NPs surface could be improved by cystamine functionalization, whereas pegylation prevents aggregation of nanoparticles and degradation of miRNA. Ekin et al. delivered miR-145 using Au-NPs to breast and prostate cancer cells [116].

1.5.5.2.5. Polycarbonate based polymers for gene delivery application

The fabrication and development of cyclic carbonate-based copolymers with well-defined structural configuration have attracted significant attention over the previous decade [117]. These polymers were extensively utilized in the pharmaceutical field as of hydrophobic drug reservoirs, nanocarrier and non-viral miRNA delivery vehicles. Research evidence suggested the potential of polymeric systems with a hydrophobic carbonate to enhance the *in vivo* gene delivery. These polycarbonates are amenable to modification with pendant groups that could efficiently deliver the oligonucleotides, including miRNA and siRNA, to the specific target tissue. Li et al., designed poly(ethylene glycol)-block-poly(2-methyl-2-carboxyl-propylene carbonate-graft-dodecanol) (PEG-PCD) lipopolymer based micellar formulation delivering hydrophobic model drug embelin. These drug-loaded micelles showed significantly improved cytotoxicity in C4-2 prostate cancer cell proliferation with no cytotoxicity observed in the blank micellar formulation [118]. In another research work, Ong et al. reported an efficient and safe non-viral gene carrier composed of galactose-functionalized cationic polycarbonate for effective hepatocyte targeting for the treatment of

hepatitis infection [119]. Further to address the challenge of chemo-resistance of prostate cancer against DTX, successful attempts were made by co-delivering microtubule destabilizer (QW-296) and hedgehog signaling pathway inhibitor (MDB5) via self-assembled micelles of mPEG-(p(TMC-MBC)) [methoxy-poly(ethylene glycol)-block-poly(trimethylene carbonate-co-2-methyl-2-benzoxycarbonyl-propylene carbonate)] with control drug release profile exhibiting enhanced in vivo anticancer efficacy [120]. The skeletal backbone of polycarbonates can be further modified by grafting with various functional moieties, including imidazole /morpholine (responsible for endosomal escape via proton sponge effect) and ethylene diamine/guanidine (responsible for efficient complexation with oligonucleotide) [121-123]. In addition to the aforementioned moieties, cholesterol grafting demonstrated enhanced transfection abilities with lower cytotoxicity and enhanced hydrophobic drug encapsulation [124]. Additionally, the inclusion of polycarbonate functionalities improved the amphiphilic nature of polymer with self-assembling properties along with enhancement in hydrophobic drug loading [125]. Several studies had demonstrated pegylation of these polycarbonate-based copolymers resulted in improved drug circulation due to the stealth effect by evading RES uptake [126]. Frere et al. synthesized biocompatible polycarbonate polymer for siRNA delivery and studied the impact of grafting various functional moieties including morpholine, and guanidinium for increasing the transfection efficiency, endosomal escape and complexation ability with the siRNA [127]. It was demonstrated that the polyplexes formed through self-assembly of siRNA with cationic polycarbonate containing guanidine/morpholine have an immense potential for gene delivery by imparting endosomal escape and avoiding lysosomal degradation.

1.6. Folate receptor targeting in cancer

Actively targeted delivery of chemotherapeutic agents and miRNA is governed by the recognition of the type of receptor expressed on to the surface of breast cancer cells. Receptor-mediated drug delivery approach serves as an important therapeutic strategy in the area of active targeting for delivering actives selectively to cancer cells resulting in improved suppression of tumor growth in comparison to non-targeted drug delivery. Adopting such a tumor-selective strategy could be very helpful in reducing the off-target cytotoxicity associated with the non-selective distribution of chemotherapeutic agents to normal healthy tissues, thereby eliminating unnecessary exposure to normal cells resulting into their lower IC50 values. Amongst various types of receptors overexpressed on breast cancer cells, folate receptors (FRα), integrin receptors (αvβ3), transferrin receptors, interleukins, Her2, estrogen, progesterone, ICAM1 and EGFR receptors are most common with triple-negative breast cancer (TNBC), involving majorly FRα that is responsible for uptake of folic acid (small molecules that is necessary for nucleic acids and DNA synthesis). Folate or vitamin-B9 or its substituents is an essential component and required in large quantities for the biosynthesis of amino acid, nucleotides and methylated substances in rapidly proliferating cells [128]. Apart from breast cancer, FRα is highly expressed in various cancers, including ovarian, lung and colorectal. Thus FRα serves as a promising targeting site for selective accumulation of actives in cancer cells [129]. For achieving active targeting, folic acid (substrate of FRα) is functionalized onto the surface of the nanocarrier system. Further, it was hypothesized that coupling this active targeting approach with combination therapy using gene and the cytotoxic drug might serve as a promising approach for effective management of breast cancer, especially, TNBC.

In a study Thapa et al. prepared the folate conjugated docetaxel and cisplatin loaded nanoparticle for treatment of TNBC. The formulation was tested in a TNBC cancer cell line

(MDA-MB-231) mice model, resulting in a significant reduction in tumor volume on treatment with folic acid conjugated nanoformulation compared to non-targeted nanoformulation or free drugs. Further, there was a significant induction of apoptosis with lower expression of Ki-67 (proliferation marker) and CD-31 (angiogenesis marker) in groups treated with folate targeted nanoformulation [130]. Recently, Orellana et al. developed a folate conjugated miR-34a for the treatment of cancer. Results suggested that there was a rapid and selective uptake of folate conjugated miR-34a in the cancer cells with enhanced in vivo stability of miR-34a [131]. Further, the anticancer efficacy of folate conjugated miR-34a was compromised due to endo-lysosomal degradation. In another study the same group developed, Folate-Nigericin-miR-34a conjugate and were able to successfully overcome the endo-lysosomal degradation due to the presence of ionophore nigericin (endosomal swelling by proton sponge effect) resulting into improved *in vivo* efficacy compared to folate conjugated miR-34a [132].

1.7. Outline of current research work

Keeping the above facts in the view, the present study is aimed to design, develop and evaluate an actively targeted non-viral lipopolymeric nanocarrier for effective delivery of miR-34a and DTX for the treatment of breast cancer. The current thesis work presented a strategy exploring the benefits of active targeting for simultaneously delivering miR-34a/DTX combination by fabricating a nanocarrier system capable of co-loading miR-34a and DTX that possessed entirely different physicochemical properties. Apart from simultaneous delivery, the proposed system could offer several advantages in terms of a) improving stability of miRNA against exogenous RNAses, b) imparting stealth property due to presence of PEG corona on the surface of nanocarrier that prevents recognition by the RES

system and c) active targeting due to presence of folic acid that enables receptor-mediated endocytosis.

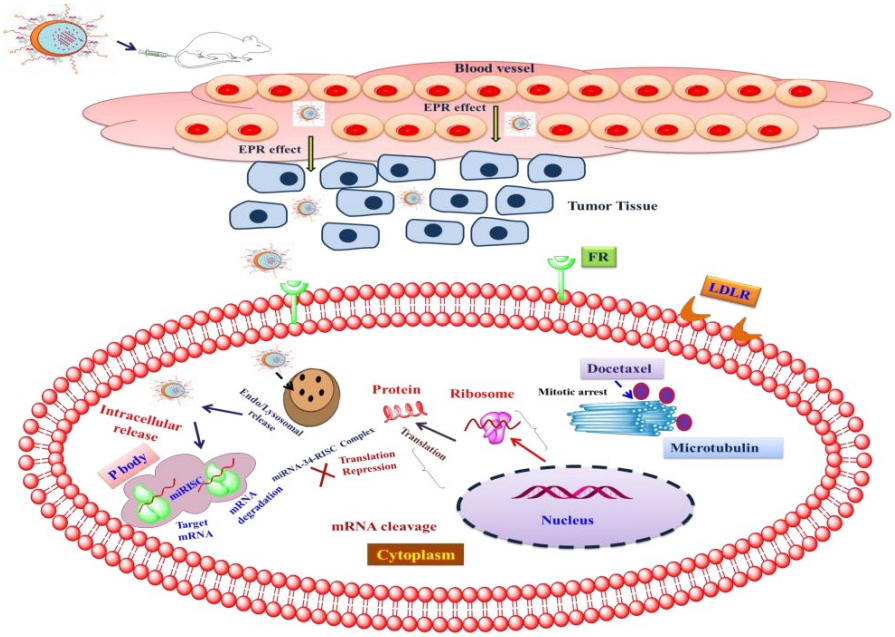

Figure 1.2. Actively targeted nanoformulation of miRNA and DTX in cancer

1.8. Objectives of the research work

To achieve the aim of the thesis, the following objectives have been designed. The thesis is divided into chapters focusing on each objective culminating in the research agenda.

Objective 1. Bioanalytical method development and validation for the analysis of docetaxel

Objective 2. Development and evaluation of cationic lipopolymeric nanoplexes containing miRNA-34a

Objective 3. Development and evaluation of folate targeted lipopolymeric nano-carrier containing docetaxel

Objective 4. Development and evaluation of folate-targeted hybrid lipopolymeric nanoplexes containing docetaxel and miRNA-34a

References

[1] D. Hanahan, R.A. Weinberg, cell, 144 (2011) 646-674.

[2] D. Nassar, C. Blanpain, Annual Review of Pathology: Mechanisms of Disease, 11 (2016) 47-76.

[3] L.A. Torre, R.L. Siegel, E.M. Ward, A. Jemal, Cancer Epidemiology and Prevention Biomarkers, 25 (2016) 16-27.

[4] A. Ahmad, Breast cancer statistics: recent trends, in: Breast Cancer Metastasis and Drug Resistance, Springer, 2019, pp. 1-7.

[5] G.N. Sharma, R. Dave, J. Sanadya, P. Sharma, K. Sharma, Journal of advanced pharmaceutical technology & research, 1 (2010) 109.

[6] D. Appleton, L. Hackney, S. Narayanan, The Annals of The Royal College of Surgeons of England, 96 (2014) 202-206.

[7] M. Chavez-MacGregor, E.A. Mittendorf, C.A. Clarke, D.Y. Lichtensztajn, K.K. Hunt, S.H. Giordano, The oncologist, 22 (2017) 1292.

[8] J. Brierley, M. Gospodarowicz, B. O'Sullivan, ecancer medical science, 10 (2016).

[9] J.M. Cejalvo, E.M. de Dueñas, P. Galván, S. García-Recio, O.B. Gasión, L. Paré, S. Antolin, R. Martinello, I. Blancas, B. Adamo, Cancer research, 77 (2017) 2213-2221.

[10] M. Arnedos, S. Drury, M. Afentakis, M. Hills, J. Salter, I. Smith, M. Dowsett, Journal of Clinical Oncology, 28 (2010) 1034-1034.

[11] A. Nagpal, R.P. Redvers, X. Ling, S. Ayton, M. Fuentes, E. Tavancheh, I. Diala, A. Lalani, S. Loi, S. David, Breast Cancer Research, 21 (2019) 1-19.

[12] E.M. Ward, C.E. DeSantis, C.C. Lin, J.L. Kramer, A. Jemal, B. Kohler, O.W. Brawley, T. Gansler, CA: a cancer journal for clinicians, 65 (2015) 481-495.

[13] W.A. Oluogun, K.A. Adedokun, M.A. Oyenike, O.A. Adeyeba, International journal of health sciences, 13 (2019) 3.

[14] C.W. Tong, M. Wu, W. Cho, K.K. To, Frontiers in oncology, 8 (2018) 227.

[15] L. Dobovišek, F. Krstanović, S. Borštnar, N. Debeljak, Cancers, 12 (2020) 525.

[16] S.M. Fragomeni, A. Sciallis, J.S. Jeruss, Surgical Oncology Clinics, 27 (2018) 95-120.

[17] T. De Marchi, N.Q. Liu, C. Stingl, M.A. Timmermans, M. Smid, M.P. Look, M. Tjoa, R.B. Braakman, M. Opdam, S.C. Linn, Molecular oncology, 10 (2016) 24-39.

[18] N.A. Satar, K.S. Fakiruddin, M.N. Lim, P.L. Mok, N. Zakaria, N.A. Fakharuzi, A.Z. Abd Rahman, Z. Zakaria, B.H. Yahaya, P. Baharuddin, Oncology reports, 40 (2018) 669-681.

[19] K. Aysola, A. Desai, C. Welch, J. Xu, Y. Qin, V. Reddy, R. Matthews, C. Owens, J. Okoli, D.J. Beech, Hereditary genetics: current research, 2013 (2013).

[20] W.D. Foulkes, I.E. Smith, J.S. Reis-Filho, New England journal of medicine, 363 (2010) 1938-1948.

[21] E. Dicks, R. Roome, J. Chafe, E. Powell, F. McCrate, C. Simmonds, H. Etchegary, Current Oncology, 26 (2019) e216.

[22] B.A. Weaver, Molecular biology of the cell, 25 (2014) 2677-2681.

[23] S. Alken, C.M. Kelly, Cancer Management and Research, 5 (2013) 357.

[24] S. Tabaczar, A. Koceva-Chyła, K. Matczak, K. Gwoździński, Postepy higieny i medycyny doswiadczalnej (Online), 64 (2010) 568-581.

[25] C. Xu, Y. Ding, J. Ni, L. Yin, J. Zhou, J. Yao, RSC advances, 6 (2016) 27542-27556.

[26] Z.-H. Peng, M. Sima, M.E. Salama, P. Kopečková, J. Kopeček, Journal of drug targeting, 21 (2013) 968-980.

[27] Z. Meng, Q. Lv, J. Lu, H. Yao, X. Lv, F. Jiang, A. Lu, G. Zhang, International Journal of Molecular Sciences, 17 (2016) 796.

[28] A. Mirza, N. Mithal, Clinical oncology, 23 (2011) 560-561.

[29] M. Ema, H. Hara, M. Matsumoto, M. Hirata-Koizumi, A. Hirose, E. Kamata, Reproductive Toxicology, 25 (2008) 89-99.

[30] MF Sohail, M. Rehman, H.S. Sarwar, S. Naveed, O. Salman, N.I. Bukhari, I. Hussain, T.J. Webster, G. Shahnaz, International Journal of Nanomedicine, 13 (2018) 3145.

[31] R.B. Rigon, M.H. Oyafuso, A.T. Fujimura, M.L. Gonçalez, A.H.d. Prado, M.P.D. Gremião, M. Chorilli, BioMed Research International, 2015 (2015).

[32] L. Zhang, N. Zhang, International Journal of Nanomedicine, 8 (2013) 2927.

[33] R. Vakili-Ghartavol, S.M. Rezayat, R. Faridi-Majidi, K. Sadri, M.R. Jaafari, Scientific Reports, 10 (2020) 1-14.

[34] X. Li, X. Tian, J. Zhang, X. Zhao, X. Chen, Y. Jiang, D. Wang, W. Pan, International Journal of Nanomedicine, 6 (2011) 1167.

[35] T. Zuo, Y. Guan, M. Chang, F. Zhang, S. Lu, T. Wei, W. Shao, G. Lin, Colloids and Surfaces B: Biointerfaces, 147 (2016) 90-99.

[36] HY. Yoon, S.S. Kwak, M.H. Jang, M.H. Kang, S.W. Sung, C.H. Kim, S.R. Kim, D.W. Yeom, M.J. Kang, Y.W. Choi, International Journal of Pharmaceutics, 523 (2017) 229-237.

[37] N. Li, T. Fu, W. Fei, T. Han, X. Gu, Y. Hou, Y. Liu, J. Yang, Journal of Pharmacy and Pharmacology, 71 (2019) 1243-1254.

[38] J.F. Deeken, R. Slack, G.J. Weiss, R.K. Ramanathan, M.J. Pishvaian, J. Hwang, K. Lewandowski, D. Subramaniam, A.R. He, I. Cotarla, Cancer chemotherapy and pharmacology, 71 (2013) 627-633.

[39] U. Bulbake, S. Doppalapudi, N. Kommineni, W. Khan, Pharmaceutics, 9 (2017) 12.

[40] J.O. Eloy, M.C. de Souza, R. Petrilli, J.P.A. Barcellos, R.J. Lee, J.M. Marchetti, Colloids and surfaces B: Biointerfaces, 123 (2014) 345-363.

[41] S. Muzammil Afzal, V.M. Naidu, N. Harishankar, V. Kishan, Drug Delivery, 23 (2016) 1355-1363.

[42] M. Cantwell, J. Robbins, A. Chen, in, AACR, 2007.

[43] R.H. Müller, K. Mäder, S. Gohla, European Journal of Pharmaceutics and Biopharmaceutics, 50 (2000) 161-177.

[44] P. Severino, T. Andreani, A.S. Macedo, J.F. Fangueiro, M.H.A. Santana, A.M. Silva, E.B. Souto, Journal of drug delivery, 2012 (2012).

[45] M.C.O. da Rocha, P.B. da Silva, M.A. Radicchi, B.Y.G. Andrade, J.V. de Oliveira, T. Venus, C. Merker, I. Estrela-Lopis, J.P.F. Longo, S.N. Báo, Journal of nanobiotechnology, 18 (2020) 1-20.

[46] S.-E. Lee, C.D. Lee, J.B. Ahn, D.-H. Kim, J.K. Lee, J.-Y. Lee, J.-S. Choi, J.-S. Park, Journal of drug delivery science and technology, 50 (2019) 365-371.

[47] P. Mathur, S. Sharma, S. Rawal, B. Patel, M.M. Patel, Journal of liposome research, 30 (2020) 182-196.

[48] J. Liu, P. Zahedi, F. Zeng, C. Allen, Journal of pharmaceutical sciences, 97 (2008) 3274-3290.

[49] Y. Guo, P. Zhang, Q. Zhao, K. Wang, Y. Luan, Macromolecular Bioscience, 16 (2016) 420-431.

[50] P. Zhang, H. Zhang, W. He, D. Zhao, A. Song, Y. Luan, Biomacromolecules, 17 (2016) 1621-1632.

[51] M.J. Ernsting, W.-L. Tang, N.W. MacCallum, S.-D. Li, Biomaterials, 33 (2012) 1445-1454.

[52] P. Rafiei, A. Haddadi, Materials Science and Engineering: C, 104 (2019) 109950.

[53] S. Jose, T.A. Cinu, R. Sebastian, M. Shoja, N. Aleykutty, A. Durazzo, M. Lucarini, A. Santini, E.B. Souto, Polymers, 11 (2019) 1905.

[54] M. Gupta, G. Agrawal, S.P. Vyas, Immunobiology, 11 (2012) 1190-1191.

[55] Z. Chen, Z. Tai, F. Gu, C. Hu, Q. Zhu, S. Gao, European Journal of Pharmaceutics and Biopharmaceutics, 107 (2016) 130-141.

[56] L. Ruiz-Gatón, S. Espuelas, E. Larrañeta, I. Reviakine, L.A. Yate, J.M. Irache, European journal of pharmaceutical sciences, 118 (2018) 165-175.

[57] A. Sorolla, E. Wang, T.D. Clemons, C.W. Evans, J.H. Plani-Lam, E. Golden, B. Dessauvagie, A.D. Redfern, K. Swaminathan-Iyer, P. Blancafort, Nanomedicine: Nanotechnology, Biology and Medicine, 20 (2019) 102003.

[58] H. Vardhan, P. Mittal, S.K.R. Adena, B. Mishra, European journal of pharmaceutical sciences, 99 (2017) 85-94.

[59] V. Sanna, N. Pala, M. Sechi, International Journal of Nanomedicine, 9 (2014) 467.

[60] H. Zhang, X. Liu, F. Wu, F. Qin, P. Feng, T. Xu, X. Li, L. Yang, International Journal of Molecular Sciences, 17 (2016) 676.

[61] L.P. Lim, N.C. Lau, E.G. Weinstein, A. Abdelhakim, S. Yekta, M.W. Rhoades, C.B. Burge, D.P. Bartel, Genes & development, 17 (2003) 991-1008.

[62] K.B. Reddy, Cancer Cell International, 15 (2015) 1-6.

[63] P. Connerty, A. Ahadi, G. Hutvagner, International journal of molecular sciences, 17 (2016) 31.

[64] C. Catalanotto, C. Cogoni, G. Zardo, International journal of molecular sciences, 17 (2016) 1712.

[65] J. Han, Y. Lee, K.-H. Yeom, Y.-K. Kim, H. Jin, V.N. Kim, Genes & development, 18 (2004) 3016-3027.

[66] S. Das, I.N. Mohamed, S.L. Teoh, T. Thevaraj, K.N. Ku Ahmad Nasir, A. Zawawi, H.H. Salim, D.K. Zhou, Mini Reviews in Medicinal Chemistry, 20 (2020) 626-635.

[67] M.-S. Song, J.J. Rossi, Biochemical Journal, 474 (2017) 1603-1618.

[68] R.W. Carthew, E.J. Sontheimer, cell, 136 (2009) 642-655.

[69] A. van den Berg, J. Mols, J. Han, Biochimica et Biophysica Acta (BBA)-Gene Regulatory Mechanisms, 1779 (2008) 668-677.

[70] X.-Z. Guo, X.-D. Shao, M.-P. Liu, J.-H. Xu, L.-N. Ren, J.-J. Zhao, H.-Y. Li, D. Wang, World Journal of Gastroenterology, 8 (2002) 1059.

[71] K. Chen, N. Rajewsky, Nature Reviews Genetics, 8 (2007) 93-103.

[72] W. Si, J. Shen, H. Zheng, W. Fan, Clinical epigenetics, 11 (2019) 25.

[73] S. Imani, R.-C. Wu, J. Fu, Journal of Cancer, 9 (2018) 3765.

[74] G. Li, L. Yao, J. Zhang, X. Li, S. Dang, K. Zeng, Y. Zhou, F. Gao, Tumor Biology, 37 (2016) 7481-7491.

[75] Z.-H. Li, X. Weng, Q.-Y. Xiong, J.-H. Tu, A. Xiao, W. Qiu, Y. Gong, E.-W. Hu, S. Huang, Y.-L. Cao, Oncotarget, 8 (2017) 106270.

[76] EY. Park, E. Chang, E.J. Lee, H.-W. Lee, H.-G. Kang, K.-H. Chun, Y.M. Woo, H.K. Kong, JY. Ko, H. Suzuki, Cancer research, 74 (2014) 7573-7582.

[77] Y. Ren, C.-S. Kang, X.-B. Yuan, X. Zhou, P. Xu, L. Han, G.X. Wang, Z. Jia, Y. Zhong, S. Yu, Journal of Biomaterials Science, Polymer Edition, 21 (2010) 303-314.

[78] A. Mittal, D. Chitkara, S.W. Behrman, R.I. Mahato, Biomaterials, 35 (2014) 7077-7087.

[79] L. Zhang, X. Yang, Y. Lv, X. Xin, C. Qin, X. Han, L. Yang, W. He, L. Yin, Scientific reports, 7 (2017) 46186.

[80] S. Shi, L. Han, L. Deng, Y. Zhang, H. Shen, T. Gong, Z. Zhang, X. Sun, Journal of Controlled Release, 194 (2014) 228-237.

[81] Q. Liu, R.-T. Li, H.-Q. Qian, J. Wei, L. Xie, J. Shen, M. Yang, X.-P. Qian, L.-X. Yu, X.-Q. Jiang, Biomaterials, 34 (2013) 7191-7203.

[82] S. Patil, Y.-G. Gao, X. Lin, Y. Li, K. Dang, Y. Tian, W.-J. Zhang, S.-F. Jiang, A. Qadir, A.-R. Qian, International journal of molecular sciences, 20 (2019) 5491.

[83] D. Chitkara, S. Singh, A. Mittal, Therapeutic Delivery, 7 (2016) 245-255.

[84] A.G. Bader, Frontiers in genetics, 3 (2012) 120.

[85] Y. Yan, X.-Q. Li, J.-L. Duan, C.-J. Bao, Y.-N. Cui, Z.-B. Su, J.-R. Xu, Q. Luo, M. Chen, Y. Xie, International journal of nanomedicine, 14 (2019) 3645.

[86] S. Sharma, V. Rajendran, R. Kulshreshtha, P.C. Ghosh, International journal of pharmaceutics, 530 (2017) 387-400.

[87] P. de Antonellis, L. Liguori, A. Falanga, M. Carotenuto, V. Ferrucci, I. Andolfo, F. Marinaro, I. Scognamiglio, A. Virgilio, G. De Rosa, Naunyn-Schmiedeberg's archives of pharmacology, 386 (2013) 287-302.

[88] B. Santos-Carballal, L. Aaldering, M. Ritzefeld, S. Pereira, N. Sewald, B.M. Moerschbacher, M. Götte, F.M. Goycoolea, Scientific reports, 5 (2015) 13567.

[89] L.M. Vermeulen, S.C. De Smedt, K. Remaut, K. Braeckmans, European journal of pharmaceutics and biopharmaceutics, 129 (2018) 184-190.

[90] V. Baumann, J. Winkler, Future medicinal chemistry, 6 (2014) 1967-1984.

[91] H.J. Lee, R. Namgung, W.J. Kim, J.I. Kim, I.-K. Park, Macromolecular Research, 21 (2013) 1201-1209.

[92] HM Abdelaziz, M. Gaber, M.M. Abd-Elwakil, M.T. Mabrouk, M.M. Elgohary, N.M. Kamel, D.M. Kabary, M.S. Freag, M.W. Samaha, S.M. Mortada, Journal of controlled release, 269 (2018) 374-392.

[93] A. Zakeri, M.A.J. Kouhbanani, N. Beheshtkhoo, V. Beigi, S.M. Mousavi, S.A.R. Hashemi, A. Karimi Zade, A.M. Amani, A. Savardashtaki, E. Mirzaei, Nano reviews & experiments, 9 (2018) 1488497.

[94] T. Sun, Y.S. Zhang, B. Pang, D.C. Hyun, M. Yang, Y. Xia, Angewandte Chemie International Edition, 53 (2014) 12320-12364.

[95] T. Zhang, X. Xue, D. He, J.-T. Hsieh, Cancer Letters, 365 (2015) 156-165.

[96] D. Putnam, C.A. Gentry, D.W. Pack, R. Langer, Proceedings of the National Academy of Sciences, 98 (2001) 1200-1205.

[97] C.-J. Chen, J.-C. Wang, E.-Y. Zhao, L.-Y. Gao, Q. Feng, X.-Y. Liu, Z.-X. Zhao, X.-F. Ma, W.-J. Hou, L.-R. Zhang, Biomaterials, 34 (2013) 5303-5316.

[98] S.W.L. Lee, C. Paoletti, M. Campisi, T. Osaki, G. Adriani, R.D. Kamm, C. Mattu, V. Chiono, Journal of Controlled Release, 313 (2019) 80-95.

[99] E. Calzoni, A. Cesaretti, A. Polchi, A. Di Michele, B. Tancini, C. Emiliani, Journal of functional biomaterials, 10 (2019) 4.

[100] E. Sah, H. Sah, Journal of Nanomaterials, 2015 (2015).

[101] S. Wang, J. Zhang, Y. Wang, M. Chen, Nanomedicine: Nanotechnology, Biology and Medicine, 12 (2016) 411-420.

[102] V. Kumar, G. Mondal, P. Slavik, S. Rachagani, S.K. Batra, R.I. Mahato, Molecular pharmaceutics, 12 (2015) 1289-1298.

[103] L. Zhu, F. Perche, T. Wang, V.P. Torchilin, Biomaterials, 35 (2014) 4213-4222.

[104] C. Zheng, M. Zheng, P. Gong, J. Deng, H. Yi, P. Zhang, Y. Zhang, P. Liu, Y. Ma, L. Cai, Biomaterials, 34 (2013) 3431-3438.

[105] X. Qian, L. Long, Z. Shi, C. Liu, M. Qiu, J. Sheng, P. Pu, X. Yuan, Y. Ren, C. Kang, Biomaterials, 35 (2014) 2322-2335.

[106] T.-M. Sun, J.-Z. Du, Y.-D. Yao, C.-Q. Mao, S. Dou, S.-Y. Huang, P.-Z. Zhang, K.W. Leong, E.-W. Song, J. Wang, ACS Nano, 5 (2011) 1483-1494.

[107] E. Abbasi, S.F. Aval, A. Akbarzadeh, M. Milani, H.T. Nasrabadi, S.W. Joo, Y. Hanifehpour, K. Nejati-Koshki, R. Pashaei-Asl, Nanoscale Research Letters, 9 (2014) 247.

[108] M.C. Gohel, R. Parikh, S. Bariya, S. Nagori, A. Gandhi, V. Patel, T. Patel, R. Pandya, S. Kharadi, P. Patel, Targeted drug delivery systems, 7 (2009).

[109] V. Dzmitruk, E. Apartsin, A. Ihnatsyeu-Kachan, V. Abashkin, D. Shcharbin, M. Bryszewska, Pharmaceutics, 10 (2018) 126.

[110] M. Mei, Y. Ren, X. Zhou, X.B. Yuan, F. Li, L.H. Jiang, C.S. Kang, Z. Yao, Journal of applied polymer science, 114 (2009) 3760-3766.

[111] M. Mei, Y. Ren, X. Zhou, X.-b. Yuan, L. Han, G.-x. Wang, Z. Jia, P.-y. Pu, C.-s. Kang, Z. Yao, Technology in cancer research & treatment, 9 (2010) 77-86.

[112] C. Song, Y. Xiao, Z. Ouyang, M. Shen, X. Shi, Journal of Materials Chemistry B, 8 (2020) 2768-2774.

[113] Y. Ren, X. Zhou, M. Mei, X.-B. Yuan, L. Han, G.-X. Wang, Z.-F. Jia, P. Xu, P.-Y. Pu, C.-S. Kang, BMC cancer, 10 (2010) 27.

[114] N. Kamaly, B. Yameen, J. Wu, O.C. Farokhzad, Chemical reviews, 116 (2016) 2602-2663.

[115] Y. Xiao, K. Shi, Y. Qu, B. Chu, Z. Qian, Molecular Therapy-Methods & Clinical Development, 12 (2019) 1-18.

[116] A. Ekin, OF Karatas, M. Culha, M. Ozen, The journal of gene medicine, 16 (2014) 331-335.

[117] W. Guerin, M. Helou, M. Slawinski, J.-M. Brusson, J.-F. Carpentier, S.M. Guillaume, Polymer Chemistry, 6 (2015) 1972-1985.

[118] F. Li, M. Danquah, R.I. Mahato, Biomacromolecules, 11 (2010) 2610-2620.

[119] ZY. Ong, C. Yang, S.J. Gao, X.Y. Ke, J.L. Hedrick, Y. Yan Yang, Macromolecular rapid communications, 34 (2013) 1714-1720.

[120] R. Yang, H. Chen, D. Guo, Y. Dong, D.D. Miller, W. Li, RI. Mahato, Journal of Pharmacology and Experimental Therapeutics, 370 (2019) 864-875.

[121] I. Ullah, K. Muhammad, M. Akpanyung, A. Nejjari, A.L. Neve, J. Guo, Y. Feng, C. Shi, Journal of Materials Chemistry B, 5 (2017) 3253-3276.

[122] S.K. Samal, M. Dash, S. Van Vlierberghe, D.L. Kaplan, E. Chiellini, C. Van Blitterswijk, L. Moroni, P. Dubruel, Chemical Society Reviews, 41 (2012) 7147-7194.

[123] A.M. Fiore, V. Naik, D.V. Spracklen, A. Steiner, N. Unger, M. Prather, D. Bergmann, P.J. Cameron-Smith, I. Cionni, W.J. Collins, Chemical Society Reviews, 41 (2012) 6663-6683.

[124] L. Zhu, R.I. Mahato, Expert opinion on drug delivery, 7 (2010) 1209-1226.

[125] Y. Xie, X. Liu, Z. Hu, Z. Hou, Z. Guo, Z. Chen, J. Hu, L. Yang, Nanomaterials, 8 (2018) 195.

[126] Y. Fang, J. Xue, S. Gao, A. Lu, D. Yang, H. Jiang, Y. He, K. Shi, Drug delivery, 24 (2017) 22-32.

[127] A. Frère, M. Kawalec, S. Tempelaar, P. Peixoto, E. Hendrick, O. Peulen, B. Evrard, P. Dubois, L. Mespouille, D. Mottet, Biomacromolecules, 16 (2015) 769-779.

[128] D.J. O'Shannessy, E.B. Somers, J. Maltzman, R. Smale, Y.-S. Fu, Springerplus, 1 (2012) 22.

[129] B.M. Necela, J.A. Crozier, C.A. Andorfer, L. Lewis-Tuffin, J.M. Kachergus, X.J. Geiger, K.R. Kalari, D.J. Serie, Z. Sun, A.M. Aspita, PloS one, 10 (2015) e0122209.

[130] P. Thapa, M. Li, R. Karki, M. Bio, P. Rajaputra, G. Nkepang, S. Woo, Y. You, ACS omega, 2 (2017) 6349-6360.

[131] E.A. Orellana, S. Tenneti, L. Rangasamy, L.T. Lyle, P.S. Low, A.L. Kasinski, Science translational medicine, 9 (2017).

[132] E.A. Orellana, A.M. Abdelaal, L. Rangasamy, S. Tenneti, S. Myoung, P.S. Low, A.L. Kasinski, Molecular Therapy-Nucleic Acids, 16 (2019) 505-518.

CHAPTER 2

BIOANALYTICAL METHOD DEVELOPMENT AND VALIDATION

- Analytical method for the analysis of DTX
- Bioanalytical Method Development and Validation

This chapter is divided into two sections i.e. 2.1 and 2.2. In the section 2.1, analytical method for the analysis of docetaxel is discussed, while in section 2.2 the bioanalytical method for the analysis of docetaxel in plasma is provided. The analytical method is adopted from a previously published thesis of our laboratory; hence only the chromatographic conditions used and calibrations curves are provided (Tushar Date, M. Pharm. Thesis, 2016, Department of Pharmacy, BITS-Pilani, Pilani Campus).

2 .1. Analytical method for the analysis of DTX

2.1.1. Chromatographic Conditions

The analysis was performed on a Shimadzu HPLC system equipped with an autosampler (SIL-HTC) and SPD-M20A PDA detector. The chromatographic separation of DTX was carried out on Intersil ODS 3V column (250× 4.6 mm, 5 µm) with a mobile phase consisting of acetonitrile and water in the ratio 70:30 v/v run at a flow rate at 1 mL/min at ambient temperature. The injection volume was kept to be 20 µL and wavelength for the analysis was kept at 227 nm wavelength. Spectral interpretations were performed using LC solution software [1].

2.1.2. Preparation of stock solution and working solution

DTX stock solution (100 µg/mL) was prepared by dissolving 10 mg of DTX in 100 mL of acetonitrile. The working solution was prepared by appropriately diluting the stock solution with acetonitrile.

2.1.3. Calibration curve and quality control samples

The calibration curves were prepared through serial dilution of a working solution containing 50 µg/mL of DTX. Seven different concentrations were prepared over the linearity

range of 0.5 μg/mL to 50 μg/mL. Similarly, for quality control samples, four replicate of LQC, MQC and HQC were prepared with a concentration of 0.8, 8 and 40 µg/ml respectively from the working solution. As above mentioned concentration range was analyzed using least-square linear regression analysis. Further, the regression equation was used to calculate the drug concentration in quality control samples and unknown samples. The method has been validated by Date et al. (M. Pharm. Thesis, 2016, Department of Pharmacy, BITS-Pilani, Pilani Campus) for the linearity, specificity, intra- and inter-day accuracy and precision, the limit of detection and limit of quantitation and system suitability parameters [2].

2.1.4. Result and discussion

The retention time for DTX was found to be 4.6 min. Representative chromatogram for DTX (8 µg/mL) is shown in figure 1. The developed method has shown the linearity over the range of 0.5 µg/mL to 50 µg/mL with an equation of *y = 22707x - 362.95*. The regression coefficient (R^2) over the specified range was found to be 0.9999 (Figure 2.1). The method was reported to be specific for docetaxel with a peak purity index of 0.9999, indicating a pure peak (Figure 2.2). The tailing factor for the DTX was 1.110 and the theoretical plate count was 8539.446. The LOD and LOQ for DTX were found to be found 0.8 µg/mL and 0.36 µg/mL, respectively. The Intra-day and Inter-day accuracy and precision of the reported analytical method were within the recommended limits.

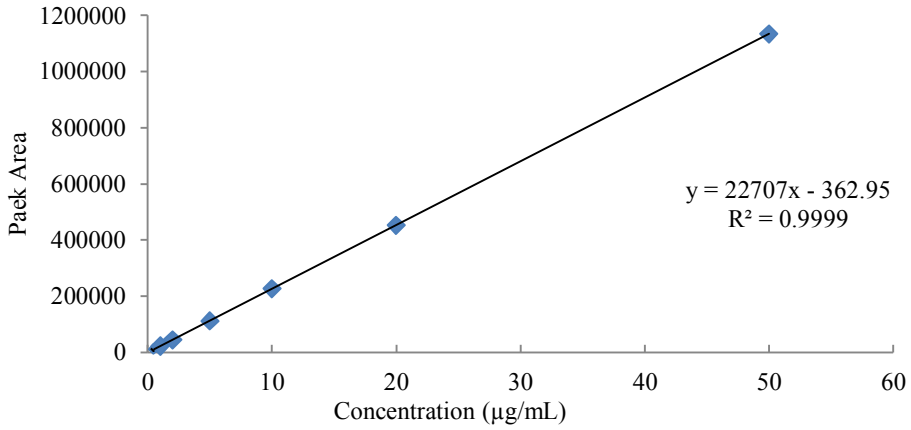

Figure 2.1. Calibration curve for DTX over a range of 0.5 µg/mL to 50 µg/mL

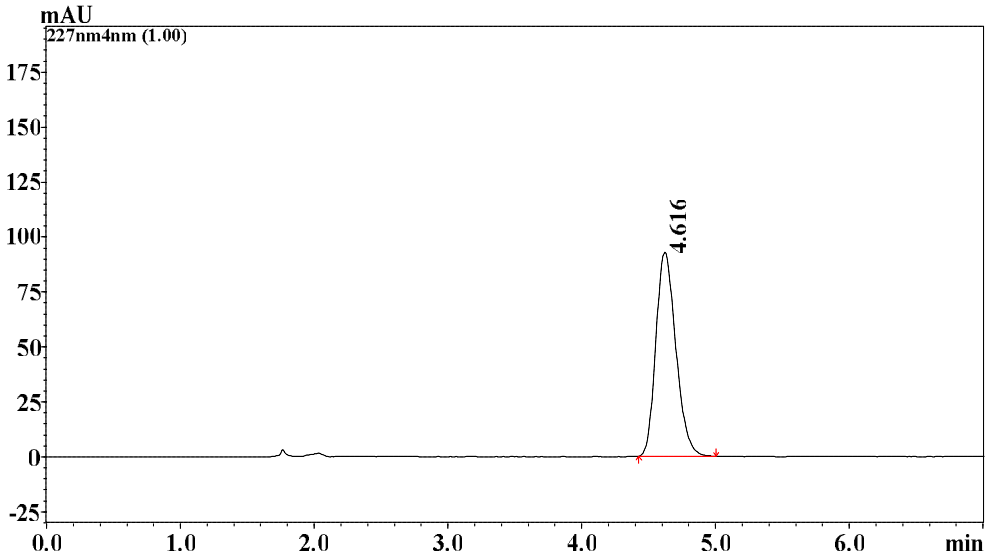

Figure 2.2. Representative chromatogram of DTX (RT= 4.6 min)

2.2. Bioanalytical Method Development and Validation

2.2.1. Liquid Chromatographic conditions

Shimadzu HPLC system (Kyoto, Japan) with an autosampler (SIL-HTC), a binary pump (LC-20AD) and SPD-M20A PDA detector were used for the analysis.

Chromatographic separation of DTX and paclitaxel (PTX; as an internal standard) from the plasma interferences was achieved with on an Inertsil-ODS 3V column (250 × 4.6 mm, 5 μm) with a mobile phase consisting of acetonitrile and water at a ratio of 48:52% v/v. The flow rate was kept at 1 mL/min with an injection volume of 80 µl. The separation was monitored at a wavelength of 227 nm and chromatograms were recorded. The hardware control and data interpretation were performed by using LC solution software version 1.22 SP1 [1, 3, 4]. The method has also been tranwsferred to Waters HPLC system equipped with dual binary pump (#515) connected with Pump controlled module, UV detector (#2489), and auto-sampler (#2707) with simila chromatographic conditions.

Plasma specimen was collected from the *Sprague Dawley* (SD rats; females; 8–10 weeks, 200–220 g) were procured from the Central Animal Facility, BITS-Pilani (Pilani, Rajasthan India) and plama sample was stored at -80 ± 15 °C. The Institutional Animal Ethics Committee (IAEC) approved the animal protocol, BITS-Pilani (IAEC/RES/23/09) and experiments were conducted as per CPCSEA guidelines.

2.2.2. Preparation of stock solution of DTX and PTX

A stock solution of 100 μg/mL was prepared by dissolving 10 mg of DTX in 100 mL of HPLC grade acetonitrile. The PTX stock solution (IS) was prepared by dissolving 2 mg of PTX in 100 mL of HPLC grade acetonitrile to achieve a concentration of 20 μg/mL. Further, the working solution of IS was prepared at a concentration of 7 μg/mL by diluting the stock solution of PTX with acetonitrile.

2.2.3. Calibration curve and linearity range

The calibration standards were prepared from the stock solution (100 μg/mL) using serial dilution with the mobile phase to obtain working solutions with concentrations of 1, 2, 4, 5, 10, 20, 25, 40 and 100 μg/mL. From these working solutions, nine different

concentrations were prepared over the linearity range of 50 ng/mL to 5000 ng/mL and the calibration curve was plotted. The calibration standard samples were prepared by spiking 80 μL of fresh plasma with 5 μL of corresponding working solutions of drug and IS (350 ng/mL). All the calibration standard samples were prepared with the concentration of 50, 100, 200, 250, 500, 1000, 1250, 2000, 5000 ng/mL for the analysis.

2.2.4. Preparation of quality control (QC) samples

For the preparation of quality control (QC) samples, four working solutions, i.e., 1, 1.5, 12 and 90 μg/mL were prepared from the stock solution by dilution with the mobile phase. The quality control (QC) samples were prepared from working stock solutions at four QC levels, i.e., LLOQC (50 ng/mL), LQC (75 ng/mL), MQC (600 ng/mL) and HQC (4500 ng/mL). The samples were prepared by spiking 5 μL of corresponding working solutions of DTX and IS (350 ng/mL) in 80 μL of plasma. All the QC samples were prepared in five replicates independent of the calibration standards. All the quality control samples were interpolated from the calibration curve to determine the concentrations of DTX. Linearity was determined with the help of the least square linear regression analysis. Further, the regression equation was used to calculate the DTX in quality control samples.

2.2.5. Extraction procedure

The protein-precipitation method was used for the extraction of DTX from the plasma [5, 6]. Briefly, 5 μL of IS (350 ng/mL) and DTX stock solution (7 μg/mL) was spiked in 80 μL fresh plasma in a 1.5 mL microcentrifuge tube and vortexed for 1 min on a cyclomixer (Tarsons, India). Further, 0.6 mL acetonitrile was added to the tube as an extraction solvent; herein, blank plasma was taken as a negative control. Vortexing was done for 4 minutes for proper mixing of the components followed by centrifugation for 20 min at 15000 rpm at 4°C. The supernatant (0.5 mL) was separated and dried under vacuum at 37 °C ± 0.5 °C. The

residue was reconstituted in 100 μL of mobile phase and analysis was performed using an HPLC system.

2.2.6. Validation of the developed method

The method was validated as per the US Food and Drug Administration (US-FDA, 2018) guidelines for bioanalytical method validation. The following parameters were determined.

2.2.6.1. Selectivity

The method selectivity was performed to analyze the major chromatographic interferences from the matrix of the plasma samples. To perform the selectivity, plasma from six different rats was collected and used in the analysis by keeping other parameters constant [7].

2.2.6.2. Linearity and calibration curve

Nine calibration standards ranging from 50 ng/mL to 5000 ng/mL were prepared and analyzed, followed by plotting the peak area ratios of the analyte (DTX) and IS (PTX). The relationship between the concentration (on the x-axis) and its corresponding peak area ratio (on the y- axis), was expressed by the equation y = mx + c, for the analyte, where m is slope and c is the intercept. The linear regression analysis was performed on calibration data.

2.2.6.3. The lower limit of quantitation (LLOQ) and limit of detection (LOD)

The sensitivity of the bioanalytical method was analyzed through visual analysis of the signal to noise ratios (S/N) of the response of drug in the samples. As recommended, the S/N ratio should be >3 for the LOD and >10 for the LLOQ. LLOQ was determined as the concentration of the DTX that showed acceptable accuracy and precision (± 20%). The LOD

was analyzed by spiking DTX at concentrations less than the LLOQ at which the drug could be detected [8, 9].

2.2.6.4. Accuracy and precision

The intra-day and inter-day accuracy and precision were determined by analyzing five replicates (n = 5) of QC samples at LLOQ, LQC, MQC and HQC. The accuracy was expressed as % Bias and precision expressed as % RSD or %Coefficient of Variation . The acceptability criteria for accuracy is ± 15% standard deviation from nominal concentration and for precision is ±15% standard deviation from nominal concentration except for LLOQ, where it should not be more than ±20% for both accuracy and precision [9]. % Bias is determined using the following formula:

$$\%\ Bias\ = \frac{Observed\ concentration - Nominal\ concentration}{Nominal\ concentration}\ X100$$

2.2.6.5. Recovery (%)

The absolute percentage recoveries of DTX and IS were analyzed by comparing the area of five replicates (n=5) of all three QC levels (LQC, MQC and HQC) in the plasma samples with corresponding standard concentrations. The percentage recovery of IS was also calculated at a single concentration at 350 ng/mL in six replicates (n = 6).

2.2.6.6. Carry-over effect

The carry-over was analyzed in two blank samples (zero samples) after injecting the HQC samples. For zero samples, an acceptable limit should be lesser than 20% as compared to LLOQ sample response as per the guidelines [9].

2.2.6.7. Stability studies

Stability studies including bench-top stability, ambient temperature 25 ± 2°C for 24 h, short-term stability (4°C ± 2°C , 7 days), long-term stability (−20°C ± 2°C for 1 month), 0 h (for all Initials) and stock solution stability were conducted in the replicate of six (n = 6) at three QC levels (LQC, MQC, and HQC). Samples were processed and analyzed in comparison to fresh calibration curves and fresh QC samples. As per US-FDA acceptance criteria, the limits of accuracy and precision should be within ±15 % for all stability studies samples [9].

2.2.7. Results and discussion

2.2.7.1. Bioanalytical Method development

The bioanalytical method for DTX was developed and validated according to the US-FDA guidelines for bioanalytical method validation. The bioanalytical method optimization was carried out by making systematic changes in LC conditions which include a selection of column, column temperature, mobile phase composition, flow rate, various system suitability parameters such as retention time (Rt), peak tailing (10%), resolution (Rs), theoretical plate number (N), and height equivalent to theoretical plate. The better retention and separation of DTX and IS were obtained using an Inertsil ODS 3 V column (250× 4.6 mm, 5 µm) as stationary phase and isocratic flow of mobile phase consisting acetonitrile and Mili-Q water in the ratio of 48:52 % v/v run at a flow rate at 1 mL/min. DTX and IS (PTX) showed a retention time of 19 min and 24 min, respectively. The standard curves were plotted from 50 ng/mL-5000 ng/mL and the injection volume was kept at 80 µL with 30 min run time. Figure 2.3 shows the representative chromatogram for a sample containing DTX and PTX.

2.2.7.2. Plasma sample extraction

The extraction of drugs from plasma samples is a tedious task and plays an important role in the selectivity and sensitivity of the bioanalytical method. To improve the percentage recovery from the plasma matrix, different strategies of sample preparation technique, selection of appropriate solvent, the volume of sample and solvent, and duration of sample preparation were crucial. Hence two different extraction methods were performed, i.e., liquid-liquid (LLE) and protein precipitation method. Finally, the protein precipitation method was adopted with acetonitrile as a protein precipitating solvent because it showed the optimum recovery, clear samples, no matrix effect and better extraction of DTX from the plasma

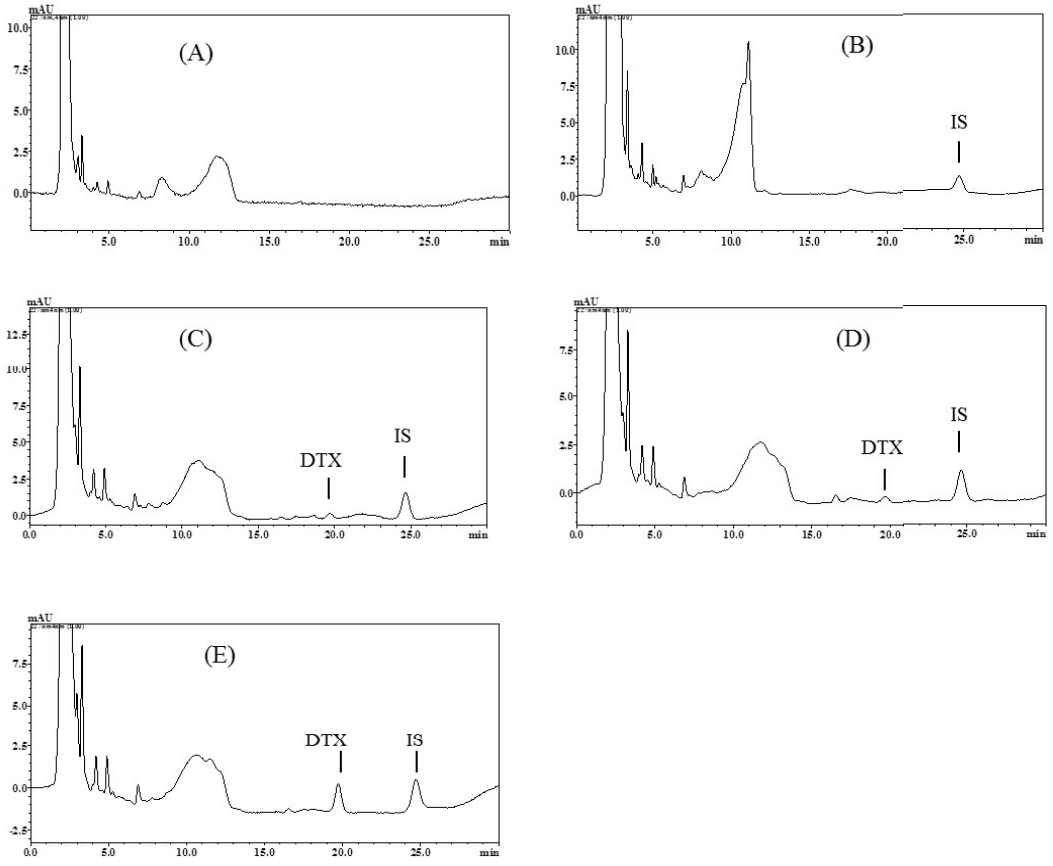

Figure 2.3. RP-HPLC chromatograms of plasma samples. (A) blank plasma, (B) zero sample (*i.e.* IS spiked with plasma), (C) DTX and IS spiked at LLOQ, (D) DTX and IS spiked at LOD and (E) DTX and IS spiked at MQC

matrix as compared to LLE method. The sample preparation, extractions were found robust and simple. The solvent was evaporated and reconstituted in a small volume (100 µL) of the mobile phase. Only 0.6 mL acetonitrile was required to achieve the sufficient percentage recovery (≥ 75 %) of DTX and PTX with better resolution (R_s 4.12 ± 0.12) and retention time (R_t (DTX) ~19 min and R_t (IS) ~ 24 min respectively), without any interference from the plasma matrix with peak purity of <0.999.

2.2.7.3. Selectivity and Specificity

For analyzing the selectivity, six plasma samples were spiked with DTX and IS followed by processing as per the optimized extraction procedure. To analyze the specificity, blank plasma samples were analyzed with the developed bioanalytical method to check the interferences wherein no interference was observed from the matrix near the retention time (Rt) of DTX and IS, as shown in figure 2.3.

2.2.7.4. Calibration Curve, Linearity, LLOQ and LOD

The bioanalytical method was characterized by analyzing plasma samples spiked with different DTX concentrations. The linear calibration curves were obtained at the concentrations range from 50 ng/mL to 5000 ng/mL with DTX and IS concentration (350

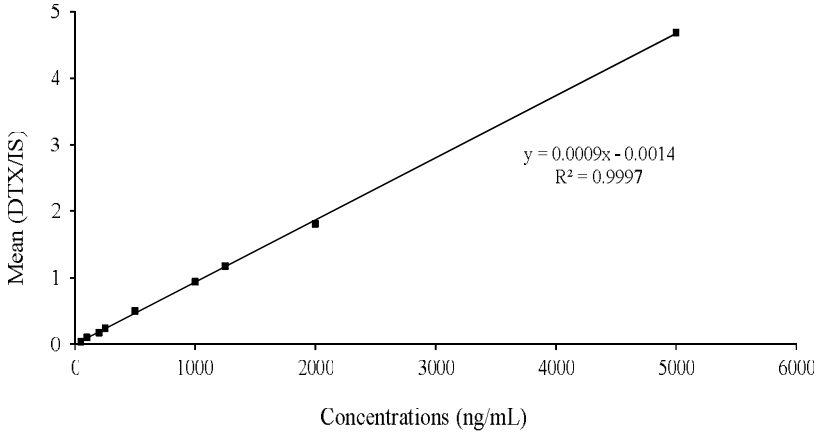

Figure 2.4. Calibration curve of DTX in rat plasma

ng/mL) that showed an R^2 of 0.9997 (figure 2.4 and Table 2). Five calibration curves were prepared consisting of nine non-zero concentrations sample (containing DTX and IS), zero sample (IS only) and blank sample. The obtained calibration curves accurately fitted with linear regression (y = mx + c). The equation; y = 0.0009x - 0.0014 with correlation coefficient R^2 of 0.9997. The percentage RSD for LLOQ (50 ng/mL) was found to be < 20%. The precision (% RSD) and accuracy (% Bias) was calculated for calibration standards with corresponding concentration previously calculated by a linear equation. For LLOQ, % RSD and % Bias were 9.59 % and -12.60 %, respectively. By using signal to noise (S/N) ratio method, S/N ratio was observed to be 3.92 and 13.86, respectively, for LOD and LLOQ that were within the acceptable limits (for LOD ≥3 and for LLOQ ≥10). LOD and LLOQ by S/N visual method were found to be 16 ng/mL and 50 ng/mL, respectively (Figure 2.3).

Table 2.1. %RSD and %Bias in the calibration standards of DTX

S. No.	Conc (ng/ml)	Observed Conc (ng/mL) Mean ± SD	% RSD	% Bias
1	5000	4889.00 ± 480	4.14	-0.22
2	2000	2009.70 ± 265.08	4.58	0.49
3	1250	1226.08 ± 120.28	5.86	4.49
4	1000	1042.19 ± 93.86	6.10	4.22
5	500	556.78 ± 45.61	5.21	11.36
6	250	254.05 ± 25.91	7.80	1.62
7	200	196.38 ± 14.90	8.18	-1.81
8	100	105.13 ± 12.53	8.39	5.13
9	50	42.70 ± 3.68	9.59	-12.60

2.2.7.5. Accuracy and Precision

The Intra-day and inter-day precision (% RSD) and accuracy (% Bias) were determined for DTX in plasma samples at four QC levels, i.e., HQC, MQC, LQC and LLOQ and data are shown in Table 2.2. The accuracy and precision data showed that the method was accurate and % bias range was found from – 6.74% to -13.99% within the acceptable limits ±15% at LQC, MQC and HQC and ±20% for LLOQ. The Intra-day and Inter-day precision value (% RSD) was found to be in the range of 1.00% -7.82% that gave the confirmation of method suitability and acceptability for the analysis of DTX in plasma samples.

Table 2.2. Intra-day and Inter-day precision and accuracy of DTX in rat plasma

		Intra-day			**Inter-day**		
Level	**Nominal Conc (ng/mL**	**Observed Conc (ng/mL)** **Mean ± SD**	**% RSD**	**% Bias**	**Observed Conc (ng/mL)** **Mean ± SD**	**% RSD**	**% Bias**
LLOQ	50	46.69 ± 2.05	4.39	-7.71	43.86 ± 2.21	5.04	-13.99
LQC	75	72.98 ± 3.60	4.94	-7.75	73.76 ± 5.77	7.82	-10.50
MQC	600	553.76 ± 19.25	3.48	-9.29	534.99 ± 23.17	4.33	-11.31
HQC	4500	4196.73 ± 145.47	3.47	-6.74	4093.04 ± 41.03	1.00	-9.04

2.2.7.6. Recovery % and carry-over effect

For DTX and IS, the mean absolute percentage recoveries were found to be > 77 % and 75%. The method integrity was determined by five times and ten times dilution of DTX spiked plasma samples (2000 ng/mL) that showed percentage accuracy as 101.12 % ± 2.05 and 98.25 % ± 3.18, respectively. The drug and IS carry over were not detected in the blank rat plasma processed sample after injected the HQC and LQC.

2.2.7.7. Stability studies

The stability of DTX in plasma samples was analyzed under different conditions and the results were depicted in Table 2.3. These stability data were found to be within the range of acceptable limits [10].

Table 2.3. Stability studies of DTX at four QC levels in rat plasma

Stability conditions	**Level**	**Nominal Conc (ng/mL**	**Observed Conc (ng/mL) Mean ± SD**	**% RSD**	**% Bias**
0 h (for all Initials)	LLOQ	50	44.92 ± 2.07	4.61	-10.18
	LQC	75	72.94 ± 4.18	5.74	-7.32
	MQC	600	548.78 ± 17.95	3.27	-6.48
	HQC	4500	4481.51 ± 37.57	5.84	-4.62
Auto sampler stability (4°C)	LLOQ	50	42.67 ± 1.97	4.61	-10.11
	LQC	75	72.28 ± 4.97	5.77	-10.05
	MQC	600	532.31 ± 13.59	2.55	-12.02
	HQC	4500	4364.77 ± 201.65	4.62	-3.01
Bench top stability at room temperature (24 h)	LLOQ	50	43.27 ± 1.74	4.02	-10.18
	LQC	75	72.21 ± 4.62	6.40	-10.11
	MQC	600	550.15 ± 17.0	3.09	-11.25
	HQC	4500	4374.12 ± 265.04	6.06	-2.80
Short-term stability (4°C, 7 days)	LLOQ	50	42.75 ± 0.58	1.36	-13.71
	LQC	75	74.39 ± 3.77	5.06	-6.23
	MQC	600	546.93 ± 31.14	5.69	-11.76
	HQC	4500	4360.07 ± 197.13	4.52	-3.11
Long-term stability (−20°C, 1 month)	LLOQ	50	43.52 ± 4.71	10.82	-10.11
	LQC	75	72.14 ± 4.51	6.25	-10.09
	MQC	600	588.74 ± 45.81	7.78	-6.49
	HQC	4500	4377.28 ± 179.10	4.09	-2.73

2.3. Conclusion

A reverse-phase HPLC based analytical for the analysis of DTX was adopted from a previously reported method of our lab (Tushar Date, M.Pharm. Thesis, 2016, Department of Pharmacy, BITS-Pilani, Pilani Campus). The bioanalytical method for the analysis of DTX in plasma was developed and validated as per US-FDA guidelines for bioanalytical method validation. Results supported the selectivity, sensitivity, lower plasma matrix interference and good recovery of DTX using the developed method. The standard calibration curve depicted the better correlation coefficient and linearity in the concentration range from 50-5000 ng/mL of DTX in plasma samples. The developed method could be employed for the *in vivo* pharmacokinetic studies of DTX in animals.

References

[1] K.S. Italiya, S. Sharma, I. Kothari, D. Chitkara, A. Mittal, Journal of Chromatography B, 1061 (2017) 49-56.

[2] B.M. Rao, A. Chakraborty, M. Srinivasu, M.L. Devi, P.R. Kumar, K. Chandrasekhar, A. Srinivasan, A. Prasad, J. Ramanatham, Journal of pharmaceutical and biomedical analysis, 41 (2006) 676-681.

[3] I.R. Kothari, S. Mazumdar, S. Sharma, K. Italiya, A. Mittal, D. Chitkara, Therapeutic Delivery, 10 (2019) 227-240.

[4] I.R. Kothari, K.S. Italiya, S. Sharma, A. Mittal, D. Chitkara, Journal of Chromatographic Science, 56 (2018) 888-894.

[5] S. Taymouri, J. Varshosaz, S.H. Javanmard, F. Hassanzadeh, Advanced biomedical research, 7 (2018).

[6] J. Wang, Z. Lan, L. Zhang, H. Guo, Z. Liu, Y. Yu, Cell biochemistry and biophysics, 73 (2015) 623-629.

[7] M.M. Deshpande, V.S. Kasture, M. Mohan, M.J. Chavan, Bioanalytical method development and validation: a review, in: Recent Advances in Analytical Chemistry, IntechOpen, 2019.

[8] B. Posocco, M. Buzzo, A. Follegot, L. Giodini, R. Sorio, E. Marangon, G. Toffoli, PloS one, 13 (2018) e0193500.

[9] U.D.o. Health, H. Services, http://www.fda.gov./cder/guidance/4252fnl.htm, (2001).

[10] G.R. Valicherla, P. Tripathi, S.K. Singh, A.A. Syed, M. Riyazuddin, A. Husain, D. Javia, K.S. Italiya, P.R. Mishra, J.R. Gayen, Journal of Chromatography B, 1031 (2016) 123-130.

CHAPTER 3

DEVELOPMENT AND EVALUATION OF CATIONIC LIPOPOLYMERIC NANOPLEXES CONTAINING MIRNA-34A

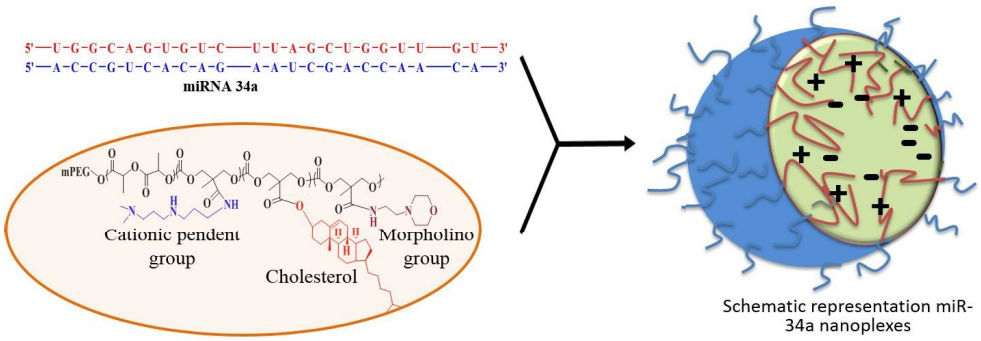

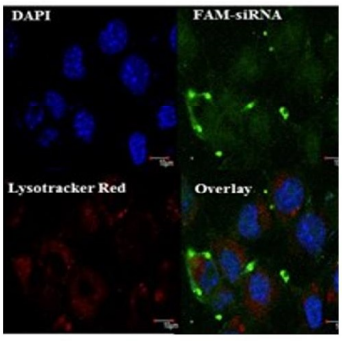

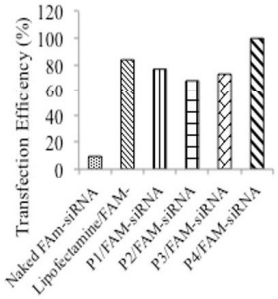

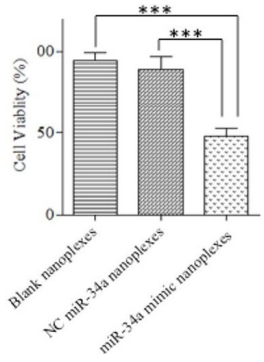

- Introduction
- Experimental section
- Results
- Discussion

3.1. Introduction

MicroRNAs (miRNAs), a class of highly conserved, endogenous noncoding, small RNA with a length of 20-25 nucleotides, control the expression of endogenous genes by unique binding to 3'-untranslated region (3'UTR) of target messenger RNAs (mRNAs), causing either translation repression or target mRNA degradation [1]. Their aberrant expression has been involved in numerous diseases, including cancers wherein either oncogenic miRNAs are upregulated or tumor suppressor miRNAs are downregulated [2]. Among various miRNAs, miRNA-34a (miR-34a) is dysregulated in multiple cancers and known as a master tumor suppressor. It is the first miRNA, which is proven to be directly regulated by transcriptional activation by p53 in response to DNA damage and plays a crucial role in cell proliferation, apoptosis and metastasis [2]. Its role has been implicated in several cancers including breast cancer [3], prostate cancer [4], lung cancer [5] and pancreatic cancer [6], wherein, it suppresses cell proliferation and induces apoptosis by targeting several mRNAs including LMTK3 [7], SIRT1 [8], cSRC [9] and CD44 [10]. Although the potential of miRNA therapeutics is now well established; however, to achieve its optimal benefits in the clinic, several biopharmaceutical issues need to be addressed. Physicochemical properties of miRNAs such as hydrophilicity, high molecular weight, and supranegative charge, make them impermeable to the cellular membranes [11]. Further, these naked miRNAs are easily filtered through the glomerulus and are unstable in biological milieu due to the presence of RNAses/nucleases, thus making their systemic administration impractical. Several non-viral vectors, including lipoplexes [12], cationic solid lipid nanoparticles [13], polyplexes [14], micelleplexes [15] and dendriplexes [16] have been reported for miRNA delivery. The use of a biocompatible cationic amphiphilic copolymer to deliver these negatively charged miRNAs based on their electrostatic complexation is an attractive strategy. Zhang et al., used poly (ethylene glycol-b-lactide-b-arginine) copolymer for preparing reducible nanoformulation for

anti-miR-21 delivery to cerebrospinal fluid [17]. In another study, dual stimuli-sensitive mixed polymeric micelles efficiently delivered miR-34a and doxorubicin in tumor tissue [18]. One significant advantage of these systems is their block copolymer structure and composition, which could be suitably modified to overcome the hurdles of miRNA delivery. In another study, cationic amphiphilic mPEG-polycarbonate based copolymers have delivered miR-205 and gemcitabine to pancreatic cancer cells *in vitro* and *in vivo* [18]. Also, a hedgehog inhibitor, GDC-0449, and miR-let7b were co-delivered using polymeric micelles for treating pancreatic cancer [19].

To further improve the therapeutic outcome of miRNA delivery, essential aspects including efficient transfection into the cells followed by their endosomal escape and release of the miRNA in the cytoplasm needs to be controlled. Attempts have been made to improve the delivery by incorporating cholesterol in the carrier system. Cholesterol conjugated chitosan has been used for delivering small molecules, including curcumin, paclitaxel, and doxorubicin [20-23]. Huang et al. prepared poly(β-amino esters) and PEG-based triblock copolymers grafted with cholesterol for the delivery of doxorubicin [24]. In another study, incorporation of cholesterol-poly(2-(dimethylamino)ethyl methacrylate) in lecithin liposomes showed enhanced internalization with no colocalization with acidic compartments in HEK-293 cells [25]. Further, incorporation of a weak base like imidazole group or histamine and guanidine in the polymer has shown to impart endosomal escape by proton sponge effect. Frere et al. showed that morpholine functionality in a polycarbonate-based polymer confers buffering ability and proton sponge effect to the polymeric carrier [26].

This chapter describes the development and evaluation of amphiphilic copolymers containing cholesterol, morpholine, and cationic pendant groups (N,N-dimethyldipropylenetriamine) on the polycarbonate backbone that could form stable nanoplexes with miR-34a at low N/P ratios. Nanoplexes were prepared by film hydration

method and double emulsion method followed by their thorough characterization for size, zeta potential, and complexation ability. Flow cytometric analysis was performed to study the transfection efficiency of FAM-siRNA loaded nanoplexes in 4T1 (murine) and MCF-7 (human) breast cancer cells. Further colocalization of the nanoplexes with the endo/lysosomes was determined by confocal microscopy. Hemocompatibility of the nanoplexes was determined by hemolysis assay. Cytotoxicity and apoptosis assessment of miR-34a containing nanoplexes were then performed in 4T1 and MCF-7 breast cancer cells by MTT assay and annexin-V/propidium staining, respectively.

3.2. Experimental section

3.2.1. Materials

miRNA-34a-5p mimic, mirVana™ miRNA Mimic #1 Negative control, and LysoTracker Red DND-99, Lipofectamine-2000®, Fetal Bovine Serum (FBS), Dulbecco's Modified Eagle Medium (DMEM), Annexin V Alexa fluor® 488 conjugate and TrypLE were purchased from Invitrogen (Carlsbad, CA, USA). FAM-siRNA was purchased from GeneCust Europe (Dudelange, Luxembourg). Bis(hydroxymethyl) propionic acid, benzyl bromide, tin(II) 2-ethylhexanoate, methoxy poly(ethylene glycol) (mPEG, 5000 Da), 4-(2-aminoethyl)morpholine, cholesterol, N,N-dimethyldipropylenetriamine and propidium iodide (PI) were purchased from Sigma Aldrich (St. Louis, MO). DL-Lactide and N, N-diisopropylethylamine (DIPEA) were purchased from TCI Chemicals (Japan). All other chemicals and reagents were of analytical grade and purchased from local vendors.

3.2.2. Synthesis of cationic amphiphilic copolymers

A series of cationic amphiphilic copolymers with different ligands on the hydrophobic segment were synthesized using a multi-step reaction consisting of the synthesis of cyclic monomer, 2-methyl-2-benzyloxy carbonyl propylene carbonate (MBC), synthesis of mPEG-

b-P(CB-co-LA) diblock copolymer followed by its reduction and coupling of ligands including N,N-dimethyldipropylenetriamine, cholesterol and/or 4-(2-aminoethyl) morpholine by EDC/HOBT coupling chemistry as shown in (Figure 3.1).

3.2.2.1. Synthesis of benzyl 5-methyl-2-oxo-1,3-dioxane-5-carboxylate (MBC, 4)

The monomer was synthesized in two steps, i.e., synthesis of benzyl 3-hydroxy-2-(hydroxymethyl)-2-methylpropanoate (BHMP-OBn, **3**) and synthesis of benzyl 5-methyl-2-oxo-1,3-dioxane-5-carboxylate (MBC, **4**).

In the first step, 2,2- bis(hydroxymethyl)propionic acid (90 g, 0.2 mol) and potassium hydroxide (44 g, 0.2 mol) were dissolved in 500 mL of N, N dimethylformamide (DMF) and stirred for 1 h at 100 °C in the oil bath. Benzyl bromide (138 mL, 0.24 mol) was added dropwise to the above solution and kept for stirring at 100 °C over 14 h under reflux condition. The reaction was monitored by thin-layer chromatography (TLC). After completion of the reaction, DMF was evaporated using a rotary evaporator, and the resulting crude residue was dissolved in 350 mL of ethyl acetate followed by washing twice with the equal quantity of chilled water. The ethyl acetate layer was collected and dried using anhydrous sodium sulfate. The solvent was evaporated, and the crude product was obtained, which was further recrystallized with toluene (1.3 mL/g of crude product). Thereafter, dried product was further washed with cold toluene and keep under reduced pressure to get benzyl 3-hydroxy-2-(hydroxymethyl)-2-methylpropanoate.; Yield: 62% (56.58 g); ^{1}H NMR (400 MHz, CDCl3): δ 1.10 (s, -CH_3), 3.73 (d, -CH_2OH), 4.82 (d, -CH_2OH), 5.21 (s, -CH_2Ar), 7.28 (m, ArH).

In the second step, 0.05 mol of benzyl 3-hydroxy-2-(hydroxymethyl)-2-methylpropanoate (BHMP-O-Bn, **3**) was dissolved in a mixture of pyridine (25 mL) and dichloromethane (DCM) (200 mL) in the ratio of 1:10. The resulting reaction mixture was cooled to -78 °C in dry ice/isopropyl alcohol mixture. Thereafter, a solution of triphosgene

(25 mmol) in DCM was added dropwise in the reaction mixture followed by stirring for 2 h at room temperature. The reaction was quenched by adding a saturated solution of ammonium chloride (NH_4Cl). The organic layer was separated and washed with 1 M HCl and saturated solution of sodium bicarbonate ($NaHCO_3$) one after the other. The organic layer was dried over anhydrous sodium sulfate (Na_2SO_4) and evaporated under reduced pressure using a rotary evaporator to get crude MBC, which was further recrystallized in ethyl acetate to get pure MBC as white crystals. Yield: 85% (38 g); mp 72-73 °C, reference mp 71-73 °C [27]. ^{1}H NMR of MBC showed peaks corresponding to δ 1.23 (CH_3, s, 1H), δ 4.35 (CH_2, d, 2H) and 4.72 (CH_2, d, 2H), δ 5.25 (CH_2, s, 2H) and δ 7.34 (C_6H_5, m, 5H). HRMS (ESI-TOF) *m/z*: M+H$^+$ calculated for $(C_{13}H_{14}O_5)+H]^+$ 251.0914; Found 251.0909.

3.2.2.2. Synthesis of mPEG-b-P(CB-co-LA) (9)

Methoxy poly(ethylene glycol) (mPEG, **6**) (1.445 g) was taken in a dried round bottom flask and kept at 130 °C followed by addition of MBC (**4**) (5.42 g), DL-Lactide (**5**) (3.126 g) and stannous 2-ethyl hexanoate ($Sn(Oct)_2$; 10 mol% of mPEG in anhydrous toluene) to the reaction mixture. Further, the reaction mixture was subjected to heating at 130 °C for 20 h under N_2 atmosphere to obtain mPEG-b-(CB-co-LA) diblock polymer (**7**) as a result of ring-opening polymerization (ROP). The crude polymer was purified by precipitation method, wherein it was dissolved in chloroform followed by precipitation with an excess amount of cold isopropanol followed by cold diethyl ether one after other. Purification was done twice, and the polymer thus obtained was dried under vacuum. Yield: 91% (7.52 g); ^{1}H NMR of polymer showed characteristics peaks for mPEG protons at δ 3.56 (CH_2, m, 4H), for 2-methyl-2-benzyoxycarbonyl-propylene carbonate (CB) unit protons at δ 1.24 (CH_3, s, 3H), δ 4.34 (CH_2, m, 4H), δ 5.25 (CH_2, s, 2H), δ 7.34 (C_6H_5, m, 5H) and for lactic acid (LA) protons at δ 1.67 (CH_3, s, 3H) and δ 5.23 (CH, q, 1H); (Figure 3.2A). ^{13}C NMR (100 MHz, $CDCl_3$) shown in (Figure 3.2B) of mPEG-b-P(CB-co-LA) showed peaks at

δ 171.9, 169.6, 169.4, 169.3, 154.3, 154, 135.3, 128.6, 128.6, 128.4, 128.3, 128.1, 127.9, 71.5, 70.6, 69.2, 69, 68.6, 67.1, 66.1, 46.6, 17.4 and 16.7.

3.2.2.3. Synthesis of mPEG-b-P(CB-{g-COOH}-co-LA) (8)

To remove the bulky benzyl groups from mPEG-b-P(CB-co-LA), (**7**), the polymer was subjected to hydrogenation under pressure. Briefly, mPEG-b-P(CB-co-LA) (6 g) polymer was dissolved in 100 mL of tetrahydrofuran (THF): Methanol (MeOH) mixture (1:1) containing 1.2 g of palladium on activated carbon (20%) (Pd/C). Initially, the reaction flask containing the polymer mixture along with Pd/C was purged with nitrogen followed by vigorous shaking for 3 h in the presence of hydrogen under pressure. At the end of the reaction, Pd/C was removed by centrifugation at 8000 rpm/5 min until Pd/C was completely removed from the mixture. The solvent was evaporated under vacuum to obtain a sticky mPEG-b-P(CB-{g-COOH}-co-LA) reduced copolymer (**8**). Yield 90% (3.52 g); ^{1}H NMR (400 MHz, DMSO-d6) (Figure 3.2C) of mPEG-b-P(CB-{g-COOH}-co-LA) showed peaks at δ 12.24 (COOH, s, 1H) and absence of phenylic protons. The broad peak corresponding to carboxylic acid protons was observed in the ^{1}H NMR taken in DMSO-d6 and was thus used as a solvent of choice for this polymer; ^{13}C NMR (100 MHz, CDCl3) (Figure 3.2D) showed peaks at δ 169.6, 169.4, 128.6, 128.3, 128.2, 127.9, 70.6, 69.2, 69.0, 67.9, 46.6, 25.6 and 16.7.

3.2.2.4. Synthesis of cationic copolymers grafted with different pendant groups (P1 to P4)

Carbodiimide/N-hydroxy benzotriazole (HOBT) coupling was used to graft 4-(2-aminoethyl) morpholine, cholesterol and/or N,N-dimethyldipropylenetriamine on the free carboxyl pendant groups of mPEG-b-P(CB-{g-COOH}-co-LA) copolymer to yield four cationic copolymers, i.e., containing only cation chain, cation chain + morpholine group, cation chain + cholesterol and cation chain + cholesterol + morpholine group and named as

P1, P2, P3, and P4, respectively (Table 3.1). Briefly, to a solution of mPEG-b-P(CB-{g-COOH}-co-LA polymer (1g) in DMSO (15 mL), EDC.HCl (730 mg), anhydrous HOBT (820 mg), triethylamine (690 µL), morpholine (155 µL), N,N-dimethyldipropylenetriamine (167 µL) and cholesterol (548 mg) were added, and the reaction mixture was stirred for 24 h at room temperature. After completion of the reaction, DMF was evaporated using a rotary evaporator, and the resulting all four (P1 – P4) crude copolymers residue were dissolved in chloroform and purified by precipitation with cold isopropanol followed by precipitation in cold diethyl ether. The purified polymers obtained were dried under vacuum, followed by characterization using ^{1}H NMR and ^{13}C NMR to predict the structure, composition, and molecular weight [28]. For this purpose, copolymers were dissolved in deuterated chloroform ($CDCl_3$) except for mPEG-b-P(CB-{g-COOH}-co-LA), which was dissolved in DMSO-d6 and analyzed using Bruker (400 MHz) NMR spectrometer. ^{1}H NMR analysis showed characteristics peaks corresponding to protons of mPEG, LA and CB units as given above in addition to the peaks of functional moieties such as cholesterol (at δ 0.83 - 1.05 (CH_3, s, 6H), δ 4.56 (CH, q, 1H), δ 5.42 (CH, d, 1H)), N,N-dimethyldipropylenetriamine (at δ 2.10 (NH, s, 1H), δ 7.40 (Amidic NH, s, 1H)) and 4-(2-aminoethyl) morpholine (at δ 3.78 (CH_2, m, 4H)), thus indicating the effective coupling of ligands. ^{13}C NMR (100 MHz, $CDCl_3$) of the synthesized copolymers is shown in Figure 3.3. Copolymer P1 (**10)** showed peaks at δ (ppm) 171.8, 169.5, 169.3, 135.4, 128.6, 128.4, 128.1, 127.9, 70.6, 69.2, 69.0, 67.1, 67.0, 65.9, 46.6, 25.3, 17.4, 16.7 and 15.3. Copolymer P2 (**12)** showed peaks at δ (ppm) 176.6, 171.9, 135.3, 128.6, 128.4, 128.1, 127.9, 71.9, 71.2, 68.9, 67.0, 64.3, 58.9, 46.6 and 16.7. Copolymer P3 (**14)** showed peaks at δ (ppm) 169.6, 169.4, 169.3, 169.1, 135.3, 128.6, 128.3, 128.0, 127.9, 70.6, 69.2, 69, 65.8, 46.6, 25.1, 16.7 and 15.3, and copolymer P4 (**15)** showed peaks at δ (ppm) 171.9, 169.7, 169.6, 169.3, 128.6, 128.4, 128.1, 128.0, 71.6, 70.6, 69.0, 67.0, 65.8, 46.6, 17.5, 16.7 and 15.3. The molecular weight of the copolymers (P1, P2, P3, and P4) were

determined using ^{1}H NMR and found to be 30209, 24342, 43523, and 35436 Da, respectively. Total carbon, hydrogen, and nitrogen content of the cationic copolymers P1 (**10)**, P2 (**12**), P3 (**13**), and P4 (**15**) were determined by elemental analysis, as shown in Table 3.1.

3.2.2.5 Characterization

Nuclear magnetic resonance (NMR) spectra were recorded with Bruker 400 spectrometer. The ^{1}H NMR experiments were reported in δ units, parts per million (ppm), and were measured relative to residual chloroform (7.26 ppm) or DMSO (2.50 ppm) in the deuterated solvent. The ^{13}C NMR spectra were reported in ppm relative to CDCl3 (77.0 ppm) or DMSO-d6 (39.5 ppm). All coupling constants (J) were reported in Hz. The following abbreviations were used to describe the peak splitting patterns when/where appropriate: s = singlet, d = doublet, t = triplet, dd = doublet of doublet, m = multiplet and brs = broad singlet. Melting points were determined on a capillary point apparatus equipped with a digital thermometer and are uncorrected. Reactions were monitored by using thin-layer chromatography (TLC) on 0.2 mm silica gel F254 plates (Merck). The molecular weights of final products were confirmed by a high-resolution ESI/APCI- hybrid quadrupole time-of-flight mass spectrometer. High-resolution mass spectrometry (HRMS) was performed with waters synapt G2 HDMS instrument using time-of-flight (TOF-MS) with ESI/APCI- hybrid quadrupole. Elemental composition of synthesized copolymers was determined using Elementar Vario EL III C-H-N analyzer (Sophisticated Test and Instrumentation Centre (STIC), Cochin University of Science and Technology, Kerala, India) which is based on combustion analysis. An accurately weighed sample was burned in excess of oxygen followed by a collection of the combustion products such as carbon dioxide, water, and nitric oxide by different traps. Masses of these combustion products were used to calculate the percentage of C, H, and N present in the copolymers.

3.2.3. Formulation of miR-34a nanoplexes

The nanoplexes of all four copolymers with miR-34a were prepared by two methods i.e., film hydration (FH) method and double emulsion solvent evaporation method [29]. Briefly, in the film hydration method, polymer (10 mg) was dissolved in dichloromethane (1 mL) followed by evaporation of the solvent under reduced pressure to obtain a thin film. The film was redispersed with DNAse/RNAse free purified water containing miR-34a (200 pmole; 1 ml). The mixture was allowed to stand for 30 min at room temperature to form nanoplexes followed by centrifugation at 2000 rpm for 5 min at 4°C. In the DE method, the internal aqueous phase consisting of miR-34a solution (40 µL; 5 pmole/µL) in DNAse/RNAse free purified water was first prepared. The organic phase was prepared by dissolving polymer (10 mg) in DCM (0.5 mL). The internal aqueous phase was added dropwise into the organic phase and sonicated for 30 seconds at 20°C on bath sonicator (Ultrasonic, Macroscientific) to form primary water in oil (w/o) emulsion which was subsequently added to 1 mL of DNAse/RNAse free purified water and kept for bath sonication for 1 min at 25°C to obtain w/o/w double emulsion. The resulting double emulsion was stirred at room temperature for 2 h (to evaporate the organic solvent) centrifuged at 2000 rpm/5 min at 4°C and filtered using 0.22 µm membrane filter. For particle size, polydispersity index, and zeta potential analysis, nanoplexes were taken at a concentration equivalent to 1 mg/mL of polymer in DNase/RNase free purified water and analyzed using Zetasizer (Malvern Nano ZS).

3.2.4. Agarose gel retardation assay

Agarose gel retardation assay was performed to determine the N/P (nitrogen (N) and phosphate (P)) ratio for effective complexation between synthesized cationic copolymers and miR-34a, as reported earlier [30]. Briefly, nanoplexes were prepared by double emulsion

method at N/P ratio ranging from 1/1 to 16/1 and loaded on an agarose gel (2% w/v) containing 0.5 μg/mL ethidium bromide (EtBr) and run for 30 min at 90 V in 0.5X Tris-Borate-EDTA (TBE) buffer. The electrophoretic mobility of miR-34a was visualized on a Gel Doc™ XR+ Gel Documentation system.

Post complexation release behavior of miRNA from nanoplexes was examined through heparin competition assay. Briefly, freshly prepared miRNA-nanoplexes were incubated with different concentrations of heparin for 30 minutes at 37° C temperature. Thereafter, samples were loaded on 2% agarose gel to evaluate the release of miRNA from nanoplexes. Herein, naked miRNA and miRNA-nanoplexes without heparin were taken as control.

3.2.5. Hemocompatibility assay

Pooled blood sample (2 mL) was collected from *swiss albino* mice and mixed with EDTA to prevent coagulation. RBCs were obtained from the blood by centrifugation at 1500 rpm at 4 ºC for 15 min, followed by washing with normal saline solution [31]. Washed RBCs were resuspended in 5 mL of normal saline to obtain RBCs dispersion. P4/miR-34 nanoplexes, blank nanoplexes, and distilled water (positive control) were added to 1 mL of RBCs dispersion and incubated at 37 °C for 1 h followed by centrifugation at 2000 rpm for 5 min. The supernatant was collected and analyzed using a UV spectrophotometer at 415 nm, and the percentage hemolysis in the samples was determined, considering the percent hemolysis induced by distilled water as 100%.

3.2.6. Cell culture studies

4T1 cells were obtained as a kind gift from Dr. Avinash Bajaj (Associate Professor, Regional Centre for Biotechnology, Haryana (NCR Delhi), India), and MCF-7 cells were obtained from National Centre for Cell Science, Pune. Both cell lines were cultured in

Dulbecco's Modified Eagle's Medium (DMEM) supplemented with 10% fetal bovine serum (FBS; HyClone, Logan, UT) and 1% antibiotics and kept in an incubator at 37°C/ 5% CO_2.

3.2.7. Transfection efficiency

FAM-siRNA nanoplexes were used for studying the transfection efficiency by flow cytometry, as reported earlier [32]. Briefly, 4T1 and MCF-7 cells were seeded at a cell density of 1×10^5 cells/well in 6-well cell culture plates and allowed to adhere for 24 h. Prior to treatment with the nanoplexes, culture media was replaced with Opti-MEM medium for 1 h. Cells were then treated with FAM-siRNA nanoplexes for 4 h. Naked FAM-siRNA and lipofectamine-2000®/FAM-siRNA lipoplexes were kept as a negative and positive control, respectively. After treatment, cells were washed thrice with PBS, trypsinized, centrifuged at 2000 rpm/5 min at 4ºC, and flow cytometric analysis was performed on Cytoflex (Beckman Coulter, USA). The FAM-siRNA was excited with an argon laser (488 nm), and fluorescence was measured at 525 nm. Data were analyzed using CytExpert 2.0 version software.

3.2.8. Endo/lysosomal escape

4T1 and MCF-7 cells (1×10^5 cells/well) were seeded onto coverslips in 6-well cell culture plates. After 24 h, cells were washed with PBS (twice), and media was replaced with Opti-MEM followed by treatment with FAM-siRNA nanoplexes or lipofectamine-2000®/FAM-siRNA lipoplexes. Cells were then incubated with LysoTracker Red DND 99 (1 µM) for 20 min for endo/lysosome labeling. Cells were washed with PBS, fixed in paraformaldehyde (4%) for 10 min, and counterstained with DAPI (for nucleus staining; 5µg/mL). The cells were observed at 100 X (Plan S-Apo, NA 1.4, WD 0.12 mm) (DIC) under a confocal laser scanning microscope (Olympus IX71, DP71, Tokyo, Japan) }16]. The colocalization of FAM-siRNA with endo/lysosomes was analyzed using BioImage XD software wherein scattergram was plotted between the FAM-siRNA fluorescence (green) and

lysosomal fluorescence (red) and Costes method was used for calculating thresholds and statistics [33, 34].

3.2.9. Cytotoxicity studies

Cytotoxicity of miR-34a nanoplexes was assessed, as reported earlier [35, 36]. Briefly, cells (4T1 or MCF-7) were seeded in 96 well plates ($5x10^3$ cells/well) and allowed to adhere for 24 h followed by treatment with nanoplexes containing 20 picomoles of miR-34a. Negative control (NC) nanoplexes (containing mirVana™ miRNA Mimic #1 Negative control, a random sequence miRNA mimic molecule) and blank nanoplexes were kept as control. After 48 h, cell viability was analyzed using 3-(4,5-dimethylthiazol-2-yl)-2,5-diphenyltetrazolium bromide (MTT) assay. Absorbance was recorded by a microplate reader (BioTek Epoch) at 560 nm and corrected for the cell debris by subtracting absorbance at 630 nm. The percentage cell viability was determined using the following formula:

$$\% \text{ Cell viability} = \frac{Absorbance\ of\ sample\ wells}{Absorbance\ of\ control\ wells} \times 100$$

3.2.10. Apoptosis assay

Annexin V, Alexa Fluor™ 488 conjugate was used to detect and quantify apoptosis induced by miR-34a nanoplexes using flow cytometry as per manufacturer's protocol. Briefly, 4T1 or MCF-7 cells were seeded ($1x10^6$ cells/well) in 6-well cell culture plates. After 24 h, the media was replaced with fresh media containing blank nanoplexes, miR-34a nanoplexes, or NC miRNA nanoplexes and incubated with cells for 24 h at 37°C/5% CO_2. After treatment, cells were washed with PBS, trypsinized, centrifuged at 2000 rpm/5 min at 4°C, resuspended in 1X binding buffer, and stained with Annexin V conjugate (5 µl) and propidium iodide (PI) (10 µl). Flow cytometric analysis was performed on Cytoflex (Beckman Coulter, USA), and data were interpreted using CytExpert software [13, 37].

3.2.11. Statistical analysis

Data are presented as the mean ± standard deviation. The difference between any two or more groups was determined by analysis of variance, and $p < 0.05$ was considered to be statistically significant.

3.3. Results

3.3.1. Synthesis and characterization of monomers and copolymers

For delivery of miR-34a, we have synthesized a series of amphiphilic cationic copolymers grafted with ligands including 4-(2-aminoethyl)morpholine, cholesterol and/or N,N-dimethyldipropylenetriamine onto the hydrophobic block of (mPEG-b-(CB-{g-COOH}-co-LA) copolymer (**8**) (Table 3.1).

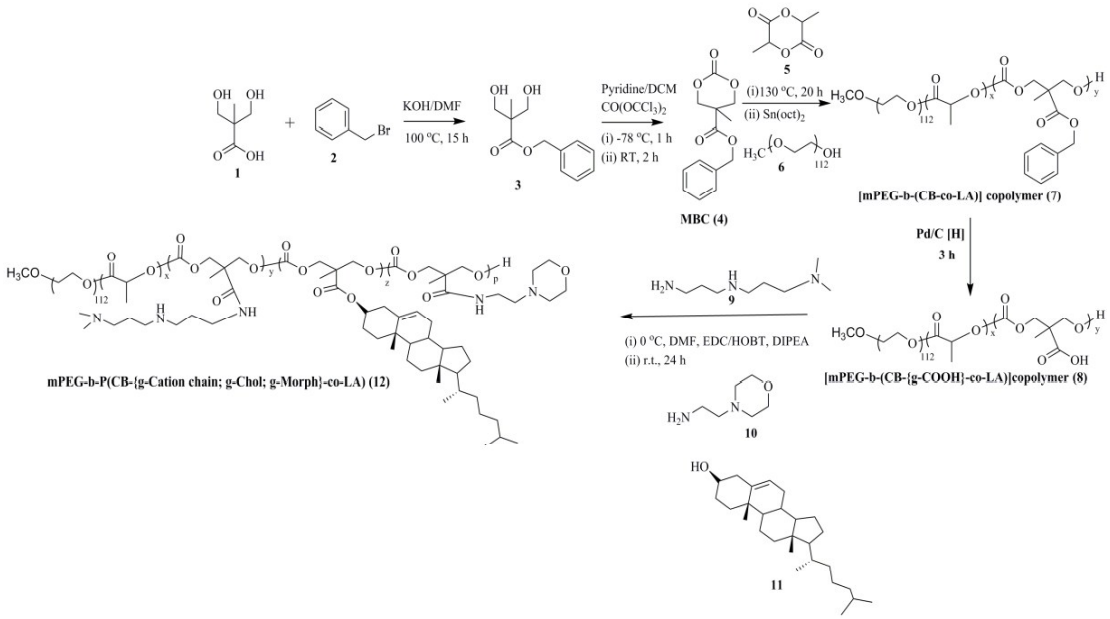

Figure 3.1. Synthesis scheme of amphiphilic copolymers (P1-P4) grafted with N,N-dimethyldipropylenetriamine (cation chain), cholesterol and 4-(2-aminoethyl) morpholine

MBC monomer was first synthesized using a reaction scheme, as shown in figure 3.1. 3-Hydroxy-2-(hydroxymethyl)-2-methylpropanoate (BHMP-O-Bn, **3**) was synthesized from 2,2- bis(hydroxymethyl)propionic acid (BHMP, **1**) by reaction with benzyl bromide (**2**),

which on ring closure with triphosgene yielded MBC (**4**) monomer. The structure of (MBC**, 4)** was confirmed from its ^{1}H NMR and ^{13}C NMR data as given in the experimental section. In the ^{13}C NMR spectrum, the carbonate and benzyl ester carbon resonances were observed at 147.36 and 170.88 ppm, respectively. Mass spectroscopy results showed a molecular ion (sodium adduct) peak at 273 m/z and its (benzylic) daughter ion peak at 90 m/z, indicating the successful synthesis of the monomer. Further, ring-opening polymerization of MBC (**4**) with DL-lactide and mPEG (**6**) as a macroinitiator in the presence of $Sn(Oct)_2$ yielded mPEG-b-P(CB-co-LA) (**7**) copolymer with 80% practical yield (Figure 3.2). In ^{1}H NMR of synthesized copolymer mPEG-b-P(CB-co-LA) (**7**) Figure 3.2A, the absence of two peaks of MBC (**4**) monomer at δ 4.34 and δ 4.72 and presence of one proton peak at δ 4.35 (CH_2, m, 4H) indicated the successful ring-opening polymerization. The percentage conversion of the copolymer (mPEG-b-P(CB-co-LA), 7) was calculated from the peak integrals of the benzylic proton (δ 7.3, δ 4.35 & δ 1.12 ppm) of MBC (**4**), methyl proton (δ 1.67 ppm) of DL-Lactide and the ethylene proton (δ 3.67 ppm) of mPEG. The characteristic peak of ethylene protons

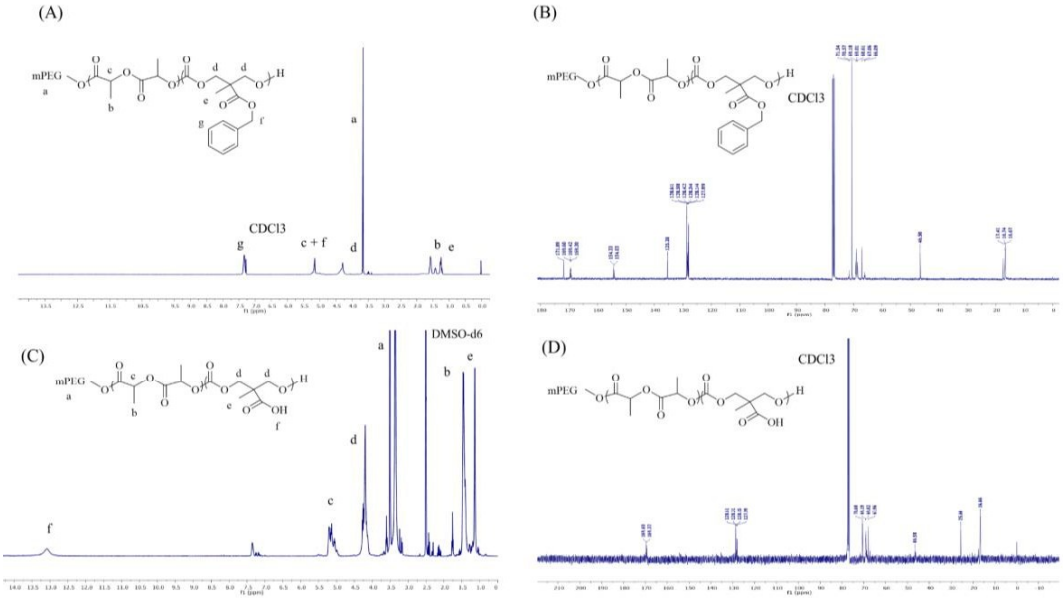

Figure 3.2. (A and B) ^{1}H NMR and ^{13}C NMR of the mPEG-b-P(CB-co-LA), (C and D) ^{1}H NMR and ^{13}C NMR of the mPEG-b-P(CB-{g-COOH}-co-LA).

of mPEG (δ 3.67 ppm) used to calculate the overall copolymer unit composition. mPEG-b-p(CB-co-LA) copolymer, (**7**) was catalytically hydrogenated to obtain mPEG-b-p(CB-{g-COOH}-co-LA) (**8**) with free carboxyl pendant groups on the polymer backbone with > 90% practical yield. ^{1}H NMR (Figure 3.2C) of mPEG-b-p(CB-{g-COOH}-co-LA) (**8**) showed peaks at δ 12.24 (COOH, s, 1H) and absence of phenylic protons. The broad peak corresponding to carboxylic acid protons was observed in the ^{1}H NMR taken in DMSO-*d6*. Finally, a series of cationic polymers, as shown in synthetic scheme (Figure 3.1) P1, P2, P3 and P4 were synthesized by grafting 4-(2-aminoethyl)morpholine, cholesterol and/or N,N-dimethyldipropylenetriamine using EDC/HOBt coupling chemistry. The cationic copolymers were characterized by ^{1}H NMR that showed the characteristics peaks of grafted moieties. The ^{1}H NMR spectra of all four cationic polymers showed ^{1}H NMR characteristics peaks at (δ 0.83 – 2.5 ppm) confirming the cholesterol conjugation; at δ 7.40 ppm indicating the formation of amide linkage due to conjugation of N,N-dimethyldipropylenetriamine and at δ 3.78 ppm signifying the conjugation of 4-(2-aminoethyl) morpholine (Figure 3.3). The molecular weights of the copolymers and percentage of carbon (C), hydrogen (H), nitrogen (N) and oxygen (O) are shown in Table 3.1.

Table 3.1. Characterization of cationic amphiphilic copolymers.

Polymer code	**Cationic Copolymers**	**Elemental Analysis**				**^{1}H NMR**
		Sample (mg)	C%	H%	N%	Molecular weight (Da)
P1	mPEG-b-P(CB_{82}-{g-Cation $chain_{11}$}-co-LA_{115})	11.98	50.39	9.78	3.76	30,209
P2	mPEG-b-P(CB_{44}-{g-Cation $chain_{13}$; g-$Morph_5$}-co-LA_{110})	4.95	45.63	7.79	7.68	24,342
P3	mPEG-b-P(CB_{78}-{g-Cation $chain_{36}$; g-$Chol_{30}$}-co-LA_{110})	4.28	46.30	7.28	6.48	43,523
P4	mPEG-b-P(CB_{65}-{g-Cation $chain_{11}$; g-$Chol_{19}$; g-$Morph_6$;}-co-LA_{120})	2.56	45.73	5.36	7.55	35,436

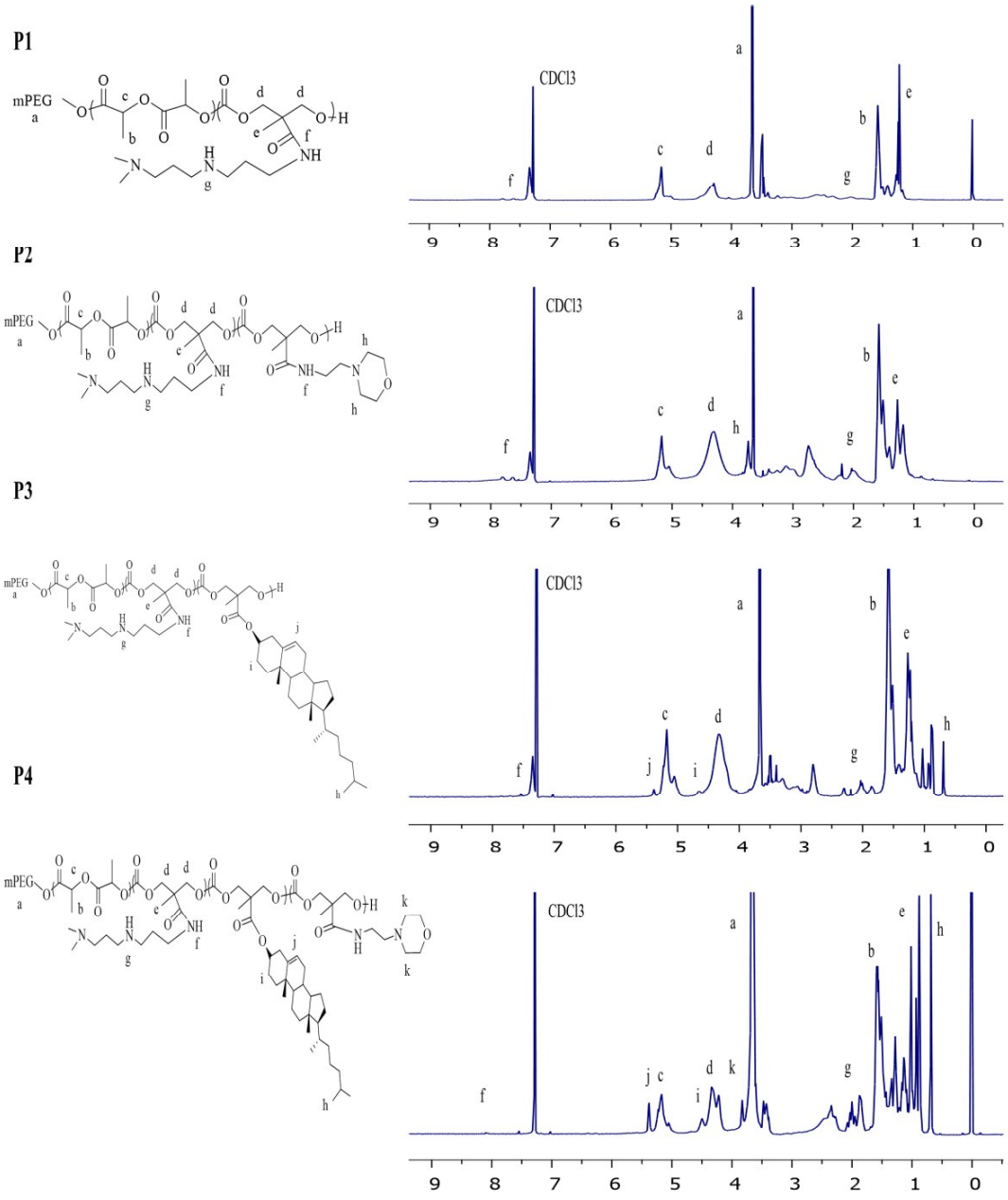

Figure 3.3. ^{1}H NMR of the synthesized cationic copolymers. P1: mPEG-b-P(CB-{g-Cation chain}-co-LA), P2: mPEG-b-P(CB-{g-Cation chain; g-Morph}-co-LA), P3: mPEG-b-P(CB-{g-Cation chain; g-Chol}-co-LA) and P4: mPEG-b-P(CB-{g-Cation chain; g-Chol; g-Morph}-co-LA).

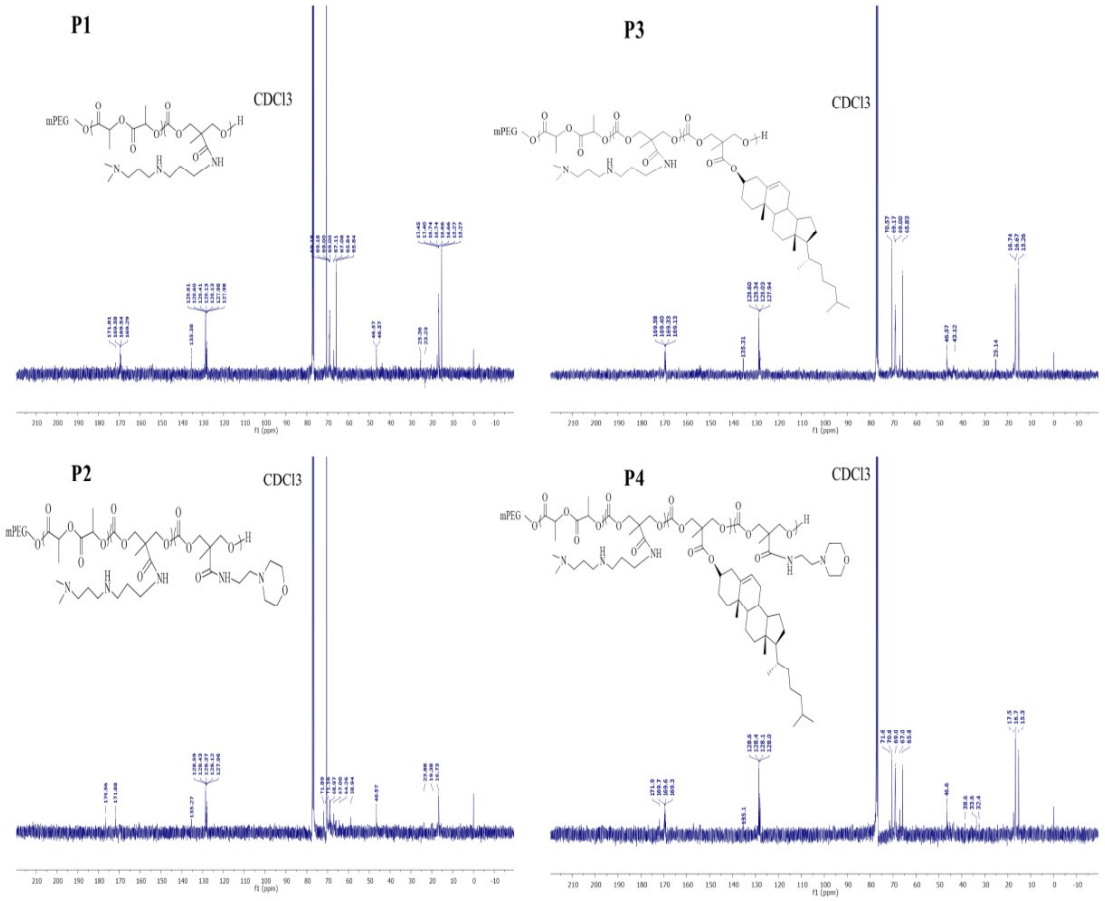

Figure 3.4. ^{13}C NMR of the synthesized cationic copolymers. P1: mPEG-b-P(CB-{g-Cation chain}-co-LA), P2: mPEG-b-P(CB-{g-Cation chain; g-Morph}-co-LA), P3: mPEG-b-P(CB-{g-Cation chain; g-Chol}-co-LA) and P4: mPEG-b-P(CB-{g-Cation chain; g-Chol; g-Morph}-co-LA).

3.3.2. Particle size, polydispersity index and zeta potential

miRNA-34a nanoplexes prepared by DE method exhibited a mean particle size of <200 nm along with zeta potential ranging from +12 to +39 mV and unimodal distribution showing bell shape curve with a polydispersity index (PDI) ranging from 0.112-0.263 (Figure 3.5 and Table 3.2). In the case of the film hydration method, nanoplexes exhibited a particle size <200 nm, but the polydispersity index (PDI) was high (0.58-0.632) with bimodal particle size distribution.

3.3.3. Agarose gel retardation assay

The complexation ability of copolymers with miR-34a was performed by agarose gel retardation assay. The assay was based on the retardation mobility of miR-34a due to binding with a cationic polymer, thus resulting in the disappearance of miRNA bands in the agarose gel. miR-34a nanoplexes were prepared by the DE method at N/P ratio ranging from 1/1 to 16/1. The results demonstrated that the electrophoretic mobility of miR-34a was fully

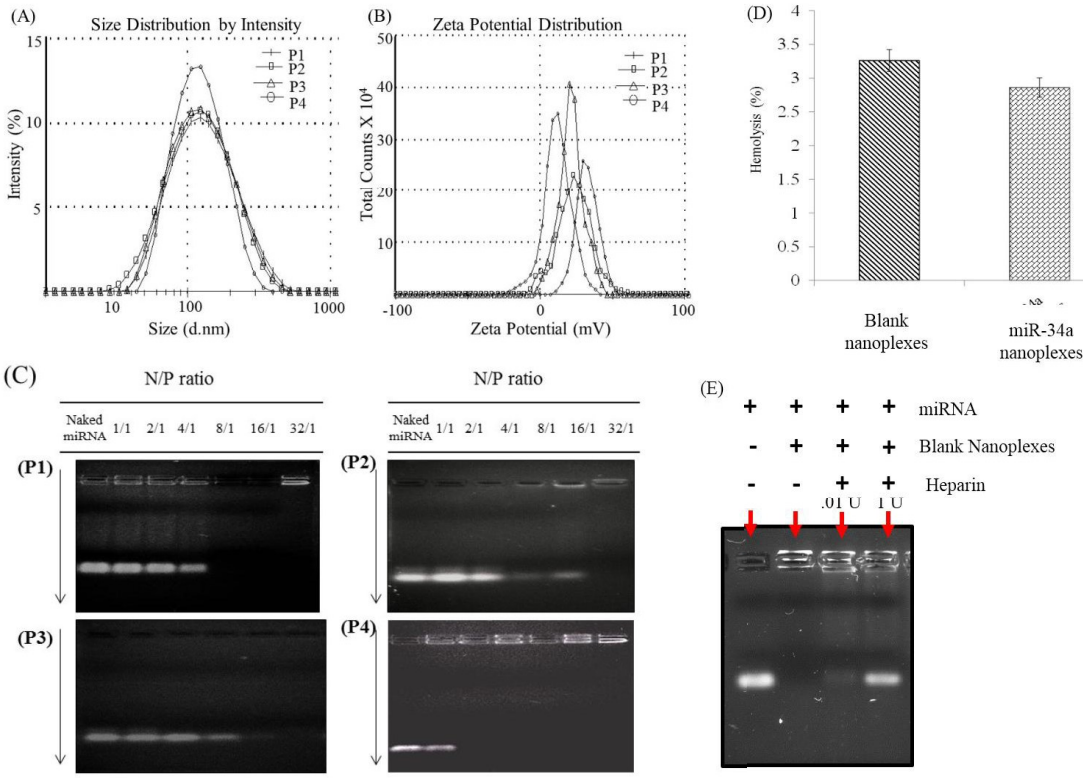

Figure 3.5. (A) Particle size*, (B) Zeta potential* of the nanoplexes prepared using cationic polymers, (C) miRNA binding ability of cationic polymers investigated by agarose gel electrophoresis, (D) Hemolysis assay of nanoplexes and (E) Heparin completion assay prepared using P4 copolymer.

*(P1: mPEG-b-P(CB-{g-Cation chain}-co-LA), P2: mPEG-b-P(CB-{g-Cation chain; g-Morph}-co-LA), P3: mPEG-b-P(CB-{g-Cation chain; g-Chol}-co-LA) and P4: mPEG-b-P(CB-{g-Cation chain; g-Chol; g-Morph}-co-LA).

retarded at N/P of 2/1 for miR-34a nanoplexes prepared using P4 copolymer while miR-34a nanoplexes prepared using P1, P2 and P3 polymer showed complete retardation at N/P of 8/1, 16/1 and 8/1, respectively (Figure 3.5C). Heparin competition assay was performed to examine post complexation integrity as well as the release behavior of miRNA-34a. The gel electrophoresis data in figure 3.5(E) showing release of miRNA-34a from nanoplexes after incubation with competition anion i.e heparin (1.0 unit). As per the data, the miRNA was found intact in terms of band intensity w.r.t naked miRNA-34a.

3.3.4. Hemocompatibility assay

The hemocompatibility assay was performed to study whether the designed formulation carries any RBCs membrane destabilization potential that could be correlated to the hemotoxicity. In the hemolysis test, the nanoplexes were incubated with the RBCs for 1 h

Table 3.2. Characterization of miR-34a nanoplexes prepared using cationic amphiphilic copolymers.

S. No	Polymer	Size (d.nm)	PDI	Zeta potential (mV)
1	P1	180 ± 6.38	0.187	12 ± 0.74
2	P2	120 ± 7.42	0.170	31 ± 1.07
3	P3	112 ± 7.89	0.263	27 ± 0.94
4	P4	108 ± 4.56	0.112	39 ± 0.84

followed by determination of hemoglobin content by UV spectroscopy. It was observed that the blank nanoplexes and miR-34a nanoplexes showed 3.26% and 2.86% hemolysis, respectively, as compared to double distilled water that showed 100% hemolysis (Figure. 3.5D).

3.3.5. In vitro transfection efficiency

To demonstrate the ability of the nanoplexes to transfect 4T1 and MCF-7 breast cancer cells, we performed the flow cytometry analysis after incubation of cancer cells with FAM-siRNA/nanoplexes. Lipofectamine-2000®/FAM-siRNA lipoplexes was taken as a positive control, naked FAM-siRNA as a negative control. and four FAM-siRNA nanoplexes (P1/FAM-siRNA, P2/FAM-siRNA, P3/FAM-siRNA, and P4/FAM-siRNA) were taken as test samples. In 4T1 cells, the percentage transfection efficiency was found to be 76.61%, 67.86%, 72.96%, 99.82% for copolymers P1, P2, P3, and P4, respectively while lipoplexes

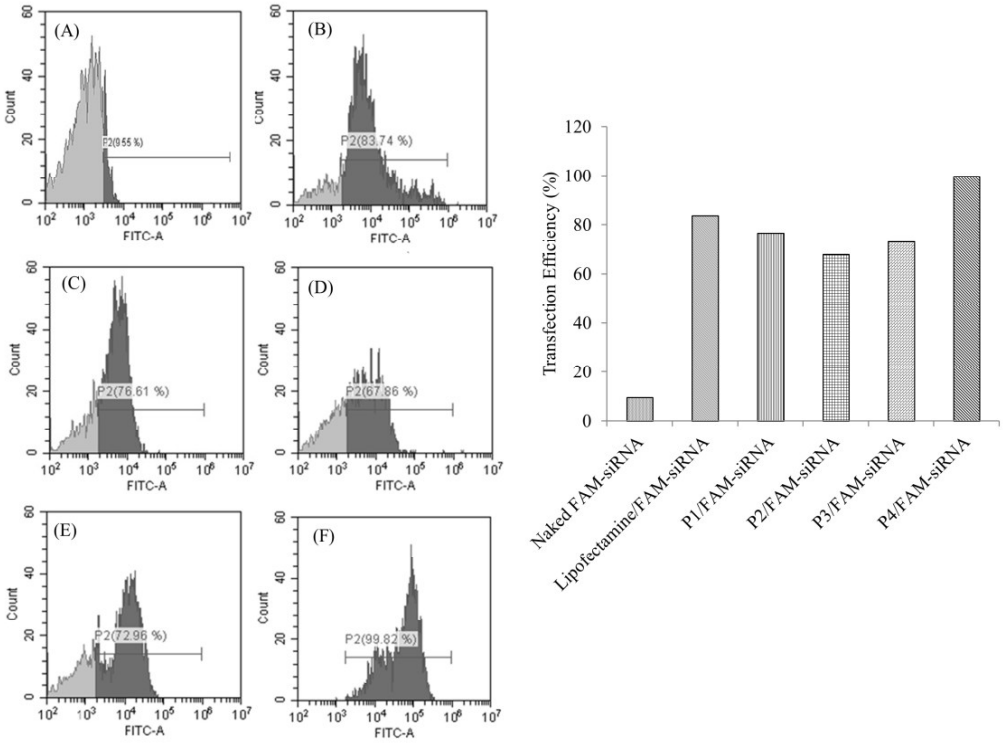

Figure 3.6. Transfection efficiency of the FAM-siRNA in 4T1 cells by flow cytometry. A) naked FAM-siRNA, B) lipofectamine-2000®/FAM-siRNA, C) P1/FAM-siRNA, D) P2/FAM-siRNA, E) P3/FAM-siRNA and F) P4/FAM-siRNA. P1: mPEG-b-P(CB-{g-Cation chain}-co-LA), P2: mPEG-b-P(CB-{g-Cation chain; g-Morph}-co-LA), P3: mPEG-b-P(CB-{g-Cation chain; g-Chol}-co-LA) and P4: mPEG-b-P(CB-{g-Cation chain; g-Chol; g-Morph}-co-LA).

(lipofectamine-2000®/FAM-siRNA) and naked FAM-siRNA showed transfection efficiency equivalent to 83.74% and 9.55% respectively (Figure 3.7). Further, in MCF-7 cells, the percentage transfection was found to be 36.69%, 39.10%, 42.34%, and 50.82% for copolymers P1, P2, P3, and P4, respectively. Lipoplexes (lipofectamine-2000®/FAM-siRNA) and naked FAM-siRNA showed a transfection efficiency of 53.94% and 4.09%, respectively (Figure 3.8).

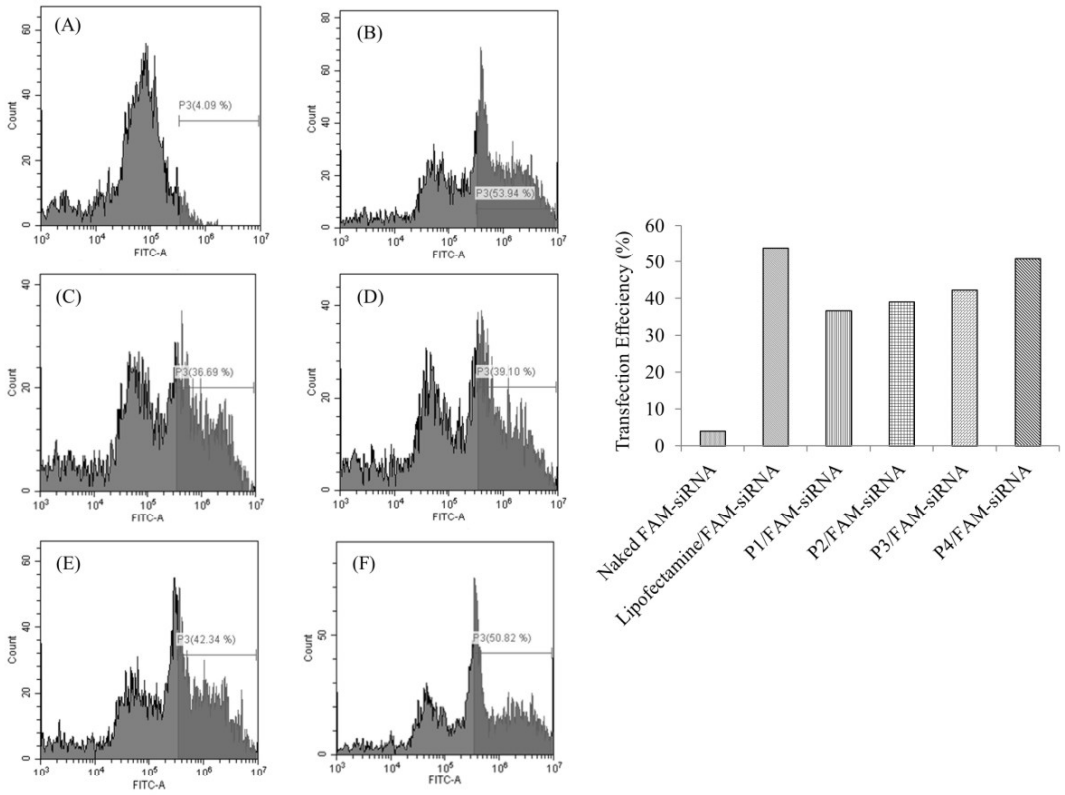

Figure 3.7. Transfection efficiency analysis of FAM-siRNA nanoplexes in MCF-7 cells by flow cytometry. A) naked FAM-siRNA, B) lipofectamine-2000®/FAM-siRNA, C) P1/FAM-siRNA, D) P2/FAM-siRNA, E) P3/FAM-siRNA and F) P4/FAM-siRNA. P1: mPEG-b-P(CB-{g-Cation chain}-co-LA), P2: mPEG-b-P(CB-{g-Cation chain; g-Morph}-co-LA), P3: mPEG-b-P(CB-{g-Cation chain; g-Chol}-co-LA) and P4: mPEG-b-P(CB-{g-Cation chain; g-Chol; g-Morph}-co-LA).

3.3.6. Endo/lysosomal escape

Intracellular trafficking and endosomal release of FAM-siRNAnanoplexes was studied using confocal microscopy (Figure 3.8). LysoTracker Red DND-99 and DAPI dyes were used to stain the acidic vesicles and nucleus, respectively. It was observed that both

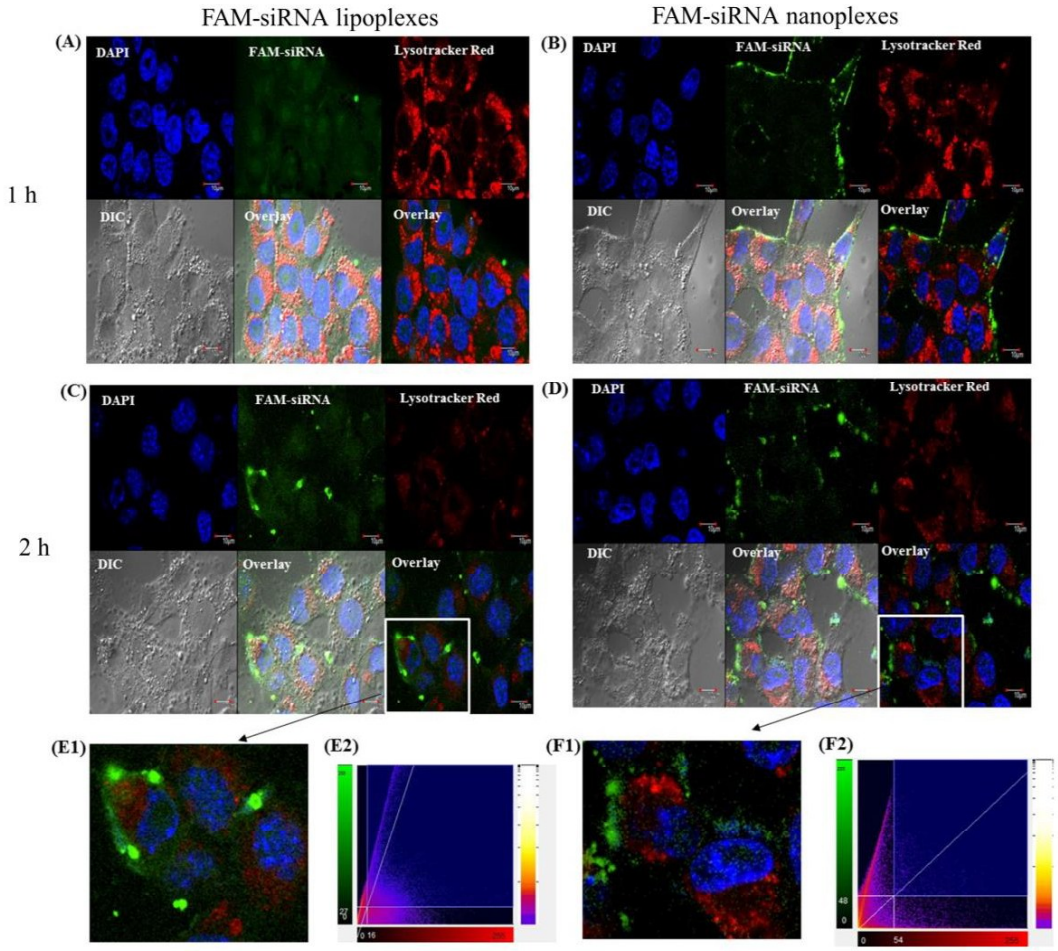

Figure 3.8. Intracellular localization of FAM-siRNA (green) in 4T1 Cells after treatment with (A and C) FAM-siRNA/lipoplexes and (B and D) FAM-siRNA/nanoplexes at 1 h and 2h, E1 and E2) colocalization analysis and scattergram between green pixel intensity (FAM-siRNA) and red pixel intensity (Lysosotracker: red) image of cells treated with siRNA/lipoplexes, F1 and F2) colocalization analysis and scattergram between green pixel intensity (FAM-siRNA) and red pixel intensity (Lysosotracker: red) image of cells treated with FAM-siRNA/nanoplexes. Scale bar represents 10 μm.

nanoplexes and lipoplexes were able to deliver FAM-siRNA (green fluorescence) into the 4T1 cells within 1 h. In the case of nanoplexes, discrete punctuate spots were observed along the cell membrane. For lipoplexes, diffused green fluorescence was observed in 1 h and 2 h samples. The colocalization was also analyzed by determining the overlap of the pixels of green fluorescence with red fluorescence. The percent of volume colocalized for lipoplexes was 22.6%, while in the case of nanoplexes, it was only 0.5% indicating no colocalization of FAM-siRNA (green) with the acidic vesicles.

3.3.7. Cytotoxicity assay miR-34a nanoplexes

miR-34a is a well-known tumor suppressor and plays an important role in cancer cell proliferation.21 Cellular cytotoxicity of miR-34a nanoplexes was determined in 4T1 and MCF-7 breast cancer cells. 4T1 is a murine mammary carcinoma cell line from a mouse that represents triple-negative breast cancer and serves as a suitable model to test miR-34a nanoplexes. Further, the sequence of hsa-miR-34a-5p mature sequence is similar to mmu-miR-34a-5p mature sequence (www.mirbase.org). Cells were treated with 20 picomoles of miR-34a nanoplexes for 48 h; afterward, the cell viability was measured by MTT assay.

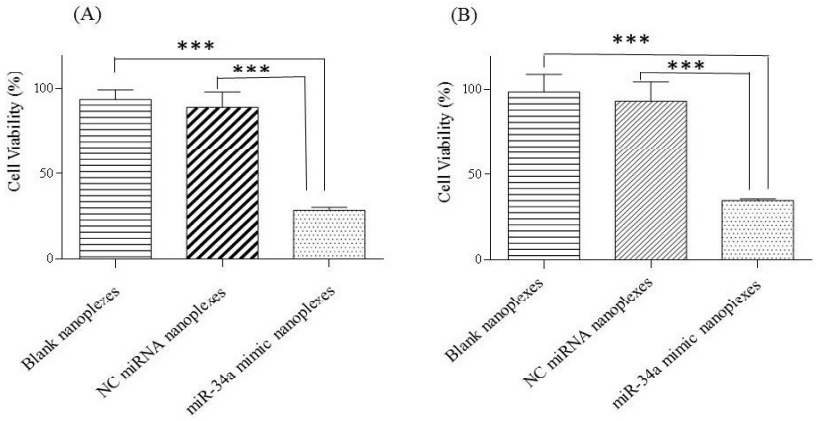

Figure 3.9 Cytotoxicity assay of miR-34a nanoplexes in A) 4T1 and B) MCF-7 cells. Data were presented as mean of three experiments in both cell lines. Statistical analysis (n=6) were performed using one-way ANOVA followed by Tukey's multiple comparison test. ***P < 0.05 was considered as statistically significant.

Blank nanoplexes and mirVana™ miRNA Mimic #1 Negative control nanoplexes were kept as control and showed no cellular cytotoxicity, while miR-34a nanoplexes showed a significant decrease in the cancer cell viability in both 4T1 (28%) and MCF-7 (34%) cells as shown in Figure 3.9.

3.3.8. Apoptosis assay

Apoptosis in 4T1 and MCF-7 cells was evaluated by flow cytometry after 24 h of treatment with miR-34a nanoplexes. In FACS plot, between FITC-A on the x-axis and propidium iodide on the y-axis, the viable cells showed annexin $V^{(-)}$ and $PI^{(-)}$ (Q_3 lower left quadrant) whereas the cells in early-phase apoptosis showed annexin $V^{(+)}$ and $PI^{(-)}$ (Q_4 at the

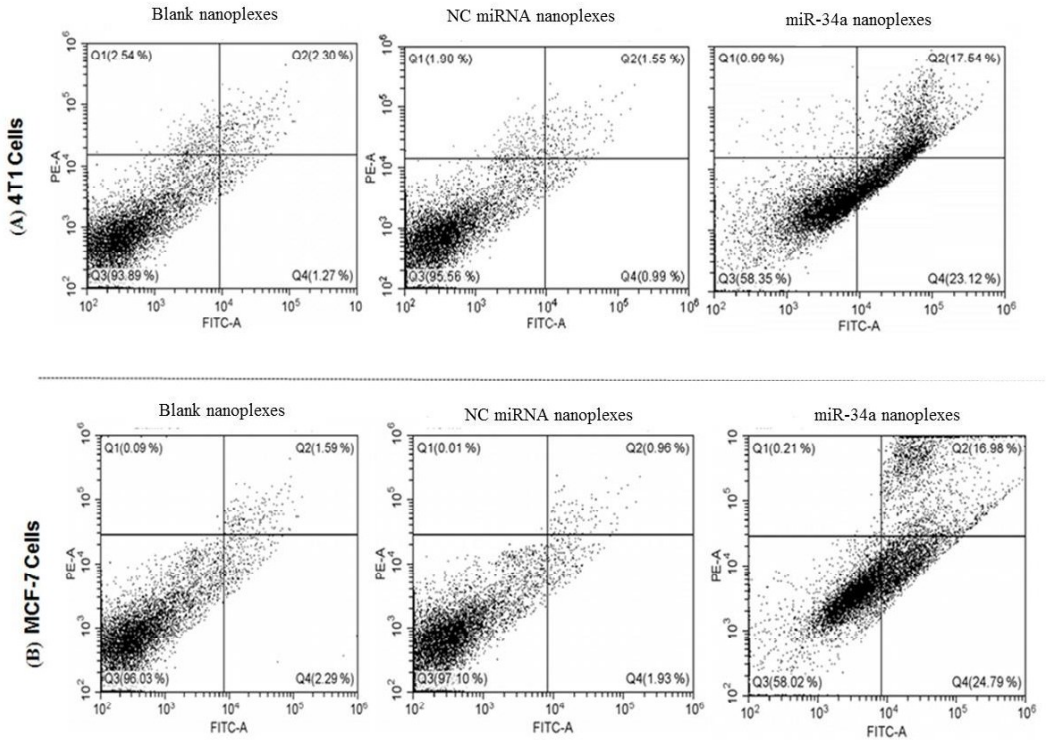

Figure 3.10. Flow cytometric analysis of apoptosis in A) 4T1 and B) MCF-7 cells after treatment with blank nanoplexes, mirVana™ miRNA Mimic #1 Negative control (NC miRNA) nanoplexes and miR-34a nanoplexes. All nanoplexes were prepared using mPEG-b-P(CB-{g-Cation chain; g-Chol; g-Morph}-co-LA) (p4) copolymer.

lower right side) and late phase apoptosis showed annexin $V^{(+)}$ and $PI^{(+)}$ (Q_2 at upper right) while necrotic cells only show $PI^{(+)}$ (Q_1 at the upper left side). It was observed that in 4T1 cells, miR-34a nanoplexes induced 40.66% apoptosis (23.12% early and 17.54% late stage) as compared to 2.54% apoptosis (0.99% early and 1.55% late stage) for NC miRNA nanoplexes and 3.57% apoptosis (1.27% early and 2.30% late stage) for blank nanoplexes. Similar results were obtained in MCF-7 cells wherein miR-34a nanoplexes induced 41.77% apoptosis (24.79% early and 16.98% late stage) as compared to 2.89% apoptosis (1.93% early and 0.96% late stage) for NC miRNA nanoplexes and 3.88% apoptosis (2.29% early and 1.59% late stage) for blank nanoplexes (Figure 3.10)

3.4. Discussion

miRNAs are known to be involved in cancer progression, invasion, and metastasis wherein their levels are either upregulated or downregulated. miRNAs as a therapeutic tool in cancer, has been explored by several research groups and have shown improved outcomes in terms of increased cytotoxicity, decreased invasion, and metastasis [2, 8, 18, 38]. Delivery strategies, including nanoplexes [39], polyplexes [14], lipoplexes [40], micelleplexes [41] and dendriplexes [42] have been reported for miRNA delivery. Since naked miRNAs could not penetrate the lipidic bilayer membrane because of high molecular weight, hydrophilicity, positive charge, and instability in the biological milieu. Apart from effectively complexing miRNAs and protecting them from degradation, another important requirement for the ideal delivery system is that they should be able to improve the uptake of miRNA by cancer cells followed by their successful endosomal escape and release into the cytoplasm so that they can get into the RISC assembly for effective mRNA degradation and/or translation repression [43].

Among various miRNA delivery systems, cationic amphiphilic copolymers offer advantages due to their self-assembly, thermodynamic stability, and lower particle size. Further, copolymers could be tailored to improve the delivery of miRNA therapeutics. In a study, Kumar et al., prepared nanoplexes of miR-let7b and a cationic copolymer, mPEG-b-PCC-g-DC-g-TEPA at N/P at 16/1, that showed an average particle size of 80 ± 10 nm }19]. In another study, Zhu et al., delivered VEGF siRNA and paclitaxel for prostate cancer by using biodegradable cationic nanoplexes of PDMAEMA-PCL-PDMAEMA triblock copolymers with micelle size of 53.6 to 132.2 nm [44].

Successful *in vivo* delivery of a miRNAs mandates a multifunctional carrier system that can ensure effective complexation with the miRNA (due to its cationic charge) along with the ability to escape from endosomes and releasing it into the cytoplasm. Herein we have designed amphiphilic cationic copolymers with different ligands *viz*. cholesterol, N,N-dimethyldipropylenetriamine and 4-(2-aminoethyl)morpholine attached on the hydrophobic block of the copolymer to enhance the complexation ability, transfection efficiency and endosomal escape. All synthesized polymers showed self-assembly into nanoplexes in size ranging from 108 to 180 nm, depending upon the ligand attached to them. For self-assembly, the double emulsion method yielded a smaller particle size and PDI as compared to the film hydration method since high hydrophobicity of the copolymer does not allow complete redispersion of the film resulting in higher polydispersity.

The synthesized copolymers were first screened for their complexation ability with the miR-34a followed by transfection efficiency in cancer cells. Complexation at lower N/P ratios is preferred since higher polymer concentration could result in cellular cytotoxicity. Use of different cationic ligands, including tetraethylenepentamine, spermine and N,N-dimethyldipropylenetriamine have been reported earlier wherein it was shown that copolymers containing N,N-dimethyldipropylenetriamine effectively complexes miRNA at

an N/P ratio of 4:1 [30]. As per our results, the P4 copolymer showed an efficient complexation with the miR-34a at an N/P ratio of 2:1 (Figure 3.5C). Furthermore, we have also performed post complexation release of miRNA-34a from nanoplexes using heparin as a competition anion. Upon incubation of nanoplexes with 1.0 unit of heparin for 30 min, an effective release of miRNA-34a was observed. At higher concentration of heparin, the release of miRNA was more prominent w.r.t the release at lower concentration. Collectively, the above data reflects the post complexation stability of miRNA-34a. Similarly, Mittal et al., showed the post complexation integrity of miRNA with cationic chain polymer, indicating that the miRNA and cationic polymer complex showed the good stability.[30]. Further, the presence of endosomal escape moieties [26] (such as imidazole, morpholine) could lead to the efficient escape of the miRNA from endosomes. Putnam et al. synthesized a poly-l-lysine-grafted-imidazole acetic acid for effective gene transfer with lower cytotoxicity [45]. In this report, the authors hypothesized that the balance between cationic amines with endosomal escaping moieties leads to efficient gene transfer with lower cytotoxicity. A weakly basic morpholine group could also have a proton sponge effect, essential for endosomal release [26]. In our copolymer, N, N-dimethyldipropylenetriamine cationic chain was incorporated for complexing with the miR-34a by charge interactions resulting in nanoplex formation while morpholine helps in the endosomal escape of the nanoplexes. Cholesterol is one of the components of cell membrane, so its incorporation in the structure of a gene carrier could help in improving biocompatibility and cellular uptake of the carrier. Cheng et al. reported cholesterol grafted bioreducible polyamidoamine polymer for delivery of siRNA, which resulted in stable siRNA nanoplexes with higher transfection ability and endosomal escape [21]. Frere et al. have also synthesized a biocompatible polycarbonate polymer containing morpholine and guanidinium for increasing the transfection efficiency, endosomal escape and complexation ability with siRNA [14]. Herein, we prepared nanoplexes by using cationic

copolymers and compared them with lipofectamine-2000® (cationic Lipid) as a positive control for *in vitro* transfection in cancer cells. The nanoplexes prepared using copolymer containing both morpholine and cholesterol have shown efficient transfection in 4T1 and MCF-7 cells as compared to lipofectamine 2000® (Figure 3.6 and 3.7). Higher transfection by this copolymer could be correlated with the zeta potential of the nanoplexes, as reported earlier by Huang et al., wherein better cellular uptake was observed with formulations having a higher positive zeta potential [24].

In order to study the endosomal escape of the nanoplexes, LysoTracker Red DND 99 dye was used to label the acidic vesicles in the cell and colocalization was studied between green fluorescence from FAM-siRNA and red fluorescence from endo/lysosomes. Similar studies were also reported by Nelson et al., for colocalization of pH-responsive siRNA polyplexes with acidic vesicles wherein polyplexes showed significantly lower colocalization relative to lipoplexes prepared using lipofectamine-2000® [46]. Our data also suggest an efficient endosomal escape of nanoplexes and thus overcome the hindrance of the endo-lysosomal barrier in delivery. Another essential aspect of miRNA delivery is the safety of the carrier system. In general cationic polymers such as polyethyleneimine (PEI) were shown to be cytotoxic, thus limiting their translational potential [47]. The developed copolymers showed negligible cellular cytotoxicity towards 4T1 and MCF-7 cells and were non-hemolytic. In order to access the in *vitro* efficacy of the miR-34a nanoplexes, cytotoxicity and apoptosis assays were performed. miR-34a has been used as a master tumor suppressor miRNA owing to its role in several cancers, including breast cancer. Zhao et al., have earlier reported that its overexpression suppresses the MCF-7 cell proliferation and cell viability [7]. We also observed a significant decrease in the cell viability of 4T1 and MCF-7 cells after treatment with miR-34a nanoplexes. While negative control miRNA nanoplexes and blank polyplexes showed no effect on cell viability, indicating their non-toxic and biocompatible

nature. Further, apoptosis assay showed miR-34a nanoplexes effectively suppressed the tumor cell growth by inducing early and late phase apoptosis in breast cancer cells.

3.5. Conclusion

Cationic copolymers (P1, P2, P3, P4) with morpholine, N,N-dimethyldipropylenetriamine and cholesterol as a pendant groups linked to polycarbonate backback bone was synthesized and characterized using 1HNMR and elemental analysis. The P4 polymer was found most effective in terms of formulation parameters and transfection efficiency. Further, all the experiments such as endosomal escape, cytotoxicity study, apoptosis assay were performed with P4 copolymer in 4T1 and MCF-7 cell lines, wherein it showed effective outcomes w.r.t naked miRNA-34a.

Collectively, miRNA-34a nanoplexes were found to have immense potential for treatment of breast cancer.

.

References

[1] D. Anglicheau, T. Muthukumar, M. Suthanthiran, Transplantation, 90 (2010) 105.

[2] W. Wang, Y.-p. Luo, Journal of Zhejiang University-SCIENCE B, 16 (2015) 18-31.

[3] E. Zhou, N. Hui, M. Shu, B. Wu, J. Zhou, Oncology letters, 10 (2015) 3488-3494.

[4] K. Duan, Y.C. Ge, X.P. Zhang, S.Y. Wu, J.S. Feng, S.L. Chen, L. Zhang, Z.H. Yuan, C.H. Fu, Oncology letters, 10 (2015) 3223-3227.

[5] Y. Shi, C. Liu, X. Liu, D.G. Tang, J. Wang, PloS one, 9 (2014) e90022.

[6] Y. Tang, Y. Tang, Y.-s. Cheng, Scientific Reports, 7 (2017) 1-11.

[7] G. Zhao, J. Guo, D. Li, C. Jia, W. Yin, R. Sun, Z. Lv, X. Cong, DNA and cell biology, 32 (2013) 699-707.

[8] L. Li, L. Yuan, J. Luo, J. Gao, J. Guo, X. Xie, Clinical and experimental medicine, 13 (2013) 109-117.

[9] B.D. Adams, V.B. Wali, C.J. Cheng, S. Inukai, C.J. Booth, S. Agarwal, D.L. Rimm, B. Győrffy, L. Santarpia, L. Pusztai, Cancer research, 76 (2016) 927-939.

[10] C. Liu, K. Kelnar, B. Liu, X. Chen, T. Calhoun-Davis, H. Li, L. Patrawala, H. Yan, C. Jeter, S. Honorio, Nature medicine, 17 (2011) 211-215.

[11] D. Ben-Shushan, E. Markovsky, H. Gibori, G. Tiram, A. Scomparin, R. Satchi-Fainaro, Drug delivery and translational research, 4 (2014) 38-49.

[12] B.J. Hong, A.J. Chipre, S.T. Nguyen, Journal of the American Chemical Society, 135 (2013) 17655-17658.

[13] N. Othman, L.L. In, J.A. Harikrishna, N. Hasima, PloS one, 8 (2013) e81735.

[14] A. Frère, A. Baroni, E. Hendrick, A.-S. Delvigne, F.o. Orange, O. Peulen, G.R. Dakwar, J.r.m. Diricq, P. Dubois, B. Evrard, ACS applied materials & interfaces, 9 (2017) 2181-2195.

[15] Y. Zhang, J.S. Buhrman, Y. Liu, J.E. Rayahin, R.A. Gemeinhart, Molecular pharmaceutics, 13 (2016) 1791-1799.

[16] A.P. Perez, M.L. Cosaka, E.L. Romero, M.J. Morilla, International Journal of Nanomedicine, 6 (2011) 2715.

[17] Y. Zhang, J.S. Buhrman, Y. Liu, J.E. Rayahin, R.A. Gemeinhart, Molecular pharmaceutics, (2016).

[18] G. Salzano, D.F. Costa, C. Sarisozen, E. Luther, G. Mattheolabakis, P.P. Dhargalkar, V.P. Torchilin, Small, 12 (2016) 4837-4848.

[19] V. Kumar, G. Mondal, P. Slavik, S. Rachagani, S.K. Batra, R.I. Mahato, Molecular pharmaceutics, 12 (2015) 1289-1298.

[20] P. Kumari, O.S. Muddineti, S.V.K. Rompicharla, P. Ghanta, A.K. BBN, B. Ghosh, S. Biswas, Drug Delivery, 24 (2017) 209-223.

[21] L.-C. Cheng, Y. Jiang, Y. Xie, L.-L. Qiu, Q. Yang, H.-Y. Lu, Oncotarget, 8 (2017) 3315.

[22] J.-M. Yu, W.-D. Li, L. Lu, X.-Y. Zhou, D.-Y. Wang, H.-M. Li, X.-Y. Xu, J. Chen, Journal of Materials Science: Materials in Medicine, 25 (2014) 691-701.

[23] J. Yu, X. Xie, M. Zheng, L. Yu, L. Zhang, J. Zhao, D. Jiang, X. Che, International Journal of Nanomedicine, 7 (2012) 5079.

[24] X. Huang, W. Liao, G. Zhang, S. Kang, C.Y. Zhang, International Journal of Nanomedicine, 12 (2017) 2215.

[25] F. Szymanowski, A.A. Hugo, P. Alves, P. Simoes, A. Gómez-Zavaglia, P.F. Pérez, Colloids and Surfaces B: Biointerfaces, 156 (2017) 38-43.

[26] A. Frère, M. Kawalec, S. Tempelaar, P. Peixoto, E. Hendrick, O. Peulen, B. Evrard, P. Dubois, L. Mespouille, D. Mottet, Biomacromolecules, 16 (2015) 769-779.

[27] K. Zhu, R. Hendren, K. Jensen, C. Pitt, Macromolecules, 24 (1991) 1736-1740.

[28] D. Wu, Y. Zheng, X. Hu, Z. Fan, X. Jing, Materials Science and Engineering: C, 53 (2015) 68-75.

[29] B.B. Lundy, A. Convertine, M. Miteva, P.S. Stayton, Bioconjugate chemistry, 24 (2013) 398-407.

[30] A. Mittal, D. Chitkara, S.W. Behrman, R.I. Mahato, Biomaterials, 35 (2014) 7077-7087.

[31] C. Dhanya, J. Jeyaraman, P. Janeesh, A. Shukla, S. Sivakumar, A. Abraham, RSC advances, 6 (2016) 55125-55134.

[32] P. Sun, W. Huang, M. Jin, Q. Wang, B. Fan, L. Kang, Z. Gao, International Journal of Nanomedicine, 11 (2016) 4931.

[33] K.W. Dunn, M.M. Kamocka, J.H. McDonald, American Journal of Physiology-Cell Physiology, (2011).

[34] T. Abraham, S.E. Allan, M.K. Levings, Micron, 41 (2010) 633-640.

[35] L. Wang, X. Zhang, G. Cui, J.Y.-W. Chan, L. Wang, C. Li, L. Shan, C. Xu, Q. Zhang, Y. Wang, Oncotarget, 7 (2016) 32054.

[36] L. Bao, S. Hazari, S. Mehra, D. Kaushal, K. Moroz, S. Dash, The American journal of pathology, 180 (2012) 2490-2503.

[37] C. Khuu, A.-M. Jevnaker, M. Bryne, H. Osmundsen, Frontiers in genetics, 5 (2014) 246.

[38] G. Misso, M.T. Di Martino, G. De Rosa, A.A. Farooqi, A. Lombardi, V. Campani, M.R. Zarone, A. Gullà, P. Tagliaferri, P. Tassone, Molecular therapy-nucleic acids, 3 (2014) e195.

[39] J. Akbuga, S. Turan, E. Salva, (2013).

[40] Y. Wu, M. Crawford, B. Yu, Y. Mao, S.P. Nana-Sinkam, L.J. Lee, Molecular pharmaceutics, 8 (2011) 1381-1389.

[41] Y. Zhang, Y. Liu, S. Sen, P. Král, R.A. Gemeinhart, Nanoscale, 7 (2015) 7559-7564.

[42] D.S. Conti, D. Brewer, J. Grashik, S. Avasarala, S.R. da Rocha, Molecular pharmaceutics, 11 (2014) 1808-1822.

[43] M. Dominska, D.M. Dykxhoorn, Journal of cell science, 123 (2010) 1183-1189.

[44] C. Zhu, S. Jung, S. Luo, F. Meng, X. Zhu, T.G. Park, Z. Zhong, Biomaterials, 31 (2010) 2408-2416.

[45] D. Putnam, C.A. Gentry, D.W. Pack, R. Langer, Proceedings of the National Academy of Sciences, 98 (2001) 1200-1205.

[46] C.E. Nelson, J.R. Kintzing, A. Hanna, J.M. Shannon, M.K. Gupta, C.L. Duvall, ACS Nano, 7 (2013) 8870-8880.

[47] H.Y. Xue, S. Liu, H.L. Wong, Nanomedicine, 9 (2014) 295-312.

CHAPTER 4

DEVELOPMENT AND EVALUATION OF FOLATE CONJUGATED LIPOPOLYMERIC NANO-CARRIER CONTAINING DOCETAXEL

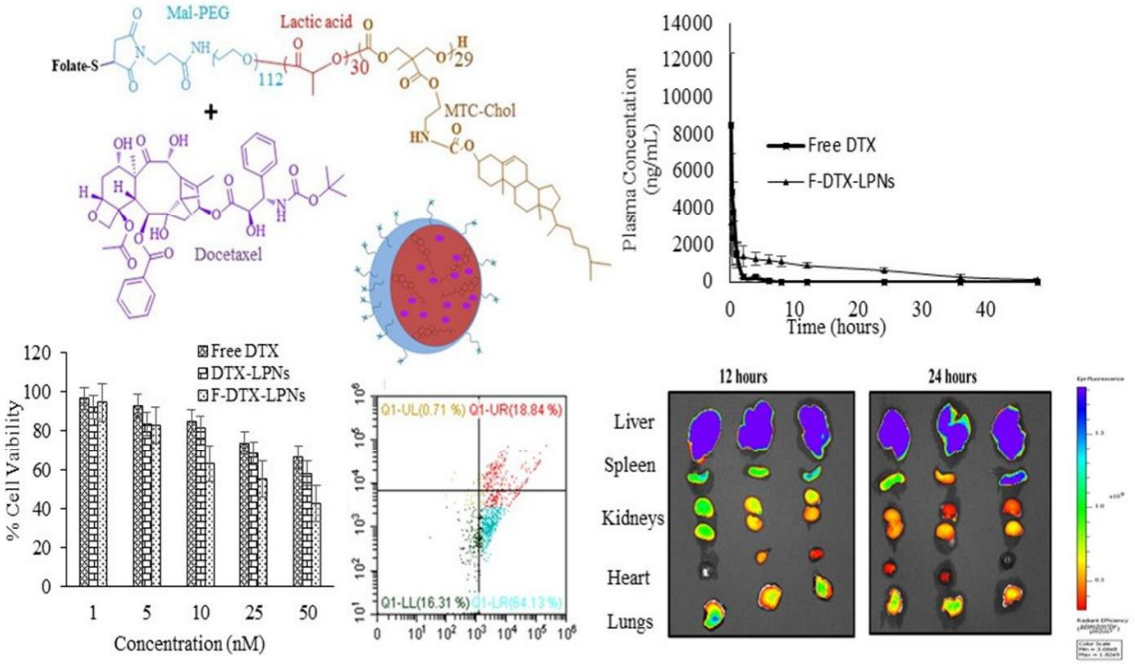

- Introduction
- Experimental section
- Results
- Discussion

4.1. Introduction

Amongst the currently available chemotherapeutics, docetaxel (DTX; a 'Taxane' derivative) is a highly potent FDA approved small molecule used as a first-line treatment for triple-negative breast cancer (TNBC). It acts by stabilizing tubulin heterodimer, resulting in impaired mitosis and inhibition of cellular proliferation in the cancer cells [1, 2]. However, DTX has poor aqueous solubility and undergoes rapid metabolism in the biological environment resulting in lower plasma half-life [3, 4]. Taxotere® is a commercially available product of docetaxel; however, its administration is associated with several undesirable side effects, including hypersensitivity reactions, fluid retention, neurotoxicity, musculoskeletal toxicity, and neutropenia [5]. There is also a risk of development of drug resistance due to its efflux by P-glycoprotein (P-gp) [6]. Also, the product has a stability issue as it should be used within 8 h post-dilution with the infusion fluid as it gets precipitated. Further, the presence of a higher amount of surfactant and ethanol necessitates the use of special tubing materials of infusion bag assembly to prevent the problem of leaching of plastic [3]. Thus, the high cost is also a major pitfall of the available product.

Over the past few decades, nanotechnology has made major contributions in cancer treatment with several nano-carriers being explored and translated to the clinic, including liposomes (Doxil® and Myocet®) [7], albumin-bound paclitaxel nanoparticle (Abraxane®) and polymeric micelles (Genexol® PM) [8]. Further, several nanotechnology-based systems are in the clinical and preclinical investigation to enable the delivery of hydrophobic drugs while largely mitigating the toxicity of chemotherapeutic agents as well as the excipients. There have been several attempts to design novel formulations of docetaxel as well to overcome its side effects along with improvement in drug delivery to the target site. These carrier systems aim to provide *in vitro* and *in vivo* stability, prolonged drug release profile, high intracellular uptake, improved pharmacokinetic profile, enhanced permeability and

retention (EPR) at the tumor site, and target specificity to tumor cells [9]. Tao et al. prepared the functionalized aptamer-based DTX loaded nanoparticles by simple surface modification method that showed efficient drug targeting to the tumor site with an effective and safe treatment as compared to Taxotere and nanoparticles without surface modification [10]. In another study, Bowerman et al. reported the PLGA based nanoparticles by using modern technology (PRINT), which can encapsulate DTX, actively transport it to the tumor site, and showed to be effective in a taxane resistant TNBC [11].

Among different materials used for preparing nanoparticles, biodegradable polymers, including polyesters and polycarbonates, have gained enormous interest owing to the advantages, such as biodegradability and biocompatibility, amenability to surface modification, tailor-made properties to suit delivery requirements, etc. Danquah et al. reported the PEGylated polyester and polycarbonate-based amphiphilic diblock copolymer for controlled delivery of hydrophobic non-steroidal antiandrogen, bicalutamide for treating prostate cancer that showed an improvement in the drug loading of the hydrophobic drug by incorporating the carbonate moiety as compared to PEG-b-PLLA [12]. In another study, Bariwal et al. reported the efficient loading of a novel tubulin destabilizing agent (QW-296) in m-PEG-b-P(CB-co-LA) nanoparticles for treating metastatic melanoma [13]. The nanoparticles showed improved QW-296 solubility, effective tumor growth inhibition, and prolong survival rate of mice bearing metastatic lung melanoma. Further, modification of the polycarbonate backbone has been attempted to improve the drug delivery of hydrophobic drugs. Feng Li *et al.,* have reported amphiphilic polycarbonate-based lipopolymers grafted with dodecanol for improved loading of a hydrophobic model drug, embelin. In other reports, drugs have been conjugated to the polycarbonate backbone to improve their delivery [14]. Chitkara *et al.,* reported self-assembling gemcitabine conjugated PEGylated polycarbonate copolymeric micelles with lower particle size, controlled drug release profile, enhanced drug

loading and reduction in plasma metabolism along with enhancement in antitumor activity in a pancreatic cancer xenograft model in NSG mice [15].

In chapter 2, we have shown the modifications of polycarbonate backbone with morpholine, cholesterol, and cationic chain to improve the delivery of miRNA-34a, wherein we have grafted the polycarbonate block of the amphiphilic copolymer by EDC/HOBT coupling [16]. Various other studies have reported the use of monomers with desired side chains, followed by ring-opening polymerization to prepare the grafted polycarbonate copolymers. Pratt *et al.,* explored different polymerization methods from aluminium alkoxide, stannous octoate, and metal-free ring-opening polymerization of functionalized cyclic carbonate monomers with various side-chain functionalities having application in biomedical science [17]. In another study, passively targeted cholesterol grafted copolymer provided a rigid fused ring structure that has improved the encapsulation efficiency of the rigid hydrophobic small anticancer molecule [18].

To develop a safe and effective delivery system for DTX, in this chapter, we report biodegradable folate-conjugated lipopolymers consisting of cholesterol grafted hydrophobic polycarbonate, polylactide and hydrophilic polyethylene block. Cholesterol modified cyclic carbonate monomer was synthesized using a multi-step approach followed by microwave-assisted ring-opening polymerization with DL-lactide in the presence of methoxy poly(ethylene glycol) afforded the copolymers. For actively targeting, folate was appended onto the PEG block. DTX was loaded in the lipopolymeric nanoparticles, followed by a thorough characterization for size, surface morphology, entrapment efficiency, on-bench stability, and *in vitro* DTX release. Cell-based assays, including intracellular uptake mechanism, cytotoxicity, apoptosis, and gene expression were performed in MDA-MB-231 breast cancer cells. *In vivo* pharmacokinetics was performed in *Sprague Dawley* rats after intravenous administration of lipopolymeric nanoformulation with a dose of 10 mg/kg.

Further, to explore the potential *in vivo* application of this targeted nanosystem, *ex vivo* tissue distribution of DiR loaded folate conjugated lipopolymeric nanoparticles was conducted in *swiss albino* mice.

4.2. Experimental section

4.2.1. Materials

Bis(hydroxymethyl) propionic acid, 2-bromoethylamine hydrobromide (99%), tin(II) 2-ethylhexanoate, cholesterylchloroformate (98%), methoxypoly(ethylene glycol) (mPEG, 5000 Da), and propidium iodide (PI) were purchased from Sigma Aldrich (St. Louis, MO) and were used as received. Maleimide poly(ethylene glycol)-hydroxyl (mal-PEG-OH, 5000 Da) was purchased from Xi'an Ruixi Biological Technology Co., Ltd (Ruixibio), Shaanxi Province, China. DL-lactide was purchased from TCI Chemicals (India) Pvt. Ltd. Docetaxel (DTX) was obtained as a kind gift from Fresenius Kabi, Bad Homburg, Germany. Fetal Bovine Serum (FBS), Dulbecco's Modified Eagle Medium (DMEM), Annexin V Alexafluor® 488 conjugate and TrypLE were obtained from ThermoFisher Scientific (MA, USA). 3-(4,5-dimethylthiazol-2-yl)-2,5-diphenyltetrazolium bromide (MTT) was procured from Sisco Research Laboratories (Mumbai, India). All other chemicals and reagents were of analytical grade and purchased from local vendors.

4.2.2. Synthesis of monomer and polymers

4.2.2.1. Synthesis of cholester-3-yl(2-bromoethyl)carbamate (Be-Chol, 3)

Cholesterylchloroformate (13.02 g, 29.1 mM, 1 equiv.) (**1**) and triethylamine (8.64 mL) were added to a solution of 2-bromoethylamine hydrobromide (6.27 g, 31.8 mM, 1.1 equiv.) (**2**) in 100 mL of chloroform in a dry round-bottom flask, under nitrogen atmosphere. The reaction mixture was stirred for 30 min. at −78°C (using dry ice bath), followed by stirring at room temperature for 12 h. After completion of the reaction, the crude mixture was

washed first with 1 N HCl solution (saturated with brine), followed by saturated sodium bicarbonate solution (saturated with brine). The organic layer was collected, dried over anhydrous sodium sulfate and evaporated to obtain a solid product that was subsequently recrystallized from ethanol, and thereafter from acetone to obtain pure Be-Chol (**3**) as a white solid.[19] Yield: 81% (10.34 g); Figure 4.4 shows the ^{1}H NMR (400 MHz, $CDCl_3$) having δ 5.42 – 5.36 (m, 1H), 5.09 (t, J = 6.1 Hz, 1H, NH), 4.60 – 4.45 (m, 1H), 3.66 – 3.55 (m, 2H), 3.49 (t, J = 5.8 Hz, 2H), 2.42 – 2.25 (m, 2H), 2.10 – 1.74 (m, 6H), 1.66 – 1.25 (m, 12H), 1.25 – 1.05 (m, 8H), 1.03 (s, 3H), 0.93 (d, J = 6.5 Hz, 3H), 0.89 (d, J = 1.9 Hz, 3H), 0.87 (d, J = 1.9 Hz, 3H), 0.69 (s, 3H); ^{13}C NMR (100 MHz, $CDCl_3$) δ 155.9 ($C{=}O_{Carbamte}$), 139.7, 122.6, 74.7, 56.7, 56.1, 50.1, 42.6, 42.3, 39.7, 39.5, 38.5, 37, 36.6, 36.2, 35.8, 32.8, 31.9, 31.9, 28.3, 28.1, 28.0, 24.3, 23.8, 22.9, 22.6, 21.0, 19.3, 18.7, 11.9.

4.2.2.2. Synthesis of (((cholester-3-yloxy)carbonyl)amino)ethyl 3-hydroxy-2-(hydroxymethyl)-2-methylpropanoate (Chol-MPA, 5)

A mixture containing 2-bis(hydroxymethyl) propionic acid (4.5g, 31.3 mM, 1.1 equiv.) (**4**) and potassium hydroxide (2.2 g, 30.3 mM, 1.1 equiv.) in dimethyl formamide (DMF; 200 mL) was heated to 100°C for 2 h. Thereafter, *N*-(2-bromoethyl) carbamoyl cholesterol (Be-Chol, **3**) (16 g, 1.12 equiv.) was added to the reaction mixture and stirred for another 18 h at 100°C. After 18 h, the mixture was dissolved in ethyl acetate and washed with saturated brine solution and distilled water. The organic layer was separated, dried using anhydrous sodium sulphate and evaporated to afford crude Chol-MPA, which was further purified by column chromatography using silica gel as an adsorbent using gradient phase ratio of ethyl acetate-hexane as the mobile phase to furnish pure Chol-MPA (**5**) as a yellowish oily semi-solid [20]. Yield: 85% (12.45 g); Figure 4.5 shows 1H NMR (400 MHz, $CDCl_3$) having δ5.44 – 5.31 (m, 2H), 4.56 – 4.46 (m, 1H), 4.28 (t, J = 5.0 Hz, 2H), 3.91 (d, J = 11.4 Hz, 2H), 3.74 (d, J = 11.5 Hz, 2H), 3.48 (q, J = 5.5 Hz, 2H), 3.42 – 3.30 (m, 2H), 2.42

– 2.24 (m, 2H), 2.11 – 1.74 (m, 7H), 1.65 – 1.40 (m, 8H), 1.39 – 1.10 (m, 11H), 1.08 (s, 3H), 1.01 (s, 3H), 0.92 (d, J = 6.5 Hz, 3H), 0.88 (d, J = 1.9 Hz, 3H), 0.87 (d, J = 1.9 Hz, 3H), 0.68 (s, 3H).; ^{13}C NMR (100 MHz, $CDCl_3$) δ 175.7 ($C{=}O_{Ester}$), 156.7 ($C{=}O_{Carbamte}$), 139.7, 122.6, 74.7, 71.8, 68.3, 4.2, 56.7, 56.1, 50.0, 49.5, 42.3, 39.7, 39.5, 38.5, 37.3, 37.3, 37.0, 36.5, 36.2, 35.8, 31.9, 31.9, 28.2, 28.1, 28.0, 24.3, 23.8, 22.8, 22.6, 21.0, 19.3, 18.7, 17.1, 11.9; HRMS (ESI-TOF) *m/z*: $[M+Na]^+$ calculated for $C_{35}H_{59}NO_6Na$ 612.4235; Found 612.4229.

4.2.2.3. Synthesis of (((cholester-3-yl)oxy)carbonyl)amino)ethyl 5-methyl-2-oxo-1,3-dioxane-5-carboxylate (MTC-Chol, 6)

Chol-MPA (10 g) (**5**) was added to 200 mL of anhydrous DCM in a round-bottom flask. This was followed by the addition of pyridine (8.0 g) to it. The reaction mixture was then cooled to -78°C using a dry ice/acetone bath. Thereafter, triphosgene (2.74 g dissolved in DCM) was added dropwise into the reaction mixture in 1 h, which was followed by continuous stirring for another 2 h at room temperature. After this, the reaction was quenched by adding saturated aqueous ammonium chloride (NH_4Cl) solution (100 mL), and the organic layer was separated, washed twice with a mixture of 1 N hydrochloric acid (HCl) solution (saturated with brine) and saturated sodium bicarbonate (saturated with brine) [20]. The organic layer was dried over anhydrous sodium sulphate and concentrated to obtain crude MTC-Chol, which was further purified using column chromatography using ethyl acetate:-hexanes as the mobile phase. The fractions containing pure MTC-Chol (**6**) were dried under vacuum to affordpure MTC-Chol as a white solid. Yield: 67% (6.7 g); Figure 4.6 shows ^{1}H NMR (400 MHz, $CDCl_3$) having δ 5.41 – 5.36 (m, 1H), 4.95 (t, J = 6.2 Hz, 1H), 4.70 (d, J = 10.9 Hz, 2H), 4.59 – 4.44 (m, 1H), 4.30 (t, J = 5.1 Hz, 2H), 4.23 (d, J = 10.9 Hz, 2H), 3.48 (q, J = 5.6 Hz, 2H), 2.42 – 2.25 (m, 2H), 2.10 – 1.93 (m, 2H), 1.92 – 1.39 (m, 12H), 1.35 (s, 6H), 1.28 – 1.03 (m, 9H), 1.02 (s, 3H), 0.93 (d, J = 6.5 Hz, 3H), 0.89 (d, J = 1.8 Hz, 3H), 0.87 (d, J = 1.8 Hz, 3H), 0.69 (s, 3H); ^{13}C NMR (100 MHz, $CDCl_3$) δ 175.7 ($C{=}O_{Ester}$), 156.2

($C=O_{Carbamte}$), 147.6 (C=O), 139.7, 122.6, 74.8, 73.0, 68.9, 65.3, 56.7, 56.1, 50.0, 42.3, 39.7, 39.5, 38.5, 37.0, 36.6, 36.2, 35.8, 31.9, 31.9, 28.2, 28.1, 28.0, 24.3, 23.8, 22.8, 22.6, 21.0, 19.3, 18.7, 17.4, 11.9; HRMS (ESI-TOF) *m/z*: $[M+Na]^+$ calculated for $C_{36}H_{57}NO_7Na$ 638.4027; Found 638.4031.

4.2.2.4. Microwave-assisted synthesis of methoxy and maleimide-terminated PEGylated lipopolymer i.e. mal-PEG-b-p(MTC-Chol-co-LA (9) and mPEG-b-p(MTC-Chol-co-LA) lipopolymers (15-18)

mPEG or maleimide PEG (mal-PEG-OH) (Mn 5000 Da; 0.216 g) (**8**) was taken in a 10 mL microwave specific vial and kept at 120º C for 5 min. in a Microwave chamber (Monowave 400, Anton Parr). After 5 min., MTC-Chol monomer (0.636 g) (**6**) and DL-lactide (0.148 g) (**7**) and stannous 2-ethyl hexanoate ($Sn(Oct)_2$; 10 mol% of mPEG or mal-PEG-OH) solution in anhydrous toluene were subsequently added. The reaction mixture was irradiated under microwave at 150º C for 1 h to obtain mPEG-b-p(MTC-Chol-co-LA) or mal-PEG-b-p(MTC-Chol-co-LA) *via* ring-opening polymerization (ROP). The crude lipopolymer was purified by precipitation method, wherein it was dissolved in chloroform followed by precipitation with an excess amount of cold diethyl ether. Purification was performed twice, and the lipopolymer thus obtained was dried under vacuum. Figure 4.8 showed ^{1}H NMR (400 MHz, $CDCl_3$) of mal-PEG-b-p(MTC-Chol-co-LA) lipopolymer showed the characteristic peaks at δ7.2 (-C<u>H</u>=C<u>H</u>-) of mal-PEG, δ5.45 to 5.05 (-CH_2-C=C<u>H</u>-CH_2- and -CO-C<u>H</u>(CH_3)-O-CO-) of cholesterol and DL-lactide, δ4.65 to 4.40 (-COO-C<u>H_2</u>-CH(CH_3)-C<u>H_2</u>-O-), δ3.85 - 3.5 (-C<u>H_2</u>C<u>H_2</u>-O) of mal-PEG, δ2.45 - 0.55 (protons from cholesterol and CH_3 in the carbonate monomer and DL-lactide) (Figure 4.5A). Similarly the above ring-opening polymerization of methoxy polyethylene glycol (mPEG, **14**) was carried using varying ratios of MTC-Chol and DL-lactide to afford a series of lipopolymers, mPEG-b-p(MTC-$Chol_{11}$-co-LA_5) (**15**), mPEG-b-p(MTC-$Chol_{15}$-co-LA_{15}) (**16**), mPEG-b-p(MTC-$Chol_{11}$-co-LA_{27}) (**17**), mPEG-b-p(MTC-$Chol_{29}$-co-LA_{30}) (**18**) (Figure 4.3).

4.2.2.5. Synthesis of folate-thiol (folate-SH, 12)

N-hyrodxysuccinimide derivative of folic acid (FA-NHS 1.02 g, (**10**)) and triethylamine (0.2 mL) were dissolved in anhydrous DMSO (10 mL), followed by the addition of cysteamine hydrochloride (**11**) (0.059 g, 0.8 mmol). The reaction was stirred for 48 h at room temperature under dark conditions. After this, the mixture was diluted with diethyl ether to precipitate the crude product, which was filtered and washed with excess diethyl ether to afford pure folate-SH (**12**) as an orange solid.[21] Yield: 56% (0.625 g); In (Figure 4.7) showed ^{1}H NMR (400 MHz, DMSO-d_6) δ8.64 (, J = Hz, -CO-NH-, 1H), δ7.61, 6.64 (benzyl protons of folate, 4H), 4.48 (-NH-CH(COOH)-CH_2-, 2H),4.36 (-CH_2-NH-, 2H), 3.76 (-NH-CH_2-CH_2-SH, 2H), 2.91(-CH_2-CH_2-SH, 2H), 2.69 (-CH_2-CH_2-CO-NH-, 2H); ^{13}C NMR (100 MHz, $CDCl_3$)δ174.4 (CH_2-CO-NH-), 167.1 (-NH-CH(COOH)), 151.7 (-C=N-), 129.4, 128.1, 121.4, 111.73 (aromatic C=C of benzyl).

4.2.2.6. Synthesis of folate-PEG-b-p(MTC-Chol-co-LA) lipopolymer (13)

To a solution of mal-PEG-b-p(MTC-Chol-co-LA) lipopolymer(200 mg) (**9**) in DMSO (2 mL), folate-SH (10 mg dissolved in DMSO) (**12**) and triethylamine (20 μL) were added, and the reaction mixture was stirred for 24 h at room temperature. After this, the reaction mixture was dialyzed using a Snake Skin dialysis membrane (molecular weight cut-off 3500 Da, Thermofisher Scientific) against purified water for 48 h and lyophilized to obtain folate-PEG-b-p(MTC-Chol-co-LA) lipopolymer (**13**). Figure 4.8 showed ^{1}H NMR (400 MHz, $CDCl_3$) of fol-PEG-b-p(MTC-Chol-co-LA) lipopolymer having the characteristic peaks at δ6.9, 7.5 and 8.67 for the corresponding to folate moiety, δ7.2 (-CH=CH-) of mal-PEG, δ5.45 to 5.05 (-CH_2-C=CH-CH_2- and -CO-CH(CH_3)-O-CO-) of cholesterol and DL-lactide, δ4.65 to 4.40 (-COO-CH_2-CH(CH_3)-CH_2-O-), δ3.85 - 3.5 (-CH_2CH_2-O) of mal-PEG, δ2.45 - 0.55 (protons from cholesterol and CH_3 in the carbonate monomer and DL-lactide).

4.2.3. Characterization of intermediates, monomer and lipopolymers

All the intermediates, monomers and lipopolymers were characterized by ^{1}H and ^{13}C NMR spectroscopy (AVANCE II Bruker NMR Using TOPSPIN) at 400 and 100 MHz, respectively. For Be-Chol, Chol-MPA and MTC-Chol, samples were prepared in deuterated chloroform ($CDCl_3$), while deuterated dimethyl sulphoxide (DMSO-d_6) was used for folate-SH monomer, mal-PEG-b-p(MTC-Chol-co-LA) lipopolymer and folate-PEG-b-p(MTC-Chol-co-LA). HRMS of the intermediates was determined by High-Resolution Mass Spectrometry (6545 Q-TOF LC/MS, Agilent) equipped with an auto-sampler in ESI^+ mode.

4.2.4. Quantification of Folate in folate-PEG-b-p(MTC-Chol-co-LA) lipopolymer

The extent of folate conjugated to the lipopolymer was determined by using a UV spectrophotometer (UV-1800, Shimadzu (SSI), Kyoto, Japan) method, as reported earlier [22]. The folate conjugated lipopolymer was dissolved in DMSO at a concentration of 10 µg/mL and its absorbance was measured at 280 nm. The standard calibration curve of folate-thiol was constructed in the concentration range of 3-30 µg/mL in dimethyl sulphoxide, and from the equation generated, the amount of folate conjugated to the lipopolymer was determined.

4.2.5. Preparation and characterization of DTX loaded folate conjugated lipopolymeric nanoparticles (F-DTX-LPNs)

Single emulsion-solvent evaporation method was adopted for the preparation of DTX loaded lipopolymeric nanoparticles [23, 24]. Briefly, a solution of DTX (5 mg) and folate-PEG-b-p(MTC-Chol-co-LA) lipopolymer (**13**) (95 mg) in DCM (400 μL) was added to 3 mL of purified water containing tween 80 (1% w/v) and sonicated using a probe sonicator (Sonics Vibra cell™, Newtown, CT, USA) at 25% amplitude for 3 min to form an o/w emulsion. It was then kept on stirring overnight at RT to remove DCM, resulting in the formation of

nanoparticles that were subsequently centrifuged at 5000 rpm for 5 min. to remove unentrapped drug or larger particles as a pellet. The supernatant containing DTX loaded nanoparticles was collected and analyzed for particle size and ζ- potential using Malvern Zetasizer. The DTX content in the nanoparticles was analyzed by RP-HPLC analytical method as given in chapter 2. The drug entrapment efficiency was determined by taking 100 μL of nanoparticle suspension and diluted with 900 μL acetonitrile followed by heating on water batch at 60°C till a clear solution was observed followed by bath sonication for 5 min. to extract the DTX. The samples were centrifuged at 17500 rpm for 10 min, filtered, and analyzed using the developed HPLC method. Morphological characterization of DTX loaded nanoparticles was determined using Field Emission-Scanning Electron Microscopy (FE-SEM) (FEI, ApreoLoVac). On-bench stability of DTX-loaded nanoparticles was determined for five days to determine any changes in its particle size, polydispersity index (PDI), and ζ-potential.

4.2.6. In vitro DTX release from lipopolymeric nanoparticles

DTX release from the DTX loaded nanoparticles was determined using a dialysis bag method. Briefly, dialysis bag (3.5 KDa cut-off; SnakeSkin® Dialysis Tubing, Thermo Fischer Scientific) containing the free drug or drug-loaded nanoparticles F-DTX-LPNs was placed in 30 mL of phosphate buffer saline (100 mM; pH 7.4) containing tween 80 (1% w/v), sodium azide (0.2% w/v) and ethanol (2% v/v) to maintain the sink condition. Studies were performed at 37ºC/100 rpm in an incubator. Release samples (2 mL) were taken at regular time intervals, i.e., 0.25, 0.5, 1, 2, 4, 8, 12 (time, h), 1, 2, 3, 4, 5, 6 and 7 (time, days) and replaced with the equal quantity of fresh release media at each time point. The amount of DTX in the release samples was determined by RP-HPLC method as given in chapter 2 and cumulative release was plotted against time.

4.2.7. In vitro Cell-based assays

In vitro cell culture studies were performed in MDA-MB-231 breast cancer cells obtained from National Centre for Cell Science, Pune, India. MDA-MB-231 cells are epithelial human breast cancer cell line that was established from a pleural effusion of a 51-year-old Caucasian female with metastatic mammary adenocarcinoma and is one of the most commonly used breast cancer cells throughout medical research laboratories. These cells were cultured in Dulbecco's Modified Eagle's Medium (DMEM) supplemented with 10% fetal bovine serum (FBS; HyClone, Logan, UT) and 1% antibiotics (100 U/mL penicillin/streptomycin) and kept in an incubator at 37°C/ 5% CO_2.

4.2.8. Cellular uptake studies and pathway mediated endocytosis

To evaluate the potential of lipopolymeric nanoparticles for intracellular delivery of loaded cargo, *in vitro* cellular uptake studies were conducted on MDA-MB-231 cells. A hydrophobic fluorescent dye (coumarin-6; C6) was loaded in the nanoparticles as a hydrophobic model drug to enable visualization of their uptake in the cells. Briefly, MDA-MB-231 cells were seeded at a cell density of 1×10^5 cells/well in a 6-well cell culture plate and allowed to adhere for 24 h. Before treatment with the nanoparticles, cells were washed with PBS (10 mM, pH 7.4) and culture media was replaced with the fresh serum-free DMEM media for 1 h followed by addition of folate-targeted and non-targeted C6 loaded nanoparticles (C6 dye ~ 150 ng/mL), and blank nanoparticles to the respective well and further incubated for 4 h. After incubation, cells were washed with PBS, fixed with paraformaldehyde (4% v/v) for 10 min, counterstained with DAPI (for nucleus labeling; 300 nM) and observed under a fluorescence microscope (Vert.A1, ZEISS, Oberkochen, Germany) [16].

To further understand the uptake mechanism of the folate-targeted nanoparticles (F-C6-LPNs) in MDA-MB-231 cells (1×10^5cells/well), four endocytic inhibitors, i.e., methyl β-cyclodextrin (Mβ-CD), nystatin (mycostatin), chlorpromazine (CPZ) and amiloride.HCl (AMD) were used. Briefly, cells were seeded in 6-well cell culture plates and allowed to adhere for 24 h. After 24 h, cells were washed with PBS (twice), and media was replaced with 1mL of serum-free DMEM followed by treatment with methyl β-CD (3 mM), nystatin (27μM), CPZ (10μM) and AMD (1mM) for 30 min. After treatment, cells were washed thrice with PBS. Further cells were treated with C6 loaded nanoparticles (F-C6-LPNs) for 4 h. After incubation, cells were washed with PBS, fixed with paraformaldehyde (4% v/v) for 10 min., counterstained with DAPI (for nucleus labeling; 300 nM) and observed under a fluorescence microscope (Vert.A1, ZEISS, Oberkochen, Germany) [16].

4.2.9. In vitro cytotoxicity studies

Cytotoxicity studies of folate-targeted and non-targeted lipopolymeric nanoparticles loaded with DTX were performed in MDA-MB-231 breast cancer cells. Briefly, MDA-MB-231 cells were seeded in 96 well cell culture plates ($5x10^3$ cells/well) and allowed to adhere for 24 h followed by treatment with free DTX (in DMSO), DTX loaded folate targeted and non-targeted lipopolymeric nanoparticles at a concentration range from 1 nM to 50 nM equivalent to DTX [25, 26]. Untreated cells and DMSO (0.001%) treated cells were kept as controls. The cytotoxicity of the folate conjugated lipopolymer (folate-PEG-b-p(MTC-Chol-co-LA)) was also studied at a concentration range from 1μg/mL- 1 mg/mL. After 48 h, the cells were washed with PBS and fresh media containing 3-(4,5-dimethylthiazol-2-yl)-2,5-diphenyltetrazolium bromide (MTT) dye (100 μg/well) was added to each well and incubated for 5 h. At the end of 5 h, the culture media was removed, cells were washed with PBS and formed formazan crystals were dissolved in 150 μL of DMSO. The absorbance of the samples was recorded by a microplate reader (BioTek Epoch) at 570 nm and corrected for the

cell debris by subtracting absorbance at 630 nm [16]. The percentage cell viability was determined using the following formula:

$$\%\ \text{Cell viability} = \frac{Absorbance\ of\ sample wells}{Absorbance\ of\ control\ wells} \times 100$$

4.2.10. Apoptosis assay

MDA-MB-231 cells ($1x10^6$ cells/well) were seeded in 6-well cell culture plates and allowed to adhere for 24 h. After 24 h, the media was replaced with the fresh media containing free DTX (50 nM), DTX loaded folate-targeted and non-targeted lipopolymeric nanoparticles equivalent to 50 nM of DTX. After 48 h incubation, the cells were washed with PBS, trypsinized, centrifuged at 1700 rpm/5 min at 4º C and treated with FITC-Annexin V Apoptosis Detection Kit (ThermoFisher Scientific, USA) as per the manufacturer's protocol. The cells undergoing early and late apoptosis were quantified by flow cytometry using Cytoflex (Beckman Coulter, USA) and data were interpreted using CytExpert software [27, 28].

4.2.11. Gene expression study

MDA-MB-231 cells ($1x10^6$ cells/well) were seeded in a 6-well cell culture plate and allowed to adhere for 24 h followed by treatment with free DTX (50 nM) (in DMSO), DTX loaded folate-targeted and non-targeted lipopolymeric nanoparticles equivalent to 50 nM of DTX for 48 h. After 48 h, cells were washed, trypsinized and total RNA was extracted using PureLink® RNA Mini Kit (Ambion®, ThermoFisher Scientific) according to the manufacturer's protocol. RNA samples were quantified by Nanodrop (Simplinano™ spectrophotometer, Biochrom, Harvard Bioscience. Inc.) and cDNA was synthesized from RNA using GeneMax™First Strand cDNA Synthesis Kit (PUREGENE, Genetix Biotech Asia, Pvt. Ltd.) on a thermal cycler (Bio-Rad; Hercules, CA) according to the manufacturer's protocol [27]. Gene quantification was performed using Maxima SYBR Green/ROX qPCR

Master Mix (2X) assay kit (Thermo Fisher Scientific Baltics UAB, Vilnius, Lithuania). Real-time PCR primers were designed for BCL2, BAX, ki67, SIRT1 and GAPDH gene were used as given below [29].

BCL2: Forward sequence- 5'-gtccaagaatgcaaagcaca -3'

Reverse sequence- 5'-ccggttatcgtaccctgttc-3',

BAX: Forward sequence- 5'-gctggacattggacttcctc-3'

Reverse sequence- 5'-ctcagcccatcttcttccag-3'

ki67: Forward sequence-5'-tctgacctgacagacctcaaga-3'

Reverse sequence- 5'-gtgtgtgttggggtgtttattg-3'

SIRT1: Forward sequence- 5'-gaacatagacacgctggaac-3'

Reverse sequence- 5'-ctaggacatcgaggaactacc-3'

GAPDH: Forward sequence- 5'-tggcttgtgctgtaagatcg'-3

Reverse sequence5'-aatctccactttgccactgc-'3

4.2.12. Pharmacokinetic studies in Sprague Dawley (SD) rats

Pharmacokinetic studies were performed in *Sprague Dawley* (SD rats; females; 8–10 weeks, 200–220 g). SD Rats procured from the Central Animal Facility, BITS-Pilani (Pilani, Rajasthan India). The Institutional Animal Ethics Committee (IAEC) approved the animal protocol, BITS-Pilani (IAEC/RES/23/09) and experiments were conducted as per CPCSEA guidelines. Animals were housed in well-ventilated cages at standard laboratory conditions with regular light/dark cycles for 12 h and fed with standard diet ab libitum.

Animals (N=6) were injected with free DTX (Taxotere®) or DTX-loaded folate-targeted lipopolymeric nanoparticles (F-DTX-LPNs) *via* tail vein injection at the dose of 10 mg/kg. Blood samples were collected from retro-orbital plexus into disodium EDTA containing microcentrifuge tubes for each pre-set time points (0.08, 0.25, 0.5, 1, 2, 4, 6, 8, 12,

24, 48 and 72 h) and centrifuged at 6500 rpm for 15 min to obtain plasma that was subsequently stored at -80°C until analyzed using a bioanalytical method outlined in chapter 2. Plasma concentration-time profiles of DTX were plotted and analyzed by a non-compartmental model approach using Phoenix 8.0 WinNonlin (Pharsight Corporation, USA) to determine $t_{1/2}$, elimination half-life; C_0, drug concentration in plasma at t=0; AUC_{0-t}, the area under the curve from zero to the last time point; $AUC_{0-\infty}$, the area under the curve from zero to infinity; MRT, mean residence time; CL, clearance and V_z, apparent volume of distribution [30].

4.2.13. In vivo bioimaging

DiR dye was used as a fluorescent marker to examine the *in vivo* distribution of folate targeted lipopolymeric nanoparticles in *Swiss albino mice*. All experiments were performed as per CPCSEA guidelines after approval from IAEC, BITS-Pilani (IAEC/RES/27/7). Herein, DiR dye was loaded in the nanoparticle using a similar method as that of F-DTX-LPNs. For the biodistribution study, mice were divided into three groups (N=3) and were given DiR loaded F-LPNs (DiR equivalent to 400 μg/kg) intravenously. At specific time points i.e., 30 min, 6, 12 and 24 h, animals were sacrificed and vital organs including liver, heart, kidney, lungs and spleen were isolated. DiR dye accumulation in the isolated tissues was determined by *ex-vivo* bioimaging using *In Vivo* Imaging System (IVIS) Lumina XR (Perkin Elmer, UK) at excitation and an emission wavelength of 745 and 788 nm, respectively [31].

4.2.14. Statistical analysis

Data are presented as the mean ± standard deviation. The difference between any two or more groups was determined by analysis of variance (ANOVA) followed by Tukey's test. $p \leq 0.05$ was considered to be statistically significant.

4.3. Results

Low solubility and permeability of DTX hinder its optimal therapeutic utilization. Taxotere®, the conventional formulation of DTX, utilizes a high concentration of surfactant and ethanol to solubilize DTX for parenteral application [32]. To improve its delivery, several nanotechnology-based approaches have been reported in the literature. Herein we have designed the folate-targeted lipopolymer containing cholesterol as pendant groups for efficient delivery of DTX. Initially, mal-PEG-b-p(MTC-Chol$_{29}$-co-LA$_{30}$) was synthesized by ring-opening polymerization (ROP) using a cyclic carbonate monomer (with cholesterol side-

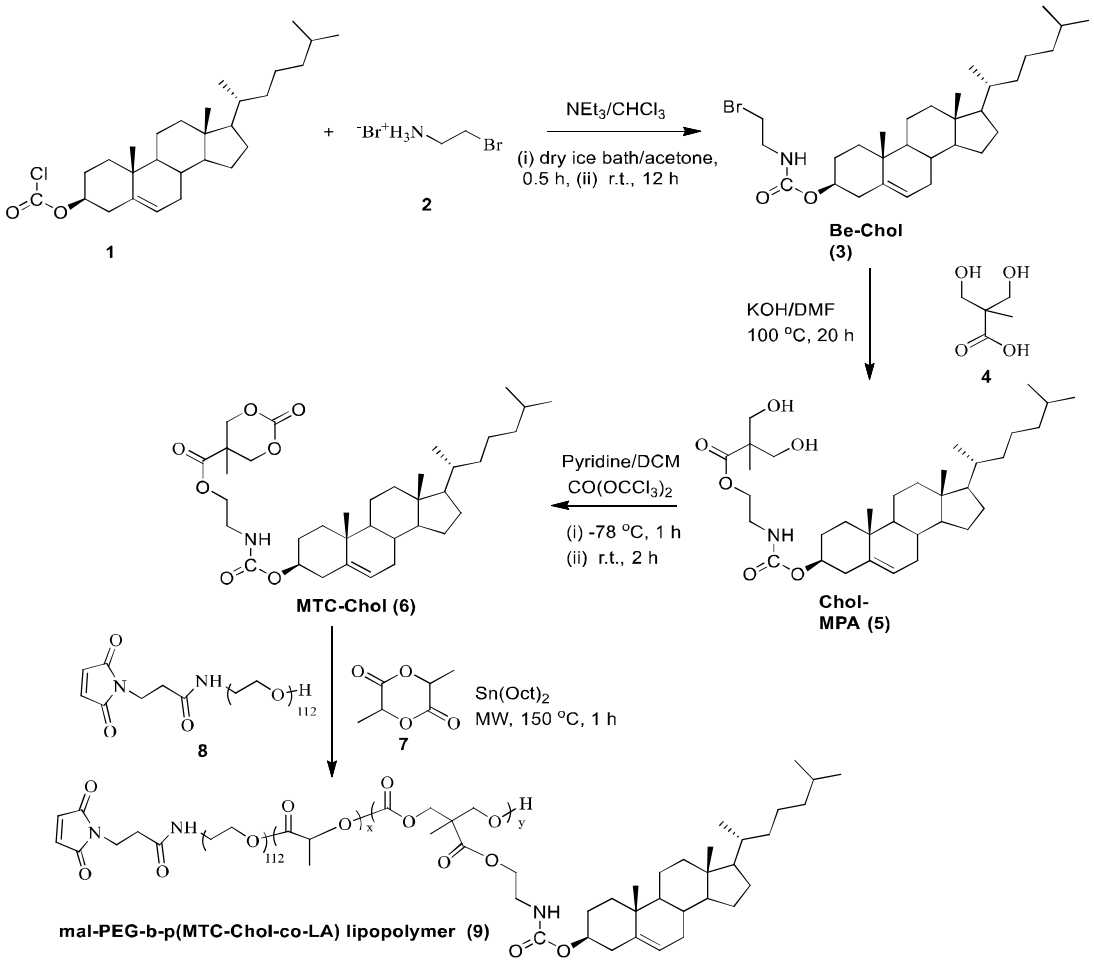

Figure 4.1. Synthetic scheme of mal-PEG-b-p(MTC-Chol-co-LA) lipopolymer **(9)**

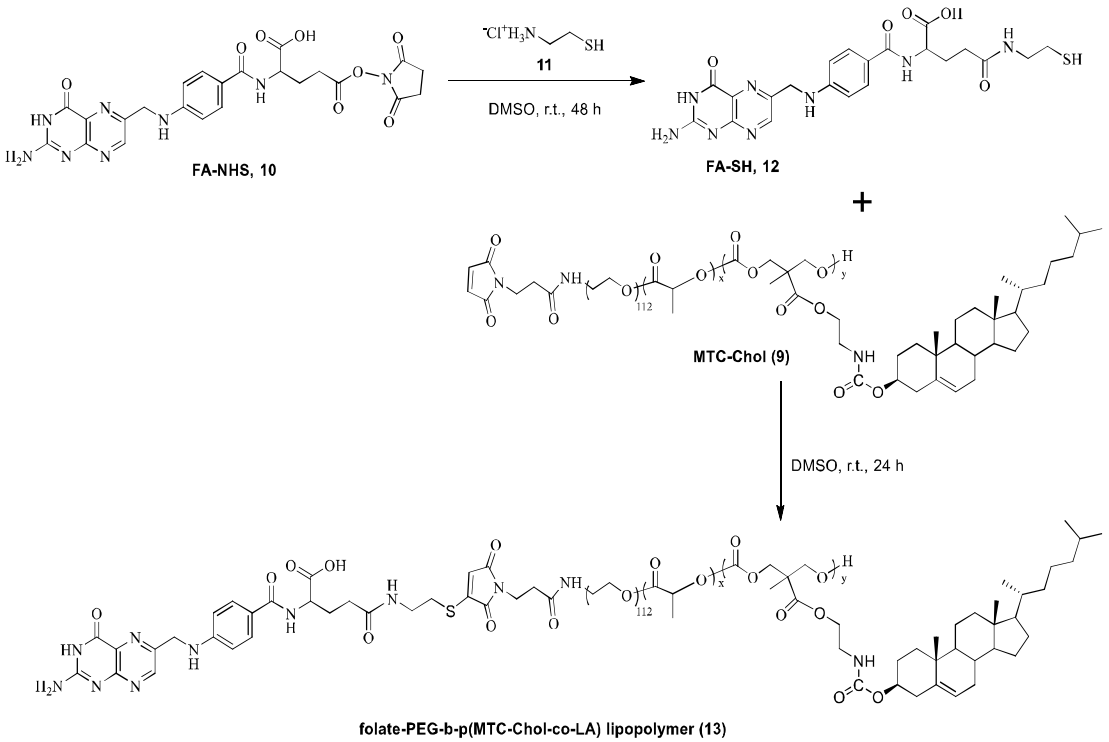

Figure 4.2. Synthesis scheme of folate-PEG-b-p(MTC-Chol-co-LA) lipopolymer (**13**)

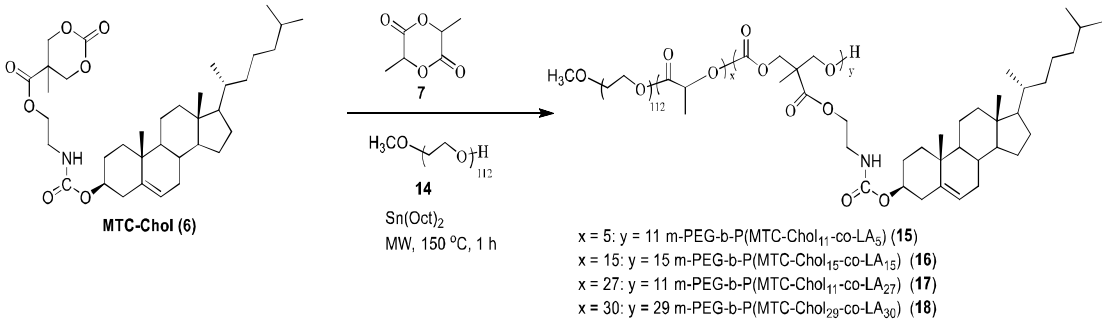

Figure 4.3. Synthetic scheme of mPEG-b-p(MTC-Chol-co-LA) lipopolymers **(15-18)**

chain), DL-lactide and maleimide-PEG-OH as a chain initiator in the presence of stannous octanoate as a catalyst. This above-synthesized lipopolymer was covalently linked to thiol-derivatized folate (folate-SH) to form folate-targeted lipopolymer, folate-PEG-b-p(MTC-Chol-co-LA).

MTC-Chol monomer was synthesized using a reaction scheme as shown in figure 4.1 The synthesis commenced with the preparation of *N*-(2-bromoethyl) carbamoyl cholesterol

(Be-Chol, **3**) from 2-bromoethylamine hydrobromide (**2**) and cholesterylchloroformate (**1**). Be-Chol (**3**) was then reacted with 2-bis(hydroxymethyl) propionic acid (**4**) to afford cholesteryl 2,2-bis(hydroxymethyl)-5-carboxyloyloxy ethyl carbamate (Chol-MPA, **5**), which on ring closure with triphosgene yielded MTC-Chol monomer (**6**) [18]. Thereafter, microwave-assisted ring-opening polymerization of MTC-Chol (**6**) with DL-lactide (**7**) and mal-PEG-OH (**8**) as a macroinitiator in the presence of $Sn(Oct)_2$ yielded maleimide-terminated PEGylated lipopolymer (mal-PEG-b-p(MTC-Chol-co-LA, **9**) (Figure 4.1). Subsequently, the thiol-derivative of folic acid (folate-SH, **12**) was synthesized by reacting active *N*-hydroxysuccinimide ester of folic acid (**10**) with cysteamine (**11**) in the presence of a triethylamine to afford folate-SH product (**12**). Finally, folate-SH (**12**) on reaction with mal-PEG-b-p(MTC-Chol-co-LA) lipopolymer (**9**) in DMSO at room temperature afforded folate-PEG-b-p(MTC-Chol-co-LA) lipopolymer (**13**) (Figure 4.1). FA-SH; 24.24 μmol/g of polymer. Further, a series of lipopolymers, mPEG-b-P(MTC-$Chol_{11}$-co-LA_5) (**14**), mPEG-b-P(MTC-$Chol_{15}$-co-LA_{15}) (**15**) and mPEG-b-P(MTC-$Chol_{11}$-co-LA_{27}) (**16**) were also synthesized by varying ratios of MTC-Chol and DL-lactide with mPEG (methoxy polyethylene glycol) (**14**) following above strategy as shown in synthetic scheme (Figure 4.3**)**

*4.3.1. Preparation and characterization of DTX loaded folate conjugated lipopolymeric nanoparticles (F-DTX-LPN*s**)**

The emulsion solvent evaporation method was adopted to prepare DTX loaded lipopolymeric nanoparticles (DTX-LPNs). Among different lipopolymers, mPEG-b-p(MTC-$Chol_{29}$-co-LA_{30}) showed an encapsulation efficiency of 91.2% with a particle size of 140 ± 7.24 nm (PDI-0.164). DTX loaded nanoparticles prepared using folate-conjugated lipopolymer (F-DTX-LPNs) showed a particle size 115.17 ± 5.74 (PDI- 0.205) nm and encapsulation efficiency of 80.14%. ζ-potential of these nanoparticles was found to be -9.13 ± 0.86 mV (Figure 4.9A).

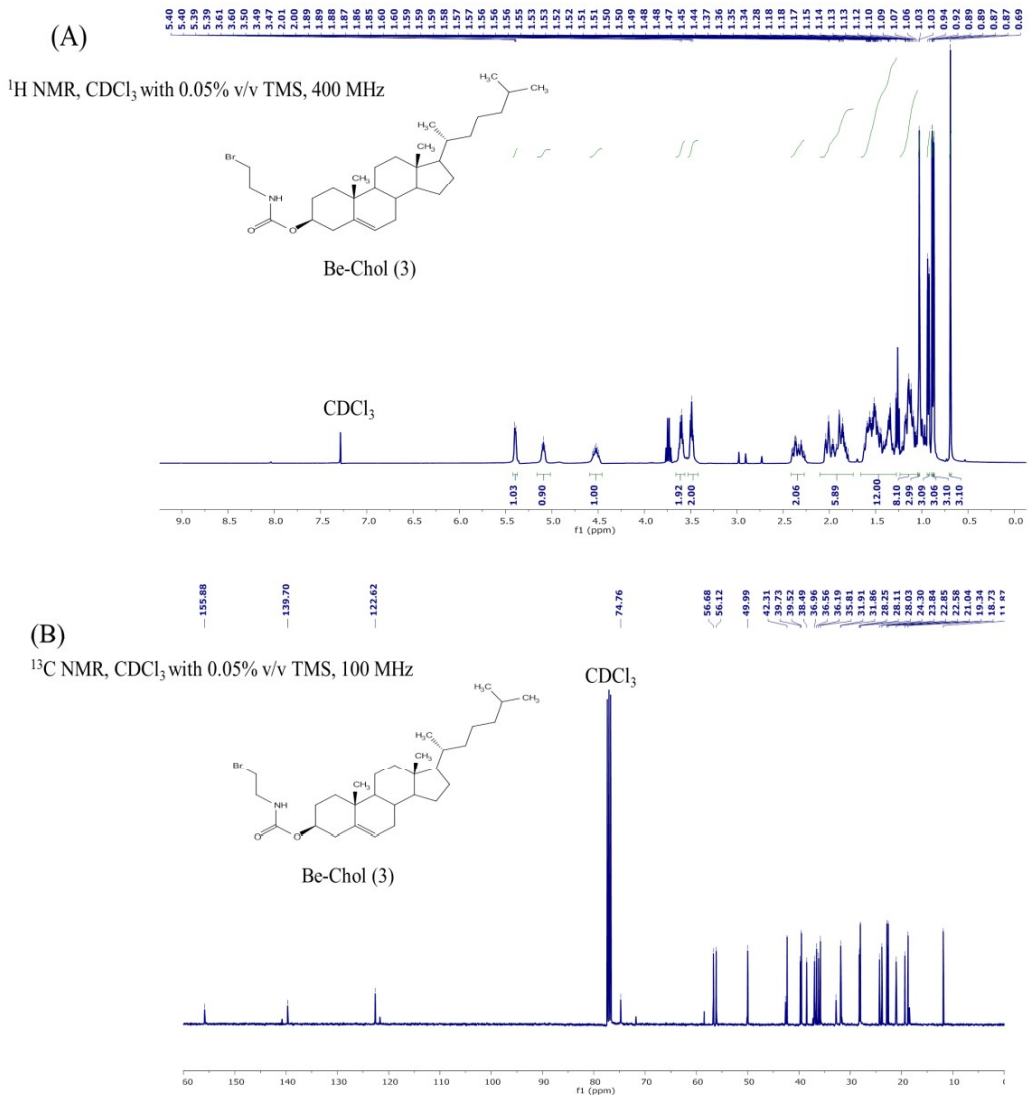

Figure 4.4. (A) ^{1}H NMR and (B) ^{13}C NMR of *N*-(2-bromoethyl) carbamoyl cholesterol (Be-Chol)

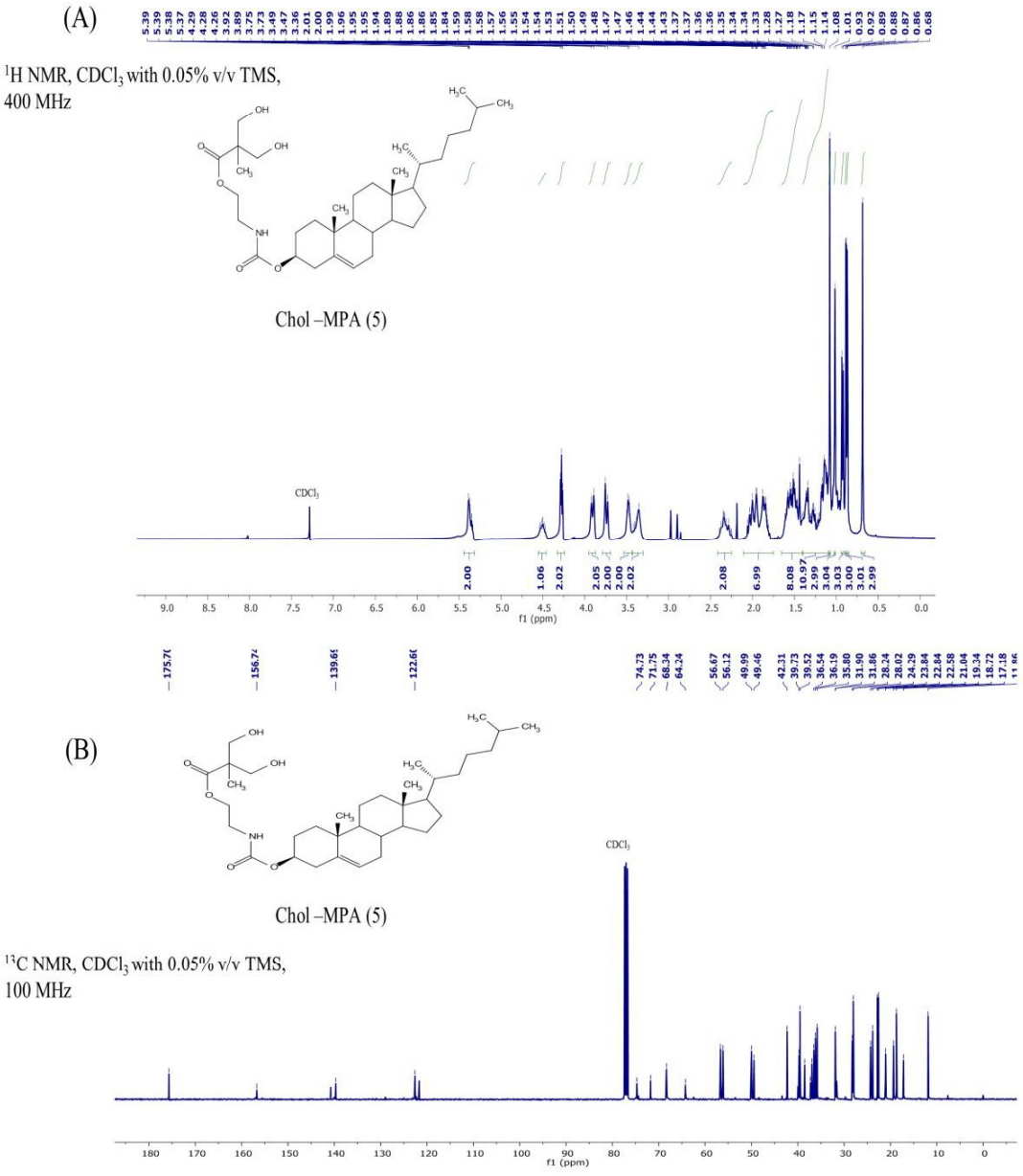

Figure 4.5. **(**A) ^{1}H NMR and (B) ^{13}C NMR of Chol-MPA monomer

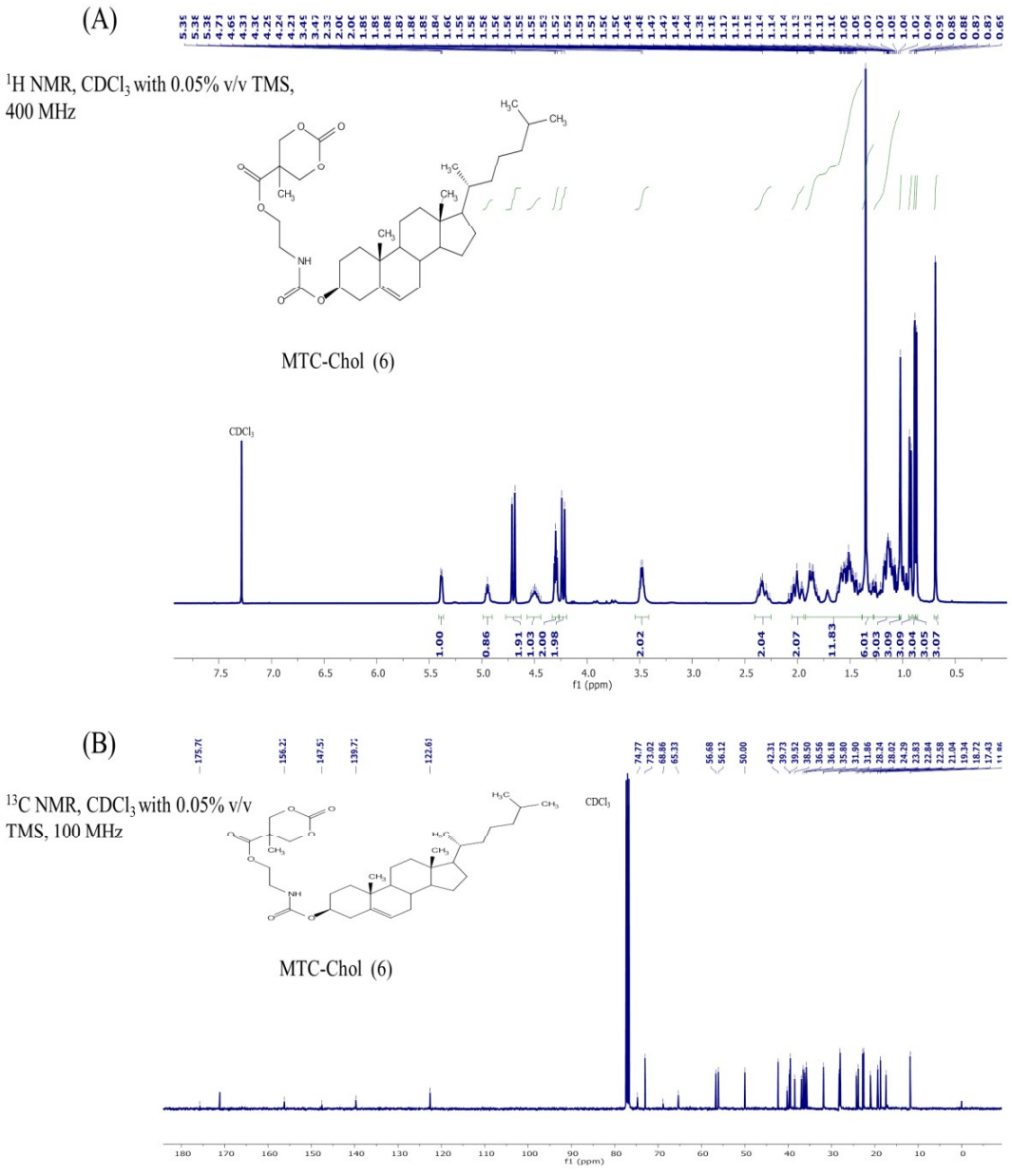

Figure 4.6. (A) ^{1}H NMR and (B) ^{13}C NMR and mass spectrum of the MTC-Chol

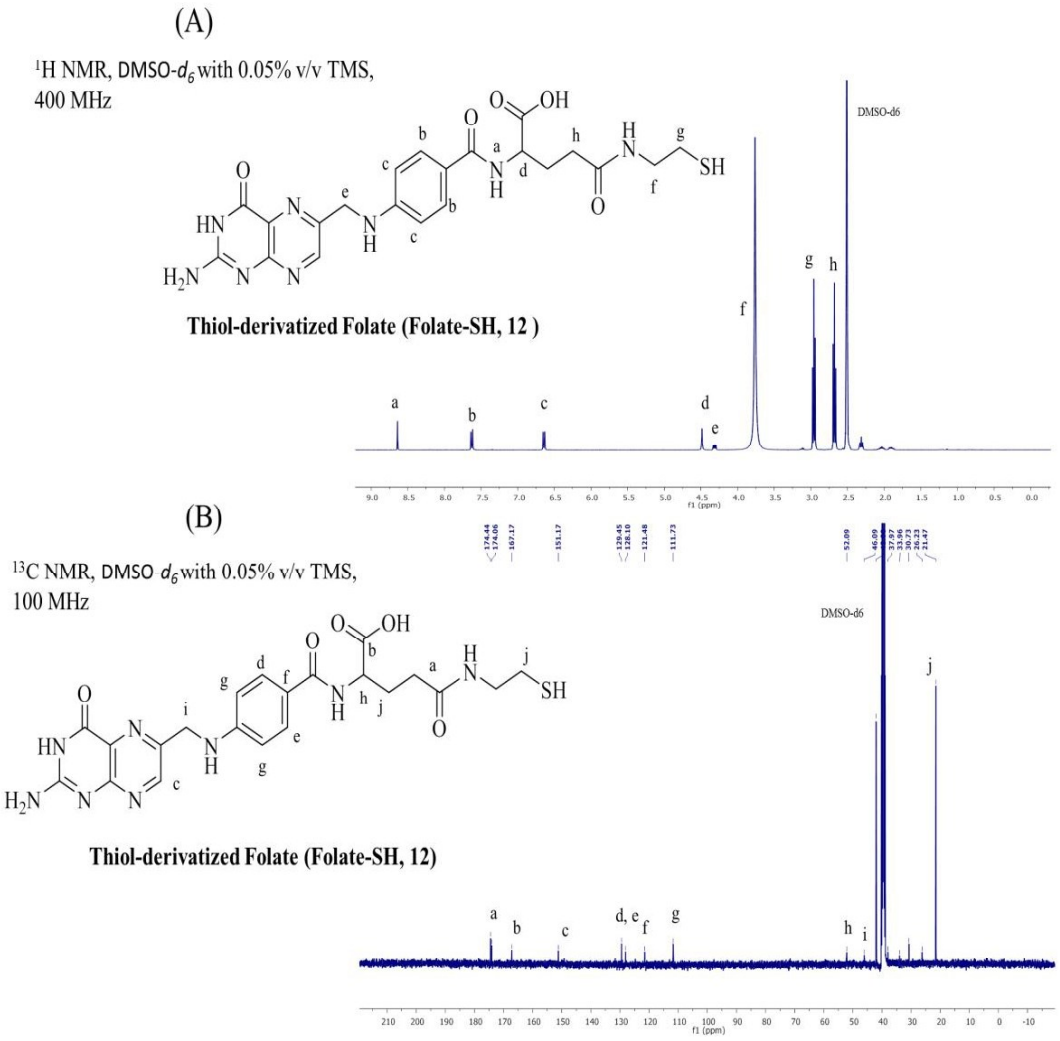

Figure 4.7. (A) ^{1}H NMR and (B) ^{13}C NMR of Thiol-derivatized folate (folate-SH)

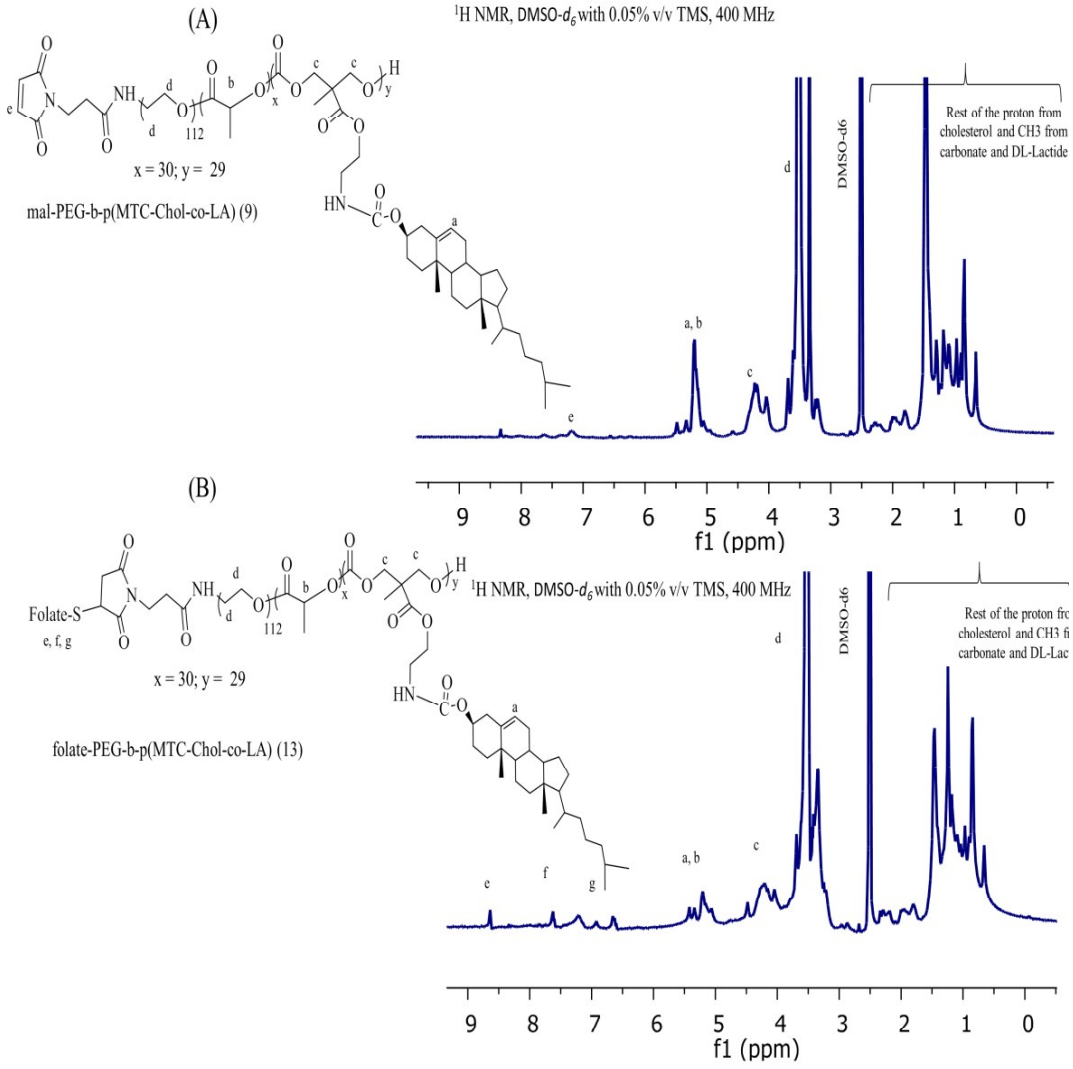

Figure 4.8. ^{1}H NMR of (A) mal-PEG-b-p(MTC-Chol-co-LA) and (B) folate-PEG-b-p(MTC-Chol-co-LA) lipopolymers

Nanoparticles showed good colloidal on-bench stability for at least 5 days without any significant change in the particle size, PDI, and ζ-potential (Figure 4.9C). *In-vitro* drug release studies indicated that the F-DTX-LNPs exhibited a sustained drug release profile of DTX for 7 days in contrast to the free drug, that showed a complete drug release within 4 h (Figure 4.9D).

Table 4.1. Characterization of amphiphilic lipopolymers

Lipopolymers	Lactic Acid (Units)	MTC-CHOL (Units)	Ratio	^{1}H NMR Mn[a](Da)
mPEG-b-p(MTC-Chol$_{11}$-co-LA$_{5}$) (15)	5	11	1:2.2	11927
mPEG-b-p(MTC-Chol$_{15}$-co-LA$_{15}$) (16)	15	15	1:1	15035
mPEG-b-p(MTC-Chol$_{11}$-co-LA$_{27}$) (17)	27	11	2.7:1	13511
mPEG-b-p(MTC-Chol$_{29}$-co-LA$_{30}$) (18)	30	29	1:1	24480
mal-PEG-b-p(MTC-Chol$_{29}$-co-LA$_{30}$) (9)	30	29	1:1	24570
fol-PEG-b-p(MTC-Chol$_{29}$-co-LA$_{30}$) (13)	30	29	1:1	24972

[a]Average molecular weight determined by ^{1}H NMR

3.3.2. Cellular uptake and pathway mediated endocytosis

Cellular uptake studies were performed in MDA-MB-231 breast cancer cells. C6 was loaded in the nanoparticles as a fluorescent hydrophobic model drug to investigate the uptake efficiency and endocytosis process. Efficient intracellular uptake was observed for both the targeted and non-targeted nanoparticles, wherein the folate-targeted nanoparticles showed higher intracellular uptake, as evident from the intense green fluorescence in the cells. Blank nanoparticles and free C6 were kept as controls that showed negligible fluorescence in the cells (Figure 4.10).

In order to delineate the pathway for the endocytosis, MDA-MB-231 cells were also treated with the endocytosis pathway inhibitors before the treatment with the C6 loaded nanoparticles. It was evident from the fluorescence microscopy images that folate-targeted nanoparticles followed the lipid raft mediated intracellular uptake since the treatment of the cell with methyl beta-cyclodextrin (Mβ-CD) (cholesterol-depleting agent, used to disrupt several lipid rafts mediated endocytic pathways), completely inhibited the green fluorescence in the cells while the cells treated with other inhibitors such as chlorpromazine (CPZ; clathrin-dependent pathway inhibitor), mycostatin (deplete cholesterol from membranes and block the formation of caveolae) and amiloride (macopinocytic pathway inhibitor) showed green fluorescence indicating the uptake of these nanoparticles (Figure 4.10) [33, 34].

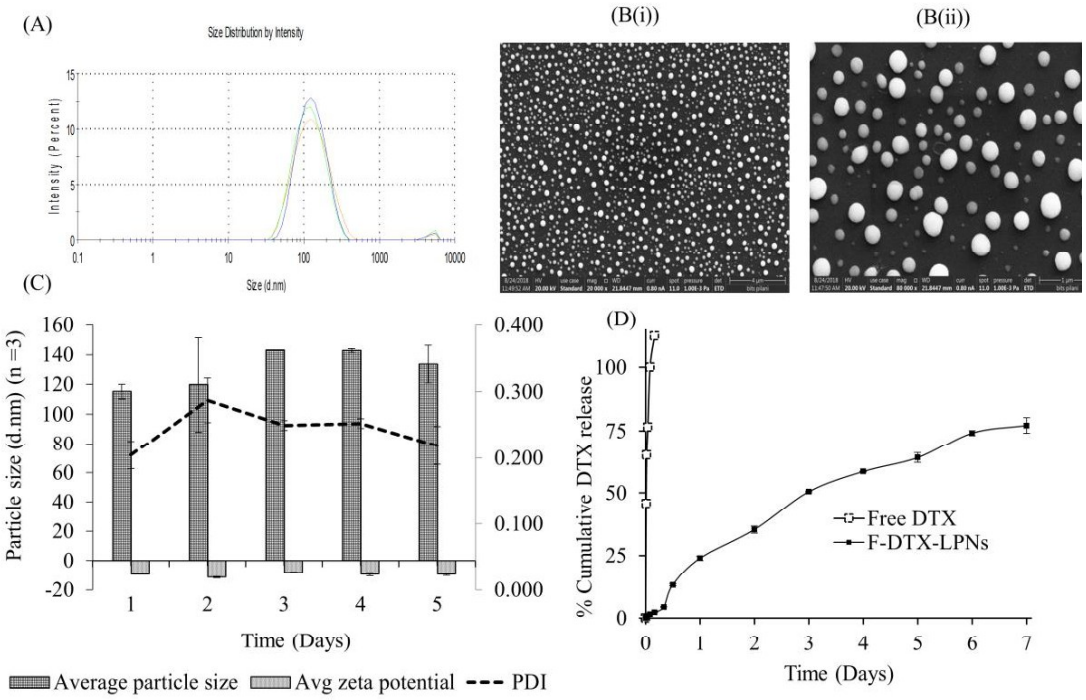

Figure 4.9. (A) Characterization of of docetaxel loaded folate-PEG-b-p(MTC-Chol-co-LA) lipopolymeric nanoparticles (F-DTX-LPNs) obtained by using Malvern Zetasizer (Nano-ZS) (n=3), (B) (i) and (ii) SEM image of spherical F-DTX-LPNs, (C) On-bench stability of F-DTX-LPNs for a period of five days and (D) *In-vitro* drug release from free DTX and F-DTX-LPNs. Each point represents the mean ± SD

4.3.3. In vitro cytotoxicity, apoptosis and gene expression analysis

Cytotoxicity, apoptosis, and gene expression analysis were performed in MDA-MB-231 cells, wherein it was observed that F-DTX-LPNs showed improved cytotoxicity, apoptosis and significant fold-change in expression levels of Bcl-2, BAX and Ki-67 as compared to DTX-LPNs and free DTX. Cell viability of 42.70% was observed with F-DTX.

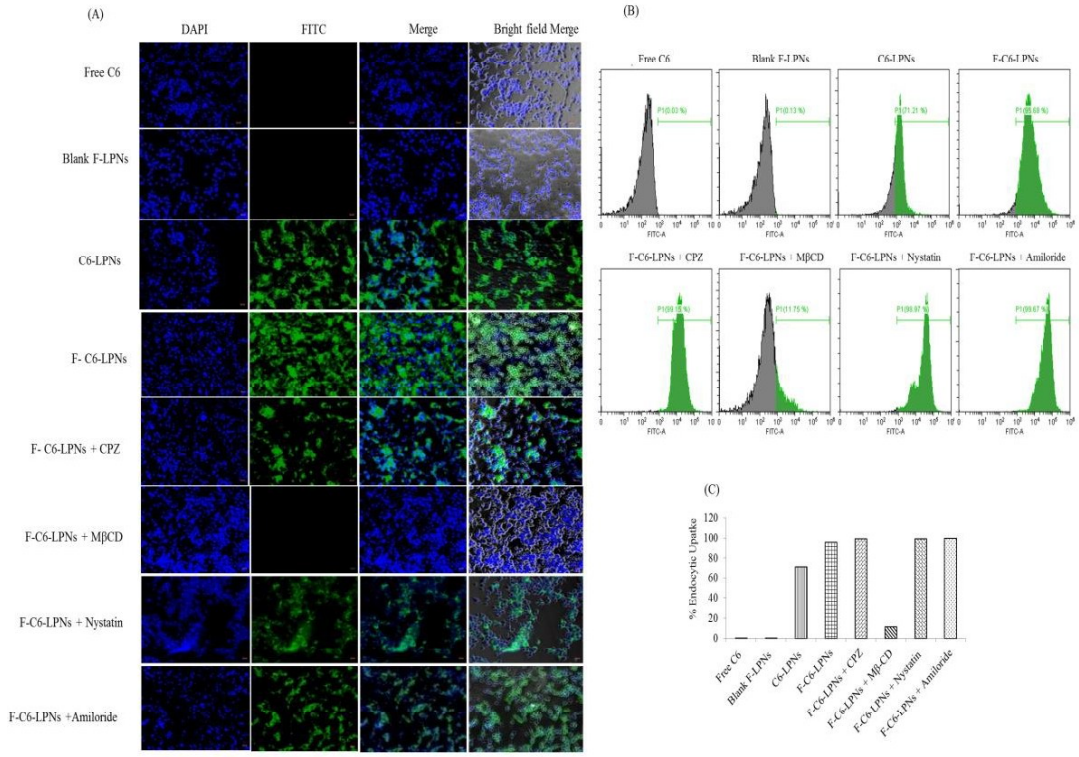

Figure 4.10. Fluorescence microscopic images of MDA-MB-231 cells treated with green fluorescent dye (Coumarin 6) loaded lipopolymeric nanoparticles. Cells were treated with various endocytosis inhibitors followed by treatment with free C6 or C6 loaded targeted or non-targeted LPNs and analyzed under fluorescent microscope. Cells were counterstained with DAPI to stain the nucleus. The scale bar is 100 μm.

LPNs at 50 nM concentration, while DTX-LPNs and the free DTX showed 58.14% and 66.43% cell viability, respectively (Figure 4.11A). Blank folate-targeted nanoparticles did not show any significant change in the cell viability up to a polymer concentration as high as 100 μg/ml (Figure 4.11B). Flow cytometry analysis of apoptosis indicated that F-DTX-

LPNs induced 82.97% apoptosis (64.13% early and 18.84% late stage) while non-targeted lipopolymeric nanoparticles induced 53.80% apoptosis (43.94% early and 9.86% late stage) and free DTX induced 39.13% apoptosis (25.79% early and 13.34% late stage). Blank folate-targeted nanoparticles did not show any apoptosis-inducing potential (Figure 4.11C). The real-time PCR analysis of Bcl-2, Ki67, BAX, and SIRT1 gene was performed to understand the impact on the downstream targets of DTX when it was delivered using folate-targeted nanoparticles. A significant downregulation in the expression of the Bcl-2 and Ki67, whereas the expression of BAX was increased after treatment with the F-DTX-LPNs as compared to the DTX-LPNs and free DTX. Further, the expression of the SIRT1 gene showed no significant difference in the cells treated with the DTX loaded nanoparticles or free DTX (Figure 4.11D).

4.3.4. In vivo pharmacokinetics and bioimaging

The comparative *in vivo* pharmacokinetics of DTX solution (Taxotere®) and F-DTX-LPNs was studied in SD rats at a dose of 10 mg/kg given intravenously. The plasma concentration profiles are shown in (Figure 4.12A), and their pharmacokinetic parameters are shown in Table 4.2 folate-targeted lipopolymeric nanoparticles showed a significantly lower Cmax (μg/mL) (3.20 ± 1.78 versus 8.29±3.48) and higher $AUC_{0-\infty}$ (μg*h/L) (35379.89 ± 8527.41 versus 5515.93 ± 1824.90) as compared to the free DTX. Further, the plasma half-life ($t_{1/2}$) (h) was observed to be 14.64 ± 3.99 h for DTX delivered using folate-targeted nanoparticles (F-DTX-LPNs) as compared to 2.51 ± 2.68 h for free DTX.

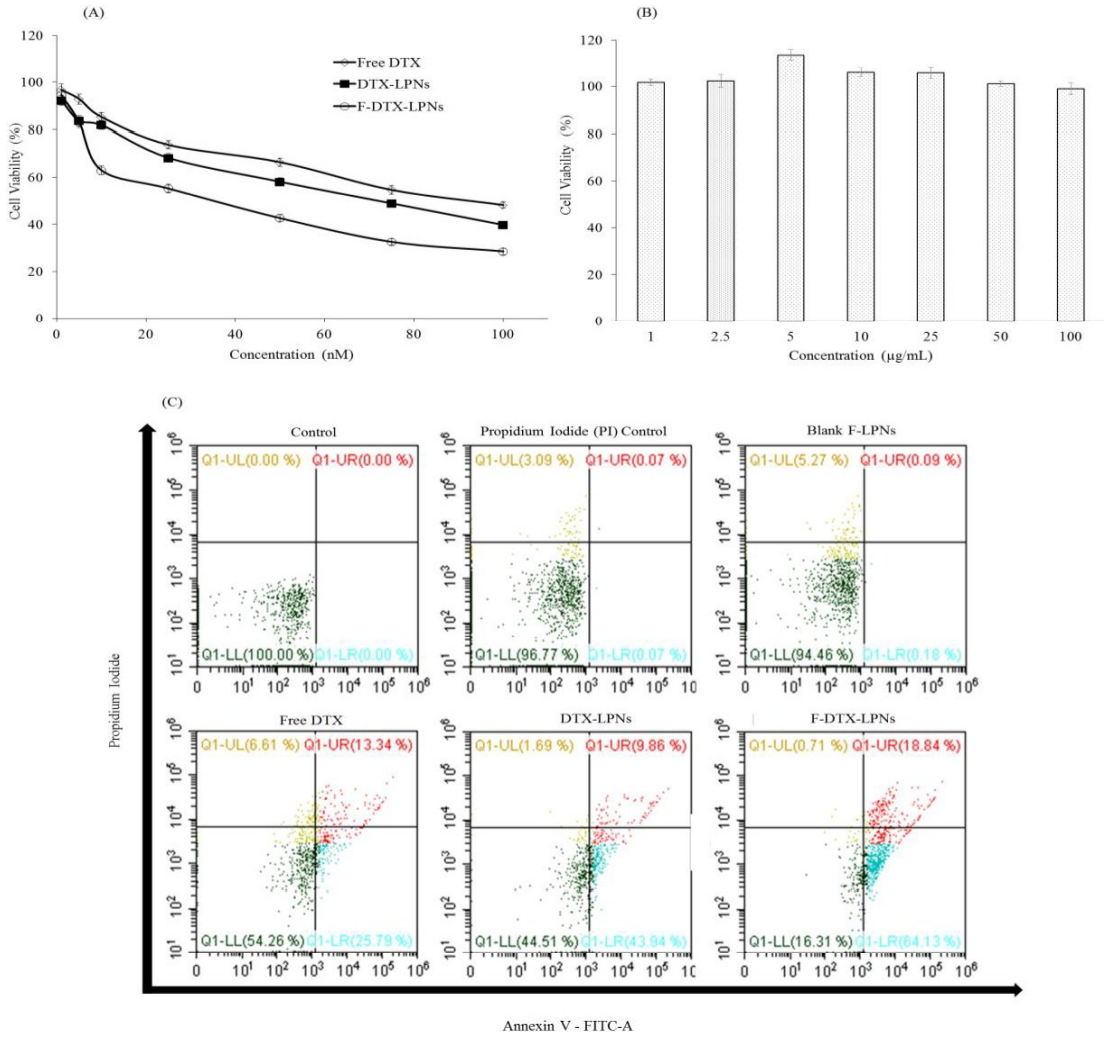

Figure 4.11. *In vitro* cytotoxicity evaluation of (A) free DTX, DTX-LPNs and F-DTX-LPNs, and (B) blank lipopolymeric nanoparticles in MDA-MB-231 breast cells following treatment. DTX and DTX loaded LPNs were tested in the concentation range from 1-50 nM DTX concetration while blank lipopolymeric nanoparticles were tested in the concentration range 1 µg/mL-100 µg/mL (polymer concentration). Each point represents the mean ± SD. Statistical analysis were performed using one way ANOVA followed by Tukey's multiple comparison test. ns: (Non significant), *(Free DTX vs DTX-LPNs), ** (DTX-LPNs vs F-DTX-LPNs) (* $P \leq 0.05$, ** $P \leq 0.01$) was considered as statistically significant) **(C)** Flow cytometric analysis of apoptosis in MDA-MB-231 cell line treated with free DTX, DTX-LPNs and F-DTX-LPNs at a concetration of 50 nM for 48 h. Untreated cells, propidium iodide treated cells and blank LPNs treated cells were kept as controls.

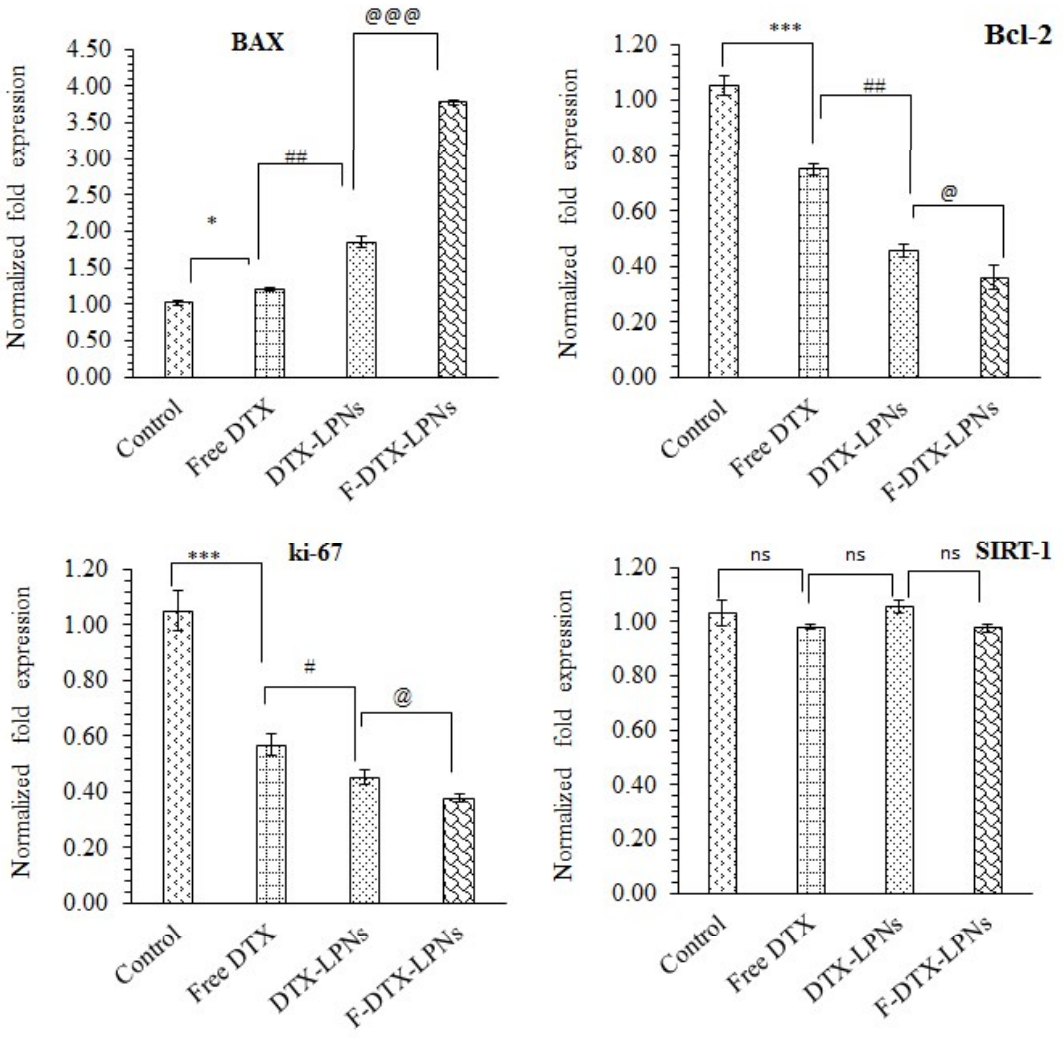

Figure 4.12. Gene expression analysis of BAX, Bcl-2, Ki-67 and SIRT-1 in MDA-MB 231 cells treated with Free DTX, DTX-LPNs and F-DTX-LPNs. Each point represents the mean ± SD (n=3). Statistical analysis were performed using one way ANOVA followed by Tukey's multiple comparison test. ns: (non-significant) ***(Control vs Free DTX), #(Free DTX vs DTX-LPNs) and @(DTX-LPNs vs F-DTX-LPNs). (* $P < 0.05$, ## $P < 0.01$, @@@ and *** $P < 0.001$) was considered as statistically significant.

Biodistribution of DiR loaded nanoparticles (F-DiR-LPNs) was examined by measuring the fluorescence of DiR dye in isolated tissues with excitation and emission wavelength at 745 nm and 788 nm, respectively at different time points. DiR dye has been reported for its unique fluorophore nature as it emits photons at the highest wavelength and itself reduces the risk of auto-fluorescence due to the blood and fur of the mice. (Figure 4.14 B) showed that nanoparticles have biodistributed to different organs with major accumulation in the liver with respect to other organs at 6, 12 and 24 h.

Table 4.2. Pharmacokinetic parameters of free DTX (Taxotere®) and F-DTX-LPNs following intravenous administration at a dose of 10 mg/kg (equivalent to DTX) in *Sprague Dawley* rats. Data are presented as mean ±SD (n=6)

Pharmacokinetic Parameters	Free DTX (Taxotere®)	F-DTX-LPNs
AUC(0-t) (µg*h/L)	5408.00 ± 1624.77	31434.80 ± 5929.47
$AUC_{0-\infty}$ (µg*h/L)	5515.93 ± 1824.90	35379.89 ± 8527.41
MRT(0-t) (h)	0.946 ± 0.33	14.60 ± 3.96
MRT(0-inf) (h)	1.37 ± 1.36	20.20 ± 7.69
Kel	0.48 ± 0.29	0.05 ± 0.012
t1/2kel (h)	2.51 ± 2.68	14.64 ± 3.98
Cmax (µg /mL)	8.29 ± 3.47	3.20 ± 1.78
Tmax (h)	0.108 ± 0.06	0.15 ± 0.17
Cl (mL/h/kg)	502.76 ± 178.42	83.83 ± 23.43
Vss (mL/kg)	464.30 ± 207.34	1150.78 ± 178.87

4.4. Discussion

Cancer remains one of the world's most devastating illnesses, with an increasing number of new cases diagnosed every year. The mortality rate has reduced in recent years due to a better understanding of the disease at the molecular level with improved diagnosis and treatment options. The use of chemotherapeutics forms a pivotal modality for treatment

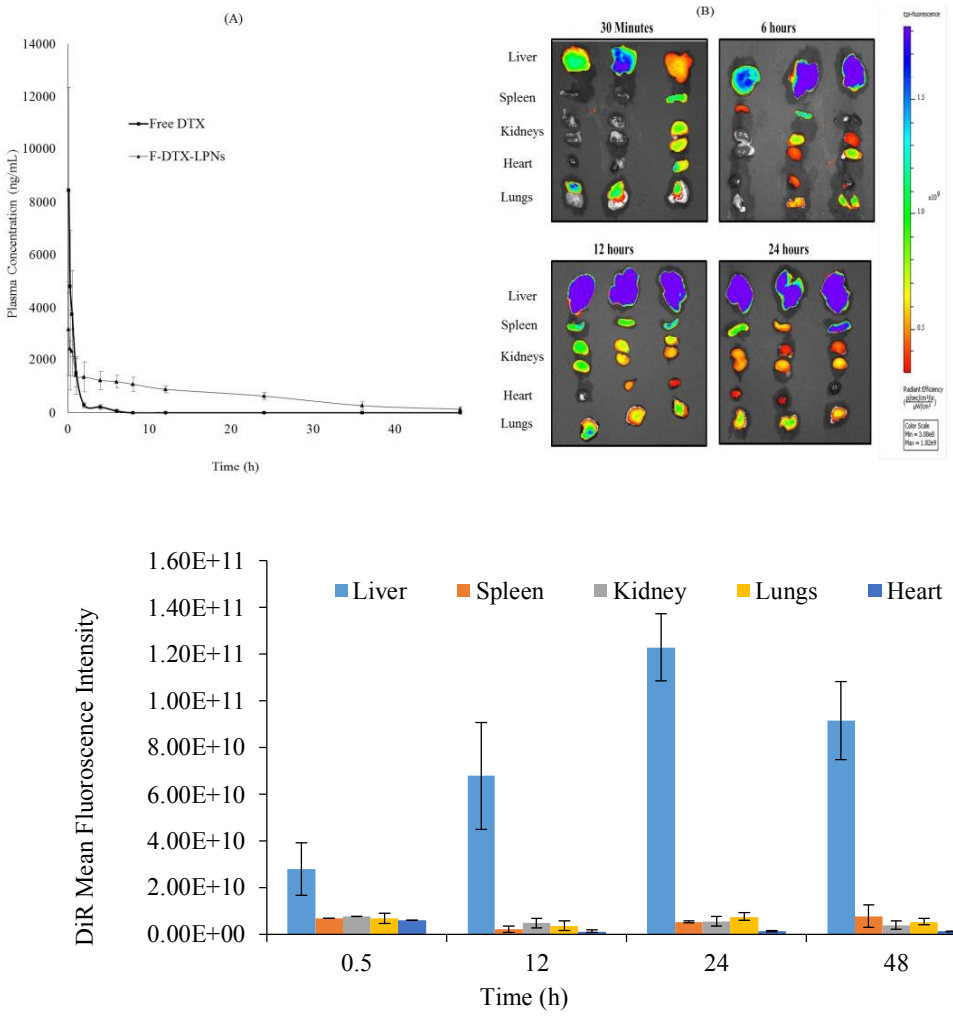

Figure 4.13. Plasma concentration–time profile in SD rats after intravenous (*i.v.*) administration via tail vein injection of free DTX (Taxotere®) and) F-DTX-LNPs at 10 mg/kg dose of DTX. Each point represents the mean ± SD (n=6) and (B) *Ex-vivo* tissue distribution shown by NIRF bio-imaging of F-DiR-LPNs in mice at different time points (n=3) (C) Mean fluorescence intensity (MFI) of DiR dye in different tissues.

with Taxanes, particularly paclitaxel and docetaxel, being used as a first-line treatment option in several cancers at advanced stages [35]. Taxotere® is the first FDA approved marketed formulation of DTX approved for the treatment of metastatic breast cancer. Although the quality of life has improved due to aggressive treatment options in the past few years [36]. However, this formulation suffers from several disadvantages such as non-specific biodistribution, acute hypersensitivity reactions, cumulative fluid retention, neurotoxicity, febrile neutropenia, nail toxicity, myalgia, nasolacrimal duct stenosis, and asthenia. The general consensus on chemotherapeutics, including DTX, is that the results would not further improve if cytotoxic treatment is the only possible treatment option for patients. Research has been envisaged to find new methods to decrease the risks of these chemotherapeutics, along with improving the efficacy. Designing new delivery systems of DTX, in particular, the nanomedicines have provided a decisive lead, as it offers several advantages owing to their nano-size range, passive and active targeting, controlled drug release, and improved pharmacokinetics resulting in a better therapeutic response and decreased toxicity.

In the current study, we have synthesized folate-targeted lipopolymers with cholesterol side chains and used the same for developing DTX loaded nanoparticles. Previously, Wang *et al.* reported the core-shell lipid-polymer hybrid (LPH) nanoparticles containing docetaxel and FTY720 to possess greater serum stability profile, longer shelf life, steady uptake by tumor cells and sustained intracellular drug release [37, 38]. In another study, it has been demonstrated by Liu et al. that docetaxel loaded folic acid conjugate nanoparticles of mixed lipid monolayer and biodegradable polymer core have greater stability, surface properties in favor of endocytic uptake, stealth effect to provide longer circulation of nanoparticles in the plasma and most effective targeting [39]. Werner et al., have also prepared folate targeted biodegradable polymeric nanoparticles containing DTX that are more effective than non-targeted NPs and free drug [40].

Aliphatic polycarbonates and polyesters are an important class of biodegradable polymers and are utilized in biomedical and pharmaceutical applications [41, 42]. A multi-step reaction was used to synthesize a cyclic carbonate monomer with a cholesterol side chain. In the first step, 2-bromoethylamine hydrobromide was reacted with cholesterylchloroformate to obtain *N*-(2-bromoethyl) carbamoyl cholesterol. Cholesterol chloroformate is highly hygroscopic and susceptible to degradation. Thus, the reaction was performed under the inert atmosphere and the product yield was improved by keeping the reaction at chilled condition under dry ice/acetone bath. The crude product obtained was recrystallized to obtain a pure product for next step wherein it was reacted with Bis(hydroxymethyl)propionic acid. The product obtained was purified by column chromatography and subjected to characterization by ^{1}H NMR and^{13}C NMR that indicated the successful synthesis of the product. For cyclization, MPA-Chol was reacted with triphosgene in the presence of a strong base, pyridine, to obtain a cyclic carbonate monomer (MTC-Chol) that was further confirmed by ^{1}H NMR, ^{13}C NMR, and HRMS data indicating the successful synthesis of the monomer.

Ring-opening polymerization was adopted for the synthesis of lipopolymers wherein FDA approved and a safe organometallic catalyst, $Sn(Oct)_2$ was employed [43-45]. The microwave irradiation method was adopted for the polymer synthesis as it provides shorter reaction time and higher percentage yield. It has been previously reported that microwave irradiation polymerization offers several advantages over conventional heating, such as non-contact, instantaneous and uniform heating of the reaction liquor, and highly specific heating with the material selectivity emerging from the wavelength of microwave irradiation that intrinsically excites dipolar oscillation and induces ionic conduction. A large number of polymeric reactions undergo an immense increase in reaction speed under microwave irradiation compared with conventional heating. Significant improvement in yield and

selectivity has been observed as a consequence of the fast and direct heating of the reactants themselves. We have synthesized series of lipopolymers with varying amounts of MTC-Chol and DL-lactide, as shown in Table 4.1. Further, folate conjugated lipopolymer was synthesized using maleimide terminated PEG-OH as a macroinitiator instead of mPEG to obtain Mal-PEG-b-p(MTC-Chol-co-LA). It was further reacted with the thiol derivative of folic acid to obtain folate conjugate lipopolymer. ^{1}H and ^{13}C NMR indicated the successful synthesis of the lipopolymers. Venkataraman et al. have earlier reported the cholesterol functionalized amphiphilic polycarbonate diblock copolymers with two different units of carbonate monomer (i.e., 4 and 11 units) in the hydrophobic block with a total molecular of weight 7500 Da and 11800 Da, respectively [20]. These copolymers were self-assembled to form disc-like micelles and stacked-like morphology. In our study, the molecular weight of the hydrophobic block was kept to 28740 DA with 30 and 29 units of LA and MTC-Chol, respectively, as this will ensure efficient loading of the hydrophobic drug in the nanoparticles.

DTX loaded nanoparticles were prepared using the synthesized lipopolymers by the emulsion solvent evaporation method. It was observed that both lactic acid and cholesterol impact the encapsulation efficiency of DTX. Higher encapsulation efficiencies were observed in the lipopolymer with 30 units and 29 units of lactic acid and cholesterol, respectively. It could be attributed to the increased hydrophobicity of the lipopolymer that enabled a higher payload of the hydrophobic drug. The particle size of DTX loaded nanoparticles was found to be 140 nm ± 7.24 mV with a PDI of 0.164, ensuring the long circulation and targeted delivery of the nanoparticles via EPR effect and folate mediated active targeting respectively. Lee *at al.,* reported the synthesis of PEG and cholesterol-containing polycarbonates based micelles for passive targeted drug delivery of highly hydrophobic molecule, PTX [18]. Their optimal compositions have sub-50 nm size with a narrow size distribution, and exceptional kinetic

stability and better *in vivo* profile. Further, they concluded that these types of delivery nano-carriers have an immense potential for the delivery of highly hydrophobic anticancer drugs with highly rigid molecular structure and conformation [18]. In another study, DIR dye loaded micelles, and PTX loaded micelles comprising cholesterol conjugated polyoxyethylene sorbitol oleate showed 164 nm and 170 nm particle size with better accumulation at the tumor site, reduced tumor growth owing to EPR effect [46]. In this study, the smaller particle size suggests that the lipopolymeric nanoparticles are having the immense potential of effective biodistribution into tumor tissues by evading immune surveillance and circulate for a prolonged period (due to EPR effect). This property makes the nanomedicines more advantageous for parenteral applications as compared to the solutions of the free drug. Further, the lower absolute value of the ζ-potential of drug-loaded nanoparticles also indicates shielding by PEG chains on the copolymer.[47-49] Field-emission scanning electron microscopy showed that the nanoparticles are spherical with narrow particle size distribution that is in agreement with the size determined by the zeta sizer (Figure 4.9).

The *in vitro* drug release profiles of the DTX loaded folate conjugated lipopolymeric nanoparticles showed a controlled release for seven days. The drug release behavior is dependent on the physical retention of the drug and intra-particular pores of the nanoparticles. It was observed approximately 13.25% of DTX was released in the initial 12 h. In the following 48 h, the percent cumulative release reached approximately 35.34% while at the end of 7 days, the percent cumulative release reached up to 77.72%, indicating a controlled and sustained drug release pattern that was due to loading of the drug inside the hydrophobic core. It has been shown that the diffusion of the hydrophobic drugs could dominantly govern the drug release over a shorter period from polymeric nanoparticles. Free DTX solution, equivalent to the Taxotere® formulation prepared *in-house,* was kept as a control in the release studies that showed 100% drug release within 4 h, indicating that the dialysis

membrane does not hinder the DTX release and sink conditions were maintained in the release media [50, 51].

For the investigation of intracellular uptake of the nanoparticles, C6 dye loaded folate-targeted and non-targeted nanoparticles were incubated with the MDA-MB-231 cells. Significantly higher green fluorescence was observed inside the cells treated with the folate-targeted nanoparticles that could be attributed to the presence of folic acid on the surface of the nanoparticles enabling their binding with folate receptors on the cancer cells and ensuring receptor-mediated endocytosis. Earlier reports have also indicated that in the breast cancer cell, especially TNBC cells have higher folate receptor expression. Nahire *et al.* prepared the folate targeted multifunctional polymersomes and analyzed the uptake in two cell line PANC-1 and MCF-7 cells. The endocytic data showed folate containing polymersomes were taken up more effectively as compared to non-targeted polymersomes. Further, the MCF-7 cells showed higher and faster uptake of folate targeted polymersome than PANC-1 cells [52, 53]. In another report, the folate targeted lipid-containing nanoformulation showed 45-fold greater internalization in MDA-MB-231 cells as compared to non-targeted formulations [54, 55]. Further, in our study, uptake of Coumarin6 (C6) loaded folate-targeted nanoparticles was completely inhibited by Mβ-CD, which acts as an inhibitor of lipid raft mediated intracellular uptake by affecting the signaling pathway resulting in cholesterol depletion [56]. Thus it could be concluded that folate-targeted lipopolymeric nanoparticles follow the lipid raft-mediated endocytic uptake.

DTX loaded folate-targeted lipopolymeric nanoparticles showed significantly higher cytotoxicity and apoptotic potential as compared to the non-targeted nanoparticles and free DTX that could be attributed to its higher intracellular uptake. Further, the blank nanoparticles did not show any cytotoxicity and apoptotic effect, suggesting the lipopolymeric nano-carrier biocompatible and non-toxic. Results in this study were in

agreement with previous reports of a folate-targeted formulation containing rhodamine-labeled folate tagged formulation showing increased internalization in MDA-MB-231 cells. In this study, the PTX loaded nanoparticles showed significant toxicity than free PTX. In another study, docetaxel showed a biphasic cytotoxicity curve with respect to drug concentration in MDA-MB231 cells (TNBC cells) [2]. In another study at the end of 48 h, docetaxel loaded chitosan nanoparticle treated with MDA-MB-231 cells at 0.05, 0.5 and 5 μg/mL concentration of DTX showed a reduction in percent cell viability from 46.09, 37.41 and 26.29% for docetaxel loaded nanoparticles and 69.98, 60.78 and 49.59% for free DTX, respectively [57].

Mitochondrial apoptosis pathway is mediated by antiapoptotic proteins such as Bcl-2, which is up-regulated by phosphorylation that lead to breast cancer malignancy. It has been reported that DTX inhibits the Bcl-2 phosphorylation [58]. On the other side, a proapoptotic protein BAX is activated by the linked BH3 protein responsible for induction for apoptosis and inhibition of the antiapoptotic Bcl-2 protein. Upon activation, BAX and BAK form a pore structure in the outer membrane of mitochondria to release cytochrome-c and activate the apoptosome [59]. In our study, we observed a significant downregulation of Bcl-2 and upregulation of BAX gene expression upon treatment with the folate targeted DTX loaded nanoparticles. Further, Ki-67 was observed to be down-regulated. It is an antigen nuclear protein expressed in all the phases of the cell cycle (G1, S, G2 and M phase) except G0 phase [60]. The nuclear expression of this gene is related to the high tumor proliferation, direly correlated to the tumor growth size and increase in the mortality rate of TNBC patients (Figure 4.12) [61].

The *in vivo* pharmacokinetics of DTX from DTX loaded folate-targeted nanoparticles showed a decrease in the C_{max} and an increase in the $t_{1/2,}$ and AUC as compared to the DTX solution (equivalent to marketed Taxotere formulation). This could be attributed to the

reduction of the clearance rate of the drug in the case of folate-targeted nanoparticles due to sustained release and longer circulation of lipopolymeric nanoparticles containing the hydrophobic drug entrapped in the lipophilic core of nanoparticles [62, 63]. Further, the hydrophilic surface of nanoparticles (due to the presence of PEG) could prevent their aggregation and prolong the systematic circulation owing to the stealth effect [64]. A NIRF molecular probe DiR dye was used for *ex vivo* tissue bioimaging of folate targeted lipopolymeric nanoparticles. The unique feature of this dye is that it emits NIR photons that have negligible absorbance minimizing the interference due to the presence of water and hemoglobin during the bioimaging study. The DiR loaded folate conjugated lipopolymeric nanoparticles were retained for a longer duration till 24 h in all tissues. We showed that the fluorescence intensity of DiR loaded nanoparticles started to saturate in the liver within 6 h after *i.v.* administration in mice. The intensity was stronger till 24 h after injection due to the high uptake of these nanoparticles by the liver as obvious due to the elimination of nanoparticles through RES [65]. Moreover, the intensity was observed in all organs after 24 h due to the sustained release of DiR dye from the nanoparticles. These folate targeted lipopolymeric nanoparticles have immense potential and application in drug delivery and improving the efficacy of treatment in a breast cancer model.

4.5. Conclusion

Folate-targeted lipopolymers containing cholesterol sub-units have been synthesized and used for the delivery of a hydrophobic drug molecule, DTX. These lipopolymers were able to efficiently load the drug and showed particle size < 140 ± 7.24 nm with a narrow size distribution, better on-bench stability, and prolonged DTX release profile up to 7 days. Further, folate-targeted nanoparticles showed higher intracellular uptake in MDA-MB-231 cells with improved cytotoxicity and apoptotic potential along with effective inhibition of antiapoptotic genes. *In vivo* pharmacokinetic profile of drug-loaded nanoformulation showed,

blood circulation ($t_{1/2}$) and mean residence time (MRT) had increased as compared to free drug. Tissue biodistribution data demonstrated that F-DTX-LPNs were successfully accumulated at the tissue for longer duration in mice. The folate-targeted nanoparticles could be an efficient drug delivery carrier for improving docetaxel chemotherapy.

References

[1] C. Dumontet, M.A. Jordan, Nature reviews Drug discovery, 9 (2010) 790-803.

[2] H. Hernández-Vargas, J. Palacios, G. Moreno-Bueno, Oncogene, 26 (2007) 2902-2913.

[3] L. Feng, R.J. Mumper, Cancer Letters, 334 (2013) 157-175.

[4] I. Ekladious, Y.L. Colson, M.W. Grinstaff, Nature reviews Drug discovery, 18 (2019) 273-294.

[5] MY. Ho, J.R. Mackey, Cancer Management and Research, 6 (2014) 253-259.

[6] H. Choudhury, B. Gorain, M. Pandey, S.A. Kumbhar, R.K. Tekade, A.K. Iyer, P. Kesharwani, International Journal of Pharmaceutics, 529 (2017) 506-522.

[7] S.M. Rafiyath, M. Rasul, B. Lee, G. Wei, G. Lamba, D. Liu, Experimental Hematology & Oncology, 1 (2012) 10-10.

[8] L.M. Witters, S.M. Santala, L. Engle, V. Chinchilli, A. Lipton, American Journal of Clinical Oncology: Cancer Clinical Trials, 26 (2003) 50-54.

[9] M.J. Ernsting, M. Murakami, E. Undzys, A. Aman, B. Press, SD. Li, Journal of Controlled Release, 162 (2012) 575-581.

[10] W. Tao, X. Zeng, J. Wu, X. Zhu, X. Yu, X. Zhang, J. Zhang, G. Liu, L. Mei, Theranostics, 6 (2016) 470.

[11] C.J. Bowerman, J.D. Byrne, K.S. Chu, A.N. Schorzman, A.W. Keeler, C.A. Sherwood, J.L. Perry, J.C. Luft, D.B. Darr, A.M. Deal, Nano letters, 17 (2017) 242-248.

[12] M. Danquah, T. Fujiwara, R.I. Mahato, Biomaterials, 31 (2010) 2358-2370.

[13] J. Bariwal, V. Kumar, H. Chen, R.S. Bhattarai, Y. Peng, W. Li, RI. Mahato, Journal of Controlled Release, 309 (2019) 231-243.

[14] F. Li, M. Danquah, R.I. Mahato, Biomacromolecules, 11 (2010) 2610-2620.

[15] D. Chitkara, A. Mittal, S.W. Behrman, N. Kumar, R.I. Mahato, Bioconjugate chemistry, 24 (2013) 1161-1173.

[16] S. Sharma, S. Mazumdar, K.S. Italiya, T. Date, RI. Mahato, A. Mittal, D. Chitkara, Molecular pharmaceutics, 15 (2018) 2391-2402.

[17] F. Nederberg, B.G. Lohmeijer, F. Leibfarth, R.C. Pratt, J. Choi, A.P. Dove, R.M. Waymouth, J.L. Hedrick, Biomacromolecules, 8 (2007) 153-160.

[18] ALZ. Lee, S. Venkataraman, S.B.M. Sirat, S. Gao, J.L. Hedrick, Y.Y. Yang, Biomaterials, 33 (2012) 1921-1928.

[19] Y. Wang, S. Gao, W.H. Ye, H.S. Yoon, Y.Y. Yang, Nature Materials, 5 (2006) 791-796.

[20] S. Venkataraman, A.L. Lee, H.T. Maune, J.L. Hedrick, V.M. Prabhu, Y.Y. Yang, Macromolecules, 46 (2013) 4839-4846.

[21] S.F. Atkinson, T. Bettinger, L.W. Seymour, J.-P. Behr, C.M. Ward, Journal of Biological Chemistry, 276 (2001) 27930-27935.

[22] I.R. Kothari, K.S. Italiya, S. Sharma, A. Mittal, D. Chitkara, Journal of Chromatographic Science, 56 (2018) 888-894.

[23] M. G Nava-Arzaluz, E. Piñón-Segundo, A. Ganem-Rondero, D. Lechuga-Ballesteros, Recent patents on drug delivery & formulation, 6 (2012) 209-223.

[24] S. Zhang, H. Gao, G. Bao, ACS Nano, 9 (2015) 8655-8671.

[25] A. Roy, M. Murakami, M.J. Ernsting, B. Hoang, E. Undzys, S.-D. Li, Molecular Pharmaceutics, 11 (2014) 2592-2599.

[26] A.M. Abou-El-Naga, G. Mutawa, I.M. El-Sherbiny, S.A. Mousa, International Journal of Nanomedicine, 13 (2018) 8153.

[27] S. Mazumdar, K.S. Italiya, S. Sharma, D. Chitkara, A. Mittal, International journal of pharmaceutics, 543 (2018) 96-106.

[28] K.S. Italiya, S. Mazumdar, S. Sharma, D. Chitkara, R.I. Mahato, A. Mittal, Nanomedicine: Nanotechnology, Biology and Medicine, 15 (2019) 175-187.

[29] ZC. Soe, J.B. Kwon, R.K. Thapa, W. Ou, H.T. Nguyen, M. Gautam, KT. Oh, H.G. Choi, S.K. Ku, C.S. Yong, J.O. Kim, Pharmaceutics, 11 (2019) 1-17.

[30] K.S. Italiya, S. Sharma, I. Kothari, D. Chitkara, A. Mittal, Journal of Chromatography B: Analytical Technologies in the Biomedical and Life Sciences, 1061-1062 (2017) 49-56.

[31] T. Tan, H. Hu, H. Wang, J. Li, Z. Wang, J. Wang, S. Wang, Z. Zhang, Y. Li, Nature Communications, 10 (2019) 1-17.

[32] S.F. Gad, J. Park, J.E. Park, G.N. Fetih, SS Tous, W. Lee, Y. Yeo, Molecular Pharmaceutics, (2018).

[33] L. Zhang, X. Yang, Y. Lv, X. Xin, C. Qin, X. Han, L. Yang, W. He, L. Yin, Scientific reports, 7 (2017) 46186.

[34] Y. Li, L. Gao, X. Tan, F. Li, M. Zhao, S. Peng, Biochimica et Biophysica Acta (BBA)-Biomembranes, 1858 (2016) 1801-1811.

[35] N. Harbeck, F. Penault-Llorca, J. Cortes, M. Gnant, N. Houssami, P. Poortmans, K. Ruddy, J. Tsang, F. Cardoso, Breast cancer, 2019.

[36] G. Mustacchi, M. De Laurentiis, Drug Design, Development and Therapy, (2015) 5669-5669.

[37] B. Mandal, H. Bhattacharjee, N. Mittal, H. Sah, P. Balabathula, L.A. Thoma, G.C. Wood, Nanomedicine: Nanotechnology, Biology and Medicine, 9 (2013) 474-491.

[38] Q. Wang, H. Alshaker, T. Böhler, S. Srivats, Y. Chao, C. Cooper, D. Pchejetski, Scientific reports, 7 (2017) 1-8.

[39] Y. Liu, K. Li, J. Pan, B. Liu, S.-S. Feng, Biomaterials, 31 (2010) 330-338.

[40] M.E. Werner, J.A. Copp, S. Karve, ND. Cummings, R. Sukumar, C. Li, M.E. Napier, R.C. Chen, A.D. Cox, A.Z. Wang, ACS Nano, 5 (2011) 8990-8998.

[41] Y. Dai, X. Zhang, Polymer Chemistry, 8 (2017) 7429-7437.

[42] K.E. Washington, R.N. Kularatne, V. Karmegam, M.C. Biewer, M.C. Stefan, Wiley Interdisciplinary Reviews: Nanomedicine and Nanobiotechnology, 9 (2017) e1446.

[43] M. Sobczak, Polymer bulletin, 68 (2012) 2219-2228.

[44] P. Lecomte, C. Jérôme, Recent developments in ring-opening polymerization of lactones, in: Synthetic biodegradable polymers, Springer, 2011, pp. 173-217.

[45] A.-C. Albertsson, I.K. Varma, Biomacromolecules, 4 (2003) 1466-1486.

[46] Y. Tian, G. Mi, Q. Chen, B. Chaurasiya, Y. Li, D. Shi, Y. Zhang, T.J. Webster, C. Sun, Y. Shen, ACS applied materials & interfaces, 10 (2018) 43411-43428.

[47] J. Chen, Q. Wu, L. Luo, Y. Wang, Y. Zhong, H.-B. Dai, D. Sun, M.-L. Luo, W. Wu, G.-X. Wang, International Journal of Nanomedicine, 12 (2017) 5745.

[48] J. Nie, W. Cheng, Y. Peng, G. Liu, Y. Chen, X. Wang, C. Liang, W. Tao, Y. Wei, X. Zeng, Drug delivery, 24 (2017) 1124-1138.

[49] X. Gong, Y. Zheng, G. He, K. Chen, X. Zeng, Z. Chen, Drug delivery, 26 (2019) 595-603.

[50] M. Han, Z. Li, D. Bi, Y. Guo, H. Kuang, X. Wang, RSC advances, 6 (2016) 64306-64314.

[51] X.-s. Wang, D.-j. Kong, T.-y. Lin, X.-c. Li, Y. Izumiya, X.-z. Ding, L. Zhang, X.-c. Hu, J.-q. Yang, S.-g. Gao, Acta Pharmacologica Sinica, 38 (2017) 931-942.

[52] J.P. Marshalek, P.S. Sheeran, P. Ingram, P.A. Dayton, R.S. Witte, T.O. Matsunaga, Journal of Controlled Release, 243 (2016) 69-77.

[53] R. Nahire, M.K. Haldar, S. Paul, A.H. Ambre, V. Meghnani, B. Layek, K.S. Katti, K.N. Gange, J. Singh, K. Sarkar, Biomaterials, 35 (2014) 6482-6497.

[54] P. Kumar, P. Huo, B. Liu, Pharmaceutics, 11 (2019) 381.

[55] R. Mukhopadhyay, R. Sen, B. Paul, J. Kazi, S. Ganguly, M.C. Debnath, Pharmaceutical research, 37 (2020) 1-19.

[56] M. Malnar, M. Kosicek, A. Lisica, M. Posavec, A. Krolo, J. Njavro, D. Omerbasic, S. Tahirovic, S. Hecimovic, Biochimica et Biophysica Acta (BBA)-Molecular Basis of Disease, 1822 (2012) 1270-1283.

[57] A. Jain, K. Thakur, P. Kush, U.K. Jain, International Journal of Biological Macromolecules, 69 (2014) 546-553.

[58] S.K. Singh, S. Banerjee, E.P. Acosta, J.W. Lillard, R. Singh, Oncotarget, 8 (2017) 17216.

[59] S. Zinkel, A. Gross, E. Yang, Cell Death and Differentiation, 13 (2006) 1351-1359.

[60] X. Sun, P.D. Kaufman, Chromosoma, 127 (2018) 175-186.

[61] T.A. Martin, L. Ye, A.J. Sanders, J. Lane, W.G. Jiang, Madame Curie Bioscience Database [Internet], (2013).

[62] C. Yang, T. Wu, Y. Qi, Z. Zhang, Theranostics, 8 (2018) 464.

[63] J.-W. Yoo, D.J. Irvine, D.E. Discher, S. Mitragotri, Nature reviews Drug discovery, 10 (2011) 521-535.

[64] E. Blanco, H. Shen, M. Ferrari, Nature biotechnology, 33 (2015) 941.

[65] C.Z. Davis ME, Shin DM. Nanoparticle therapeutics: an emerging treatment modality for cancer. 2008;7(9):771–82, Nat Rev Drug Discov, 7(9) (2008) 771-782.

CHAPTER 5

DEVELOPMENT AND EVALUATION OF FOLATE-TARGETED HYBRID LIPOPOLYMERIC NANOPLEXES CONTAINING DOCETAXEL AND MIRNA-34A

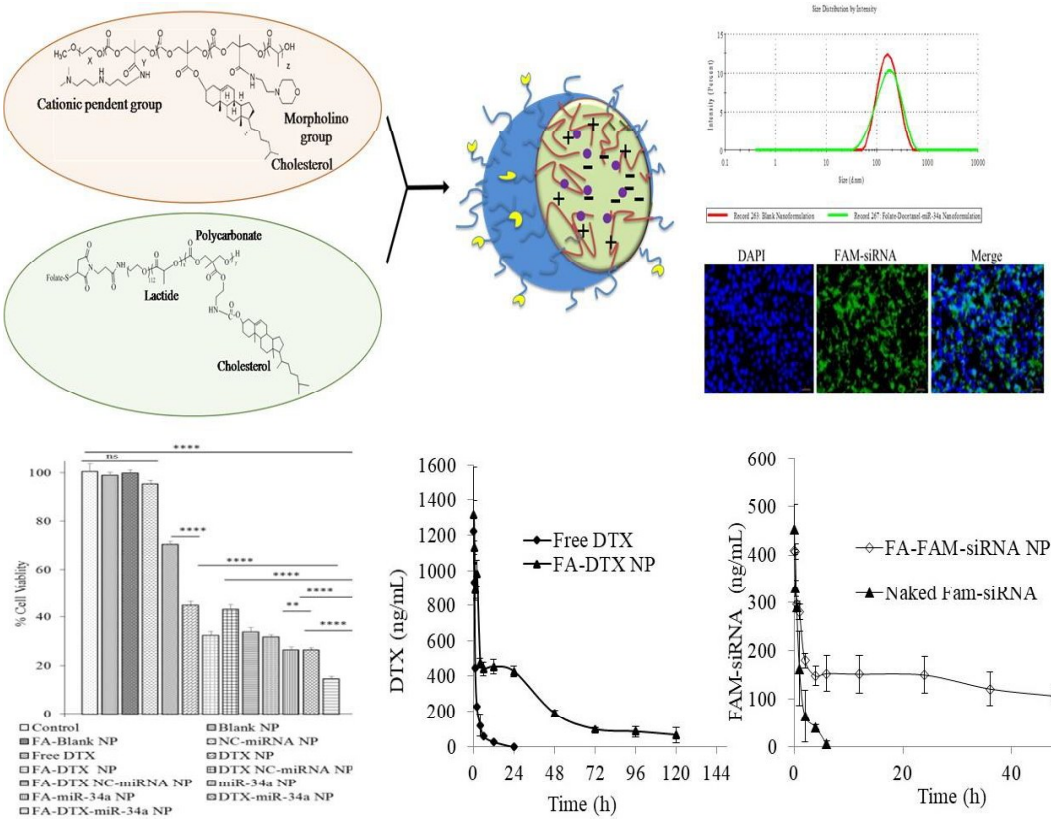

- Introduction
- Experimental section
- Results
- Discussion

5.1. Introduction

Among different types of cancer, breast cancer is the leading cause of death in women [1], and clinically 90% therapies fail due to chemo-resistance, aggressive behavior and metastasis [2, 3]. Several miRNAs that exhibit a significantly important role in breast cancer progression have become an enticing target serving an ancillary approach to other treatment strategies, such as surgery, chemotherapy, and radiotherapy [4]. miRNA profiling of human breast cancer tissues has provided several aberrantly expressed miRNAs in breast cancer. including miRNA-34a (miR-34a) that can antagonize many oncogenic processes by regulating genes involved in the cell cycle (CDK4, CDK6), apoptosis (BCL2, survivin), metastasis (JAG1, WNT1, NOTCH1), cancer cell stemness (CD44, NANOG, SOX2) and oncogenic transcription (E2F3, MYC) resulting into inhibition of tumor angiogenesis, metastasis, cellular proliferation, EMT and promoting cellular apoptosis thereby inhibiting cancer progression [5, 6]. miR-34a is known as a master tumor suppressor and has also been implicated in several other types of cancer as well including, prostate [7], lung [8] and pancreatic cancer [8] apart from breast cancer [9]. Several others, including us, have reported the potential of miR-34a in breast cancer treatment [10]. We have demonstrated the *in vitro* performance of miR-34a containing cationic nanoplexes in 4T1 and MCF-7 cells wherein efficient transfection efficiency along with significant improvement in cytotoxicity and apoptosis was observed. Recently, Fabiana et al. demonstrated enhanced *in vivo* suppression of mammary tumor using synthetic silica dioxide nanoparticles loaded with miR-34a [11].

Experimental evidence also suggests the potential of combining tumor suppressor miRNAs with small molecule drugs [12]. These combinations simultaneously harness the advantage of miRNAs to target multiple downstream oncogenic pathways along with the cytotoxic action of the anticancer drug. Particularly, miR-34a has been shown to improve the efficacy of paclitaxel, docetaxel, gemcitabine and doxorubicin [13]. Among these

chemotherapeutic agents, DTX, a broad-spectrum and highly potent FDA approved chemotherapeutic agent, possesses strong inhibitory activity against many types of human cancers, including metastatic breast cancer, through its tubulin heterodimer stabilizing mechanism, results into impaired mitosis, cell cycle arrest and promotion of apoptosis [14]. However, DTX has poor aqueous solubility, rapid body clearance rate, poor tumor penetration, development of drug resistance (P-gp efflux) and detrimental side effects due to non-specific distribution of the drug to healthy tissues [14]. Further, more than 50% of these patients develop chemo-resistance, aggressive behavior and metastasis, leading to early relapse and shorter survival [15]. Combining DTX with miR-34a could prove to be beneficial as it aims to simultaneously harness the advantage of miR-34a to target multiple downstream oncogenic pathways along with the cytotoxic action of the anticancer drug.

Inspite of the dominant role played by drug-miRNAs combination, their *in vivo* delivery has not been realized owing to their instability in the biological milieu and varied physicochemical properties [16]. miRNAs are polyanionic possessing high water-solubility and molecular weight, limited by poor cellular uptake, lack of tumor specificity and rapid *in vivo* degradation resulting in a rapid body clearance. Thus, for effective clinical translation of miRNA-drug combination therapeutics, a safer, non-toxic and clinically viable carrier systems are required. Ren et al. have used poly(amidoamine) dendrimers for co-delivery of antisense miR-21 (as-miR-21) and 5-FU. The co-delivery of as-miR-21 significantly improved the cytotoxicity of 5-FU and dramatically increased the apoptosis of U251 cells, while the migration ability of the tumor cells was decreased. miR-205 and gemcitabine, a small hydrophilic molecule, were co-delivered using cationic polymers wherein gemcitabine was chemically conjugated to the polymer chain. Core-shell nano-carriers coated by cationic albumin have been previously reported to co-deliver miR-34a and DTX with improved *in vitro* performance and significantly inhibited tumor growth and metastasis in 4T1-tumor bearing

mice model [17]. Further, Sanjun et al. reported cationic solid lipid nanoparticles loaded with miR-34a and PTX that exhibited enhanced efficacy in treating murine B16F10-$CD44^+$ melanoma metastasized to the lungs [18]. Qin et al. verified the synergetic effects of co-delivered miR-200c and DTX using gelatinases-stimuli nanoparticles on inhibition of cancer stem cells with resultant enhancement in the cytotoxicity and *in vivo* tumor suppression due to decrease in the level of class III beta-tubulin and regression of EMT [19].

Most of these nano-carriers are taken inside the cells via endocytic routes that are directed towards the endo-lysosomal pathway, leading to the degradation of payload and thus diminishing their therapeutic effects [20]. Delivering the nanoparticles in cancer cells *via* endocytic routes that bypass the endo-lysosomal pathway can lead to enhancement in the therapeutic performance of DTX and miRNAs is highly desirable. We have shown that folate-targeted cholesterol-grafted lipopolymeric nanoparticles adopted caveolae-mediated endocytic uptake in MDA-MB-231 cells [21]. Further, we demonstrated that nanoplexes composed of cholesterol and morpholine grafted cationic amphiphilic copolymers delivered miR-34a inside the cytosol of 4T1 and MCF-7 cells and demonstrated endo/lysosomal escape [22]. In this chapter, we have designed DTX and miR-34a loaded folate-targeted lipo-polymeric nanoplexes prepared using a combination of two lipopolymers *i.e.* folate-conjugated, cholesterol-grafted lipopolymer and cationic copolymer grafted with cholesterol and morpholine. These nanoplexes were thoroughly characterized for their *in vitro* performance, including transfection efficiency, endocytic uptake mechanism, cytotoxicity, apoptosis, gene expression, *in vivo* pharmacokinetic profile and *in vivo* safety profile in mice.

5.2. Experimental section

5.2.1. Materials

DTX was received as a generous gift sample from Fresenius Kabi, Bad Homburg, Germany. FAM-siRNA was procured from the GeneCust Europe (Luxembourg). LysoTracker

Red DND-99, miRNA-34a-5p mimic and mirVana miRNA Mimic #1 Negative control were purchased from Thermo Fischer Scientific (Massachusetts, USA). Lipofectamine-2000®, Fetal Bovine Serum (FBS), Dulbecco's Modified Eagle Medium (DMEM), Annexin V Alexa fluor 488 conjugate, and TrypLE were purchased from ThermoFisher Scientific (USA). N,N-dimethyldipropylenetriamine (DP), bis(hydroxymethyl) propionic acid, cholesteryl chloroformate (98%), methoxypoly(ethylene glycol) (mPEG, 5000 Da), benzyl bromide, tin(II) 2- ethylhexanoate, 2-bromoethylamine hydrobromide (99%), 4-(2-aminoethyl)morpholine, cholesterol and propidium iodide (PI) was procured from Sigma Aldrich (St. Louis, MO). Maleimide poly(ethylene glycol)-hydroxyl (mal-PEG-OH, 5000 Da) was received from Xi'an Ruixi Biological Technology Co., Ltd (Ruixibio), Shaanxi Province, China. DL-lactide was procured from TCI Chemicals (India) Pvt. Ltd. 3-(4, 5-dimethylthiazol-2-yl)-2,5-diphenyltetrazolium bromide (MTT) was purchased from Sisco Research Laboratories (Mumbai, India). All other chemicals and reagents were of analytical grade and procured from local vendors. Milli-Q water was collected from a Millipore Direct-Q ultra-pure water system (Millipore, Bedford, USA).

5.2.2. Synthesis and characterization of lipopolymers

Both cationic lipopolymer (CCM), mPEG-b-(CB_{65}-{g-Cation $chain_{11}$; g-$chol_{19}$; g-$Morph_6$;}-co-LA_{120}) and folate conjugated lipopolymer (Fol-LP), Folate-PEG-b-p(MTC-$Chol_{30}$-co-LA_{29}) were synthesized as reported in the Chapter 3 and 4, respectively [22]. Briefly, a cyclic carbonate monomer, 2-methyl-2-benzyloxycarbonylpropylene carbonate (MBC) was synthesized by a two-step reaction involving reaction of 2,2- bis(hydroxymethyl) propionic acid and potassium hydroxide with benzyl bromide in dimethylformamide (DMF) at 100 °C for 15 h to yield intermediate product, benzyl 2,2-bis(methylol)propionate that was further reacted with triphosgene in the presence of pyridine. Diblock amphiphilic copolymer, mPEG-

b-p(CB-co-LA), was synthesized by ring-opening polymerization of DL-lactide and MBC in the presence of stannous (II) 2-ethylhexanoate (10 mol % of mPEG) as catalyst and mPEG as chain initiator. mPEG-b-p(CB-co-LA) was further reduced by Pd/C under 45 psi pressure to remove the protective benzyl groups to yield the free carboxyl pendant groups on the polymer backbone. These carboxyl groups were further grafted with N,N-dimethyldipropylenetriamine, cholesterol, and 4-(2- aminoethyl)morpholine using EDC/HOBT coupling chemistry to yield cationic lipopolymer (CCM).

Folate conjugated lipopolymer was synthesized by reacting maleimide-terminated mal-PEG-b-p(MTC-Chol-co-LA) lipopolymer with thiol derivate of folic acid in the presence of trimethylamine. Briefly, a cyclic carbonate monomer with a cholesterol side chain (Cholesteryl 2-(5-methyl-2-oxo-1,3-dioxane-5-carboxyloyloxy) ethyl carbamate (MTC-Chol)) was synthesized using a multi-step reaction. Firstly, N-(2-bromoethyl) carbamoyl cholesterol (Be-chol) was synthesized by reacting 2-bromoethylamine hydrobromide with cholesterylchloroformate in the presence of trimethylamine at -78°C for 30 min using dry ice/acetone bath followed by stirring at RT for another 12 h. In the second step, 2,2-bis(hydroxymethyl) propionic acid and potassium hydroxide were reacted with N-(2-bromoethyl) carbamoyl cholesterol (Be-chol) in dimethylformamide (DMF) at 100 °C for 18 h to yield intermediate product Cholesteryl 2,2-Bis(hydroxymethyl)-5-carboxyloyloxy)ethyl carbamate (Chol-MPA) that was further reacted with triphosgene in the presence of pyridine to obtain MTC-Chol monomer. Further, microwave-assisted ring-opening polymerization of maleimide-PEG with MTC-Chol and DL-lactide was carried out in the presence of stannous (II) 2-ethylhexanoate (10 mol % of mPEG) as the catalyst to obtain mal-PEG-b-p(MTC-Chol-co-LA) lipopolymer.

Further, the thiol derivative of folic acid (folate-SH) was synthesized in two-steps by reacting folic acid (FA) with N-hydroxysuccinimide (NHS) in the presence of N, N'-

dicyclohexyl carbodiimide (DCC) followed by reaction of NHS-Folate with Cysteamine.HCl in the presence of triethylamine at RT for 24 h. The reaction of folate-SH with the mal-PEG-b-p(MTC-Chol-co-LA) lipopolymer yielded folate conjugated lipopolymer. All the intermediates, monomers, and polymers were thoroughly characterized by 1H NMR, and 13C NMR as reported earlier in Chapter 3 and 4.

5.2.3. Preparation and characterization of nanoplexes containing DTX/miR-34a

The nanoplexes containing DTX and miR-34a were prepared using a combination of cationic lipopolymer (P4) and Fol-LP at different ratios (i.e., 4:1, 2:1, 1:1, 1:2 and 1:4) by double emulsion solvent evaporation method. Briefly, an aqueous solution of miR-34a (40 μl; 5 pmol/μL) in DNAse/RNAse free purified water was emulsified in 400 µl of dichloromethane (DCM) containing P4 lipopolymer (3 mg), Fol-LP (6 mg) and DTX (1 mg). The coarse emulsion obtained was probe sonicated (Vibra-Cell tip sonicator, Sonic & Materials, Inc., CT, USA) at 25% amplitude for 30 s on an ice bath. The resulting water-in-oil (w/o) emulsion was added dropwise to DNAse/RNAase free water (2 mL) and probe sonicated at 25% amplitude for 120 s on an ice bath to form a double emulsion (w/o/w). DCM was evaporated under vacuum using a rotary evaporator to form a colloidal dispersion that was further centrifuged at 5000 rpm for 5 min. at 4°C to remove the unentrapped DTX and larger particles. Particle size, polydispersity index and zeta potential of the nanoplexes were determined by Malvern Zetasizer (Malvern Nano ZS).

For determination of DTX content in the nanoplexes, 100 μL of nanoplex dispersion was added to 900 μL of acetonitrile and subjected to heating on a water bath at 60°C till a clear solution was observed followed by bath sonication for 5 min. to extract the DTX. The samples were centrifuged at 17500 rpm for 10 min., and the supernatant was collected, filtered, and analyzed using the developed RP-HPLC method as given in chapter 2.

5.2.4. *In vitro* DTX release and agarose gel retardation assay

To have an estimate of the rate and pattern of DTX release from folate targeted nanoplexes (FA-DTX NP), an *in vitro* drug release study was performed. Briefly, dialysis bag (3.5 KDa cut-off; SnakeSkin® Dialysis Tubing, Thermo Fischer Scientific) containing free DTX or FA-DTX NP were placed in a vial containing release media (30 mL) composed of phosphate buffer saline (100 mM; pH 7.4) containing tween 80 (1% w/v), sodium azide (0.2 % w/v) and ethanol (2% v/v) kept in an incubator at 37ºC/100 rpm. Samples (2 mL) were withdrawn at regular time intervals, i.e., 0.25, 0.5, 1, 2, 4, 8, 12, 24, 48, 72, 96, 120, 144 and 168 h and replenished with the equal quantity of fresh release media at each time point. The cumulative amount of DTX released from the dialysis bag was determined by RP-HPLC method and a graph of percent cumulative DTX release against time was plotted.

Agarose gel retardation assay was performed as given in chapter 3. Briefly, nanoplexes were complexed with the miR-34a at N/P ratio ranging from 1/1 to 64/1 and loaded on an agarose gel (2% w/v) containing 0.5 μg/mL ethidium bromide (EtBr) and run for 30 min at 90 V in 0.5X Tris-Borate-EDTA (TBE) buffer. The electrophoretic mobility of miR-34a was visualized on a Gel Doc™ XR+ Gel Documentation system.

Post complexation release behavior of miRNA from nanoplexes was examined through heparin competition assay. Briefly, freshly prepared miRNA-nanoplexes were incubated with different concentrations of heparin for 30 minutes at 37° C temperature. Thereafter, samples were loaded on 2% agarose gel to evaluate the release of miRNA from nanoplexes. Herein, naked miRNA and miRNA-nanoplexes without heparin were taken as control.

5.2.5. Cell culture studies

4T1 cells were obtained as a kind gift from Dr. Avinash Bajaj (Associate Professor, Regional Centre for Biotechnology, Haryana (NCR Delhi), India) and MDA-MB-231 breast

cancer cells were purchased from National Centre for Cell Science, Pune, India. Cells were cultured in Dulbecco's Modified Eagle's Medium (DMEM) supplemented with 10% fetal bovine serum (FBS; HyClone, Logan, UT) and 1% antibiotics (100 U/mL penicillin/streptomycin) and kept in an incubator at 37°C/ 5% CO_2.

5.2.6. Gene transfection efficiency and endocytic uptake mechanism

In vitro transfection efficiency of the developed nanoplexes was performed in MDA-MB-231 and 4T1 breast cancer cells as per the reported procedure [22]. Briefly, cells were seeded at a cell density of 1×10^5 cells/well in 6-well cell culture plates and allowed to adhere overnight. After 24 h, culture media was replaced with Opti-MEM medium, and cells were incubated for 1 h followed by treatment with folate targeted and non-targeted FAM-siRNA loaded nanoplexes. The naked FAM-siRNA and FAM-siRNA/Lipofectamine-2000® lipoplexes were kept as a negative and positive control, respectively. After 4 h treatment, cells were washed with PBS, trypsinized, and centrifuged at 2000 rpm for 5 min at 4ºC. Cells were then resuspended in cold PBS (0.5 mL) followed by flow cytometric analysis using Cytoflex (Beckman Coulter, USA). The FAM-siRNA was excited with an argon laser 488 nm, and fluorescence was measured at 525 nm. Analysis of data was carried out using CytExpert version 2.0.

Further, to elucidate endocytic uptake mechanism of developed nanoplexes in both cell lines, cells were pretreated with different endocytic inhibitors including methyl-β-cyclodextrin (Mβ-CD; 3 mM), mycostatin (MST; 27 μM), chlorpromazine (CPZ; 10 μM) and amiloride (AMD; 10 μM) for 30 min followed by treatment with folate targeted FAM-siRNA nanoplexes (FA-FAM-siRNA NP) for 4 h and analyzed using flow cytometry and fluorescence microscopy. For flow cytometric analysis, the same procedure as given above was followed. For fluorescence microscopy, the cells were washed thrice with PBS, fixed using

paraformaldehyde solution (4% v/v) for 10 min. followed by counterstaining with DAPI (for nucleus labeling; 300 nM) and observed under an inverted fluorescence microscope (Vert. A1 ZEISS Axiocam 305 color).

5.2.7. In vitro cytotoxicity studies

MDA-MB-231 or 4T1 cells were seeded in 96-well cell culture plates ($5x10^3$ cells/well) and allowed to adhere for 24 h. After 24 h, media was replaced with the fresh media containing free DTX, non-targeted DTX nanoplexes (DTX NP), folate targeted DTX nanoplexes (FA-DTX NP), non-targeted negative control miRNA nanoplexes (NC-miRNA NP), folate-targeted negative control miRNA nanoplexes (FA-NC-miRNA NP), non-targeted miR-34a nanoplexes (miR-34a NP), folate targeted miR-34a nanoplexes (FA-miR-34a NP), non-targeted DTX/Negative control miRNA nanoplexes (DTX-NC-miRNA NP), folate targeted DTX/Negative control miRNA nanoplexes (FA-DTX-NC-miRNANP), non-targeted DTX/miR-34a nanoplexes (DTX-miR-34a NP) and folate targeted DTX/miR-34a nanoplexes (FA-DTX-miR-34a NP). miR-34a or negative control miRNA were used at an equivalent concentration of 20 pmol while DTX was used at a concentration of 25 nM, wherever applicable. Blank nanoplexes (Blank NP and FA-Blank NP), folate targeted and non-targeted negative control (NC) nanoplexes and untreated cells were kept as controls. After 48 h, the cells were washed with PBS, and FBS free media (120 μL) containing 3-(4,5-dimethylthiazol-2-yl)-2,5-diphenyltetrazolium bromide (MTT) dye (5 mg/mL) was added to cells. After 5 h, cells were washed with PBS, and formed formazan crystals were dissolved in DMSO (150 μL) followed by measurement of absorbance at 560 nm with a correction for cell debris by subtracting the absorbance at 630 nm using microplate reader (BioTek Epoch) [23]. The percentage cell viability was determined using the following formula:

$$\%\, Cell\ viability = \frac{Absorbance\ of\ sample\ wells}{Absorbance\ of\ control\ wells} \times 100$$

5.2.8. Apoptosis assay

Briefly, MDA-MB-231 or 4T1 cells ($1x10^6$ cells/well) were seeded in a 6-well cell culture plate and incubated for 24 h. The media was replaced with fresh media containing free DTX, DTX NP, FA-NC-miRNA NP, DTX-NC-miRNA NP, FA-DTX-NC-miRNA NP, DTX-miR-34a NP, and FA-DTX-miR-34a NP. After 24 h, the cells were washed with PBS, trypsinized, centrifuged at 1700 rpm/5 min. at 4ºC, and resuspended in 1X binding buffer. Annexin V-FITC conjugate and propidium iodide were used to detect and quantify the cellular apoptosis using flow cytometry (Cytoflex, M/s Beckman Coulter, USA) as per the supplier's protocol and data were interpreted using CytExpert version 2.0 (Beckman Coulter software) [22].

5.2.9. Gene expression study

Briefly, MDA-MB-231 or 4T1 cells ($1x10^6$ cells/well) were seeded in a 6-well cell culture plates and allowed to adhere for 24 h followed by treatment with free DTX, DTX NP, FA-DTX NP, FA-NC-miRNA NP, miR-34a NP, FA-miR-34a NP, DTX-miR-34a NP and FA-DTX-miR-34a NP. At the end of treatment, cells were washed, trypsinized and total RNA was extracted using PureLink® RNA Mini Kit (Ambion®, ThermoFisher Scientific) according to the manufacturer's protocol. Concentration and purity of RNA were quantified by Nanodrop (Simplinano™ spectrophotometer, Biochrom, Harvard Bioscience. Inc.). cDNA was synthesized from the RNA using GeneMax™ First Strand cDNA Synthesis Kit (PUREGENE, Genetix Biotech Asia, Pvt. Ltd.) on a thermal cycler (Bio-Rad; Hercules, CA) according to the manufacturer's protocol. The cycle threshold (CT) values were normalized to the housekeeping gene (GAPDH) and the fold change was calculated using the delta CT method. Gene quantification was performed using Maxima SYBR Green/ROX qPCR Master Mix (2X) assay

kit (Thermo Fisher Scientific Baltics UAB, Vilnius, Lithuania). Real-time PCR primers were designed for BCL2, BAX, ki67, and GAPDH, as given below [24].

For 4T1;

ki67: Forward sequence- 5'-ccaaccaaggacagttaaggag-3'

Reverse sequence- 5'-ctgtgggctcttcttttacacc-3'

BCL2: Forward sequence- 5'-ttgtaattcatctgccgccg-3'

Reverse sequence- 5'-aatgaatcgggagttggggt-3',

BAX: Forward sequence- 5'- tctttgtggctggagtcctc-3'

Reverse sequence- 5'-cattcccacccctcccaata-3'

For MDA-MB-231 cells;

ki67: Forward sequence- 5'-tctgacctgacagacctcaaga-3'

Reverse sequence- 5'-gtgtgtgttggggtgtttattg-3'

BCL2: Forward sequence- 5'-gtccaagaatgcaaagcaca -3'

Reverse sequence- 5'-ccggttatcgtaccctgttc-3',

BAX: Forward sequence- 5'-gctggacattggacttcctc-3'

Reverse sequence- 5'-ctcagcccatcttcttccag-3'

GAPDH: Forward sequence- 5'-tggcttgtgctgtaagatcg'-3

Reverse sequence 5'-aatctccactttgccactgc-'3

5.2.10. In vivo plasma pharmacokinetics of FAM-siRNA and DTX

All experimental procedures were conducted according to CPCSEA guidelines and were duly approved by the Institutional Animal Ethics Committee (IAEC) of BITS-Pilani (Protocol No. IAEC/RES/27/3 and IAEC/RES/27/4). *Swiss albino* mice (female; 8–10 weeks, 20-25 g) were procured from the Central Animal Facility, BITS-Pilani (Pilani, Rajasthan India)

and acclimatized for 1 week before initiation of the experiment in well-ventilated plastic cages under standard laboratory conditions with 12 h dark and 12 h light cycle, and fed with standard diet *ab libitum.*

Animals were injected with the formulations intravenously *via* tail vein at an equivalent dose of 10 mg/kg DTX and 1 mg/kg of FAM-siRNA. Blood samples were withdrawn from retro-orbital plexus into disodium EDTA containing microcentrifuge tubes at predetermined time points, centrifuged at 6500 rpm at 4°C for 15 min. to collect plasma and was subsequently stored at -80°C until further analysis. [25].

Protein precipitation method was used for extracting FAM-siRNA from the mice plasma, as reported earlier [26]. Briefly, plasma (40µL) was spiked with working standard solution FAM-siRNA (10µL) to obtain concentrations ranging from 70 to 1000 ng/mL. For extraction, sodium dodecyl sulphate (0.1% in PBS; 100µL) was added followed by vortexing and incubation at 65°C for 10 min. Further, methanol (150µL) was added to the samples, vortexed, incubated at 65°C for 10 min. followed by centrifugation at 13000 RPM for 15 min/4°C. The clear supernatant was collected (100 μL) and analyzed by spectrofluorimetry (Fluorolog^{TM} HORIBA Scientific) at a slit width of 5 mm by exciting FAM-siRNA at 485 nm using xenon arc lamp and its emission was recorded at 518 nm [27]. A protein precipitation method was used for extracting DTX from the mice plasma, and bioanalysis was carried out using the bioanalytical method outlined in chapter 2.

Concentration-time profiles of Fam-siRNA and DTX in plasma were plotted, and analysis was performed by a non-compartmental model approach using Phoenix 8.0 WinNonlin (Pharsight Corporation, USA). Various pharmacokinetic parameters including C_0, drug concentration in plasma at t=0; $t_{1/2}$, elimination half-life; AUC_{0-t}, area under the curve from zero to the last time point; $AUC_{0-\infty}$, area under the curve from zero to infinity; V_z, apparent

volume of distribution, CL, clearance, and MRT, mean residence time were determined as reported earlier [28].

5.2.11. Acute toxicity evaluation of nanoplexes

The experimental protocol was duly approved by the Institutional Animal Ethics Committee (IAEC) of BITS-Pilani (Protocol No: IAEC/RES/27/4) and was conducted as per CPCSEA guidelines. Female *swiss albino* mice weighing 25 ± 5 g were used for testing acute toxicity of nanoplexes after intravenous administration *via* tail vein at an equivalent cationic CCM lipopolymer dose of 10 mg/kg, 50 mg/kg and 100 mg/kg after overnight fasting. After subjecting to treatments, animals were returned to their home cages and observed for 10 min at 2 h interval for a total duration of 24 h. Various parameters were recorded viz., fur, skin color, eye color, tears, locomotion activity, abnormal stereotypy, respiratory deficit, food intake, water intake, seizures, and death. At the end of the observational study, whole blood was collected from retro-orbital plexus, and various hematological and biochemical parameters were evaluated. The hematological parameters evaluated include hematocrit and hemoglobin value, total red blood cells count (TRBC), total leukocytes count (TLC), differential leucocytes count (DLC), total platelets count (TPC), packed cell volume (PCV), mean corpuscular volume (MCV), mean corpuscular hemoglobin (MCH) and blood sugar level. Biochemical parameters examined were total protein, albumin, serum creatinine, serum alkaline phosphate, bilirubin, urea, cholesterol, and triglyceride. Additionally, liver and kidney function tests were also conducted. Animals were sacrificed, and all the vital organs (lungs, heart, kidney, liver, and spleen) were collected for histopathological examination [29].

5.2.12. Statistical analysis

Data were presented as the mean ± standard deviation or standard error of the mean. The difference between any two or more groups was determined by analysis of variance

followed by Tukey's multiple comparison test. (*P ≤ 0.05, **P ≤ 0.01, ***P ≤ 0.005 and ****P ≤ 0.001) was statistically significant.

5.3. Results

5.3.1. Synthesis and characterization of lipopolymers

Both folate conjugated lipopolymer (Fol-LP), folate-PEG-b-p(MTC-Chol$_{29}$-co-LA$_{30}$) and cationic amphiphilic lipopolymer (CCM), mPEG-b-(CB$_{65}$-{g-Cation chain$_{11}$; g-chol$_{19}$; g-

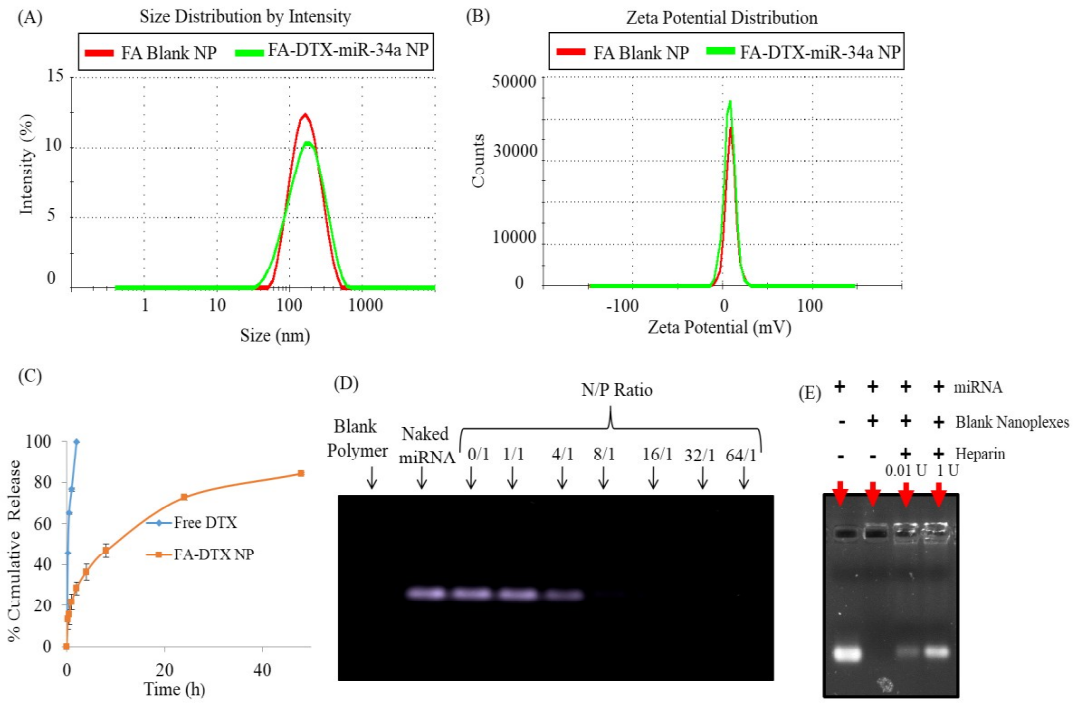

Figure 5.1. (A-B) Comparative particle size distribution and zeta potential of FA-DTX-miR-34a NP and blank NP obtained using Malvern zetasizer, (C) *In vitro* drug (DTX) release from FA-DTX-NP and Free DTX (Taxotere®), (D) Gel retardation assay of miRNA-34a and folate targeted nanoplexes and E) Heparin competition assay

Morph$_6$;}-co-LA$_{120}$) were synthesized as reported earlier and characterized using 1H and 13C NMR to confirm the structure and molecular weight (Chapter 3 and Chapter 4). The molecular weight of this Fol-LP and CCM were found to be 24972 and 35436 Da, respectively.

5.3.2. Characterization of DTX/miR-34a Nanoplexes

Nanoplexes were prepared from a combination of CCM and Fol-LP showed higher DTX loading and entrapment efficiency as compared to the nanoparticles prepared by using either CCM or Fol-LP. The nanoplexes prepared at 1:1 ratio of CCM and Fol-LP showed particle size of 156.5 nm (PDI 0.295) with entrapment efficiency of 87.65 % at 20 % theoretical drug loading. When the ratio was changed to 1:2, the nanoplexes size reduced to 129.3 nm, with an increase in entrapment efficiency (94.8 %). On further change in ratio to 1:3, the particle size increased to 146.5 nm, with a decrease in entrapment efficiency (43%). Further, the zeta potential was found to be 11.48, 15.23 and 15.7 mV for nanoplexes prepared at 1:1, 1:2 and 1:3 ratios (Table 1), respectively. The complexation with miR-34a did not significantly alter the size and PDI and zeta potential was decreased from 15.23 to 13.47 mV (Figure 5.1 A & B). The DTX/miR-34a nanoplexes showed good hydrodynamic diameter with no visible aggregation and particle size determined using Malvern Zetasizer.

5.3.3. In vitro DTX release study and agarose gel retardation assay

It was observed that the folate targeted hybrid lipopolymeric nanoplexes demonstrated a sustained drug release profile of DTX for 3 days with approximately 12% of DTX getting released in the initial 12 h. In the following 48 h, the percent cumulative release reached approximately 85 % while up to 3rd day the percent cumulative release reached upto 90 % indicating a sustained drug release profile whereas, free DTX solution (Taxotere®) (kept as a control) showed complete release within 4 h (Figure 5.2). Agarose gel retardation assay showed the effective complexation of miR-34a when incubated with naked polymeric nanoparticles to form nanoplexes at the N/P ratio of 8/1. When nanoplexes were incubated with heparin (0.1/1 Unit), the significant release of miRNA-34a was observed (Figure 5.1 E).

Table 5.1. Impact of changing ratio of P4 and Fol-LP polymer on particle size, zeta potential and encapsulation efficiency of hybrid nanoparticles

Batch No	Ratio P4: Fol-LP	P4 (mg)	Fol-LP (mg)	DTX (mg)	MilliQ Water (mL)	% TDL	Particle size (nm)	PDI	Zeta potential (mV)	Entrapment efficiency (%)
1	3:1	6.75	2.25	1	2	10	202.4	0.443	+19.10	85.30
2	2:1	6	3	1	2	10	152.5	0.256	+14.50	99.00
3	1:1	4.5	4.5	1	2	10	156.5	0.218	+11.48	87.65
4	1:2	3	6	1	2	10	129.3	0.295	+15.23	94.80
5	1:3	2.25	6.75	1	2	10	146.5	0.316	+15.70	43.00
6	1:2	21.33	42.67	16	3.5	20	146.7	0.241	+15.58	95.76

5.3.4. Gene transfection efficiency and endocytic uptake mechanism

Transfection efficiency of the FAM-siRNA/nanoplexes was carried out in both 4T1 and MDA-MB-231 breast cancer cells using flow cytometric analysis. In 4T1 cells, the transfection efficiency (%) for non-targeted FAM-siRNA nanoplexes and folate targeted FAM-siRNA nanoplexes was found to be 85.98% and 93.63%, respectively while lipofectamine-2000/FAM-siRNA and naked FAM-siRNA showed transfection efficiency equivalent to 82.73% and 3.34%, respectively (Figure 5.3). In MDA-MB-231 cells, the percentage of transfection was found to be 91.24% and 94.59% for non-targeted and folate targeted FAM-siRNA/nanoplexes, respectively. Lipofectamine-2000/FAM-siRNA and naked FAM-siRNA showed a transfection efficiency of 92.54% and 1.57%, respectively (Figure 5.4).

Further, to elucidate the endocytic uptake mechanism of the developed nanoplexes, both qualitative and quantitative analysis using fluorescence microscopy and flow cytometry, respectively, were performed. High intracellular uptake was observed for folate targeted FAM-siRNA/ nanoplexes, evident from the intense green fluorescence in the cells. Blank nanoplexes and naked FAM-siRNA were kept as the control that showed negligible fluorescence in the

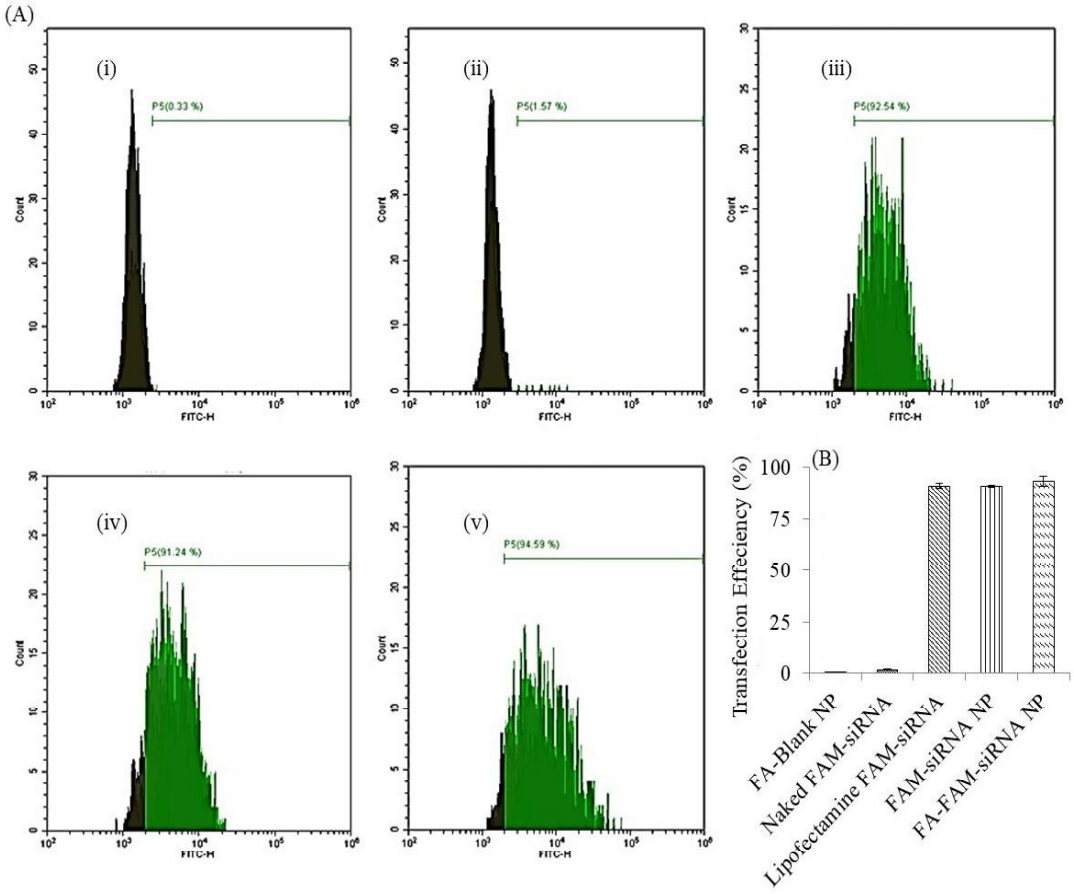

Figure 5.4. (A) Flow cytometry evaluations of the transfection efficiencies of FAM-siRNA in MDA-MB-231 cell line treated with (i) Folate targeted blank nanoparticles (FA-Blank NP), (ii) naked FAM-siRNA, (iii) Lipofectamine-FAM-siRNA (iv) non-targeted FAM-siRNA nanoplexes (FAM-siRNA NP) and (v) Folate targeted FAM-siRNA nanoplexes (FA-FAM-siRNA NP). In these graphs, y-axis represents cell counts and x-axis represents the FAM-siRNA fluorescence intensities, and (B) Transfection efficiency (%) after various treatments of FAM-siRNA formulations in MDA-MB-231 cell line. Each point represents the mean ± SD.

cells (Figure 5.3 and Figure 5.4). In order to delineate the pathway for the endocytosis, both 4T1 and MDA-MB-231 cells were pretreated with various endocytic inhibitors followed by treatment with the folate targeted FAM-siRNA/nanoplexes. It was evident from the fluorescence microscopic images that folate targeted FAM-siRNA/nanoplexes followed both lipid-raft and clathrin-mediated intracellular uptake pathways since the treatment of the cells with methyl-β-cyclodextrin (Mβ-CD) and chlorpromazine (CPZ), significantly inhibited the green fluorescence in the cells while other inhibitors such as mycostatin (caveolae pathway inhibitor) and amiloride (macopinocytic pathway inhibitor) did not show any inhibition of

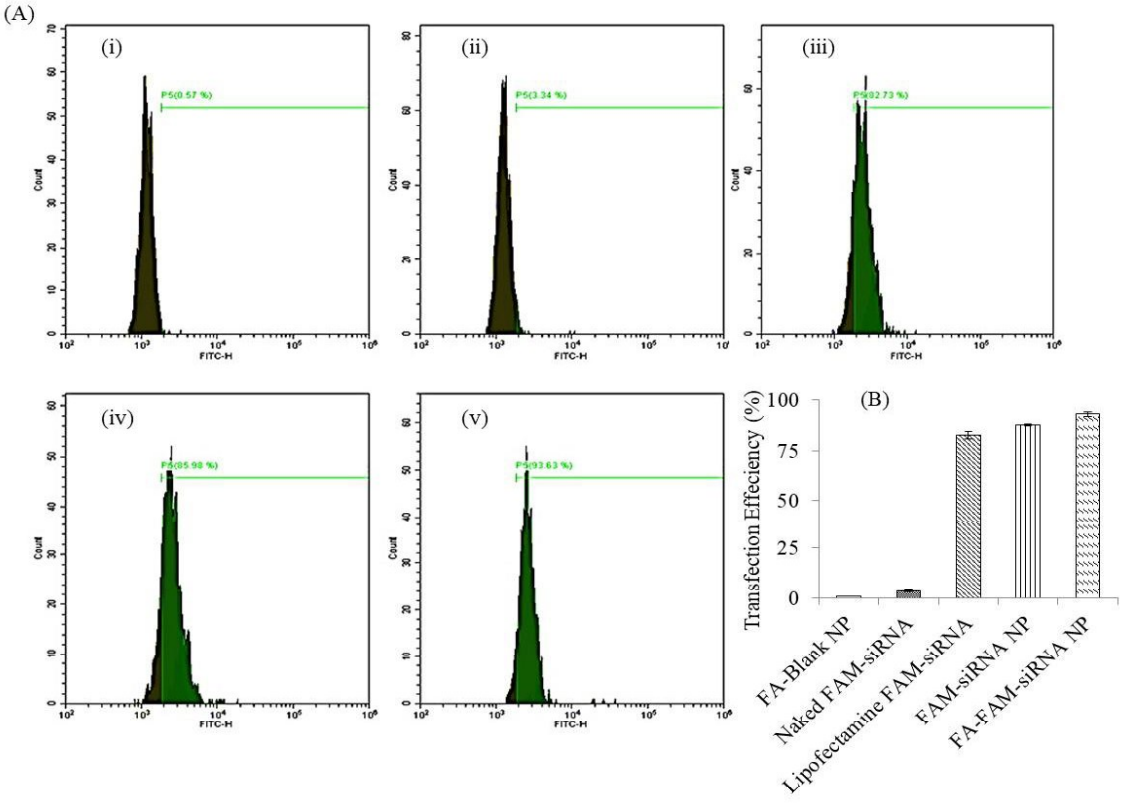

Figure 5.3. (A) Flow cytometry evaluations of the transfection efficiencies of FAM-siRNA in 4T1 cell line treated with (i) folate targeted blank nanoplexes (FA-Blank NP), (ii) naked FAM-siRNA, (iii) Lipofectamine-FAM-siRNA, (iv) non-targeted FAM-siRNA nanoplexes (FAM-siRNA NP) and (v) folate targeted FAM-siRNA nanoplexes (FA-FAM-siRNA NP). In these graphs, y-axis represents cell counts and x-axis represents the FAM-siRNA fluorescence intensities, and (B) Transfection efficiency (%) after various treatments of FAM-siRNA formulations in 4T1 cell line. Each point represents the mean ± SD.

uptake of these nanoplexes (Figure 5.5 and Figure 5.6). Percent fluorescence intensity graphs generated from the flow cytometry data indicated higher uptake of Fol-P/FAM-siRNA nanoplexes as compared to naked FAM-siRNA in both 4T1 cells and MDA-MB-231 cell. Further, decreased fluorescence intensity after treatment with MβCD and chlorpromazine indicated lipid-raft and clathrin-mediated endocytosis.

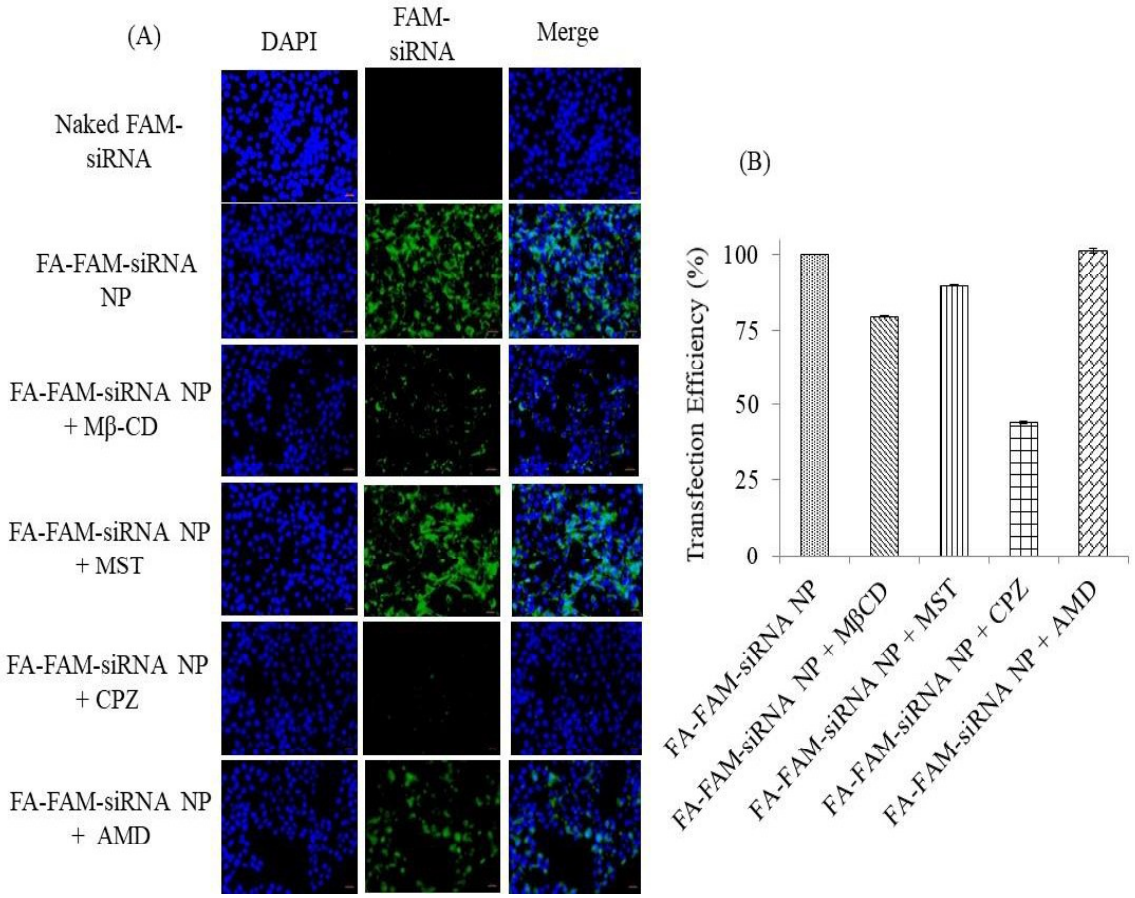

Figure 5.5. (A) Microscopic images of cellular uptake following incubation with Naked FAM-siRNA, FA-FAM-siRNA NP**,** and FA-FAM-siRNA NP with various endocytosis inhibitors for 4 h in 4T1 cell line and (B) flow cytometry based quantification of percent fluorescence intensity in 4T1 cells, indicating higher uptake of FA-FAM-siRNA NP as compared to Naked FAM-siRNA and dropping down of fluoroscence in presence of MβCD and CPZ indicating lipid-raft and clathrin mediated endocytosis. Each point represents the mean ± SD.

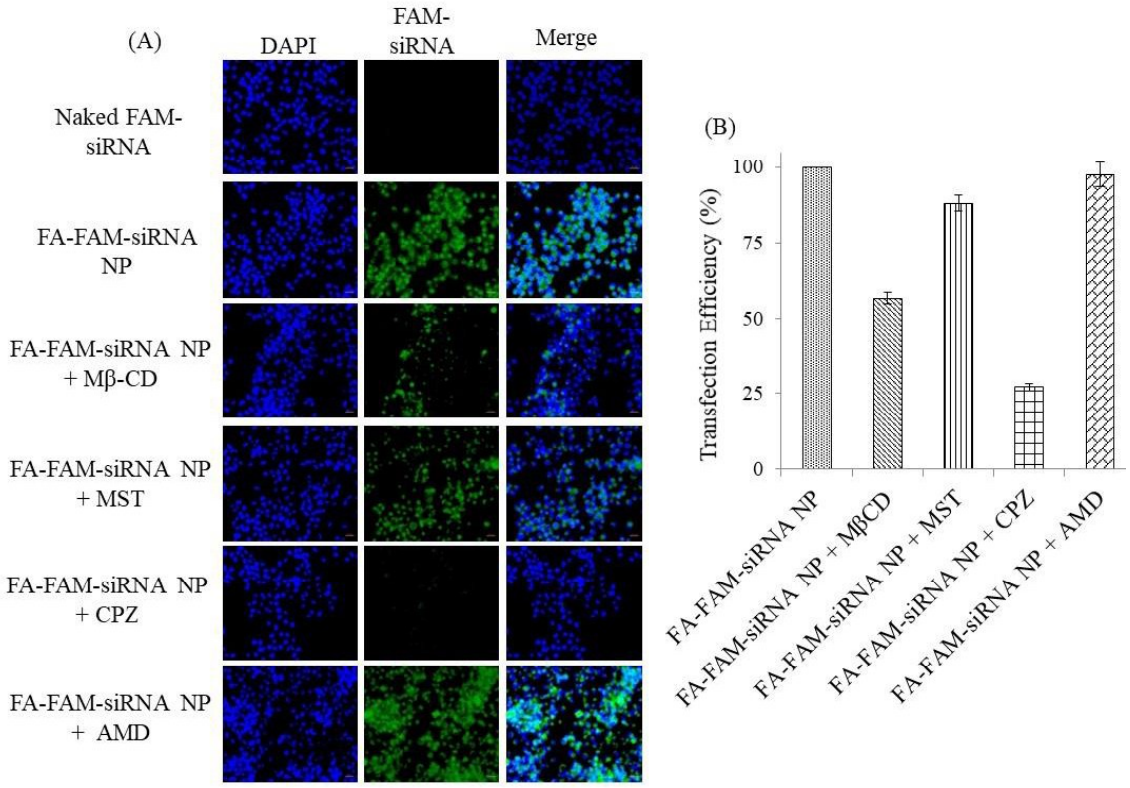

Figure 5.6. (A) Microscopic images of cellular uptake following incubation with Naked FAM-siRNA, FA-FAM-siRNA NP, and FA-FAM-siRNA NP with various endocytosis inhibitors for 4 h in MDA-MB-231 cell line and (B) flow cytometry based quantification of percent fluorescence intensity inMDA-MB-231 cells, indicating higher uptake of Fol-P/FAM-siRNA Nanoplexes as compared to Naked FAM-siRNA and dropping down of fluoroscence in presence of MβCD and chlorpromazine indicating lipid-raft and clathrin mediated endocytosis. Each point represents the mean ± SD.

5.3.5. In vitro cytotoxicity

Both DTX and miR-34a exhibit very effective tumor-suppressing activity and play a significant role in inhibiting cancer cell proliferation [30]. Cell viability of 17% and 14% were observed with folate targeted DTX/miR-34a nanoplexes in 4T1 and MDA-MB-231 cell lines, respectively as compared to non-targeted DTX/miR-34a nanoplexes that showed cell viability of 30% and 26% in 4T1 and MDA-MB-231 cells, respectively. Further, the folate targeted DTX or miR-34a containing nanoplexes also showed significantly higher cytotoxicity as compared to non-targeted nanoplexes in both 4T1 and MDA-MB-231 cells. Both folate targeted and non-targeted NC-miRNA/nanoplexes (containing mirVana™ miRNA Mimic #1 Negative control) did not show any cytotoxicity in both cell lines (Figure 5.7 and Figure 5.8).

5.3.6. Apoptosis assay

Apoptosis in 4T1 and MDA-MB-231 cells were evaluated after 24 h treatment with the nanoplexes by flow cytometry. In fluorescence-activated cell sorting (FACS) plot, X-axis represents FITC-A and Y-axis represents propidium iodide. The viable cells showed annexin V(−) and PI (−) (Q3 lower left quadrant) whereas the cells in early-phase apoptosis showed annexin V(+) and PI (−) (Q4 at the lower right side) and late phase apoptosis showed annexinV(+) and PI(+) (Q2 at upper right) while necrotic cells only show PI(+) (Q1 at upper left side). It was observed that the treatment with folate targeted DTX/miR-34a nanoplexes showed improved apoptosis i.e. 60.89% apoptosis (47.60 % early and 13.29 % late stage) and 58.44% apoptosis (10.78 % early and 47.66 % late stage) in 4T1 and MDA-MB-231 cells, respectively as compared to the non-targeted DTX/miR-34a nanoplexes that induced 59.60% apoptosis (45.80 % early and 13.80 % late stage) and 51.65% apoptosis (10.24 % early and 41.41 % late stage) in 4T1 and MDA-MB-231 cells, respectively. Rest of the treatments induced apoptosis significantly lower compared to that of folate targeted or non-targeted

DTX/miR-34a nanoplexes signifying the enhanced action of the combination of DTX and miR-34a when delivered using nanoplexes. Folate targeted mirVana miRNA Mimic #1 Negative control nanoplexes (Folate targeted and non-targeted) and blank nanoplexes (used as controls) did not show any apoptosis-inducing potential (Figure 5.7 and Figure 5.8).

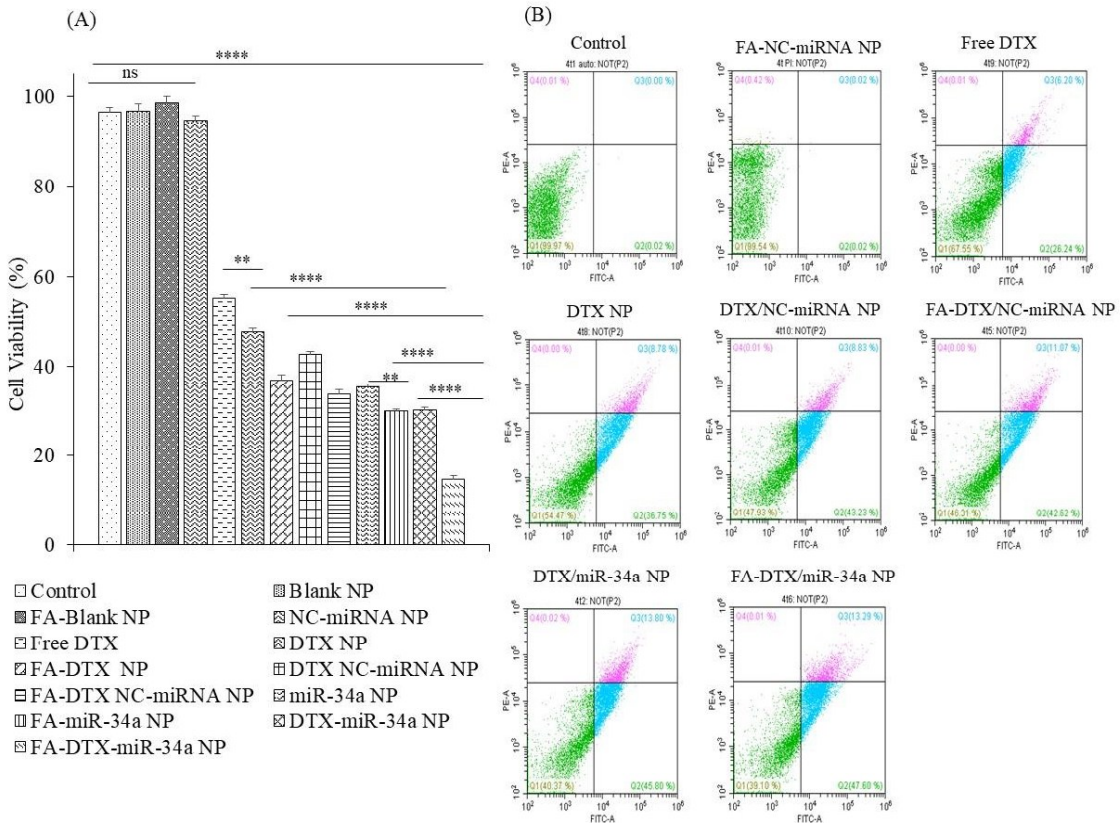

Figure 5.7. (A) *In-vitro* cytotoxicity study and (B) flow cytometric detection of apoptosis in 4T1 cell line incubated for 48 h with various nanoformulation (DTX: 25 nM and miR-34a: 20 pM). Each point represents the mean ± SD. Statistical analysis were performed using one way ANOVA followed by Tukey's multiple comparison test. ns: (non-significant). (**** $P < 0.0001$) was considered as statistically significant.

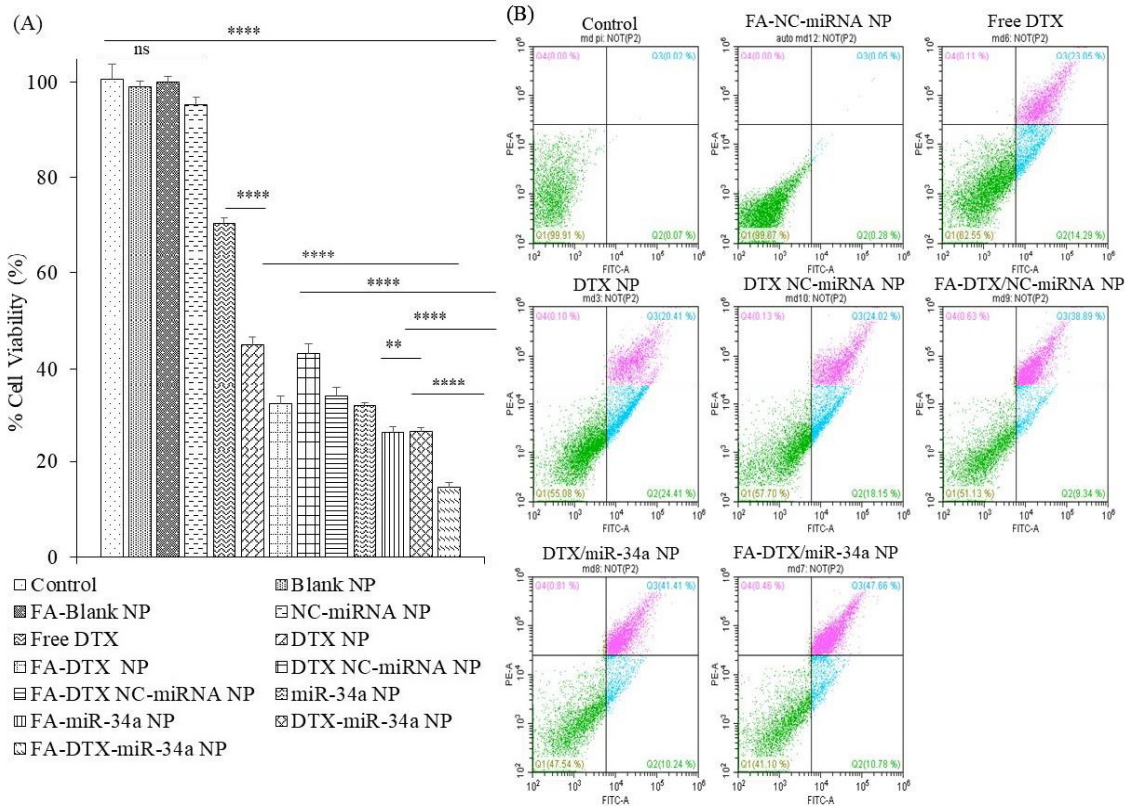

Figure 5.8. (A) *In-vitro* cytotoxicity study and (B) flow cytometric detection of apoptosis in MDA-MB-231 cell line incubated for 48 h with various nanoformulation (DTX: 25 nM and miR-34a: 20 pM). Each point represents the mean ± SD (n=3). Statistical analysis were performed using one way ANOVA followed by Tukey's multiple comparison test. ns: (non-significant). (**** $P < 0.0001$) was considered as statistically significant.

5.3.7. Gene expression analysis

The real-time PCR (RT-PCR) analysis of BAX, Bcl-2, Ki-67 and SIRT1 gene was performed to understand the impact on the downstream targets of DTX and miR-34a when they were co-delivered using folate-targeted nanoplexes. A significant suppression in the expression of both Bcl-2 and Ki67 with a concomitant increase in the expression of BAX was observed after treatment with the folate targeted DTX/miR-34a nanoplexes as compared to the non-targeted DTX/miR-34a nanoplexes in both cell lines. A similar pattern of expression was

observed in the case of folate targeted DTX nanoplexes compared to non-targeted DTX nanoplexes indicating that the folate ligand played an active role in targeting cancer cells in both cell lines. Further, the SIRT1 gene expression was significantly downregulated in MDA-MB-231 cells treated with folate targeted DTX/miR-34a nanoplexes compared to non-targeted DTX/miR-34a nanoplexes (Figure 5.9).

5.3.8. In vivo plasma pharmacokinetics of FAM-siRNA and DTX

The comparative *in vivo* pharmacokinetics of DTX and FAM-siRNA loaded folate targeted nanoplexes was studied in *Swiss albino* mice. The results demonstrated that there was a significant difference in the pharmacokinetic profiles for naked FAM-siRNA *vs.* folate targeted FAM-siRNA nanoplexes and free DTX (Taxotere®) versus folate targeted DTX loaded nanoplexes (Figure 5.10 and Table 5.2). There were the quantifiable levels of FAM-siRNA and DTX in mice plasma at 48 h and 120 h when it was administered as nanoplexes,

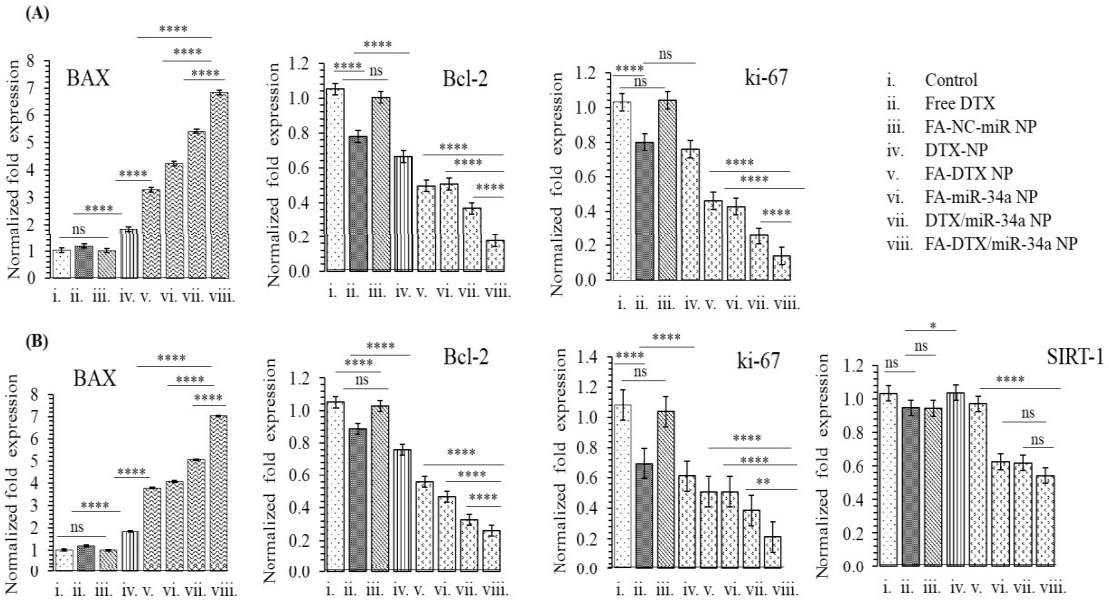

Figure 5.9. Gene expression analysis of BAX, Bcl-2, Ki-67 and SIRT-1 in 4T1 and MDA-MB-231 cells treated free DTX and DTX/miR-34a loaded nano-carriers. Each point represents the mean ± SD (n=3).

whereas in case of naked FAM-siRNA and free DTX, no detectable levels of FAM-siRNA were seen after 6 h post-injection. Further, folate-targeted FAM-siRNA nanoplexes showed a significantly lower Cmax (ng/mL) (441.22±14.48) *vs.* naked FAM-siRNA (541.09 ± 10.57) The higher $AUC_{0-\infty}$ (μg*h/L) (9059±183.72 versus 578.77±20.14) (>15 times) as compared to the naked FAM-siRNA. Similarily DTX loaded nanoplexes showed a Cmax (ng/mL) of 1658.00 ± 416.59 as compared to free DTX that showed a Cmax of 1599.41 ± 292.90. DTX loaded nanoplexes exhibited >13 times increment in $AUC_{0-\infty}$ (μg*h/L) (30812.54 ± 3289.19) as compared to the free DTX $AUC_{0-\infty}$ (μg*h/L) (2301.19 ± 92.99).

Further, the plasma half-life ($t_{1/2}$) (h) was observed to be 26.55 ± 1.17 h and 34.98 ± 6.33 for FAM-siRNA and DTX respectively, delivered using folate-targeted nanoplexes (Figure 5.10 and Table 5.2) as compared to 1.47 ± 0.05 h and 4.51 ± 1.13 h for naked FAM-siRNA and free DTX respectively (Table 5.2) indicating improved *in vivo* residence of FAM-siRNA and DTX when administered in the form of nanoplexes.

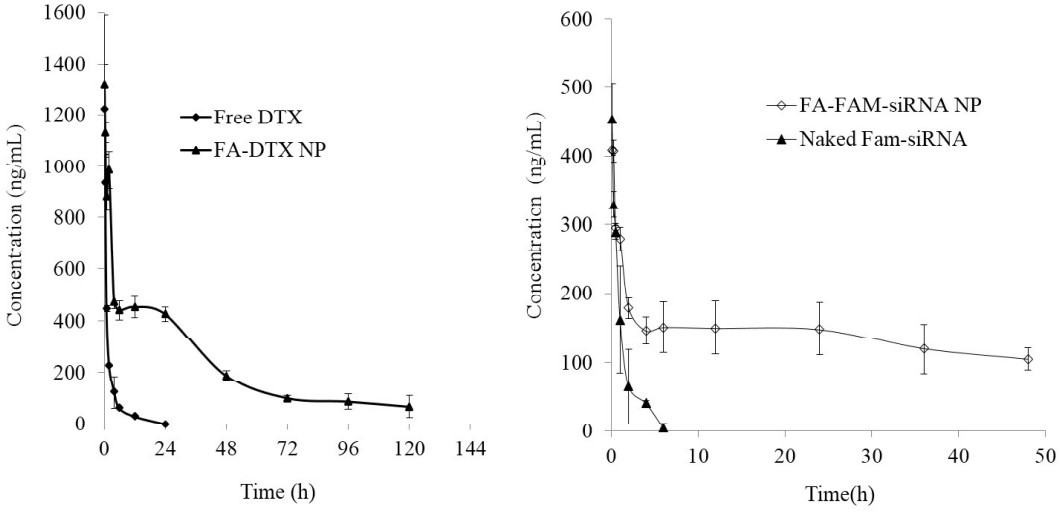

Figure 5.10. Plasma concentration profiles of DTX and Fam-siRNA after administration of (A) free DTX and FA-DTX nanoparticles and (B) Naked Fam-siRNA and Fam-siRNA Nanoplexes at dose of 10 mg/kg and 1 mg/kg of DTX and Fam-siRNA, respectively *i.v.* via tail vein (n=6).

Table 5.2. Pharmacokinetic parameters of DTX and Fam-siRNA after administration of free DTX, FA-DTX nanoparticles, naked Fam-siRNA and Fam-siRNA Nanoplexes at dose of 10 mg/kg and 1 mg/kg of DTX and Fam-siRNA, respectively *i.v.* via tail vein (n=6).

Pharmacokinetic Parameters	Naked FAM-siRNA	FA-FAM-siRNA NP	Free DTX (Taxotere®)	F-DTX-LPNs
AUC(0-t) (µg*h/L)	550.66 ± 18.64	6938.4 ± 89.62	2110.01 ± 120.37	27256.76 ± 814.12
$AUC_{0-\infty}$ (µg*h/L)	578.77 ± 20.14	9059 ± 183.72	2301.19 ± 92.99	30812.54 ± 3289.19
MRT(0-t) (h)	1.32 ± 0.02	21.97 ± 0.37	2.26 ± 0.18	34.04 ± 3.41
MRT(0-inf) (h)	1.65 ± 0.05	39.84 ± 1.43	3.64 ± 0.48	49.25 ± 14.26
Kel	0.47 ± 0.016	0.026 ± 0.0014	0.16 ± 0.05	0.02 ± 0.00
t1/2kel (h)	1.47 ± 0.05	26.55 ± 1.17	4.51 ± 1.13	34.98 ± 6.33
Cmax (µg /mL)	541.09 ± 10.57	441.22 ± 14.48	1599.41 ± 292.90	1658.00 ± 416.59
Cl (mL/h/kg)	54.53 ± 1.87	4.32 ± 0.056	4350.90 ± 175.40	327.08 ± 31.68
Vd (mL/kg)	72.02 ± 2.73	95.03 ± 2.14	28369.34 ± 7393.77	16355.07 ± 2192.32

5.3.9. Biosafety evaluation and in vivo acute toxicity study

5.3.9.1. Observational data

At the end of the toxicity study, none of the animals in any of the groups showed mortality or abnormal locomotor activity. Animals did not show diarrheal symptoms, irregular respiration or seizure during the observational periods of 24 h, and their food and water intake was normal. Each animal was showing normal stereotypy behavior like chewing, rearing, cage climbing and sniffing. Further, no deviation in the average body weights of animals was observed during the study period. Furthermore, no other abnormal or inflammatory condition

in the skin, ear, and paws was observed. Fur and eye color of the animals were also normal when compared to the control group.

5.3.9.2. Organ toxicity data

Size as well as the weight of spleen in the group exposed to a dose of 50 mg/kg and 100 mg/kg was significantly increased with respect to the control group treated with normal saline. Spleen size and weight of animals administered with a dose of 10 mg/kg did not differ significantly from the control group administered with normal saline. There was no deviation in the weights of the liver in the treatment group with no morphological difference compared to the control group administered with normal saline. No other organs, including heart, lungs

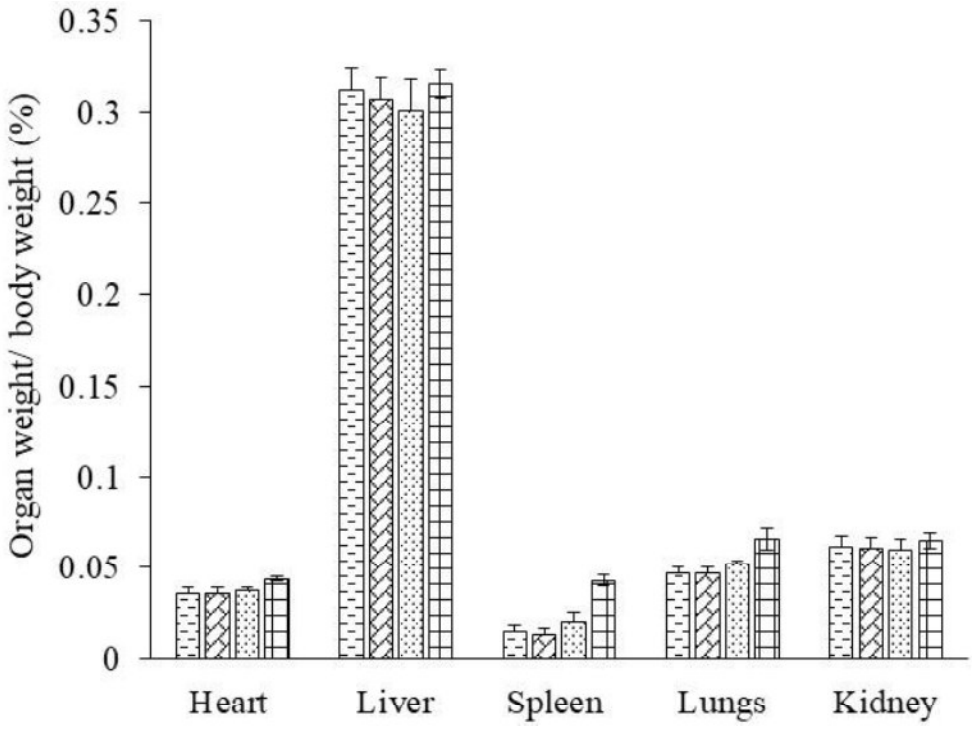

Figure 5.10. Dose dependent organ toxicity in mice treated with various doses of cationic polymer (10 mg/kg, 50 mg/kg and 100mg/kg) administered *i.v.* via tail vein compared to saline (control) (n=3). Ratio of weight of the organs (heart, liver, spleen, lungs, kidney) to animal weights in percentage was plotted.

and kidney, showed statistical difference in size and weight with respect to the control group (Figure 5.10).

5.3.9.3. Hematological and biochemical parameters

Overall, no significant differences were observed in the hematological parameters after single-dose administration of nanoplexes (Table 5.3). All the parameters were within the normal range except total red blood cell count (TRBC) and total leucocyte count (TLC) at 100 mg/kg with respect to the control group. In all the groups treated with nanoplexes, the serum level of cholesterol was more compared to the control group. Major inflammatory markers viz., AST/SGOT and ALT/SGPT were in the normal range (Table 5.3). Results of acute toxicity study revealed that nanoplexes are not toxic in a short time exposure at a single dose of 10 mg/kg in mice.

5.3.9.4. Histopathological examination

Figure 5.11 shows the histopathological evaluation of lungs, heart, kidney, liver and spleen. Histopathological sections of lungs showed toxicity signs, i.e., mild edema (congestion), interalveolar septa thickening with mild fibrosis and mild infiltration of inflammatory cells at a higher dose of 100 mg/kg. Even at a dose of 50 mg/kg, toxicity signs, i.e., mild edema (congestion), interalveolar septa thickening with mild fibrosis were observed. At a lower dose of 10 mg/kg, the histological section retained normal architecture of alveolar spaces with thin alveolar septa without any sign of toxicity and were comparable to that of the control group treated with saline suggesting its safety at a lower dose.

Histopathological sections of heart showed that at a higher dose of 100 mg/kg, there was moderate to severe disorganization of the myofibrils with severe loss of striations of cardiac myocytes with mild to moderate focal degenerating myocytes and congestion. At both moderate and lower doses, i.e., 50 mg/kg and 10 mg/kg, the normal architecture of cardiac

Table 5.3. Hematological and biochemical parameters of *Swiss albino* mice treated with various doses of cationic polymer (10 mg/kg, 20 mg/kg and 100 mg/kg) administered *i.v.* via tail vein.

Hematological and biochemical parameters	Control	Group 1 10 mg/kg	Group 2 50 mg/kg	Group 3 100 mg/kg
Animal Body weight (g)	19	19.5	20	20
Hemoglobin (Hb gm %)	11.60	12.3	11.40	11.90
Total leukocytes count (TLC)/cumm	13133	12833	13833	16300
Differential Leucocytes Count (DLC)				
Neutrophil (%)	14	19.69	65.63	76.70
Lymphocytes (%)	76	73	26	15
Eosinophils (%)	6.97	7.33	7	7.77
Total Red Blood Cell Count (TRBC) (million/cu.mm)	7.63	7.7	6.10	9.41
Total Platelets Count (TPC) (lacks/cu.mm)	5.16	4	5.99	4.69
Packed cell volume (PCV) (%)	35	36	27.30	41.57
Mean corpuscular volume (MCV)	44.33	48	44.20	44.67
Mean corpuscular hemoglobin (MCH) pg	14.33	16	14.30	12.43
Mean corpuscular hemoglobin Concentration(MCHC) g/dl	32	33	32.57	29.27
Total Eosinophils Count (TEC) cells/cumm	443	480	458.33	466.33
Blood sugar Random (mg%)	127	106	152.33	136
AST/SGOT (U/L)	22.33	21.00	25.67	23.33
ALT/SGPT (U/L)	18.33	17.67	25	22.67
Serum Bilirubin (mg%)	-	-	0.47	0.53
Total	0.50	0.47	0.47	0.53
Direct	0.27	0.30	0.30	0.37
Indirect	0.23	0.17	0.17	0.20
Serum alkaline phosphatase (U/L)	316	305	272	258
Total protein (g%)	5.6	5.13	5.47	5.50
Albumin (g%)	3.17	2.57	3.17	3.23
Serum creatinine (mg%)	0.37	0.27	0.47	0.44
Globulin (g%)	2.50	2.57	2.30	2.27
Blood urea (mg%)	13.67	13.0	14.33	10.67
Serum cholesterol (mg%)	86.33	98.33	118	124
Triglyceride (mg%)	34.33	29.67	36	37.67

myocytes with centrally placed nuclei was observed that was comparable to that of the control group treated with saline suggesting its safety at a lower dose. Histopathological sections of kidneys revealed that in all the treatment groups, the glomerulus, proximal convoluted tubules

(PCT), and distal convoluted tubules (DCT) were intact without any sign of degeneration and inflammation and were comparable to that of the control group. Histopathological sections of the liver showed that in all the treatment groups, there were normal intact hepatocytes without any sign of infiltration of inflammatory cells from the central vein that was comparable to that of the control group. Histopathological sections of the spleen revealed that at a higher dose of 100 mg/kg, there was the mixing of the red pulp (pink in color) and white pulp (blue in color) areas due to the rupture of splenocytes resulting from swelling and enlargement of the spleen. At a dose of 50 mg/kg, there was comparatively mild toxicity observed in spleen. At a lower dose of 10 mg/kg, red pulp and white pulp areas remained intact and were comparable to that of the control group.

5.4. Discussion

The combination of DTX with miR-34a is an alternative strategy for accomplishing synergistic outcomes in cancer therapy because of their complementary actions [18, 31]. DTX is an FDA approved, a first-line chemotherapeutic agent for the treatment of various types of cancer; however, due to poor solubility, high clearance rate, low tumor penetrating efficiency, development of drug resistance (P-gp efflux) and the manifestation of serious side effects, its therapeutic applications are compromised [32, 33]. miR-34a exerts its biological activity by promoting apoptosis and suppression of cancer progression by down-regulating the Bcl-2 genes reducing resistance/ increasing the sensitivity of tumor cells to conventional chemotherapeutic agents [30]. Besides this, miR-34a causes regression of the EMT, leading to the inhibition of metastasis, a major cause of death among breast cancer patients [34]. Hence, the combination of DTX and miR-34a has the potential to yield a synergistic response in breast cancer treatment. Delivering DTX and miR-34a simultaneously to the cytosol is crucial to achieving the benefit. The major hurdle encountered when miR-34a is internalized within the

cell is its degradation by the lysosomal enzymes, if it is not escaped from the endosomes [35, 36]. Designing nano-carriers for co-delivering chemotherapeutic agents and miRNAs to the cytosol of tumor cells is far challenging because of their enormously different physicochemical properties [37]. Currently available potent anticancer drug molecules are highly hydrophobic and possess very poor aqueous solubility, whereas; miRNAs are polyanionic oligonucleotides with high water-solubility having the large molecular weight and are susceptible to degradation *in vivo* [38, 39]. Zhang et al., co-delivered miRNA-34a and DTX using core-shell nano-carriers with surface coated cationic albumin in 4T1 cancer cells. These nano-carriers adopted a caveolae-mediated endocytic pathway bypassing the endo-lysosomal pathway and demonstrated enhanced *in vitro* performance with significant inhibition of tumor growth and metastasis in 4T1-tumor bearing mice model [40].

In the present work, we have demonstrated that folate targeted hybrid lipopolymeric nanoplexes could promisingly co-deliver DTX and miR-34a. These folate targeted nanoplexes were prepared from the combination of previously reported cationic CCM and Fol-LP polymers, thus forming a hybrid system with an improved loading capacity (of DTX), complexation (of miRNA) and active targeting (by folate). The hydrophobic core of the nanoplexes was composed of cholesterol and lactic acid units from both lipopolymers that could efficiently encapsulate hydrophobic DTX. The cationic chain, N,N-dimethyldipropylenetriamine, grafted on CCM imparts positive surface charge for complexation with miR-34a through electrostatic interaction and responsible for enhancing colloidal stability by improving zeta potential. Further, the morpholine moiety from cationic CCM exerts proton sponge effect, as reported earlier, resulted in the endosomal escape of nanoplexes leading to enhancement in the therapeutic effects of miR-34a [22] [41].Furthermore, the folate moiety conjugated to the PEG unit of Fol-LP was responsible for the active targeting of nanoplex to cancer cells that highly express folate receptors [42] [43].

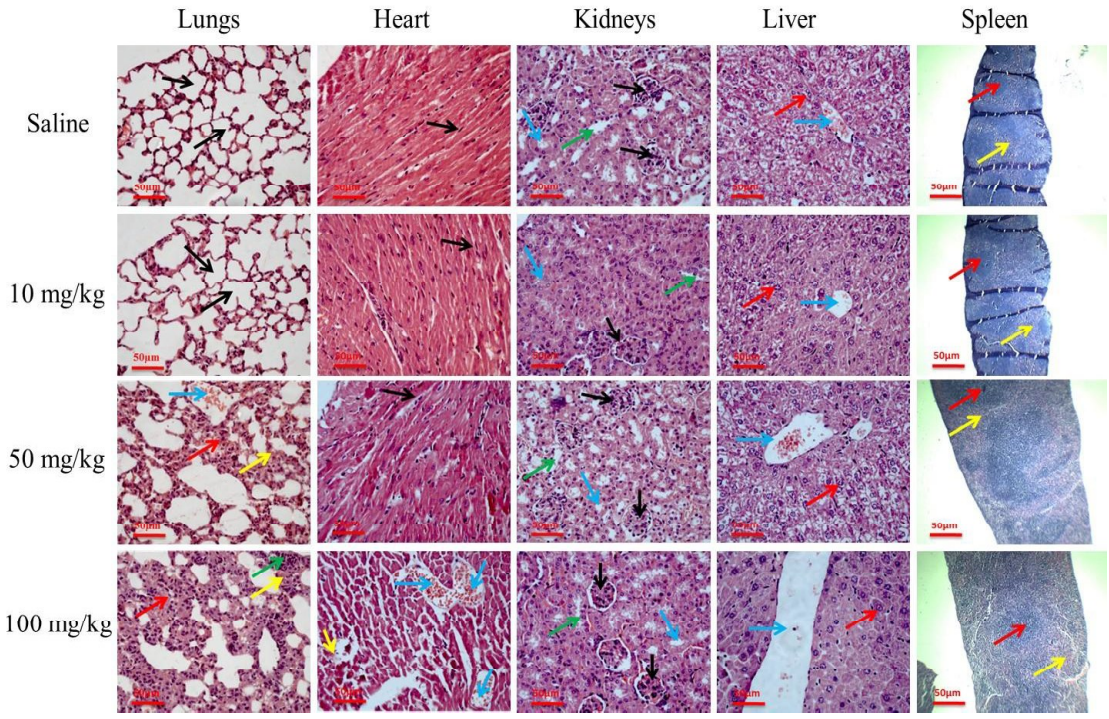

Figure 5.11 Histopathological evaluation (H&E staining, 40X) of various organs of female mice treated with various doses of cationic polymer from 10 mg/kg to 100mg/kg administered intravenously via tail vein compared to saline (control). For **lungs**, abbreviations are as follow - **black arrows**: normal architecture of alveolar spaces with thin alveolar septa; **sky blue arrow:** mild edema or congestion; **red arrow:** interalveolar septa thickening; **yellow arrow:** mild fibrosis; **green arrow:** mild infiltration of inflammatory cells. For **heart**, abbreviations are as follow- **black arrows**: normal architecture of cardiac myocytes with centrally placed nuclei; **yellow arrow**: moderate to severe disorganization of the myofibrils with severe loss of striations of cardiac myocytes with mild to moderate focal degenerating myocytes; **sky blue arrow**: congestion. For **kidneys**, abbreviations are as follow- **black arrows**: glomerulus; **sky blue arrow**: proximal convoluted tubules PCT; **green arrow**: distal convoluted tubules, DCT. For **liver**, abbreviations are as follow- **red arrow:** hepatocytes; **sky blue arrow:** central vein, CV. For **spleen**, abbreviations are as follow- **red arrow**: white pulp; **yellow arrow**: red pulp. (Magnification: 40X). Scale bar = 50 µm.

`Folate-targeted nanoplexes containing DTX/miR-34a combination were prepared at various ratios of cationic CCM and Fol-LP (i.e. at 4:1, 2:1, 1:1, 1:2 and 1:4) by double emulsion solvent evaporation method. Even though the results of batches prepared at 2:1, 1:1 and 1:2 exhibited comparable results, batch prepared at 1:2 ratio was selected as the quantity of cationic

CCM in the composition was minimum. The cationic polymer possesses amine functionality that imparts buffering capacity in endosomes, promoting the nanoparticles to undergo endosomal escape for efficiently delivering genes to the cytoplasm. As reported previously, the presence of residual positive charges could lead to the potential toxicity of the cationic polymers due to its membrane perturbation mechanism leading to cytotoxicities and restricting clinical translation [44]. The *in vitro* drug release profiles of the folate targeted nanoplexes showed a controlled release for three days. The slow and sustained drug release profile is due to the physical retention of the drug inside the hydrophobic core of nanoplexes. The formulation prepared with the combination of polymer showed effective complexation with miR-34a to form nanoplexes at the N/P ratio of 8/1. Heparin is competent anion and used to release nucleic acid from cationic polymers/lipids. Our results depict the release of miRNA-34a from nanoplexes after incubation with heparin (0.1/1 Unit), proving the improvement in post complexation miRNA-34a stability

The delivery of miRNAs to the cytosol is highly desirable for their therapeutic effect [45]. Non-viral vector-based miRNA delivery to tumor cells has emerged as a promising approach as they avoid several issues in the use of viral vectors (including potential pathogenicity, insertional mutations, and immunogenicity) as well as provide an efficient means to deliver genes based therapeutics intracellularly to cytosol or nucleus [46]. Among various non-viral vectors, polymeric micelleplexes has the advantage of simultaneous loading of hydrophobic drug and complexation with the miRNAs [47]. These systems enter the cells *via* endocytic routes such as macropinocytosis, caveolin/lipid raft, clathrin, etc., depending on the surface properties and size. Amongst these endocytic pathways, caveolin-mediated endocytosis is desirable as it bypasses the endo-lysosomal pathway of degradation and, therefore, could enhance the therapeutic efficiency [48]. Our cellular uptake data revealed that folate targeted FAM-siRNA nanoplexes showed significantly high intracellular uptake in both

4T1 and MDA-MB-231 cell lines that could be credited to the presence of folic acid conjugated to the nanoplexes enabling their binding with folate receptors expressed on the surface of cancer cells. The breast cancer cell lines, especially TNBC cells, demonstrated higher surface folate receptor expression. Nahire et al. formulated the folate targeted multifunctional polymersomes and reported that these targeted polymersomes were effectively internalized within the MCF-7 cells as compared to PANC-1 cells [49]. In another study, it was found that the folate targeted lipid nanoparticles exhibited 45-fold increased cellular uptake in MDA-MB-231 cells as compared to non-targeted formulations [50]. Further, folate-targeted FAM-siRNA nanoplexes followed lipid-raft and clathrin-mediated intracellular uptake since the treatment with methyl beta-cyclodextrin (Mβ-CD) (cholesterol-depleting agent used to disrupt several lipid-raft mediated endocytic pathways) and chlorpromazine (CPZ; clathrin-dependent pathway inhibitor), completely inhibited the green fluorescence in the cells with a significant reduction in the percent fluorescence intensity. The portion of nanoplexes that adopted the lipid-raft mediated pathway bypassed the endo-lysosomal pathway that is responsible for drug or gene degradation and has fascinated increasing scrutiny due to their enhanced therapeutic effects of gene-based drugs. Further, in our previous work, we found that our constructed nanoplexes composed of cholesterol and morpholine grafted cationic amphiphilic copolymers delivered miR-34a inside the cytosol of 4T1 and MCF-7 cells [49].

Folate targeted DTX/miR-34a nanoplexes showed significantly higher cytotoxicity, apoptotic potential and significant fold-change in expression levels of Bcl-2, BAX, SIRT-1 and Ki-67 as compared to non-targeted DTX/miR-34a nanoplexes and free DTX in 4T1 and MDA-MB-231 cells that could be credited to its higher intracellular uptake. The SIRT1 gene expression was significantly downregulated in MDA-MB-231 cells treated with folate targeted DTX/miR-34a nanoplexes compared to DTX nanoplexes and non-targeted DTX/miR-34a nanoplexes. miR-34a, the first identified miRNA that is known to regulate the expression of

SIRT-1. The exact mechanism by which miR-34a regulates the cell proliferation is still under investigation but most of the reports consolidate its tumor suppressor property. Yamakuchi M. et. al. explored its role in regulation of apoptosis and cell cycle via. interfering transcriptional target of p53 through SIRT-1 inhibition. Interestingly, transfection of antisense-miR-34a led to marked increase in expression of SIRT-1 in HEK-293 cells [51]. Similarly, our data coincides the most of the published reports. On the other hand, SIRT-1 is not a direct target of DTX. But it It has been reported in several studies that patients with higher SIRT-1 levels are more prone to development of chemoresistance with respect to those with lower SIRT-1 levels. Furthermore, more than 70 percent of patients with high SIRT-1 levels did not responded to DTX treatment. Yousafzai et al. reported deacetylation in SIRT-1 led to stabilization of XRCC1 which is responsible for induction of chemoresistance in lung cancer [52]. Recently, Motamedi et al. showed effect of DTX on SIRT1 expression, wherein, slight increase in SIRT1 level was reported [53]. Hence, our data could be the possible result of the same. Further, the blank and negative control (NC) nanoplexes did not show any cytotoxicity and apoptosis, suggesting that the nanoplexes are non-toxic and biocompatible. Bcl-2 is an anti-apoptotic protein whose up-regulation can prevent cell death *via* the mitochondrial apoptosis pathway, rendering the tumor cells resistant to conventional chemotherapeutic agents. Therefore, it is desirable that Bcl-2 be down-regulated that could suppress tumor growth and enhance the sensitivity of cancer cells to anti-cancer drugs. DTX inhibits the phosphorylation step of Bcl-2 that is responsible for its up-regulation [54]. Among the various mechanisms of miR-34a, down-regulation of Bcl-2 is considered as one of the important mechanisms [55]. BAX is a pro-apoptotic protein and responsible for inhibiting anti-apoptotic Bcl-2 protein and hence promoting apoptosis of cancer cells. BAX is activated by the linked BH3 protein, and together with BAK, that form pores in the outer membrane of mitochondria, releasing cytochrome-c leading to activation of apoptosome [56]. Ki-67 is an antigen nuclear protein, and its high

expression is found to be associated with tumor cell proliferation and is directly correlated to the cancer progression and increase in the mortality rate amongst TNBC patients. In our study, we observed a significant downregulation of BCL-2 and Ki-67 along with the upregulation of BAX gene expression upon treatment with the FA-DTX-miR-34a nanoplexes.

There was a significant improvement in the *in vivo* pharmacokinetic profile of the FAM-siRNA and DTX when they were co-loaded in the folate targeted nanoplexes, as indicated by the increased MRT and increased AUC. Naked FAM-siRNA and free DTX showed rapid clearance from the body, which is one of the implicit drawbacks of free drugs requiring periodic administration of a higher dose, thus leading to poor patient compliance and incurring additional side effects. Compared to naked FAM-siRNA and free DTX, the pharmacokinetic parameters, i.e, AUC, t1/2 and MRT of FAM-siRNA and for DTX loaded folate targeted nanoplexes were increased by approximately 15, 18.06 and 24 fold and for DTX 13.3, 7.75 and 13.5, respectively. The improvement in the pharmacokinetic profile of FAM-siRNA when co-loaded in nanoplexes may be ascribed to the strong electrostatic complexation of FAM-siRNA onto the surface of nanoplexes resulting into slow and sustained drug release profile with additional stealth effect exerted due to PEG coating on the outer surface. PEG produced hydrophilic coating around the nanoplexes that reduced the interaction between actin and myosin filaments of immune cells with the surface of nano-carrier and thus protecting nanoplexes from being opsonized and thereby reducing their sequestration by the reticuloendothelial system (RES) uptake, thus attaining lower clearance rates with prolonged body residence.

The cationic nano-carriers (polymeric or lipidic) employed in the gene delivery may cause toxicity [57] and are thus required to be thoroughly tested *in vivo* at the pre-clinical level. In the present work, cationic CCM lipopolymer was employed as one of the major components of nanoplexes and its biosafety was necessary to be established in vivo. The blank nanoplexes

containing cationic CCM lipopolymer at a dose of 10 mg/kg administered intravenously *via* tail vein in mice did not show any sign of toxicity (inflammation or pathological changes) as confirmed after thorough hematological, biochemical and histopathological examination. Donato et al. developed chitosan/PLGA nanoplexes for delivering miR-34a and was found to be non-toxic in vivo. In another report by Knudsen et al. showed that the cationic polymeric micelles exhibited dose-dependent toxicity that was directly related to the positive surface charge [57].

5.5. Conclusion

In conclusion, folate targeted hybrid lipopolymeric nanoplexes demonstrated high transfection efficiency resulting in enhanced *in vitro* performance. *In vivo* results indicated substantial improvement in the pharmacokinetic profile of both DTX and FAM-siRNA delivered using these nanoplexes that proved to be non-toxic at the therapeutic quantities administered. Summarizing the research outcomes, co-delivery of DTX and miRNA-34a *via* folate targeted hybrid lipopolymeric nanoplexes proved to be a synergistic combination with translational potential. The enhancement of the anticancer efficacy was attributed to the efficient co-delivery using the targeted nanoplexes. Moreover, in comparison to typical co-delivery systems, the preparation procedure for nanoplexes was simple without using any complicated steps, entailing their potential for clinical translation. Overall, this strategy serves as a platform for the co-delivery of poorly soluble hydrophobic drugs and highly water-soluble gene and holds great potential for the treatment of breast cancer.

References

[1] R. Devulapally, T.V. Sekar, R. Paulmurugan, Molecular pharmaceutics, 12 (2015) 2080-2092.

[2] A.M. Gonzalez-Angulo, F. Morales-Vasquez, G.N. Hortobagyi, Overview of resistance to systemic therapy in patients with breast cancer, in: Breast Cancer Chemosensitivity, Springer, 2007, pp. 1-22.

[3] Y. Feng, M. Spezia, S. Huang, C. Yuan, Z. Zeng, L. Zhang, X. Ji, W. Liu, B. Huang, W. Luo, Genes & diseases, 5 (2018) 77-106.

[4] W. Si, J. Shen, H. Zheng, W. Fan, Clinical epigenetics, 11 (2019) 25.

[5] G. Misso, M.T. Di Martino, G. De Rosa, A.A. Farooqi, A. Lombardi, V. Campani, M.R. Zarone, A. Gullà, P. Tagliaferri, P. Tassone, Molecular therapy-nucleic acids, 3 (2014) e195.

[6] A.G. Bader, Frontiers in genetics, 3 (2012) 120.

[7] H. Okuda, F. Xing, P.R. Pandey, S. Sharma, M. Watabe, S.K. Pai, Y.-Y. Mo, M. Iiizumi-Gairani, S. Hirota, Y. Liu, Cancer research, 73 (2013) 1434-1444.

[8] F. Yu, H. Deng, H. Yao, Q. Liu, F. Su, E. Song, Oncogene, 29 (2010) 4194-4204.

[9] X. Sun, S. Qin, C. Fan, C. Xu, N. Du, H. Ren, Oncology reports, 29 (2013) 2079-2087.

[10] P. Bonetti, M. Climent, F. Panebianco, C. Tordonato, A. Santoro, M.J. Marzi, P.G. Pelicci, A. Ventura, F. Nicassio, Oncogene, 38 (2019) 360-374.

[11] F. Panebianco, M. Climent, M.A. Malvindi, P.P. Pompa, P. Bonetti, F. Nicassio, Nanomedicine: Nanotechnology, Biology and Medicine, 19 (2019) 95-105.

[12] R. Garzon, G. Marcucci, C.M. Croce, Nature reviews Drug discovery, 9 (2010) 775-789.

[13] J. Ma, C. Dong, C. Ji, Cancer gene therapy, 17 (2010) 523-531.

[14] H. Korkaya, M.S. Wicha, Cancer Research, 73 (2013) 3489-3493.

[15] R.X. Zhang, J. Li, T. Zhang, M.A. Amini, C. He, B. Lu, T. Ahmed, H. Lip, A.M. Rauth, X.Y. Wu, Acta Pharmacologica Sinica, 39 (2018) 825-844.

[16] X. Duan, Y. Li, Small, 9 (2013) 1521-1532.

[17] M. Zhou, Z. Liu, Y. Zhao, Y. Ding, H. Liu, Y. Xi, W. Xiong, G. Li, J. Lu, O. Fodstad, Journal of Biological Chemistry, 285 (2010) 21496-21507.

[18] S. Shi, L. Han, L. Deng, Y. Zhang, H. Shen, T. Gong, Z. Zhang, X. Sun, Journal of Controlled Release, 194 (2014) 228-237.

[19] Q. Liu, R.-T. Li, H.-Q. Qian, J. Wei, L. Xie, J. Shen, M. Yang, X.-P. Qian, L.-X. Yu, X.-Q. Jiang, Biomaterials, 34 (2013) 7191-7203.

[20] S.-J. Kim, J.-S. Oh, J.-Y. Shin, K.-D. Lee, K.W. Sung, S.J. Nam, K.-H. Chun, Journal of Controlled Release, 155 (2011) 427-434.

[21] J. Kota, R.R. Chivukula, K.A. O'Donnell, E.A. Wentzel, C.L. Montgomery, H.-W. Hwang, T.-C. Chang, P. Vivekanandan, M. Torbenson, K.R. Clark, Cell, 137 (2009) 1005-1017.

[22] S. Sharma, S. Mazumdar, K.S. Italiya, T. Date, R.I. Mahato, A. Mittal, D. Chitkara, Molecular pharmaceutics, 15 (2018) 2391-2402.

[23] S. Mazumdar, K.S. Italiya, S. Sharma, D. Chitkara, A. Mittal, International Journal of Pharmaceutics, 543 (2018) 96-106.

[24] Z.C. Soe, J.B. Kwon, R.K. Thapa, W. Ou, H.T. Nguyen, M. Gautam, K.T. Oh, H.G. Choi, S.K. Ku, C.S. Yong, J.O. Kim, Pharmaceutics, 11 (2019) 1-17.

[25] S.-T. Chou, Q. Leng, P. Scaria, J.D. Kahn, L.J. Tricoli, M. Woodle, A.J. Mixson, Biomacromolecules, 14 (2013) 752-760.

[26] S.-D. Li, Y.-C. Chen, M.J. Hackett, L. Huang, Molecular Therapy, 16 (2008) 163-169.

[27] X. Huang, R.J. Lee, Y. Qi, Y. Li, J. Lu, Q. Meng, L. Teng, J. Xie, Oncotarget, 8 (2017) 96826.

[28] K.S. Italiya, S. Sharma, I. Kothari, D. Chitkara, A. Mittal, Journal of Chromatography B: Analytical Technologies in the Biomedical and Life Sciences, 1061-1062 (2017) 49-56.

[29] X. Ma, Y. Zhao, X.-J. Liang, Accounts of chemical research, 44 (2011) 1114-1122.

[30] L. Zhang, Y. Liao, L. Tang, Journal of Experimental & Clinical Cancer Research, 38 (2019) 1-13.

[31] J.A. Kemp, M.S. Shim, C.Y. Heo, Y.J. Kwon, Advanced Drug Delivery Reviews, 98 (2016) 3-18.

[32] V. Thakur, R.V. Kutty, Journal of Experimental & Clinical Cancer Research, 38 (2019) 1-22.

[33] Y. Mi, J. Zhao, S.-S. Feng, Journal of Controlled Release, 169 (2013) 185-192.

[34] H. Zheng, Y. Kang, Oncogene, 33 (2014) 1755-1763.

[35] P.L. Leopold, Lysosomes: Biology, Diseases, and Therapeutics: Biology, Diseases, and Therapeutics, (2016) 383-407.

[36] A.K. Varkouhi, M. Scholte, G. Storm, H.J. Haisma, Journal of Controlled Release, 151 (2011) 220-228.

[37] N.S. Gandhi, R.K. Tekade, M.B. Chougule, Journal of Controlled Release, 194 (2014) 238-256.

[38] F. Abedi-Gaballu, G. Dehghan, M. Ghaffari, R. Yekta, S. Abbaspour-Ravasjani, B. Baradaran, J.E.N. Dolatabadi, M.R. Hamblin, Applied materials today, 12 (2018) 177-190.

[39] Y. Chen, D.-Y. Gao, L. Huang, Advanced Drug Delivery Reviews, 81 (2015) 128-141.

[40] L. Zhang, X. Yang, Y. Lv, X. Xin, C. Qin, X. Han, L. Yang, W. He, L. Yin, Scientific Reports, 7 (2017) 46186.

[41] B. Hu, L. Zhong, Y. Weng, L. Peng, Y. Huang, Y. Zhao, X.-J. Liang, Signal transduction and targeted therapy, 5 (2020) 1-25.

[42] J. Reddy, C. Abburi, H. Hofland, S. Howard, I. Vlahov, P. Wils, C. Leamon, Gene therapy, 9 (2002) 1542-1550.

[43] K. Müller, E. Kessel, P.M. Klein, M. Höhn, E. Wagner, Molecular Pharmaceutics, 13 (2016) 2332-2345.

[44] C.H. Jones, C.-K. Chen, A. Ravikrishnan, S. Rane, B.A. Pfeifer, Molecular Pharmaceutics, 10 (2013) 4082-4098.

[45] S.S. Myoung, A.L. Kasinski, Strategies for Safe and Targeted Delivery of MicroRNA Therapeutics, in: MicroRNAs in Diseases and Disorders, 2019, pp. 386-415.

[46] B.L. Davidson, P.B. McCray, Nature Reviews Genetics, 12 (2011) 329-340.

[47] D. Chitkara, S. Singh, A. Mittal, Therapeutic Delivery, 7 (2016) 245-255.

[48] S. Patel, J. Kim, M. Herrera, A. Mukherjee, A.V. Kabanov, G. Sahay, Advanced Drug Delivery Reviews, 144 (2019) 90-111.

[49] Y. Wu, M. Crawford, Y. Mao, R.J. Lee, I.C. Davis, T.S. Elton, L.J. Lee, S.P. Nana-Sinkam, Molecular Therapy-Nucleic Acids, 2 (2013) e84.

[50] J.P. Marshalek, P.S. Sheeran, P. Ingram, P.A. Dayton, R.S. Witte, T.O. Matsunaga, Journal of Controlled Release, 243 (2016) 69-77.

[51] M. Yamakuchi, M. Ferlito, C.J. Lowenstein, Proceedings of the National Academy of Sciences, 105 (2008) 13421-13426.

[52] N.A. Yousafzai, Q. Zhou, W. Xu, Q. Shi, J. Xu, L. Feng, H. Chen, V.Y. Shin, H. Jin, X. Wang, Cell death & disease, 10 (2019) 1-12.

[53] M. Motamedi, F. Razmkhah, L. Rezakhani, S. Ghasemi, Journal of gastrointestinal cancer, (2019) 1-7.

[54] A. Savry, M. Carre, R. Berges, A. Rovini, I. Pobel, C. Chacon, D. Braguer, V. Bourgarel-Rey, Neoplasia, 15 (2013) 49-IN17.

[55] E. Slabáková, Z. Culig, J. Remšík, K. Souček, Cell death & disease, 8 (2017) e3100-e3100.

[56] Y. Dai, X. Zhang, Polymer Chemistry, 8 (2017) 7429-7437.

[57] K.B. Knudsen, H. Northeved, P.K. Ek, A. Permin, T. Gjetting, T.L. Andresen, S. Larsen, K.M. Wegener, J. Lykkesfeldt, K. Jantzen, Nanomedicine: Nanotechnology, Biology and Medicine, 11 (2015) 467-477.

Table of contents

Contents		*Page. No.*
Acknowledgements		*i*
List of Abbreviations		*vi*
List of Tables		*xiii*
List of Figures		*xiv*
Abstract		*xx*
Chapter 1	Introduction	1
Chapter 2	Bioanalytical Method Development and Validation	44
Chapter 3	Development and Evaluation of Cationic Lipopolymeric Nanoplexes Containing miRNA-34a	59
Chapter 4	Development and evaluation of folate conjugated lipopolymeric nano-carrier containing docetaxel	91
Chapter 5	Development and evaluation of folate-targeted hybrid lipopolymeric nanoplexes containing docetaxel and miRNA-34a	135
Chapter 6	Conclusions and Future Prospects	178
Appendix I	*List of Publications and Presentations*	*A1*
Appendix II	*Biographies*	*A4*

Acknowledgments

A single flower cannot make a garden, or a single star cannot make the beautiful shiny sky, the same way a research work can never be the outcome of a single individual's talent or efforts. This thesis is a synergistic product of many persons. Though only my name appears on the cover of this dissertation, a great many people have contributed to its preparation. This is the time to say sincere thanks to all those who have, in various ways, helped me to sail through my Ph.D. journey. Though it will not be enough to express my gratitude in words because words are always a poor approximation of what one intends to say, I would still like to give my sincere thanks to all those people.

At the very beginning, I would like to submit myself to the creator of everything ***"The God"*** for bequeathed with blessing, knowledge and strength to make a substantial contribution to the field of pharmacy. Without the blessings of almighty, it would not have been possible to achieve my dreams. Next, I would like to bow myself in front of parents, soul-mate, and elder brother for their blessings to provide me mental and physical well-being to finish this marathon journey on a high note.

First of all, I would like to extend my heartfelt thanks to my research supervisor **Dr**. **Deepak Chitkara**, for giving me a chance to work with him. I would also like to thank him for his guidance, illustrative discussions, having confidence in my abilities and, most importantly, trust and giving me a free hand to explore myself to the fullest of abilities that inspired me to go ahead in research with immense confidence and enthusiasm. It is with fathomless gratitude that expresses my benevolent thanks to my esteem guide and mentor, whose active guidance helped me to develop skills in research procedures, scientific writing and communication. He has boosted my morale with constant encouragement, keen interest in research, positive attitude and enduring support on all occasions. I am indebted to him for his guidance throughout my project. His kind support has been in-estimable for the

completion of my research project. I am highly obliged to him as he truly and wholeheartedly played the role of my guide with his ever helpful and supporting nature. It is my proud privilege to express my heartfelt gratitude for giving me an opportunity to carry out the doctoral research work under his supervision. Thank you, Sir, for your support, and in the future, I would try my level best to live up to your expectations and reach new heights.

My sincere and special thanks to **Dr. Anupama Mittal**, Department of Pharmacy, for her support and kind cooperation from her that made it possible for me. I have benefited very much from her research ideas, guidance, research comments, essentials cell culture facilities, conferring full liberty for research work, and constant encouragement throughout my research work.

I express my sincere and special thanks to my Doctoral Advisory Committee (**DAC Members**), **Dr. Anil Jindal** and **Dr. Aniruddha Roy** for their great cooperation during my Ph.D. and for their valuable, research informative and important suggestions to refine my proposal and thesis.

I sincerely express my gratitude to **Prof. Ram I. Mahato**, Department of Pharmaceutical Sciences, University of Nebraska Medical Center, Omaha, United States, for his valuable inputs in my research work.

I am greatly thankful to **Prof. Souvik Bhattacharyya** (Vice-Chancellor), **Prof. Sudhir Kumar Barai** (Director), **Prof. A.K. Sarkar** (Ex. Director), **Mr. Ernest Samuel Ratnakumar J** (Registrar), **Prof. S. K. Verma** (Dean, Administration), **Prof. S. Krishnaswamy** (Dean, AGSRD), Dr. **Jitendra Panwar** (Associate Dean, AGSRD, Pilani Campus), **Prof. Hemant R. Jadhav** (Head of the Department, Ex. Assoc. Dean, AGSRD, Pilani Campus) and **Prof. R. N. Saha** (Senior Professor and Director, BITS-Pilani, Dubai Campus) for allowing me to pursue my doctoral studies by providing necessary facilities.

I am thankful to all the faculty members of the Department of Pharmacy, BITS Pilani for making my stay in BITS Pilani very productive. I would like to take this opportunity to thank the faculty members of the Department of Pharmacy, **Prof. R. Mahesh** (Ex. Dean, Faculty affairs division), **Dr. Atish T. Paul** (Ex. Head of the Department), **Dr. Rajeev Taliyan**, **Dr. S. Murugesan**, **Dr. Anil B. Gaikwad**, **Dr. Sandeep Sundriyal**, **Dr. Richa Shrivastava**, **Dr. Vaibhav A. Dixit**, **Dr. Sunil Kumar Dubey**, **Dr. Gautam Singhvi** and **Dr. Murali Manohar Pandey** for their cooperation during my Ph.D. Programme. I am also delighted to thank **Dr. Rajeev Sakhuja** and **Dr. Devesh S Agarwal** of the Department of chemistry for their inspirational support during my research work. My special thanks to **Dr. Shushil Yadav** (Senior Vet. In-charge, Animal house Facility) and all non-teaching staff members for providing necessary lab requirements in a timely manner over the years and as well as essential help. My sincere thanks to **Mr. Giridhar Kunkur**, Chief Librarian, BITS Pilani and library staff for their support while utilizing the library facilities.

I would also like to thank **DST-SERB**, **CSIR** and **BITS Pilani** for providing be financial support during the tenure of my Ph.D.

This acknowledgment would be incomplete without mentioning the most basic source of my life energy: my parents, wife, and my elder brother. I have an amazing and unique family in many ways. A special acknowledgment is dedicated to my father; **Mr. Satish Sharma** and father-in-law; **Mr. Vinod Kumar Sharma**, for understanding and providing me the wings to fly high in life. I am indebted to my mother; **Mrs. Babli Sharma** and mother-in-law; **Mrs. Tarun Lata Sharma** for loving me unconditionally, believing and encouraging me. Their vision, ethical principles, moral support, endless patience and eternal inspiration to face any situation in life have guided me to the successful completion of this work and it will continue for the rest of my life for any problem. It feels great to have my wife, **Dr. Mahalaxmi Sharma**, who always have celebrated my success as their own that gave me

immense happiness to achieve the best in my life. A special acknowledgment is dedicated to my elder brother, **Mr. Gaurav Sharma** and Bhabhi **Mr**s. **Ruby Sharma**. Their support has been unconditional all these years; they have given up many things for me to be a Ph.D; they have cherished with me every great moment and supported me whenever I needed it. They have sincerely encouraged and motivated me throughout my research work and lifted me uphill this phase of life, and I have a strong feeling and confidence that they will always be there for me. The words would not be enough to acknowledge the little princess and prince of our house, **Ms. Ira Sharma**, **Mr. Ananata Vardhan** and little **Kiyan** who's smiling face is like an oasis in the desert.

The great inspiring and congenial atmosphere, along with the achievements made in our Lab, is one of the most memorable things in my life. I am fortunate and blessed to meet a fantastic bunch of labmates, **Mr. Sudeep Sudesh Pukale**, **Mr. Deepak. K. Sahel**, **Mr. Prabhjeet Singh**, **Mr. Samrat Mazumdar**, **Mr. Kishan Italiya**, **Mr. Arihant Kumar Singh**, **Mr. Sai Bhargav**, **Ms. Reena Jaytan**, **Mr. Imran Ansari**, **Ms. Moumita Basak** and **Mr. Manoj**, whose untiring and continued support is beyond the word to express. I would also like to acknowledge our collaborators **Prof. Sujata Mohanty** and **Dr. Manu Dalela** (Stem Cell Facility, DBT-Centre of Excellence for Stem Cell Research., All India Institute of Medical Sciences (AIIMS), New Delhi, India) for their continuous help and support to accomplish the research work.

My Special thanks to my friends and my seniors **Mr. Shahid Khan**, **Dr. Zeeshan**, **Dr. Devesh S. Agarwal**, **Dr. Santosh Kumar Goru**, **Dr. Sorabh Sharma**, **Dr. Almesh Kadakol**, **Dr. SNC Sridhar**, **Mr. Krishna**, **Mr. Ginson** and **Ms. Pracheta Sengupta** for their research knowledge and moral support.

I extend my warm thanks to dozens of remarkable friends belonging from the pharmacy department and other departments also for their continuous support during my

research work. Those tea breaks and unending chatting over all kinds of issues personal or professional made days in BITS easy. Without these guys, my life would have been monotonous during these years.

Finally, there are many more my well-wishers, teachers, relatives, friends, whose faith, encouragement, and constant moral support has contributed in a big way in the completion of this work. I express my sincere and special thanks to all of them.

(Saurabh Sharma)

List of Abbreviations

ALT/SGPT	Alanine Aminotransferase/ Serum Glutamic-Pyruvic Transaminase
AM	Amiloride.HCl
AST/SGOT	Aspartate Aminotransferase/ Serum Glutamic-Oxaloacetic Transaminase
AUC	Area Under the Curve
BAX	Bcl2 Associated X
BCL-2	B-Cell Lymphoma 2
BCL-XL	B-Cell Lymphoma-Extra Large
BCS	Biopharmaceutical Classification System
TNBC	Triple Negative Breast Cancer
Be-Chol	Cholester-3-yl(2-bromoethyl)carbamate
BHMP-OBn	Benzyl 3-hydroxy-2-(hydroxymethyl)-2-methylpropanoate
CCM	Cationic amphiphilic lipopolymer
CD44	Cluster of Differentiation 44
CDK4	Cyclin-Dependent Kinase 4
CDK6	Cyclin-Dependent Kinase 6
Cl	Clearance
Cmax	Maximum Concentration
CPCSEA	Committee for the Purpose of Control and Supervision of Experiments on Animals
CPZ	Chlorpromazine
DAPI	4′,6-Diamidino-2-phenylindole
DCC	N, N'- Dicyclohexylcarbodiimide
DCM	Dichloromethane
DCT	Distal Convoluted Tubules

DDAB	Dimethyldidodecylammonium bromide
DE	Double Emulsion Solvent Evaporation Method
DGCR8	DiGeorge Syndrome Chromosomal Region 8
DIC	Differential Interference Contrast
DIPEA	Diisopropylethylamine
DiR	1,1′-Dioctadecyl-3,3,3′,3′-tetramethylindotricarbocyanine iodide
DMEM	Dulbecco's Modified Eagle Medium
DMF	Dimethylformamide
DTX	Docetaxel
E2F3	E2F Transcription Factor 3
EDC	1-Ethyl-3-(3-dimethylaminopropyl)carbodiimide
EDTA	Ethylenediaminetetraacetic acid
EGFR	Epidermal Growth Factor Receptor
EMT	Epithelial-Mesenchymal Transition
EPR	Enhanced Permeation and Retention
ER	Estrogen Receptors
ESI-TOF	Electrospray Ionization Time-of-Flight
EtBr	Ethidium bromide
FA	Folate
FA-NHS	N-Hyrodxysuccinimide Derivative of Folic Acid
FBS	Fetal Bovine Serum
F-DTX-LPNs	DTX loaded folate conjugated lipopolymeric nanoparticles
FE-SEM	Field Emission-Scanning Electron Microscopy
FITC	Fluorescein isothiocyanate
folate-SH	Folate-thiol

Fol-LP	Folate conjugated lipopolymer
FRα	Folate Receptor α
HCl	Hydrochloric acid
HER2	Human Epidermal Growth Factor Receptor 2
HOBT	Hydroxybenzotriazole
HPLC	High Performance Liquid Chromatography
HQC	Higher Quality Control
HR	Hormone Receptor
HRMS	High-Resolution Mass Spectrometry
IAEC	Institutional Animal Ethics Committee
IC50	Half Maximal Inhibitory Concentration
ICAM1	Intercellular Adhesion Molecule 1
ICH	International Council for Harmonisation of Technical Requirements for Pharmaceuticals for Human Use
ICRA	International Cancer Research Agency
IHC	Immuno-Histochemistry
IS	Internal Standard
IVIS	*In Vivo* Imaging System
JAG1	Jagged1
Kel	Elimination rate constant
LDL	Low-Density Lipoprotein
LDLR	Low-Density Lipoprotein Receptor
LE-DT	Docetaxel loaded liposomes
LLE	Liquid-Liquid Extraction
LLOQC	Lower Limits of Quality Control

LMTK3	Lemur Tyrosine Kinase 3
LOD	Limit of Detection
LOQ	Limit of Quantitation
LQC	Low Quality Control
mal-PEG-OH	Maleimide-poly(ethylene glycol)-hydroxyl
MAP	Microtubule Associated Protein
MBC	2-Methyl-2-benzyloxy carbonyl propylene carbonate
MDR-1 protein	Multidrug Resistance Associated Protein
miRNA	MicroRNA
mPEG	methoxypoly(ethylene glycol)
MQC	Middle Quality Control
mRNA	messenger RNA
MRT	Mean Residence Time
MTT	3-(4,5-Dimethylthiazol-2-yl)-2,5-diphenyltetrazolium bromide
MYOD1	Myogenic Differentiation 1
Mβ-CD	Methyl β-cyclodextrin
N	Theoretical Plate Number
N/P ratio	Nitrogen to Phosphate ratio
Na_2SO_4	Sodium sulfate
$NaHCO_3$	Sodium hydrogen carbonate
NEs	Nano-emulsions
NH_4Cl	Ammonium chloride
NHS	N-hydroxysuccinimide
NPs	Nanoparticles

PAMAM	Polyamidoamine
PBS	Phosphate Buffered Saline
PCT	Proximal Convoluted Tubules
Pd/C	Pallidium/carbon
PDA	Photodiode Array
PDCs	Polymer Drug Conjugates
PDI	Polydispersity Index
PEG	Polyethylene glycol
PEI	Polyethylenimine
P-gp	P-glycoprotein
PI	Propidium iodide
PK	Pharmacokinetics
PPT	Protein precipitation
PPTE	Protein precipitation Extraction
PR	Progesterone Receptors
pRb	Phosphorylated Retinoblastoma Protein
Pre-miRNA	Precursor-microRNA
Pri-miRNA	Primary miRNA
PS-80	Polysorbate 80
PSMA	(S)-2-(3-((S)-5-Amino-1-carboxypentyl)ureido)pentanedioic Acid
PTEN	Phosphatase and Tensin Homolog
PTX	Paclitaxel
QC	Quality Control
QS	Quality Standards

RanGTP	GTP Binding Nuclear Protein
RES	Reticuloendothelial System
RISC	RNA Inducing Silencing Complex
RNA POL II/III	RNA polymerase II/III
RNAi	RNA Interference
ROP	Ring-opening polymerization
Rs	Resolution
RSD	Relative Standard Deviation
Rt	Retention time
RT-PCR	Real-Time PCR
SD	Sprague Dawley
SEER	Surveillance, Epidemiology, and End Results
shRNA	short hairpin RNA
siRNA	Small interfering RNA
SLNs	Solid-lipid nanoparticles
$Sn(Oct)_2$	Stannous 2-ethyl hexanoate
STIC	Sophisticated Test and Instrumentation Centre
t1/2	Half-life
TBE	Tris-Borate-EDTA
TGF-β	Transforming Growth Factor Beta
THF	Tetrahydrofuran
TLC	Thin Layer Chromatography
Tmax	Time taken to reach maximum concentration
TNBC	Triple-Negative Breast Cancer
TOF-MS	Time of Flight Mass Spectrometry

TP53	Tumor Protein p53
TPD52	Tumor Protein D52
TRBC	Total Red Blood Cell Count
tRNA	Transfer Ribonucleic Acid
US-FDA	US Food and Drug Administration
UTR	Untranslated Region
VEGF	Vascular Endothelial Growth Factor
Vss	Steady-state volume of distribution
W.H.O.	World Health Organization
XPO5	Exportin-5
ZEB1	Zinc Finger E-Box Binding Homeobox 1
ZEB2	Zinc Finger E-Box Binding Homeobox 2
$\alpha v\beta 3$	Integrin Receptors

List of tables

Table No.	Caption	Page No.
1.1	Physicochemical and pharmacokinetic properties of DTX	6
1.2	Docetaxel nanoformulations in clinical trials	8
1.3	Co-delivery of miRNA and small molecules	19
2.1	%RSD and %Bias in the calibration standards of DTX	54
2.2	Intra-day and Inter-day precision and accuracy of DTX in rat plasma	55
2.3	Stability studies of DTX at four QC levels in rat plasma	56
3.1	Characterization of cationic amphiphilic copolymers	73
3.2	Characterization of miR-34a nanoplexes prepared using cationic amphiphilic copolymers	77
4.1	Characterization of amphiphilic lipopolymers	114
4.2	Pharmacokinetic parameters of free DTX (Taxotere®) and F-DTX-LPNs following intravenous administration at a dose of 10 mg/kg (equivalent to DTX) in *Sprague Dawley* rats. Data are presented as mean ±SD (n=6)	120
5.1	Impact of changing ratio of P4 and Fol-LP polymer on particle size, zeta potential and encapsulation efficiency of hybrid nanoparticles	150
5.2	Pharmacokinetic parameters of DTX and Fam-siRNA after administration of free DTX, FA-DTX nanoparticles, naked Fam-siRNA and Fam-siRNA Nanoplexes at dose of 10 mg/kg and 1 mg/kg of DTX and Fam-siRNA, respectively i.v. via tail vein (n=6)	160
5.3	Hematological and biochemical parameters of *Swiss albino* mice treated with various doses of cationic polymer (10 mg/kg, 20 mg/kg and 100 mg/kg) administered *i.v.* via tail vein	163

List of figures

Figure No.	Captions	Page No.
1.1	miRNA biosynthesis and its mechanism of action	15
1.2	Actively targeted nanoformulation of miRNA and DTX in cancer	33
2.1	Calibration curve for DTX over a range of 0.5 µg/mL to 50 µg/mL	46
2.2	Representative chromatogram of DTX (RT= 4.6 min)	46
2.3	RP-HPLC chromatograms of plasma samples. (A) blank plasma, (B) zero sample (*i.e.* IS spiked with plasma), (C) DTX and IS spiked at LLOQ, (D) DTX and IS spiked at LOD and (E) DTX and IS spiked at MQC	52
2.4	Calibration curve of DTX in rat plasma	53
3.1	Synthesis scheme of amphiphilic copolymers (P1-P4) grafted with N,N-dimethyldipropylenetriamine (cation chain), cholesterol and 4-(2-aminoethyl) morpholine	71
3.2	(A and B) ^{1}H NMR and ^{13}C NMR of the mPEG-b-P(CB-co-LA), (C and D) ^{1}H NMR and ^{13}C NMR of the mPEG-b-P(CB-{g-COOH}-co-LA)	72
3.3	^{1}H NMR of the synthesized cationic copolymers. P1: mPEG-b-P(CB-{g-Cation chain}-co-LA), P2: mPEG-b-P(CB-{g-Cation chain; g-Morph}-co-LA), P3: mPEG-b-P(CB-{g-Cation chain; g-Chol}-co-LA) and P4: mPEG-b-P(CB-{g-Cation chain; g-Chol; g-Morph}-co-LA).	74
3.4	^{13}C NMR of the synthesized cationic copolymers. P1: mPEG-b-P(CB-{g-Cation chain}-co-LA), P2: mPEG-b-P(CB-{g-Cation chain; g-Morph}-co-LA), P3: mPEG-b-P(CB-{g-Cation chain; g-Chol}-co-LA) and P4: mPEG-b-P(CB-{g-Cation chain; g-Chol; g-Morph}-co-LA).	75
3.5	(A) Particle size (B) Zeta potential of the nanoplexes prepared using cationic polymers, (C) miRNA binding ability of cationic polymers investigated by agarose gel electrophoresis. (D) Hemolysis assay of nanoplexes prepared using P4 copolymer. P1: mPEG-b-P(CB-{g-Cation chain}-co-LA), P2: mPEG-b-P(CB-{g-Cation chain; g-Morph}-co-LA), P3: mPEG-b-P(CB-{g-Cation chain; g-Chol}-co-LA) and P4: mPEG-b-P(CB-{g-Cation chain; g-Chol; g-Morph}-co-LA).	76

3.6	Transfection efficiency of the FAM-siRNA in 4T1 cells by flow cytometry. A) Naked FAM-siRNA, B) Lipofectamine-2000®/FAM-siRNA, C) P1/FAM-siRNA, D) P2/FAM-siRNA, E) P3/FAM-siRNA and F) P4/FAM-siRNA. P1: mPEG-b-P(CB-{g-Cation chain}-co-LA), P2: mPEG-b-P(CB-{g-Cation chain; g-Morph}-co-LA), P3: mPEG-b-P(CB-{g-Cation chain; g-Chol}-co-LA) and P4: mPEG-b-P(CB-{g-Cation chain; g-Chol; g-Morph}-co-LA).	78
3.7	Transfection efficiency analysis of FAM-siRNA nanoplexes in MCF-7 cells by flow cytometry. A) Naked FAM-siRNA, B) Lipofectamine-2000®/FAM-siRNA, C) P1/FAM-siRNA, D) P2/FAM-siRNA, E) P3/FAM-siRNA and F) P4/FAM-siRNA. P1: mPEG-b-P(CB-{g-Cation chain}-co-LA), P2: mPEG-b-P(CB-{g-Cation chain; g-Morph}-co-LA), P3: mPEG-b-P(CB-{g-Cation chain; g-Chol}-co-LA) and P4: mPEG-b-P(CB-{g-Cation chain; g-Chol; g-Morph}-co-LA).	79
3.8	Intracellular localization of FAM-siRNA (green) in 4T1 Cells after treatment with (A and C) FAM-siRNA/lipoplexes and (B and D) FAM-siRNA/nanoplexes at 1 h and 2h, E1 and E2) colocalization analysis and scattergram between green pixel intensity (FAM-siRNA) and red pixel intensity (Lysosotracker: red) image of cells treated with siRNA/lipoplexes, F1 and F2) colocalization analysis and scattergram between green pixel intensity (FAM-siRNA) and red pixel intensity (Lysosotracker: red) image of cells treated with FAM-siRNA/nanoplexes. Scale bar represents 10 μm.	80
3.9	Cytotoxicity assay of miR-34a nanoplexes in A) 4T1 and B) MCF-7 cells. Data were presented as mean of three experiments in both cell lines. Statistical analysis were performed using one way ANOVA followed by Tukey's multiple comparison test. ***P < 0.05 was considered as statistically significant.	81
3.10	Flow cytometric analysis of apoptosis in A) 4T1 and B) MCF-7 cells after treatment with blank nanoplexes, mirVana™ miRNA Mimic #1 Negative control (NC miRNA) nanoplexes and miR-34a nanoplexes. All nanoplexes were prepared using mPEG-b-P(CB-{g-Cation chain; g-Chol; g-Morph}-co-LA) (p4) copolymer.	82
4.1	Synthetic scheme of mal-PEG-b-p(MTC-Chol-co-LA) lipopolymer **(9)**	106

4.2	Synthesis scheme of folate-PEG-b-p(MTC-Chol-co-LA) lipopolymer (13)	107
4.3	Synthetic scheme of mPEG-b-p(MTC-Chol-co-LA) lipopolymers (15-18)	107
4.4	(A) 1H NMR and (B) 13C NMR of N-(2-bromoethyl) carbamoyl cholesterol (Be chol)	109
4.5	(A) 1H NMR and (B) 13C NMR of Chol-MPA monomer	110
4.6	(A) 1H NMR and (B) 13C NMR and mass spectrum of the MTC-Chol	111
4.7	(A) 1H NMR and (B) 13C NMR of Thiol-derivatized folate (folate-SH)	112
4.8	1H NMR of (A) mal-PEG-b-p(MTC-Chol-co-LA) and (B) folate-PEG-b-p(MTC-Chol-co-LA)	113
4.9	(A) Characterization of of docetaxel loaded folate-PEG-b-p(MTC-Chol-co-LA) lipopolymeric nanoparticles (F-DTX-LPNs) obtained by using Malvern Zetasizer (Nano-ZS) (n=3), (B) (i) and (ii) SEM image of spherical F-DTX-LPNs, (C) On-bench stability of F-DTX-LPNs for a period of five days and (D) *In-vitro* drug release from free DTX and F-DTX-LPNs. Each point represents the mean ± SD	115
4.10	Fluorescence microscopic images of MDA-MB-231 cells treated with green fluorescent dye (Coumarin6) loaded lipopolymeric nanoparticles. Cells were treated with various endocytosis inhibitors followed by treatment with free C6 or C6 loaded targeted or non-targeted LPNs and analyzed under fluorescent microscope. Cells were counterstained with DAPI to stain the nucleus. The scale bar is 100 μm.	116
4.11	*In vitro* cytotoxicity evaluation of (A) free DTX, DTX-LPNs and F-DTX-LPNs, and (B) blank lipopolymeric nanoparticles in MDA-MB-231 breast cells following treatment. DTX and DTX loaded LPNs were tested in the concentation range from 1-50 nM DTX concetration while blank lipopolymeric nanoparticles were tested in the concentration range 1 μg/mL-100 μg/mL (polymer concentration). Each point represents the mean ± SD. Statistical analysis were performed using one way ANOVA followed by Tukey's multiple comparison test. ns: (Non significant), *(Free DTX vs DTX-LPNs), ** (DTX-LPNs vs F-DTX-LPNs) (* $P \leq 0.05$, ** $P \leq 0.01$) was considered as statistically significant) **(C)** Flow cytometric analysis of apoptosis in MDA-MB-231 cell line treated with free DTX, DTX-LPNs and F-DTX-LPNs at a concetration of 50 nM for 48 h.	118

	Untreated cells, propidium iodide treated cells and blank LPNs treated cells were kept as controls.	
4.12	Gene expression analysis of BAX, Bcl-2, Ki-67 and SIRT-1 in MDA-MB 231 cells treated with Free DTX, DTX-LPNs and F-DTX-LPNs. Each point represents the mean ± SD. Statistical analysis were performed using one way ANOVA followed by Tukey's multiple comparison test. ns: (non-significant) ***(Control vs Free DTX), #(Free DTX vs DTX-LPNs) and @(DTX-LPNs vs F-DTX-LPNs). (* $P < 0.05$, ## $P < 0.01$, @@@ and *** $P < 0.001$) was considered as statistically significant.	119
4.13	Plasma concentration–time profile in SD rats after intravenous (*i.v.*) administration via tail vein injection of free DTX (Taxotere®) and) F-DTX-LNPs at 10 mg/kg dose of DTX. Each point represents the mean ± SD (n=6) and (B) *Ex-vivo* tissue distribution shown by NIRF bio-imaging of F-DiR-LPNs in mice at different time points (n=3) (C) Mean fluorescence intensity (MFI) of DiR dye in different tissues.	121
5.1	(A-B) Comparative particle size distribution and zeta potential of FA-DTXmiR-34a NP and blank NP obtained using Malvern zetasizer, (C) In vitro drug (DTX) release from FA-DTX-NP and Free DTX (Taxotere®), (D) Gel retardation assay of miRNA-34a and folate targeted nanoplexes and E) Heparin competition assay	148
5.2	(A) Flow cytometry evaluations of the transfection efficiencies of FAM-siRNA in 4T1 cell line treated with (i) folate targeted blank nanoplexes (FA-Blank NP), (ii) naked FAM-siRNA, (iii) Lipofectamine-FAM-siRNA, (iv) non-targeted FAM-siRNA nanoplexes (FAM-siRNA NP) and (v) folate targeted FAM-siRNA nanoplexes (FA-FAM-siRNA NP). In these graphs, y-axis represents cell counts and x-axis represents the FAM-siRNA fluorescence intensities, and (B) Transfection efficiency (%) after various treatments of FAM-siRNA formulations in 4T1 cell line. Each point represents the mean ± SD.	151
5.3	(A) Flow cytometry evaluations of the transfection efficiencies of FAM-siRNA in MDA-MB-231 cell line treated with (i) folate targeted blank nanoparticles (FA-Blank NP), (ii) naked FAM-siRNA, (iii) Lipofectamine-FAM-siRNA , (iv) non-targeted FAM-siRNA nanoplexes (FAM-siRNA	152

	NP) and (v) folate targeted FAM-siRNA nanoplexes (FA-FAM-siRNA NP). In these graphs, y-axis represents cell counts and x-axis represents the FAM-siRNA fluorescence intensities, and (B) Transfection efficiency (%) after various treatments of FAM-siRNA formulations in MDA-MB-231 cell line. Each point represents the mean ± SD.	
5.4	(A) Microscopic images of cellular uptake following incubation with Naked FAM-siRNA, FA-FAM-siRNA NP, and FA-FAM-siRNA NP with various endocytosis inhibitors for 4 h in 4T1 cell line and (B) Percent fluorescence intensity of 4T1 cells, indicating higher uptake of FA-FAM-siRNA NP as compared to Naked FAM-siRNA and dropping down of fluoroscence in presence of MβCD and CPZ indicating lipid-raft and clathrin mediated endocytosis. Each point represents the mean ± SD.	153
5.5	(A) Microscopic images of cellular uptake following incubation with Naked FAM-siRNA, FA-FAM-siRNA NP, and FA-FAM-siRNA NP with various endocytosis inhibitors for 4 h in MDA-MB-231 cell line and (B) Percent fluorescence intensity of 4T1 cells and MDA-MB-231 cell, indicating higher uptake of Fol-P/FAM-siRNA Nanoplexes as compared to Naked FAM-siRNA and dropping down of fluoroscence in presence of MβCD and chlorpromazine indicating lipid-raft and clathrin mediated endocytosis. Each point represents the mean ± SD.	154
5.6	(A) *In-vitro* cytotoxicity study and (B) flow cytometric detection of apoptosis in 4T1 cell line incubated for 48 h with various nanoformulation (DTX: 25 nM and miR-34a: 20 pM). Each point represents the mean ± SD. Statistical analysis were performed using one-way ANOVA followed by Tukey's multiple comparison test. ns: (non-significant). (**** $P < 0.0001$) was considered as statistically significant.	156
5.7	(A) *In-vitro* cytotoxicity study and (B) flow cytometric detection of apoptosis in MDA-MB-231 cell line incubated for 48 h with various nanoformulation (DTX: 25 nM and miR-34a: 20 pM). Each point represents the mean ± SD. Statistical analysis were performed using one-way ANOVA followed by Tukey's multiple comparison test. ns: (non-significant). (**** $P < 0.0001$) was considered as statistically significant.	157
5.8	Gene expression analysis of BAX, Bcl-2, Ki-67 and SIRT-1 in 4T1 and	158

	MDA-MB-231 cells treated free DTX and DTX/miR-34a loaded nano-carriers. Each point represents the mean ± SD (n=).	
5.9	Plasma concentration profiles of DTX and Fam-siRNA after administration of (A) free DTX and FA-DTX nanoparticles and (B) Naked Fam-siRNA and Fam-siRNA Nanoplexes at dose of 10 mg/kg and 1 mg/kg of DTX and Fam-siRNA, respectively *i.v.* via tail vein (n=4).	159
5.10	Dose dependent organ toxicity in mice treated with various doses of cationic polymer (10 mg/kg, 50 mg/kg, 100mg/kg) administered *i.v.* via tail vein compared to saline (control). Ratio of weight of the organs (heart, liver, spleen, lungs, kidney) to animal weights in percentage was plotted.	161
5.11	Histopathological evaluation (H&E staining, 40X) of various organs of female mice treated with various doses of cationic polymer from 10 mg/kg to 100mg/kg administered intravenously via tail vein compared to saline (control). For **lungs**, abbreviations are as follow - **black arrows**: normal architecture of alveolar spaces with thin alveolar septa; **sky blue arrow:** mild edema or congestion; **red arrow:** interalveolar septa thickening; **yellow arrow:** mild fibrosis; **green arrow:** mild infiltration of inflammatory cells. For **heart**, abbreviations are as follow- **black arrows**: normal architecture of cardiac myocytes with centrally placed nuclei; **yellow arrow**: moderate to severe disorganization of the myofibrils with severe loss of striations of cardiac myocytes with mild to moderate focal degenerating myocytes; **sky blue arrow**: congestion. For **kidneys**, abbreviations are as follow- **black arrows**: glomerulus; **sky blue arrow**: proximal convoluted tubules PCT; **green arrow**: distal convoluted tubules, DCT. For **liver**, abbreviations are as follow- **red arrow:** hepatocytes; **sky blue arrow:** central vein, CV. For **spleen**, abbreviations are as follow- **red arrow**: white pulp; **yellow arrow**: red pulp. (Magnification: 40X). Scale bar = 50 μm.	166

Abstract

Cancer, being one of the fatal diseases, is of global concern as it affects all strata of populations across all the countries with varying incidences. Among all the cancers, breast cancer is the second leading cause of mortality in women with limited therapeutic options. Thus, it is a need of an hour to prevent incidences of breast cancer and to find effective treatment ways that could prolong the patient's survival as well as the quality of life. Many diagnosed breast cancers are $HER2^+$ and ER^-/PR^-, or $HER2^-/ER^-/PR^-$ triple-negative (TNBC) with poor prognosis. Therapeutic regimen employed in TNBC consist of chemotherapeutic agents, including taxanes (paclitaxel, docetaxel), anthracyclines (doxorubicin), 5-fluorouracil and cyclophosphamide. Among these, docetaxel has been explored widely due to its higher potency and better physico-chemical properties; however, it still offers several challenges in delivery that needs to be addressed. Several nanotechnology-based systems are in the clinical and preclinical investigation to enable the delivery of hydrophobic drugs while largely mitigating the toxicity of chemotherapeutic agents as well as the excipients. There have been several attempts to design novel formulations of docetaxel as well to overcome its side effects along with improvement in drug delivery to the target site. These carrier systems aim to provide *in vitro* and *in vivo* stability, prolonged drug release profile, high intracellular uptake, improved pharmacokinetic profile, enhanced permeability and retention (EPR) at the tumor site, and target specificity to tumor cells.

Further, literature evidence suggested that a combination of small molecules with RNA interference (RNAi) therapeutics such as microRNA (miRNA) could improve the therapeutic outcome. These miRNAs provide the advantage of targeting multiple oncogenic pathways, thus providing a rationale for combining them with chemotherapeutic agents. miRNA-34a (miR-34a) is a master tumor suppressor and can antagonize many oncogenic processes by regulating genes involved in the cell cycle (CDK4, CDK6), apoptosis (BCL2,

survivin), metastasis (JAG1, WNT1, NOTCH1), cancer cell stemness (CD44, NANOG, SOX2) and oncogenic transcription (E2F3, MYC). Literature evidence also suggested that combining DTX with miR-34a could improve the therapeutic outcome in cancer. However, these therapeutics pose challenges for the delivery because of their different physico-chemical properties. miRNAs are high molecular weight, hydrophilic and negatively charged while DTX has poor aqueous solubility and the emergence of resistance that limits its optimal therapeutic use. Additionally, the carrier should deliver the payload at the desired site, could be efficiently uptaken by the cells, undergo endosomal escape and release the payload in the cytoplasm. The research work disclosed in the present thesis entitled **"Development and Evaluation of Lipo-polymeric Nano-carriers Containing MicroRNA-34a and Docetaxel for the Treatment of Breast Cancer"** systematically provides development of a nano-carrier for the delivery of DTX and miR-34a alone and in combination followed by *in vitro* and *in vivo* evaluation of the developed formulations. This doctoral work has been divided into six chapters to achieve the objective of the thesis.

C**hapter 1** of the thesis provides an introduction to breast cancer and TNBC, different treatment strategies, limitation of conventional formulations, particularly DTX formulations and nano-carriers used for delivering DTX. Further, the miRNAs, their biogenesis and therapeutic use in cancer have been discussed. Furthermore, non-viral vectors used for delivering the RNAi therapeutics in particular miRNA and their combination is discussed.

Chapter 2 of the thesis describes the high-performance liquid chromatography (HPLC) methods for the analysis docetaxel in formulation and drug release study samples and its bioanalysis in blood plasma.

Chapter 3 of the thesis describes cationic amphiphilic copolymers grafted with cholesterol (chol), N,N-dimethyldipropylenetriamine (cation chain) and 4-(2-aminoethyl)-morpholine (morph) for miR-34a delivery. The amphiphilic copolymer was synthesized using

a multi-step scheme followed by their thorough characterization using 1H-NMR and elemental analysis. The synthesized copolymer interacts with miR-34a at low N/P ratios (∼2/1) to form nanoplexes of size ∼108 nm and a zeta potential ∼ +39 mV. *In vitro* studies in 4T1 and MCF-7 cells indicated efficient transfection efficiency. The intracellular colocalization suggested that the copolymer effectively transported the FAM-labeled siRNA into the cytoplasm within 2 h and escaped from the endo-/ lysosomal environment. The developed miR-34a nanoplexes inhibited breast cancer cell growth as confirmed by MTT assay wherein 28% and 34% cancer cell viability was observed in 4T1 and MCF-7 cells, respectively. Further, miR-34a nanoplexes possess immense potential to induce apoptosis in both cell lines.

Chapter 4 outlines the folate targeted amphiphilic lipopolymer prepared by microwave-assisted ring-opening polymerization of cholesterol conjugated cyclic carbonate monomer and DL-lactide in the presence of mPEG or maleimide-PEG as a macroinitiator. The synthesized polymer was conjugated with the thiol derivative of folic acid to form a folate targeted lipopolymer. The DTX-loaded folate targeted lipopolymeric nanoparticles (F-DTX-LPNs) prepared by the emulsion solvent evaporation method exhibited a size of ∼115.17 nm with a PDI of 0.205 and encapsulation efficiency of > 80 %. Further, these lipopolymeric nanoparticles showed a good on bench stability and sustained DTX release for seven days. Cell-based assays in MDA-MB 231 cells revealed a significant enhancement in the intracellular uptake of folate targeted lipopolymeric nanoparticles compared to non-targeted nanoparticles. Further, methyl beta-cyclodextrin (Mβ-CD) completely inhibited the uptake of these nanoparticles in the cells, indicating a lipid raft-mediated uptake mechanism. The developed F-DTX-LPNs showed improved cytotoxicity, apoptosis, and significant fold-change in expression levels of Bcl-2, BAX and Ki-67 as compared to non-targeted DTX-LPNs and free DTX. Further, F-DTX-LPNs showed an improved *in-vivo* pharmacokinetic

profile in *Sprague Dawley* rats as compared to the free DTX. The bio-imaging of *ex-vivo* tissues demonstrated that the DiR loaded folate targeted LPNs exhibited intense signals after 24 h due to the sustained release of DiR dye from the nanoparticles.

Chapter 5 presents the folate targeted hybrid lipopolymeric nanoplexes for co-delivering DTX and miR-34a. These nanoplexes were prepared using a combination of the cationic amphiphilic copolymer (outlined in chapter 3) and folate targeted lipopolymer (outlined in chapter 4). These nanoplexes exhibited an average particle size of 129.3 nm, efficient complexation with miR-34a and high entrapment efficiency of DTX (94.8%) with a sustained release profile. These nanoplexes demonstrated significantly high transfection efficiency following both lipid-raft and clathrin-mediated endocytic uptake mechanisms in 4T1 and MDA-MB-231 breast cancer cells. These nanoplexes showed improved cytotoxicity and apoptosis along with significant fold-change in expression levels of Bcl-2, BAX and Ki-67. Further, an improved *in vivo* pharmacokinetics of both DTX and FAM-siRNA was observed in *swiss albino* mice. These cationic polymers used for the preparation of nanoplexes exhibited a safety profile in mice evaluated by hematological parameters, clinical biochemical parameters and histopathology of the tissues.

Chapter 6 provides conclusions of the work and its future scope. These hybrid nanoplexes could serve as a platform for co-delivering hydrophobic small molecules and gene-based therapeutics with a potential synergy for cancer treatment.

APPENDIX

[APPENDIX 1]

List of Publications, Book Chapters & Patents

Publications

From Ph.D. Thesis

1. **Sharma S**, Mazumdar S, Italiya KS, Date T, Mahato RI, Mittal A, Chitkara D. Cholesterol and Morpholine grafted cationic Amphiphilic copolymers for miRNA-34a delivery. Molecular pharmaceutics. 2018 May 10;15(6):2391-402.
2. **Sharma S**, Pukale SS, Sahel DK, Agarwal DS, Dalela M, Mohanty S, Sakhuja R, Mittal A, Chitkara D. Folate-Targeted Cholesterol-Grafted Lipo-Polymeric Nanoparticles for Chemotherapeutic Agent Delivery. AAPS PharmSciTech. 2020 Oct;21(7):1-21.
3. **Sharma S**, Pukale SS, Sahel DK, Singh P, Mittal A, Chitkara D. Folate Targeted Hybrid Lipo-Polymeric Nanoplexes Containing Docetaxel and miRNA-34a for Breast Cancer Treatment. 2020 Nov (Submitted)
4. **Sharma S**, Pukale SS, Mittal A, Chitkara D. Docetaxel and its nanoformulations: how delivery strategies could impact the therapeutic outcome?. Future Science, Therapeutic delivery doi/10.4155/tde-2020-0088(2020).

Book Chapters

5. Vinayak Sadashiv Mharugde, Sudeep Pukale, **Saurabh Sharma**, Anupama Mittal, Deepak Chitkara, Chapter 16: Advancement in Polymeric System for Nucleic Acid Delivery. In Molecular Medicines for Cancer: Concepts and Applications of Nanotechnology, In Molecular Medicines for Cancer: Concepts and Applications of Nanotechnology, Eds. Deepak Chitkara, Anupama Mittal, and Ram I. Mahato, September 2018, CRC Press, Taylor Francis, Florida, USA

Other Publications

6. **Sharma S**, Italiya K, Mittal A, Chitkara D. New strategies for cancer management: how can temozolomide carrier modifications improve its delivery?.Therapeutic delivery, 8 (2017): 475-477.
7. Pukale SS, **Sharma S**, Dalela M, kumar Singh A, Mohanty S, Mittal A, Chitkara D. Multi-component clobetasol-loaded monolithic lipid-polymer hybrid nanoparticles ameliorate imiquimod-induced psoriasis-like skin inflammation in Swiss albino mice. Acta Biomaterialia. 2020 Oct 1;115:393-409.
8. Italiya KS, Mazumdar S, **Sharma S**, Chitkara D, Mahato RI, Mittal A. Self-assembling lisofylline-fatty acid conjugate for effective treatment of diabetes mellitus. Nanomedicine: Nanotechnology, Biology and Medicine. 2019 Jan 1;15(1):175-87.
9. Mazumdar S, Italiya KS, **Sharma S**, Chitkara D, Mittal A. Effective cellular internalization, cell cycle arrest and improved pharmacokinetics of Tamoxifen by cholesterol based lipopolymeric nanoparticles. International Journal of Pharmaceutics. 2018 May 30;543(1-2):96-106.
10. Thotakura N, **Sharma S**, Khurana RK, Babu PV, Chitkara D, Kumar V, Singh B, Raza K. Aspartic acid tagged carbon nanotubols as a tool to deliver docetaxel to breast cancer cells: Reduced hemotoxicity with improved cytotoxicity. Toxicology in Vitro. 2019 Sep 1;59:126-34.
11. Harsha PJ, Thotakura N, Kumar M, **Sharma S**, Mittal A, Khurana RK, Singh B, Negi P, Raza K. A novel PEGylated carbon nanotube conjugated mangiferin: An explorative nanomedicine for brain cancer cells. Journal of Drug Delivery Science and Technology. 2019 Oct 1;53:101186.

12. Kothari IR, Mazumdar S, **Sharma S**, Italiya K, Mittal A, Chitkara D. Docetaxel and alpha-lipoic acid co-loaded nanoparticles for cancer therapy. Therapeutic delivery. 2019 Apr;10(4):227-40.
13. Italiya KS, **Sharma S**, Kothari I, Chitkara D, Mittal A. Simultaneous estimation of lisofylline and pentoxifylline in rat plasma by high performance liquid chromatography-photodiode array detector and its application to pharmacokinetics in rat. Journal of Chromatography B. 2017 Sep 1;1061:49-56.
14. Kothari IR, Italiya KS, Sharma S, Mittal A, Chitkara D. A rapid and precise liquid chromatographic method for simultaneous determination of alpha lipoic acid and docetaxel in lipid-based Nanoformulations. Journal of chromatographic science. 2018 Nov 1;56(10):888-94.

Patents

1. Deepak Chitkara, Sudeep S. Pukale, Arihant K Singh, Anupama Mittal, **Saurabh Sharma**. Applicant- Incisive Element LLC., USA A lipid-polymer hybrid nanoparticle (PCT, filed on 02 Feb 2020; Application no. PCT/IB2020/050819)
2. Deepak Chitkara, Deepak K. Sahel, Kishan S. Italiya, **Saurabh Sharma**, Shruti Saha, Anupama Mittal, Reena Jatyan, A self-assembling drug conjugate and method of preparation thereof. (Indian Patent Application filed on 08 May 2019; Application no. 201911018304)

APPENDIX II

Brief Biography of Dr. Deepak Chitkara

Dr. Deepak Chitkara has obtained his M.S. (Pharm) in Pharmaceutics and Ph.D. (in pharmaceutical Sciences) from the Department of Pharmaceutics, National Institute of Pharmaceutical Education and Research (NIPER), SAS Nagar, Punjab. During his Ph.D., he went to the University of Tennessee Health Science Center (UTHSC), Memphis, TN, USA, as a visiting scholar for one year. He pursued his postdoctoral research with Prof. Ram I. Mahato at the University of Nebraska Medical Center (UNMC), Omaha, NE, USA. He joined the Department of Pharmacy, BITS Pilani, Pilani Campus, as an Assistant Professor since June 2014. He is leading an independent research group wherein his current research interest lies in the development of nano-carriers for the delivery of small molecules, RNAi therapeutics and genome editing tools and their evaluation *in vitro* as well as *in vivo*. Dr. Chitkara has been working in the area of designing Advanced drug delivery systems for small molecules, proteins and gene delivery applications. He has worked extensively in the synthesis of monomers and polymers with different chemical modifications and designing nanomedicines and their evaluation in cell culture and in vivo models. At BITS-Pilani, His lab has well-equipped laboratory for synthesis, formulation development, characterization and evaluation of nanocarriers. His work primarily focuses on the development of novel nanocarrier systems including polymeric nanoparticles, lipid nanoparticles, lipid-polymeric hybrid nanoparticles, micelles, polymer drug conjugate, that can be utilized to deliver several small and macromolecules, and further improving clinical outcomes.

His active contribution in these areas has fetched him more than fourty research and review articles with several international and national patents. Further, he edited an international book entitled "*Molecular medicines for cancer: concepts and applications of nanotechnology*" in 2019. He has successfully completed three projects and is currently running seven sponsored projects funded by various funding agencies viz., DST, DBT and ICMR. He is also running an industry sponsored project from Incisive Element LLC, USA.

Brief Biography of Mr. Saurabh Sharma

Mr. Saurabh Sharma has obtained his Bachelor of Pharmacy in 2013 from Manipal College of Pharmaceutical Sciences (MCOPS), Manipal Campus, Manipal Academy of Higher Education (MAHE) University, Madhav Nagar, Udupi, Karnataka, India and Master of Pharmacy in Pharmaceutics from B. K. Mody Govt. College of Pharmacy, Gujarat Technological University, Ahmedabad, Gujarat, India, in 2015. He worked as an Amrut Mody Research fellow (AMRF) at the Bombay College of Pharmacy, Mumbai University, and as a Project Trainee (Formulation & Development Division) for one year in formulation and development division at Alkem Research Centre, Taloja, Navi Mumbai. In January 2016, he joined BITS-Pilani, Pilani Campus to pursue his doctoral research under the guidance Dr. Deepak Chitakra and worked in a DST-SERB funded project. He also received the CSIR-SRF award in 2018.

His Ph.D. is in the area of nanotherapeutics that encompasses the delivery of microRNA-34a and an anticancer molecule, docetaxel, using a non-viral vector for the treatment of cancer. Over the course of his study, he has been actively engaged in the polymer design and synthesis, formulation development and biological evaluation of designed formulations. He also well versed in performing cell culture-based studies like MTT assay, transfection assay, endocytic uptake pathway, apoptosis, cell cycle analysis, and RT-PCR study. Apart from this, he also has hands-on experience on various instruments like high-pressure homogenizer, fluidized bed processor, spray dryer, pan coater, tablet punching machine and analytical instruments like flow cytometer (Cytoflex), fluorescence microscopy, gel permeation chromatography, gel electrophoresis, HPLC, NMR, FTIR, DSC, UV and spectrofluorimetry. He has 12 original research and 2 review publications in peer-reviewed

journals. Apart from this, he has contributed in one book chapter and is a part of two filed patents. He has also given two oral presentations at the international and national level. He has also presented posters in two international and two national conferences.

molecular pharmaceutics

Article

Cite This: *Mol. Pharmaceutics* 2018, 15, 2391−2402

Cholesterol and Morpholine Grafted Cationic Amphiphilic Copolymers for miRNA-34a Delivery

Saurabh Sharma,[†] Samrat Mazumdar,[†] Kishan S. Italiya,[†] Tushar Date,[†] Ram I. Mahato,[‡] Anupama Mittal,[†] and Deepak Chitkara*[,†]

[†]Department of Pharmacy, Birla Institute of Technology and Science-Pilani (BITS), Pilani Campus, Vidya Vihar, Pilani - 333031, Rajasthan, India

[‡]Department of Pharmaceutical Sciences, College of Pharmacy, University of Nebraska Medical Center, 986125 Nebraska Medical Center, Omaha, Nebraska 68198-6125, United States

ABSTRACT: miR-34a is a master tumor suppressor playing a key role in the several signaling mechanisms involved in cancer. However, its delivery to the cancer cells is the bottleneck in its clinical translation. Herein we report cationic amphiphilic copolymers grafted with cholesterol (chol), *N,N*-dimethyldipropylenetriamine (cation chain) and 4-(2-aminoethyl)-morpholine (morph) for miR-34a delivery. The copolymer interacts with miR-34a at low N/P ratios (~2/1) to form nanoplexes of size ~108 nm and a zeta potential ~ +39 mV. *In vitro* studies in 4T1 and MCF-7 cells indicated efficient transfection efficiency. The intracellular colocalization suggested that the copolymer effectively transported the FAM labeled siRNA into the cytoplasm within 2 h and escaped from the endo-/lysosomal environment. The developed miR-34a nanoplexes inhibited the breast cancer cell growth as confirmed by MTT assay wherein 28% and 34% cancer cell viability was observed in 4T1 and MCF-7 cells, respectively. Further, miR-34a nanoplexes possess immense potential to induce apoptosis in both cell lines.

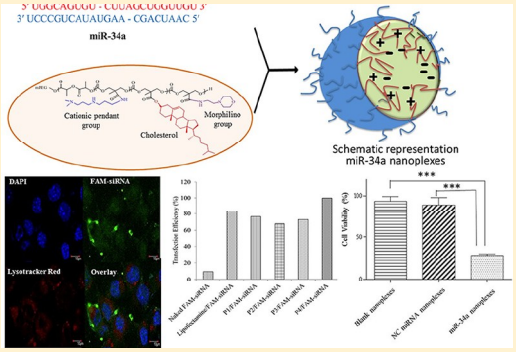

KEYWORDS: *nanoplexes, miR-34a, amphiphilic cationic polymer, anticancer therapy*

INTRODUCTION

miRNAs are endogenous, short, noncoding, 20−25 base pair long oligonucleotides involved in gene expression regulation via mRNA degradation or translation repression.[1] Their abberant expression has been implicated in several diseases including cancer wherein either oncogenic miRNAs are overexpressed or tumor suppressor miRNAs are underexpressed.[2] Among various miRNAs, miRNA-34a (miR-34a) is known as a master tumor suppressor which is transcriptionally activated by p53 and plays a key role in cell proliferation, apoptosis, and metastasis.[2] Its role has been implicated in several cancers including breast cancer,[3] prostate cancer,[4] lung cancer,[5] and pancreatic cancer[6] wherein it suppresses cell proliferation and induces apoptosis by targeting several mRNAs including LMTK3,[7] SIRT1,[8] cSRC,[9] and CD44.[10] Although the potential of miRNA therapeutics is now well established, to achieve its optimal benefit in clinic, several biopharmaceutical issues need to be addressed. Physicochemical properties of miRNAs such as hydrophilicity, high molecular weight, and negative charge make them impermeable to the cellular membranes.[11] Further naked miRNAs are easily filtered through the glomerulus and are unstable in biological milieu due to the presence of RNases, thus making their systemic administration impractical. Several nonviral vectors including lipoplexes,[12] cationic solid lipid nanoparticles,[13] polyplexes,[14] micelleplexes,[15] and dendriplexes[16] have been reported for miRNA delivery. Use of cationic amphiphilic copolymers forms an attractive strategy for complexation with negatively charged miRNA. In a study by Zhang et al. poly(ethylene glycol-*b*-lactide-*b*-arginine) copolymer was used for preparing a reducible nanoformulation for anti-miR-21 delivery to cerebrospinal fluid.[15] In another study, dual stimuli-sensitive mixed polymeric micelles efficiently delivered miR-34a and doxorubicin in tumor tissue.[17] One major advantage of these systems is that their block copolymer structure and composition could be suitably modified to overcome the hurdles of miRNA delivery. Previously, we have also shown that cationic amphiphilic mPEG-polycarbonate based copolymers could deliver miR-205 and gemcitabine to pancreatic cancer cells in vitro and in vivo.[18] In another study, a hedgehog inhibitor, GDC-0449, and miR-let7b was codelivered using these micelles for treating pancreatic cancer.[19]

To further improve the therapeutic outcome of miRNA delivery, important aspects including efficient transfection into the cells followed by their endosomal escape and release of the miRNA in the cytoplasm needs to be controlled. Attempts have been made to improve the delivery by incorporating cholesterol in the carrier system. Cholesterol conjugated chitosan has been

Received: March 2, 2018
Revised: May 5, 2018
Accepted: May 10, 2018
Published: May 10, 2018

DOI: 10.1021/acs.molpharmaceut.8b00228
Mol. Pharmaceutics 2018, 15, 2391−2402

Table 1. Characterization of Cationic Amphiphilic Copolymers

polymer code	cationic copolymers	elemental analysis				^{1}H NMR
		sample weight (mg)	C%	H%	N%	molecular weight (Da)
P1	mPEG-*b*-P(CB$_{82}$-{g-Cation chain$_{11}$}-*co*-LA$_{115}$)	11.98	50.39	9.78	3.76	30 209
P2	mPEG-*b*-P(CB$_{44}$-{g-Cation chain$_{13}$; g-Morph$_5$}-*co*-LA$_{110}$)	4.95	45.63	7.79	7.68	24 342
P3	mPEG-*b*-P(CB$_{78}$-{g-Cation chain$_{36}$; g-Chol$_{30}$}-*co*-LA$_{110}$)	4.28	46.30	7.28	6.48	43 523
P4	mPEG-*b*-P(CB$_{65}$-{g-Cation chain$_{11}$; g-Chol$_{19}$; g-Morph$_6$;}-*co*-LA$_{120}$)	2.56	45.73	5.36	7.55	35 436

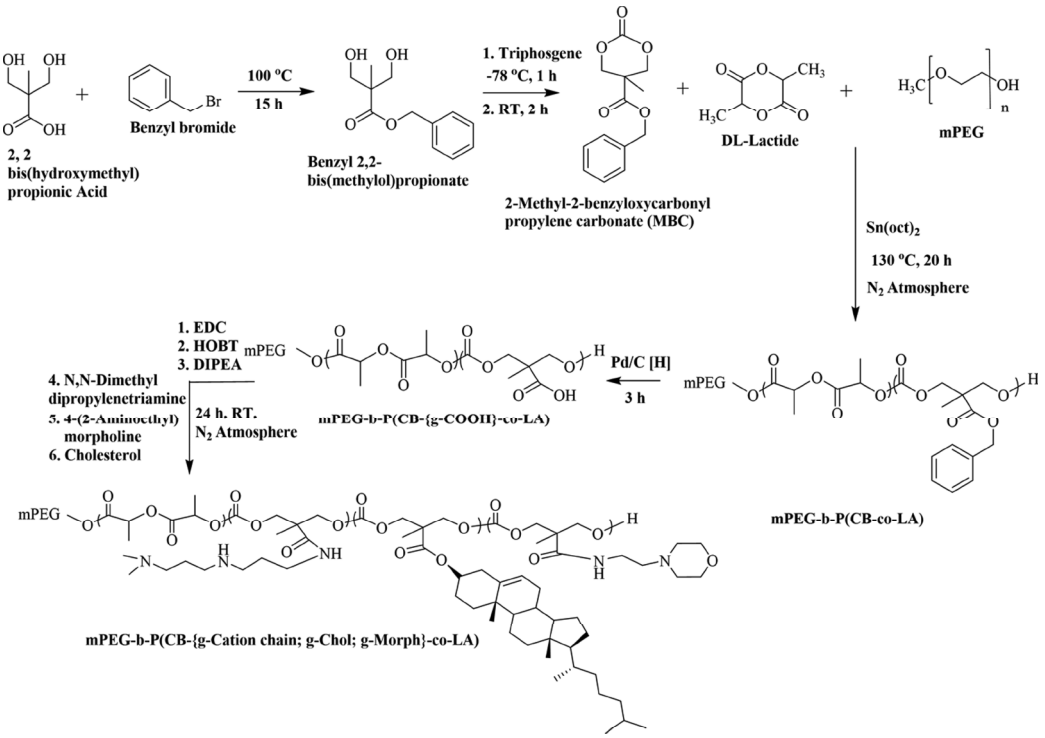

Figure 1. Synthesis of amphiphilic copolymers grafted with *N,N*-dimethyldipropylenetriamine (cation chain), cholesterol, and 4-(2-aminoethyl) morpholine.

used for delivering small molecules including curcumin, paclitaxel, and doxorubicin.[20−23] Huang et al. prepared poly(β-amino esters) and PEG based triblock copolymers grafted with cholesterol for doxorubicin delivery.[24] In a recent study, incorporation of cholesterol-poly(2-(dimethylamino)-ethyl methacrylate) in lecithin liposomes showed enhanced internalization with no colocalization with acidic compartments in HEK-293 cells.[25] Incorporation of a weak base such as an imidazole group or histamine and guanidine in the polymer have been shown to impart endosomal escape by proton sponge effect. Frere et al. showed that morpholine functionality in a polycarbonate based polymer confers buffering ability and proton sponge effect to the polymer.[26]

Herein we report amphiphilic copolymers containing cholesterol, morpholine, and cationic pendant groups (*N,N*-dimethyldipropylenetriamine) on the polycarbonate backbone that could form stable nanoplexes with miR-34a at low N/P ratios. Nanoplexes were prepared by a film hydration method or double emulsion method followed by their thorough characterization for size, zeta potential, and complexation ability. Flow cytometric analysis was performed to study the transfection efficiency of FAM-siRNA loaded nanoplexes in 4T1 (murine) and MCF-7 (human) breast cancer cells. Further colocalization of the nanoplexes with the endo-/lysosomes was determined by confocal microscopy. Hemocompatibility of the nanoplexes was determined by hemolysis assay. Cytotoxicity and apoptosis assessment of miR-34a containing nanoplexes were then performed in 4T1 and MCF-7 breast cancer cells by MTT assay and annexin-V/propidium staining, respectively.

EXPERIMENTAL SECTION

Materials. miRNA-34a-5p mimic, mirVana miRNA Mimic #1 Negative control, and LysoTracker Red DND-99 were purchased from ThermoFischer scientific (Massachusetts, USA). Lipofectamine-2000, Fetal Bovine Serum (FBS), Dulbecco's Modified Eagle Medium (DMEM), Annexin V Alexa fluor 488 conjugate, and TrypLE were obtained from ThermoFisher Scientific (USA). FAM-siRNA was purchased from the GeneCust Europe (Luxembourg). Bis-(hydroxymethyl) propionic acid, benzyl bromide, tin(II) 2-ethylhexanoate, methoxy poly(ethylene glycol) (mPEG, 5000 Da), 4-(2-aminoethyl)morpholine, cholesterol, *N,N*-dimethyl-dipropylenetriamine (DP), and propidium iodide (PI) were purchased from Sigma-Aldrich (St. Louis, MO). DL-Lactide and *N,N*-diisopropylethylamine (DIPEA) were purchased from TCI Chemicals (Japan). All other chemicals and reagents were of analytical grade and purchased from local vendors.

DOI: 10.1021/acs.molpharmaceut.8b00228
Mol. Pharmaceutics 2018, 15, 239−2402

Synthesis of Cationic Amphiphilic Copolymers. A series of cationic amphiphilic copolymers with different ligands (Table 1) on the hydrophobic segment were synthesized using a multistep reaction consisting of synthesis of cyclic monomer, 2-methyl-2-benzyloxycarbonylpropylene carbonate (MBC), synthesis of mPEG-*b*-P(CB-*co*-LA) diblock copolymer followed by its reduction, and coupling of ligands including *N*,*N*-dimethyldipropylenetriamine, cholesterol, and/or 4-(2-aminoethyl)morpholine by EDC/HOBT coupling chemistry as shown in Figure 1. Briefly, a cyclic monomer, MBC, was synthesized in a two-step reaction, wherein a mixture of 2,2-bis(hydroxymethyl) propionic acid and potassium hydroxide was reacted with benzyl bromide in dimethylformamide (DMF) at 100 °C for 15 h. Workup of the crude product was performed followed by recrystallization from toluene to yield a pure intermediate product, benzyl 2,2-bis(methylol)-propionate. In the second step, benzyl 2,2-bis(methylol)-propionate (in a dichloromethane−pyridine mixture) was reacted with triphosgene to obtain MBC as a crude product, which was further recrystallized from ethyl acetate to obtain MBC as white crystals.[27] An amphiphilic copolymer, viz. mPEG-*b*-P(CB-*co*-LA), was synthesized by ring opening polymerization of mPEG with MBC and DL-lactide in the presence of tin(II) 2-ethylhexanoate (10 mol % of mPEG) as the catalyst. The reaction was allowed to continue for 20 h at 130 °C under nitrogen. The crude polymer obtained was dissolved in chloroform and purified by precipitation using diethyl ether and isopropyl alcohol followed by drying under vacuum. The protective benzyl groups from mPEG-*b*-P(CB-*co*-LA) copolymer were removed by catalytic hydrogenation using Pd/C under 45 psi pressure to obtain mPEG-*b*-P(CB-{g-COOH}-*co*-LA) with free carboxyl pendant groups on the polymer backbone.[28]

Carbodiimide/*N*-hydroxybenzotriazole (HOBt) coupling was used to graft 4-(2-aminoethyl)morpholine, cholesterol and/or *N*,*N*-dimethyldipropylenetriamine on the free carboxyl pendant groups of the mPEG-*b*-P(CB-{g-COOH}-*co*-LA) copolymer to yield four cationic copolymers (i.e., containing only cation chain, cation chain + morpholine group, cation chain + cholesterol, and cation chain + cholesterol + morpholine group) and named as P1, P2, P3, and P4, respectively (Table 1). Crude polymers were subsequently purified by precipitation in isopropanol and diethyl ether followed by drying under vacuum. These copolymers were then characterized by ^{1}H NMR and ^{13}C NMR to determine the structure, composition, and molecular weight.[28] For this purpose, copolymers were dissolved in deuterated chloroform ($CDCl_3$) except for mPEG-*b*-P(CB-{g-COOH}-*co*-LA) which was dissolved in DMSO-d6 and analyzed using a Bruker (400 MHz) NMR spectrometer. Elemental composition of synthesized copolymers was determined using the Elementar Vario EL III C−H−N analyzer (Sophisticated Test and Instrumentation Centre (STIC), Cochin University of Science and Technology, Kerala, India) which is based on combustion analysis. An accurately weighed sample was burned in an excess of oxygen followed by collection of the combustion products such as carbondioxide, water, and nitric oxide by different traps. Masses of these combustion products were used to calculate the percentage of C, H, and N present in the copolymers.

Formulation of miR-34a Nanoplexes. The nanoplexes of all four copolymers with miR-34a were prepared by two methods, i.e. a film hydration (FH) method and double emulsion solvent evaporation method (DE).[29−31] In the film hydration method, the copolymer (10 mg) was dissolved in dichloromethane (1 mL) followed by evaporation of the solvent under reduced pressure to obtain a thin film. The film was further redispersed with DNase/RNase free purified water containing miR-34a (200 pmole; 1 mL). The formed nanoplexes were allowed to stand for 30 min at room temperature followed by centrifugation at 2000 rpm for 5 min at 4 °C. In the DE method, the internal aqueous phase consisting of miR-34a solution (40 μL; 5 pmol/μL) in DNase/RNase free purified water was first prepared. The organic phase was prepared by dissolving a copolymer (10 mg) in dichloromethane (0.5 mL). The internal aqueous phase was added dropwise into the organic phase and sonicated for 30 s on a bath sonicator (Ultrasonic, Macroscientific) to form a primary water in oil (w/o) emulsion which was subsequently added to 1 mL of DNase/RNase free purified water and kept for bath sonication for 1 min to obtain w/o/w double emulsion. The resulting double emulsion was stirred at room temperature for 2 h (to evaporate the organic solvent), centrifuged at 2000 rpm for 5 min at 4 °C, and filtered using a 0.22 μm membrane filter. For particle size, polydispersity index, and zeta potential analysis, nanoplexes were taken at a concentration equivalent to 1 mg/mL of polymer in DNase/RNase free purified water and analyzed using Zetasizer (Malvern Nano ZS).

Agarose Gel Retardation Assay. Agarose gel retardation assay was performed to determine the N/P ratio for effective complexation between synthesized cationic copolymers and miR-34a as reported earlier.[18] Briefly, nanoplexes were prepared by the double emulsion method at N/P ratios ranging from 1/1 to 16/1 and loaded on an agarose gel (2% w/v) containing 0.5 μg/mL ethidium bromide (EtBr) and run for 30 min at 90 V in 0.5X Tris-Borate-EDTA (TBE) buffer. The electrophoretic mobility of miR-34a was visualized on a Gel Doc XR+ Gel Documentation system.

Hemocompatibility Assay. A pooled blood sample (2 mL) was collected from swiss albino mice and mixed with EDTA to prevent coagulation. RBCs were obtained from the blood by centrifugation at 1500 rpm at 4 °C for 15 min followed by washing with normal saline solution.[31] These washed RBCs were resuspended in 5 mL of normal saline to obtain RBC dispersion. P4/miR-34 nanoplexes, blank nanoplexes, and distilled water (positive control) were added to 1 mL of RBC dispersion and incubated at 37 °C for 1 h followed by centrifugation at 2000 rpm for 5 min. The supernatant was collected and analyzed using a UV spectrophotometer at 415 nm, and the percentage hemolysis in the samples was determined considering the percent hemolysis induced by distilled water as 100%.

Cell Culture Studies. 4T1 cells were obtained as a kind gift from Dr. Avinash Bajaj (Associate Professor, Regional Centre for Biotechnology, Haryana (NCR Delhi), India), and MCF-7 cells were obtained from the National Centre for Cell Science, Pune. Both cell lines were cultured in Dulbecco's Modified Eagle's Medium (DMEM) supplemented with 10% fetal bovine serum (FBS; HyClone, Logan, UT) and 1% antibiotics and kept in an incubator at 37 °C/5% CO_2.

Transfection Efficiency. FAM-siRNA nanoplexes were used for studying the transfection efficiency by flow cytometry as reported earlier.[32] Briefly, 4T1 and MCF-7 cells were seeded at a cell density of 1×10^5 cells/well in a six-well cell culture plate and allowed to adhere for 24 h. Prior to treatment with the nanoplexes, the culture medium was replaced with Opti-MEM medium for 1 h. Cells were treated then with FAM-

DOI: 10.1021/acs.molpharmaceut.8b00228
Mol. Pharmaceutics 2018, 15, 239−2402

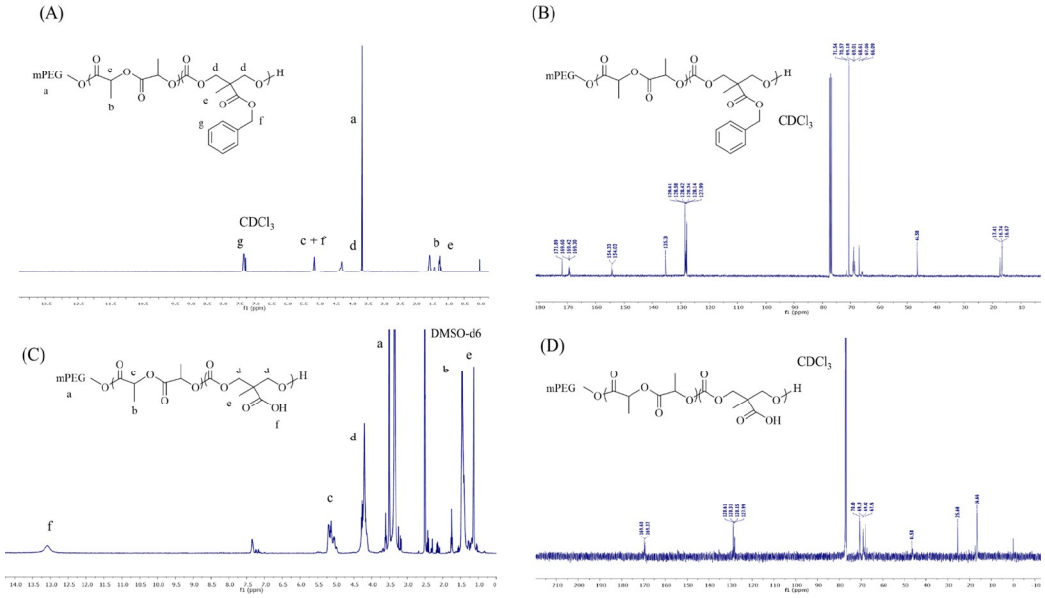

Figure 2. (A and B) ^{1}H NMR and ^{13}C NMR of the mPEG-*b*-P(CB-*co*-LA); (C and D) ^{1}H NMR and ^{13}C NMR of the mPEG-*b*-P(CB-{g-COOH}-*co*-LA).

siRNA nanoplexes for 4 h. Naked FAM-siRNA and lipofectamine-2000/FAM-siRNA lipoplexes were kept as negative and positive control, respectively. After treatment, cells were washed thrice with PBS, trypsinized, and centrifuged at 2000 rpm/5 min at 4 °C and flow cytometric analysis was performed on Cytoflex (Beckman Coulter, USA). The FAM-siRNA was excited with an argon laser (488 nm), and fluorescence was measured at 525 nm. Data were analyzed using CytExpert software.[33]

Endo-/Lysosomal Escape. 4T1 and MCF-7 cells (1×10^5 cells/well) were seeded onto coverslips in six-well cell culture plates. After 24 h, cells were washed with PBS (twice) and the medium was replaced with Opti-MEM followed by treatment with FAM-siRNA nanoplexes or lipofectamine-2000/FAM-siRNA lipoplexes. Cells were then incubated with LysoTracker Red DND 99 (1 μM) for 20 min for endo-/lysosome labeling. Cells were washed with PBS, fixed in paraformaldehyde (4%) for 10 min, and counterstained with DAPI (for nucleus staining; 5 μg/mL). The cells were observed at 100 X (Plan S-Apo, NA 1.4, WD 0.12 mm) (DIC) under a confocal laser scanning microscope (Olympus IX71, DP71, Tokyo, Japan).[16] The colocalization of FAM-siRNA with endo-/lysosomes was analyzed using BioImage XD software wherein a scattergram was plotted between the FAM-siRNA fluorescence (green) and lysosomal fluorescence (red), and the Costes method was used for calulating thresholds and statistics.[34−36]

Cytotoxicity Studies. The cytotoxicity of miR-34a nanoplexes was assessed as reported earlier.[37,38] Briefly, cells (4T1 or MCF-7) were seeded in 96-well plates (5×10^3 cells/well) and allowed to adhere for 24 h followed by treatment with nanoplexes containing 20 pmol of miR-34a. Negative control (NC) nanoplexes (containing mirVana miRNA Mimic **#1** Negative control, a random sequence miRNA mimic molecule) and blank nanoplexes were kept as controls. After 48 h, cell viability was analyzed using the 3-(4,5-dimethylthiazol-2-yl)-2,5-diphenyltetrazolium bromide (MTT) assay. The absorbance was recorded by a microplate reader (BioTek Epoch) at 560 nm and corrected for the cell debris by subtracting the absorbance at 630 nm. The percentage cell viability was determined using the following formula:

$$\%\text{Cell viability} = (\text{Absorbance of sample wells} / \text{Absorbance of control wells}) \times 100$$

Apoptosis Assay. Annexin V, an Alexa Fluor 488 conjugate, was used to detect and quantify apoptosis induced by miR-34a nanoplexes using flow cytometry as per manufacturer's protocol. Briefly, 4T1 or MCF-7 cells were seeded (1×10^6 cells/well) in a 6-well cell culture plate. After 24 h, the media were replaced with fresh media containing blank nanoplexes, miR-34a nanoplexes, or NC miRNA nanoplexes and incubated with cells for 24 h at 37 °C/5% CO_2. After treatment, cells were washed with PBS, trypsinized, centrifuged at 2000 rpm/5 min at 4 °C, resuspended in 1× binding buffer, and stained with Annexin V conjugate (5 μL) and propidium iodide (PI) (10 μL). Flow cytometric analysis was performed on Cytoflex (Beckman Coulter, USA), and data were interpreted using CytExpert software.[13,39]

Statistical Analysis. Data are presented as the mean ± standard deviation. The difference between any two or more groups was determined by analysis of variance. $P < 0.05$ was considered to be statistically significant.

RESULTS

Synthesis and Characterization of Monomers and Copolymers. For delivery of miR-34a, we have synthesized amphiphilic cationic copolymers grafted with ligands including 4-(2-aminoethyl)morpholine, cholesterol, and *N*,*N*-dimethyldipropylenetriamine onto the hydrophobic block (Table 1). A cyclic carbonate monomer, MBC (2-methyl-2-benzyoxycarbonyl propylene carbonate), was synthesized as reported earlier.[27] ^{1}H NMR of MBC showed peaks corresponding to δ 1.2 (CH_3, s, 1H), δ 4.3 (CH_2, d, 2H), 4.7 (CH_2, d, 2H), δ 5.2 (CH_2, s, 2H) and δ 7.3 (C_6H_5, m, 5H). Mass spectroscopy results showed a molecular ion (sodium adduct) peak at 273 *m*/*z* and its (benzylic) daughter ion peak at 90 *m*/*z* indicating the

DOI: 10.1021/acs.molpharmaceut.8b00228
Mol. Pharmaceutics 2018, 15, 239−2402

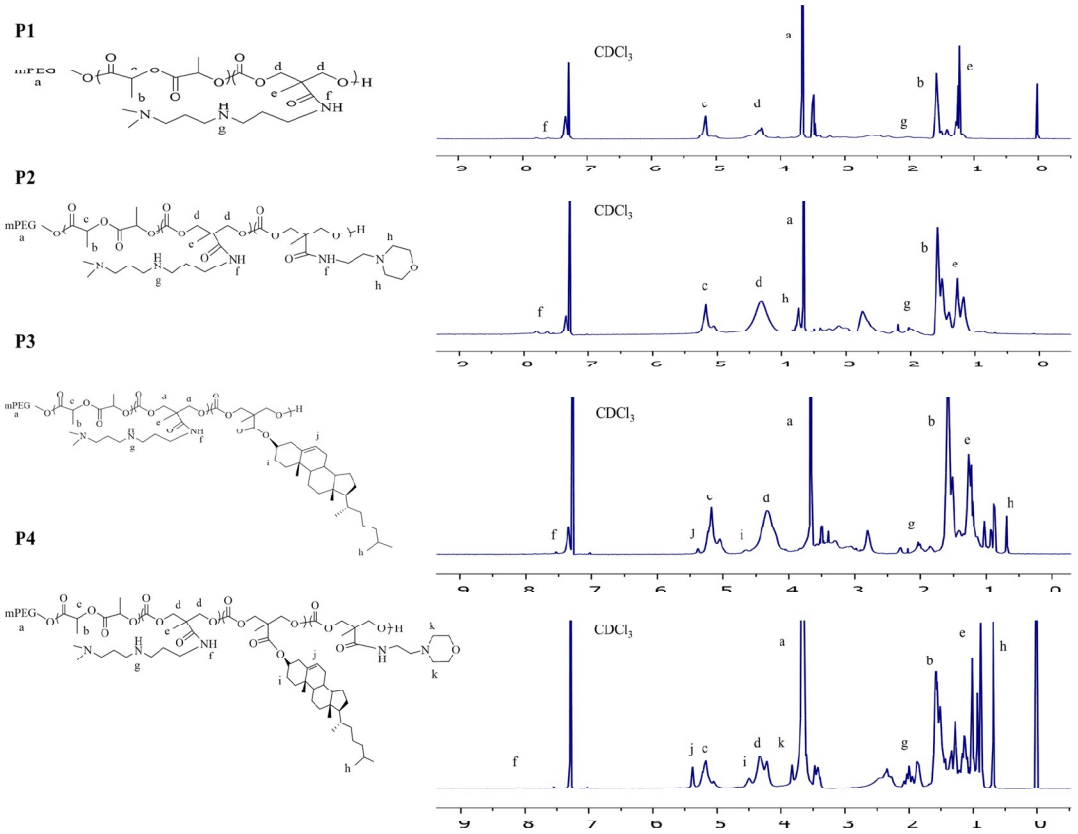

Figure 3. ^{1}H NMR of the synthesized cationic copolymers. P1: mPEG-*b*-P(CB-{g-Cation chain}-*co*-LA). P2: mPEG-*b*-P(CB-{g-Cation chain; g-Morph}-*co*-LA). P3: mPEG-*b*-P(CB-{g-Cation chain; g-Chol}-*co*-LA). P4: mPEG-*b*-P(CB-{g-Cation chain; g-Chol; g-Morph}-*co*-LA).

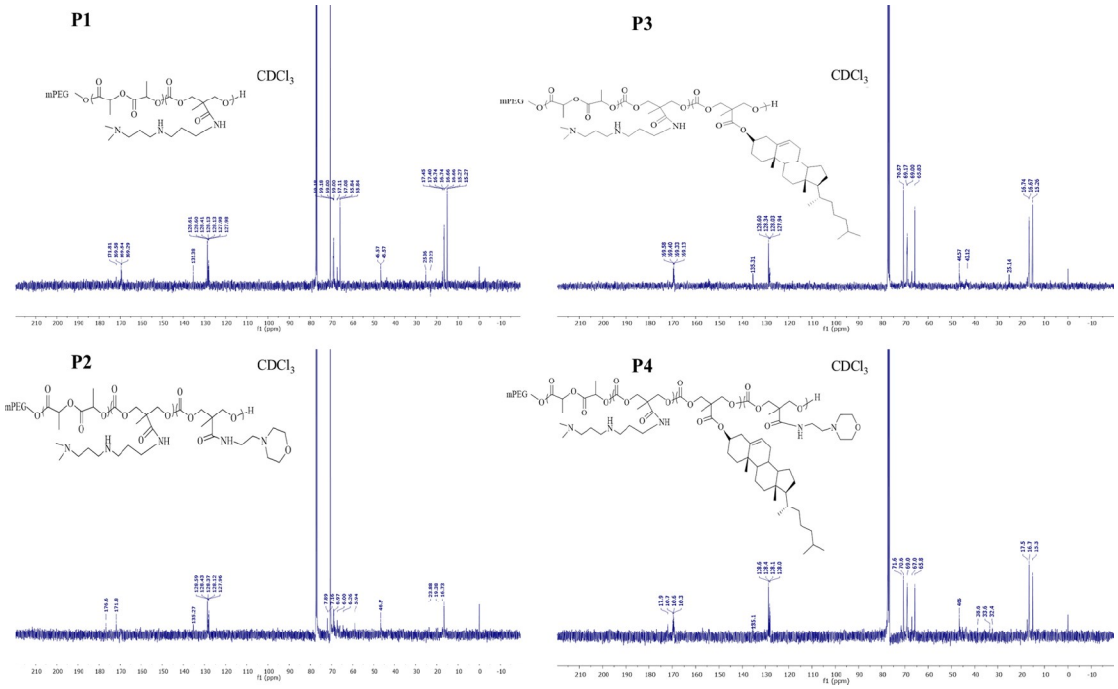

Figure 4. ^{13}C NMR of the synthesized cationic copolymers. P1: mPEG-*b*-P(CB-{g-Cation chain}-*co*-LA). P2: mPEG-*b*-P(CB-{g-Cation chain; g-Morph}-*co*-LA). P3: mPEG-*b*-P(CB-{g-Cation chain; g-Chol}-*co*-LA). P4: mPEG-*b*-P(CB-{g-Cation chain; g-Chol; g-Morph}-*co*-LA).

successful synthesis of the monomer. Further ring opening polymerization of mPEG with DL-lactide and MBC in the presence of tin(II) 2-ethylhexanoate yielded the mPEG-*b*-P(CB-*co*-LA) copolymer with 80% practical yield. Figure 2 A

DOI: 10.1021/acs.molpharmaceut.8b00228
Mol. Pharmaceutics 2018, 15, 2391−2402

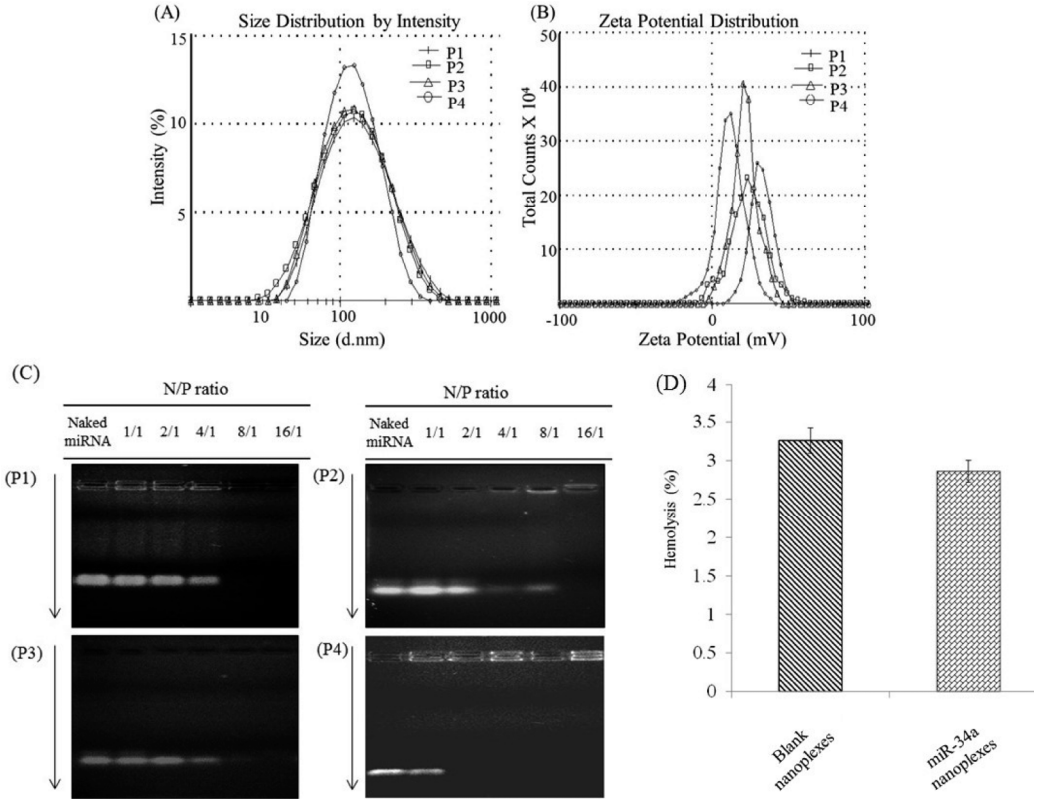

Figure 5. (A) Particle size and (B) zeta potential of the nanoplexes prepared using cationic polymers, (C) miRNA binding ability of cationic polymers investigated by agarose gel electrophoresis and (D) hemolysis assay of nanoplexes prepared using P4 copolymer. P1: mPEG-*b*-P(CB-{g-Cation chain}-*co*-LA). P2: mPEG-*b*-P(CB-{g-Cation chain; g-Morph}-*co*-LA). P3: mPEG-*b*-P(CB-{g-Cation chain; g-Chol}-*co*-LA). P4: mPEG-*b*-P(CB-{g-Cation chain; g-Chol; g-Morph}-*co*-LA).

shows ^{1}H NMR (400 MHz,$CDCl_3$) of synthesized copolymer mPEG-*b*-P(CB-*co*-LA) that showed peaks for mPEG protons at δ 3.56 (CH_2, m, 4H), for 2-methyl-2-benzyoxycarbonyl-propylene carbonate (CB) unit protons at δ 1.24 (CH_3, s, 3H), δ 4.3 (CH_2, m, 4H), δ 5.2 (CH_2, s, 2H), δ 7.3 (C_6H_5, m, 5H) and for lactic acid (LA) protons at δ 1.6 (CH_3, s, 3H) and δ 5.2 (CH, q, 1H). Further, the absence of two peaks (of MBC monomer) at δ 4.3 and δ 4.7 and presence of one proton peak at δ 4.3 (CH_2, m, 4H) indicated the successful ring opening polymerization. Further ^{13}C NMR (100 MHz, $CDCl_3$) (Figure 2 B) of mPEG-*b*-P(CB-*co*-LA) showed peaks at δ 171.9, 169.6, 169.4, 169.3, 154.3, 154, 135.3, 128.6, 128.6, 128.4, 128.3, 128.1, 127.9, 71.5, 70.6, 69.2, 69, 68.6, 67.1, 66.1, 46.6, 17.4, and 16.7. The mPEG-*b*-P(CB-*co*-LA) copolymer was catalytically hydrogenated to obtain mPEG-*b*-P(CB-{g-COOH}-*co*-LA) with free carboxyl pendant groups on the polymer backbone with >90% practical yield. ^{1}H NMR (400 MHz, DMSO-d_6) (Figure 2 C) of mPEG-*b*-P(CB-{g-COOH}-*co*-LA) showed peaks at δ 12−13 (COOH, s, 1H) and the absence of phenylic protons. The broad peak corresponding to carboxylic acid protons was observed in the ^{1}H NMR taken in DMSO-d_6 and was thus used as a solvent of choice for this polymer. Its ^{13}C NMR (100 MHz, $CDCl_3$) (Figure 2 D) showed peaks at δ 169.6, 169.4, 128.6, 128.3, 128.2, 127.9, 70.6, 69.2, 69.0, 67.9, 46.6, 25.6, and 16.7.

Carbodiimide/*N*-hydroxybenzotriazole (HOBt) coupling was used to graft 4-(2-aminoethyl) morpholine, cholesterol, and *N*,*N*-dimethyldipropylenetriamine onto the free carboxyl pendant groups of the mPEG-*b*-P(CB-{g-COOH}-*co*-LA) copolymer to yield a series of cationic copolymers as shown in Table 1. ^{1}H NMR analysis showed peaks corresponding to protons of mPEG, LA, and CB units as given above in addition to the peaks of functional moieties such as cholesterol (at δ 0.8−1.0 (CH_3, s, 6H), δ 4.5 (CH, q, 1H), δ 5.4 (CH, d, 1H)), *N*,*N*-dimethyldipropylenetriamine (at δ 2.1 (NH, s, 1H), δ 7.4 (Amidic NH, s, 1H)), and 4-(2-aminoethyl) morpholine (at δ 3.7 (CH2, m, 4H)), thus indicating the effective coupling of ligands (Figure 3). ^{13}C NMR (100 MHz, $CDCl_3$) of the synthesized copolymers is shown in Figure 4. Copolymer P1 showed peaks at δ (ppm) 171.8, 169.5, 169.3, 135.4, 128.6, 128.4, 128.1, 127.9, 70.6, 69.2, 69.0, 67.1, 67.0, 65.9, 46.6, 25.3, 17.4, 16.7, and 15.3. Copolymer P2 showed peaks at δ (ppm) 176.6, 171.9, 135.3, 128.6, 128.4, 128.1, 127.9, 71.9, 71.2, 68.9, 67.0, 64.3, 58.9, 46.6, and 16.7. Copolymer P3 showed peaks at δ (ppm) 169.6, 169.4, 169.3, 169.1, 135.3, 128.6, 128.3, 128.0, 127.9, 70.6, 69.2, 69, 65.8, 46.6, 25.1, 16.7, and 15.3, and copolymer P4 showed peaks at δ (ppm) 171.9, 169.7, 169.6, 169.3, 128.6, 128.4, 128.1, 128.0, 71.6, 70.6, 69.0, 67.0, 65.8, 46.6, 17.5, 16.7, and 15.3. The molecular weights of the copolymers (P1, P2, P3, and P4) were determined using ^{1}H NMR and found to be 30 209, 24 342, 43 523, and 35 436 Da, respectively. The total carbon, hydrogen, and nitrogen content of the cationic copolymers (P1, P2, P3, and P4) were determined by elemental analysis as shown in Table 1.

Characterization of miRNA-34a Nanoplexes. miRNA-34a nanoplexes prepared by the DE method exhibited a mean particle size of <200 nm with positive zeta potentials ranging from 12 to 39 mV and unimodal distribution showing a bell

DOI: 10.1021/acs.molpharmaceut.8b00228
Mol. Pharmaceutics 2018, 15, 239−2402

shape curve with polydispersity indexes (PDI) ranging from 0.112 to 0.263 (Figure 5 and Table 2). In the case of the film hydration method, nanoplexes exhibited a particle size <200 nm but the polydispersity index (PDI) was high (0.58−0.632) with bimodal particle size distribution.

Table 2. Characterization of miR-34a Nanoplexes Prepared Using Cationic Amphiphilic Copolymers

s. no.	polymer	size (d.nm)	PDI	zeta potential (mV)
1	P1	180 ± 6.38	0.187	12 ± 0.74
2	P2	120 ± 7.42	0.170	31 ± 1.07
3	P3	112 ± 7.89	0.263	27 ± 0.94
4	P4	108 ± 4.56	0.112	39 ± 0.84

Agarose Gel Retardation Assay. The complexation ability of copolymers with miR-34a was analyzed by agarose gel retardation assay. The assay was based on the restricted mobility of miR-34a due to binding with cationic polymers thus resulting in the disappearance of miRNA bands in the agarose gel. miR-34a nanoplexes were prepared by the DE method at N/P ratios ranging from 1/1 to 16/1. The results demonstrated that the electrophoretic mobility of miR-34a was fully retarded at N/P = 2/1 for miR-34a nanoplexes prepared using the P4 copolymer, indicating complete complex formation with miR-34a while miR-34a nanoplexes of P1, P2, and P3 showed complex formation at N/P = 8/1, 16/1, and 8/1, respectively (Figure 5C).

Hemocompatibility Assay. The hemocompatibility assay was performed to study whether the designed formulation carries any RBCs membrane destabilization potential that could be correlated to the hemotoxicity. In hemolysis testing, the nanoplexes were incubated with the RBCs for 1 h followed by determination of hemoglobin content by UV spectroscopy. It was observed that the blank nanoplexes and miR-34a nanoplexes showed 3.26% and 2.86% hemolysis respectively, as compared to double distilled water that showed 100% hemolysis (Figure 5D).

In Vitro Transfection Efficiency. To demonstrate the ability of the nanoplexes to transfect 4T1 and MCF-7 breast cancer cells, we performed the flow cytometry analysis after incubation of cancer cells with FAM-siRNA/nanoplexes. Lipofectamine-2000/FAM-siRNA lipoplexes were taken as a positive control, naked FAM-siRNA was taken as a negative control, and four FAM-siRNA nanoplexes (P1/FAM-siRNA, P2/FAM-siRNA, P3/FAM-siRNA and P4/FAM-siRNA) were taken as test samples. In 4T1 cells, the percentage transfection efficiency was found to be 76.61%, 67.86%, 72.96%, and 99.82% for copolymers P1, P2, P3, and P4, respectively, while lipoplexes (lipofectamine-2000/FAM-siRNA) and naked FAM-siRNA showed transfection efficiency equivalent to 83.74% and 9.55%, respectively (Figure 6). Further in MCF-7 cells the percentage transfection was found to be 36.69%, 39.10%, 42.34%, and 50.82% for copolymers P1, P2, P3, and P4 respectively. Lipoplexes (lipofectamine-2000/FAM-siRNA) and naked FAM-siRNA showed a transfection efficiency of 53.94% and 4.09%, respectively (Figure 7).

Endo-/Lysosomal Escape. Intracellular trafficking and endosomal release of FAM-siRNA from the nanoplexes were studied using confocal microscopy (Figure 8). LysoTracker Red

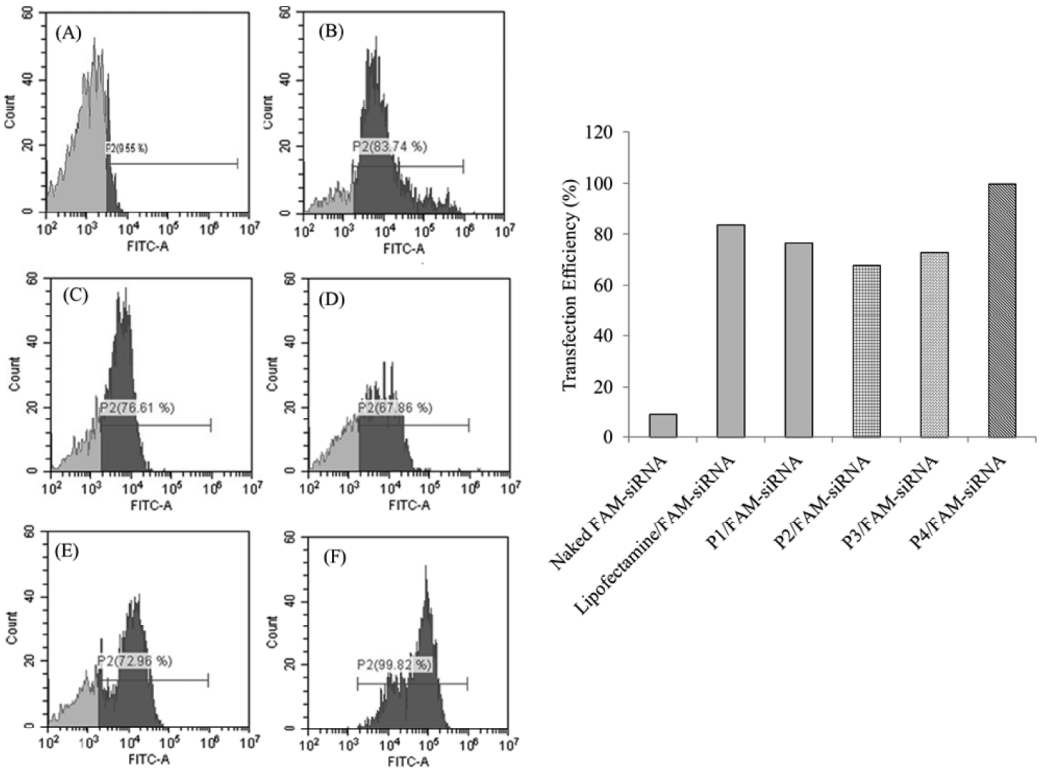

Figure 6. Transfection efficiency of the FAM-siRNA in 4T1 cells by flow cytometry. (A) Naked FAM-siRNA, (B) Lipofectamine-2000/FAM-siRNA, (C) P1/FAM-siRNA, (D) P2/FAM-siRNA, (E) P3/FAM-siRNA, and (F) P4/FAM-siRNA. P1: mPEG-*b*-P(CB-{g-Cation chain}-*co*-LA). P2: mPEG-*b*-P(CB-{g-Cation chain; g-Morph}-*co*-LA). P3: mPEG-*b*-P(CB-{g-Cation chain; g-Chol}-*co*-LA). P4: mPEG-*b*-P(CB-{g-Cation chain; g-Chol; g-Morph}-*co*-LA).

DOI: 10.1021/acs.molpharmaceut.8b00228
Mol. Pharmaceutics 2018, 15, 239−2402

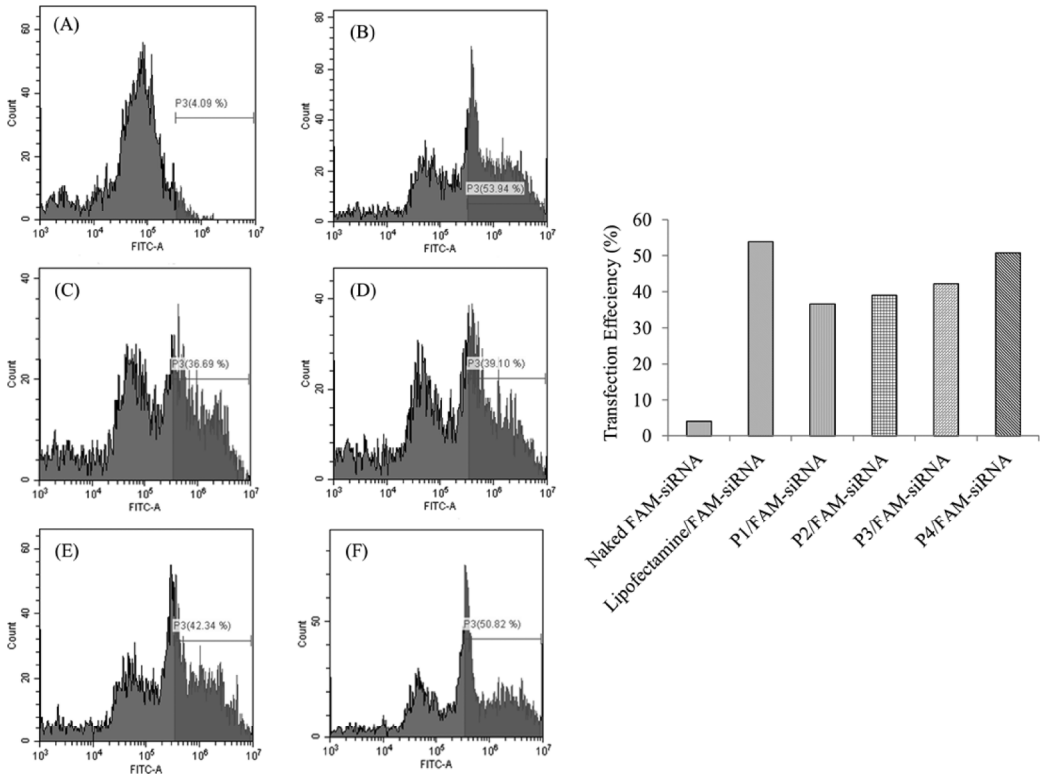

Figure 7. Transfection efficiency of FAM-siRNA in MCF-7 cells by flow cytometry. (A) Naked FAM-siRNA, (B) Lipofectamine-2000/FAM-siRNA, (C) P1/FAM-siRNA, (D) P2/FAM-siRNA, (E) P3/FAM-siRNA, and (F) P4/FAM-siRNA. P1: mPEG-*b*-P(CB-{g-Cation chain}-*cc*-LA). P2: mPEG-*b*-P(CB-{g-Cation chain; g-Morph}-*co*-LA). P3: mPEG-*b*-P(CB-{g-Cation chain; g-Chol}-*co*-LA). P4: mPEG-*b*-P(CB-{g-Cation chain; g-Chol; g-Morph}-*co*-LA).

DND-99 and DAPI dyes were used to stain the acidic vesicles and nucleus, respectively. It was observed that both nanoplexes and lipoplexes were able to deliver FAM-siRNA (green fluorescence) into the 4T1 cells within 1 h. In the case of nanoplexes, discrete punctuated spots were observed along the cell membrane. For lipoplexes, diffused green fluorescence was observed in 1 and 2 h samples. The colocalization was also analyzed by determining the overlap of the pixels of green fluorescence with red fluorescence. The percent of volume colocalized for lipoplexes was 22.6% while in the case of nanoplexes it was only 0.5% indicating no colocalization of FAM-siRNA (green) with the acidic vesicles.

Cytotoxicity Assay miR-34a Nanoplexes. miR-34a is a well-known tumor suppressor and plays an important role in cancer cells proliferation.[21] Cellular cytotoxicity of miR-34a nanoplexes was determined in 4T1 and MCF-7 breast cancer cells. 4T1 is a murine mammary carcinoma cell line from a BALB/cfC3H mouse that represents triple-negative breast cancer and serves as a suitable model to test miR-34a nanoplexes. Further, the hsa-miR-34a-5p mature sequence is similar to the mmu-miR-34a-5p mature sequence (www.mirbase.org). Cells were treated with 20 pmol of miR-34a nanoplexes for 48 h; afterward, the cell viability was measured by MTT assay. Blank nanoplexes and mirVana miRNA Mimic #1 Negative control nanoplexes were kept as controls and showed no cellular cytotoxicity, while miR-34a nanoplexes showed a significant decrease in the cancer cell viability in both 4T1 (28%) and MCF-7 (34%) cells as shown in Figure 9.

Apoptosis Assay. Apoptosis in 4T1 and MCF-7 cells was evaluated after 24 h treatment with miR-34a nanoplexes by flow cytometry. In an FACS plot between FITC-A on the *x*-axis and propidium iodide on the *y*-axis, the viable cells showed annexin $V^{(-)}$ and PI $^{(-)}$ (Q_3 lower left quadrant) whereas the cells in early phase apoptosis showed annexin $V^{(+)}$ and PI $^{(-)}$ (Q_4 at the lower right side) and late phase apoptosis showed annexin$V^{(+)}$ and $PI^{(+)}$ (Q_2 at upper right) while necrotic cells only show $PI^{(+)}$ (Q_1 at upper left side). It was observed that, in 4T1 cells, miR-34a nanoplexes induced 40.66% apoptosis (23.12% early and 17.54% late stage) as compared to 2.54% apoptosis (0.99% early and 1.55% late stage) for NC miRNA nanoplexes and 3.57% apoptosis (1.27% early and 2.30% late stage) for blank nanoplexes. Similar results were obtained in MCF-7 cells wherein miR-34a nanoplexes induced 41.77% apoptosis (24.79% early and 16.98% late stage) as compared to 2.89% apoptosis (1.93% early and 0.96% late stage) for NC miRNA nanoplexes and 3.88% apoptosis (2.29% early and 1.59% late stage) for blank nanoplexes (Figure 10).

■ DISCUSSION

miRNAs are known to be involved in cancer progression, invasion and metastasis wherein their levels are either upregulated or down regulated. miRNAs as therapeutic tool in cancer has been explored by several research groups which have shown improved outcome in terms of increased cytotoxicity, decreased invasion and metastasis.[2,8,17,40] Delivery strategies including nanoplexes,[41] polyplexes,[14] lipoplexes,[42] micelleplexes[15,43] and dendriplexes[44] have been reported for miRNA delivery since naked miRNAs could not penetrate the bilayer lipidic membrane because of high molecular weight, hydrophilic and anionic nature and instability in biological

DOI: 10.1021/acs.molpharmaceut.8b00228
Mol. Pharmaceutics 2018, 15, 239−2402

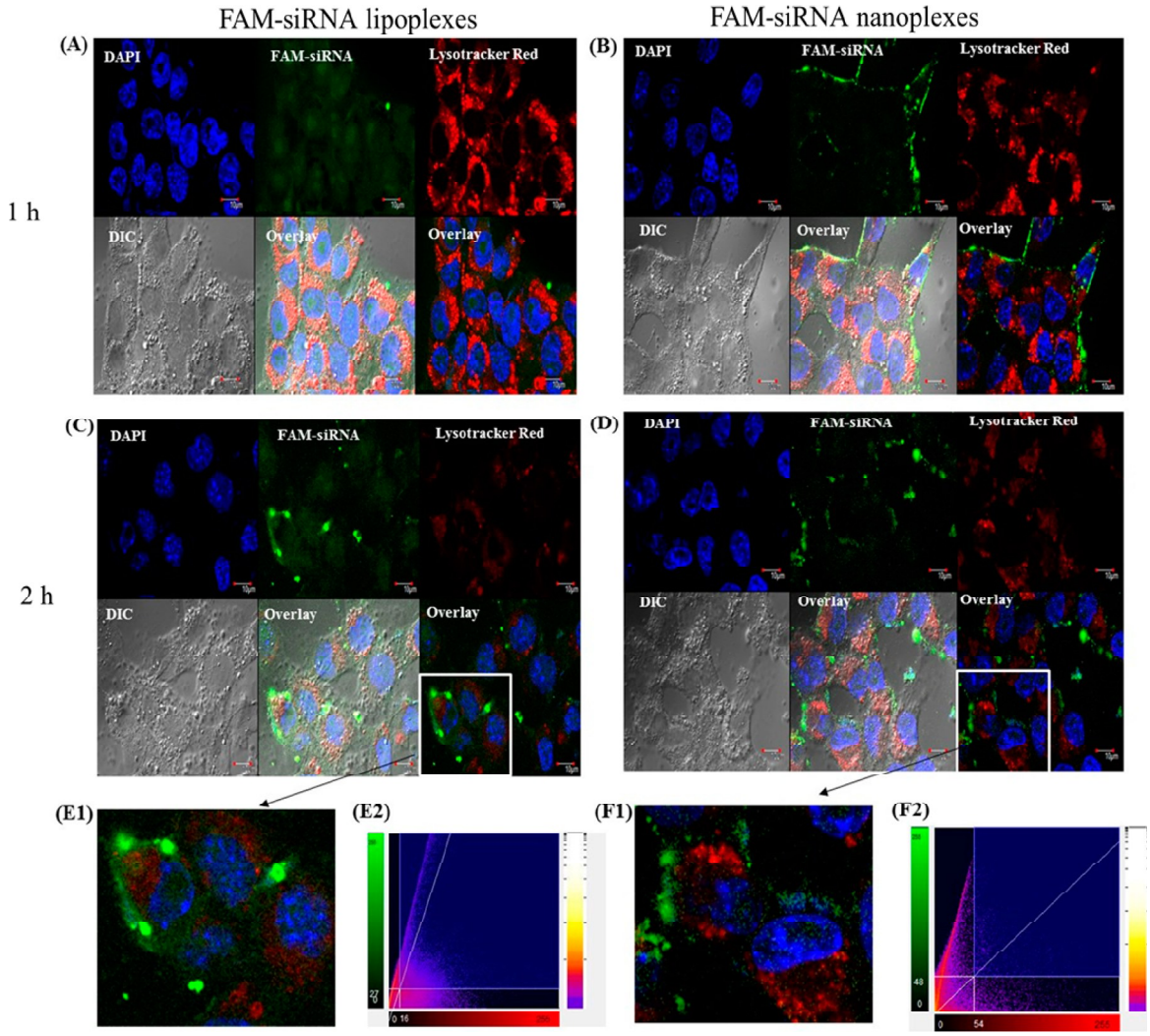

Figure 8. Intracellular localization of FAM-siRNA (green) in 4T1 cells after treatment with (A and C) FAM-siRNA/lipoplexes and (B and D) FAM-siRNA/nanoplexes at 1 h and 2 h, (E1 and E2) colocalization analysis and scattergram between green pixel intensity (FAM-siRNA) and red pixel intensity (Lysosotracker: red) image of cells treated with siRNA/lipoplexes, (F1 and F2) colocalization analysis and scattergram between green pixel intensity (FAM-siRNA) and red pixel intensity (Lysosotracker: red) image of cells treated with FAM-siRNA/nanoplexess. Scale bar represents 10 μm.

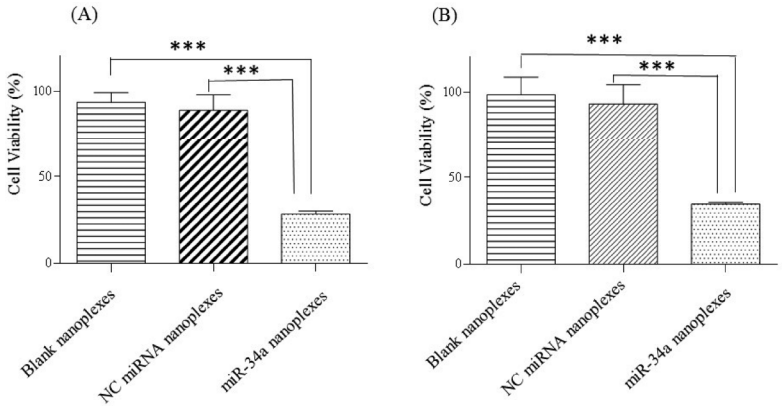

Figure 9. Cytotoxicity assay of miR-34a nanoplexes in (A) 4T1 and (B) MCF-7 cells. Data were presented as mean of three experiments in both cell lines. Statistical analysis were performed using one way ANOVA followed by Tukey's multiple comparison test. ***P < 0.05 was considered as statistically significant.

DOI: 10.1021/acs.molpharmaceut.8b00228
Mol. Pharmaceutics 2018, 15, 2391−2402

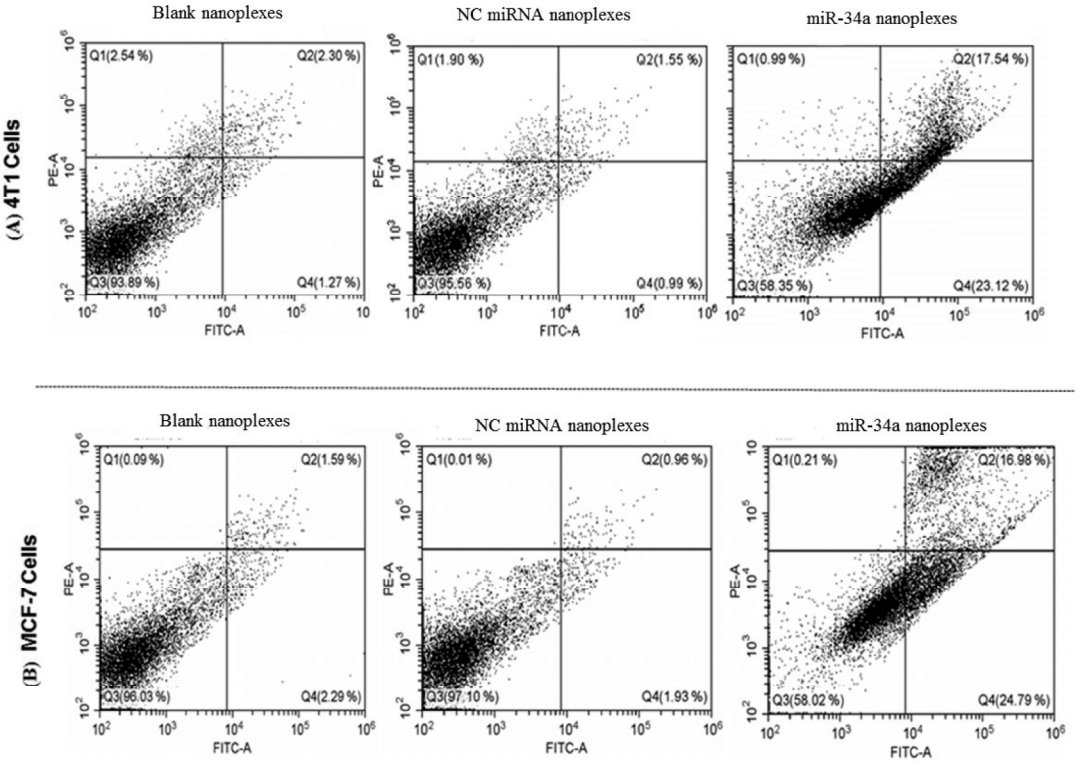

Figure 10. Flow cytometric analysis of apoptosis in (A) 4T1 and (B) MCF-7 cells after treatment with blank nanoplexes, mirVana miRNA Mimic #1 Negative control (NC miRNA) nanoplexes, and miR-34a nanoplexes. All nanoplexes were prepared using mPEG-*b*-P(CB-{g-Cation chain; g-Chol; g-Morph}-*co*-LA) copolymer.

milieu. Apart from effectively complexing miRNAs and protecting them from degradation, another important requirement for ideal delivery system is that they should be able to improve the uptake of miRNA by cancer cells followed by their successful endosomal escape and release into the cytoplasm so that they can get into the RISC assembly for effective mRNA degradation and/or translation repression.[45]

Among various miRNA delivery systems, cationic amphiphilic copolymers offer advantages due to their self-assembly, thermodynamic stability, and lower particle size. Further copolymers could be tailored to improve the delivery of miRNA therapeutics. In a recent study, Kumar et al. prepared nanoplexes of miR-let7b and a cationic copolymer, mPEG-*b*-PCC-*g*-DC-*g*-TEPA at N/P = 16/1, that showed an average particle size of 80 ± 10 nm.[19] In another study,[46] Zhu et al. delivered VEGF siRNA and paclitaxel for prostate cancer by using biodegradable cationic nanoplexes of PDMAEMA-PCL-PDMAEMA triblock copolymers with micelle sizes of 53.6 to 132.2 nm.[46]

Successful *in vivo* delivery of a miRNAs mandates a multifunctional carrier system which can ensure effective complexation with the miRNA (due to its cationic charge) along with the ability to escape from endosomes and release it into the cytoplasm. In the present study, we have designed amphiphilic cationic copolymers with different ligands viz. cholesterol, *N*,*N*-dimethyldipropylenetriamine, and 4-(2-aminoethyl)morpholine attached on the hydrophobic block of the copolymer to enhance the complexation ability, transfection efficiency, and endosomal escape. All synthesized polymers showed self-assembly into nanoplexes in sizes ranging from 108 to 180 nm depending upon the ligand attached to them. For self-assembly, the double emulsion method yielded a smaller particle size and PDI as compared to the film hydration method since the high hydrophobicity of the copolymer does not allow complete redispersion of the film resulting in higher polydispersity.

The synthesized copolymers were first screened for their complexation ability with the miR-34a followed by transfection efficiency in cancer cells. Complexation at lower N/P ratios is preferred since a higher polymer concentration could result in cellular cytotoxicity. Use of different cationic ligands including tetraethylenepentamine, spermine, and *N*,*N*-dimethyldipropylenetriamine has been reported earlier wherein it was shown that copolymers containing *N*,*N*-dimethyldipropylenetriamine effectively complexes miRNA at an N/P ratio of 4:1.[18] Our results indicate efficient complexation with the miR-34a at an N/P ratio of 2:1 for copolymer P4 (Figure 5C). Further, the presence of endosomal escape moieties[26] (such as imidazole, morpholine) could lead to the efficient escape of the miRNA from endosomes. Putnam et al. synthesized a poly L-lysine-grafted-imidazole acetic acid for effective gene transfer with lower cytotoxicity.[47] In this report, authors hypothesized that the balance between cationic amines with endosomal escaping moieties leads to efficient gene transfer with lower cytotoxicity. A weakly basic morpholino group could also have a proton sponge effect, essential for endosomal release.[26] In our copolymer, the *N*,*N*-dimethyldipropylenetriamine cationic chain was incorporated for complexing with the miR-34a by charge interactions resulting in nanoplex formation while morpholine helps in the endosomal escape of the nanoplexes. Cholesterol is one of the components of the cell membrane, so its incorporation in the structure of gene carrier could help in

DOI: 10.1021/acs.molpharmaceut.8b00228
Mol. Pharmaceutics 2018, 15, 2391−2402

improving the biocompatibility and cellular uptake of the carrier. Cheng et al. reported a cholesterol grafted bioreducible (polyamidoamine) polymer for delivery of siRNA which resulted in stable siRNA nanoplexes with higher transfection ability and endosomal escape.[21] Frere et al. have also synthesized a biocompatible polycarbonate polymer containing morpholine and guanidinium for increasing the transfection efficiency, endosomal escape, and complexation ability with siRNA.[14] In the present study, we prepared nanoplexes by using cationic copolymers with FAM labeled siRNA and compared them with lipofectamine-2000 (cationic Lipid) as a positive control for in vitro transfection in cancer cells. The nanoplexes prepared using the copolymer containing both morpholine and cholesterol have showed efficient transfection in 4T1 and MCF-7 cells as compared to lipofectamine-2000 (Figures 6 and 7). Higher transfection by this copolymer could be correlated with the zeta potential of the nanoplexes as reported earlier by Huang et al. wherein better cellular uptake was observed with formulations having higher zeta potential.[24]

In order to study the endosomal escape of the nanoplexes, LysoTracker Red DND 99 dye was used to label the acidic vesicles in the cell and colocalization was studied between the green fluorescence from FAM-siRNA and red fluorescence from endo-/lysolomes. Similar studies were also reported by Nelson et al. for colocalization of pH responsive siRNA polyplexes with acidic vesicles wherein polyplexes showed significantly lower colocalization relative to lipoplexes prepared using lipofectamine-2000.[48] Our data also suggest an efficient endosomal escape of nanoplexes, thus overcoming the hindrance of an endolysosomal barrier in delivery. Another important aspect of miRNA delivery is the safety of the carrier system. In general cationic polymers such as polyethylenimine (PEI) were shown to be cytotoxic thus limiting their translational potential.[49] The developed copolymers showed negligible cellular cytotoxicity toward 4T1 and MCF-7 cells and were nonhemolytic. In order to access the in vitro efficacy of the miR-34a nanoplexes, cytotoxicity and apoptosis assays were performed. miR-34a has been used as a master tumor suppressor miRNA owing to its role in several cancers including breast cancer. Zhao et al. have earlier reported that its overexpression suppresses the MCF-7 cell proliferation and cell viability.[7] We also observed a significant decrease in the cell viability of 4T1 and MCF-7 cells after treatment with miR-34a nanoplexes. Negative control miRNA nanoplexes and blank polyplexes showed no effect on cell viability, indicating their nontoxic and biocompatible nature. Further, the apoptosis assay showed miR-34a nanoplexes effectively suppressed the tumor cell growth by inducing early and late phase apoptosis in breast cancer cells. In summary, the cationic copolymers containing morpholine and cholesterol in the backbone could be used as potential nonviral carriers for delivering miR-34a. They self-assemble to form stable nanoplexes of <200 nm at a low N/P ratio and exhibit improved transfection, endosomal escape, and the ability to inhibit cancer cell growth.

AUTHOR INFORMATION

Corresponding Author

*E-mail: deepak.chitkara@pilani.bits-pilani.ac.in. Phone: 01596 515 835 (O), +91 9660 456 009 (M).

ORCID

Ram I. Mahato: 0000-0003-3588-0434

Deepak Chitkara: 0000-0003-4174-7664

Notes

The authors declare no competing financial interest.

ACKNOWLEDGMENTS

The funding support from Department of Science and Technology (DST), Government of India to D.C. through a young scientist award (YSS/2014/000521) is duly acknowledged. The authors gratefully acknowledge Advanced Instrumentation Research Facility (AIRF), Jawaharlal Nehru University (JNU), New Delhi, India for providing instrumental support for Confocal Laser Scanning Microscopy (CLSM). We also thank Mr. Ashok Kumar Sahu from AIRF, JNU, New Delhi for his help in taking confocal images. Also, we thank Sophisticated Test & Instrumentation Centre (STIC), Cochin University of Science and Technology, Kerala, India for elemental analysis.

REFERENCES

(1) Reddy, K. B. MicroRNA (miRNA) in cancer. *Cancer Cell Int.* **2015**, *15*, 38.

(2) Wang, W.; Luo, Y. P. MicroRNAs in breast cancer: oncogene and tumor suppressors with clinical potential. *J. Zhejiang Univ., Sci., B* **2015**, *16*, 18−31.

(3) Zhou, E.; Hui, N. A.; Shu, M.; Wu, B.; Zhou, J. Systematic analysis of the p53-related microRNAs in breast cancer revealing their essential roles in the cell cycle. *Oncol. Lett.* **2015**, *10*, 3488−3494.

(4) Duan, K.; Ge, Y. C.; Zhang, X. P.; Wu, S. Y.; Feng, J. S.; Chen, S. L.; Zhang, L. I.; Yuan, Z. H.; Fu, C. H. miR-34a inhibits cell proliferation in prostate cancer by downregulation of SIRT1 expression. *Oncol. Lett.* **2015**, *10*, 3223−3227.

(5) Shi, Y.; Liu, C.; Liu, X.; Tang, D. G.; Wang, J. The microRNA miR-34a inhibits non-small cell lung cancer (NSCLC) growth and the CD44hi stem-like NSCLC cells. *PLoS One* **2014**, *9*, e90022.

(6) Tang, Y.; Tang, Y.; Cheng, Y. S. miR-34a inhibits pancreatic cancer progression through Snail1-mediated epithelial-mesenchymal transition and the Notch signaling pathway. *Sci. Rep.* **2017**, *7*, 38232.

(7) Zhao, G.; Guo, J.; Li, D.; Jia, C.; Yin, W.; Sun, R.; Lv, Z.; Cong, X. MicroRNA-34a suppresses cell proliferation by targeting LMTK3 in human breast cancer mcf-7 cell line. *DNA Cell Biol.* **2013**, *32*, 699−707.

(8) Li, L.; Yuan, L.; Luo, J.; Gao, J.; Guo, J.; Xie, X. MiR-34a inhibits proliferation and migration of breast cancer through down-regulation of Bcl-2 and SIRT1. *Clin. Exp. Med.* **2013**, *13*, 109−117.

(9) Adams, B. D.; Wali, V. B.; Cheng, C. J.; Inukai, S.; Booth, C. J.; Agarwal, S.; Rimm, D. L.; Gyorffy, B.; Santarpia, L.; Pusztai, L.; Saltzman, W. M.; Slack, F. J. miR-34a Silences c-SRC to Attenuate Tumor Growth in Triple-Negative Breast Cancer. *Cancer Res.* **2016**, *76*, 927−939.

(10) Liu, C.; Kelnar, K.; Liu, B.; Chen, X.; Calhoun-Davis, T.; Li, H.; Patrawala, L.; Yan, H.; Jeter, C.; Honorio, S.; Wiggins, J. F.; Bader, A. G.; Fagin, R.; Brown, D.; Tang, D. G. The microRNA miR-34a inhibits prostate cancer stem cells and metastasis by directly repressing CD44. *Nat. Med.* **2011**, *17*, 211−215.

(11) Ben-Shushan, D.; Markovsky, E.; Gibori, H.; Tiram, G.; Scomparin, A.; Satchi-Fainaro, R. Overcoming obstacles in microRNA delivery towards improved cancer therapy. *Drug Delivery Transl. Res.* **2014**, *4*, 38−49.

(12) Hong, B. J.; Chipre, A. J.; Nguyen, S. T. Acid-degradable polymer-caged lipoplex (PCL) platform for siRNA delivery: facile cellular triggered release of siRNA. *J. Am. Chem. Soc.* **2013**, *135*, 17655−17658.

(13) Othman, N.; In, L. L.; Harikrishna, J. A.; Hasima, N. Bcl-xL silencing induces alterations in hsa-miR-608 expression and subsequent cell death in A549 and SK-LU1 human lung adenocarcinoma cells. *PLoS One* **2013**, *8*, e81735.

(14) Frere, A.; Baroni, A.; Hendrick, E.; Delvigne, A. S.; Orange, F.; Peulen, O.; Dakwar, G. R.; Diricq, J.; Dubois, P.; Evrard, B.; Remaut,

DOI: 10.1021/acs.molpharmaceut.8b00228
Mol. Pharmaceutics 2018, 15, 2391−2402

K.; Braeckmans, K.; De Smedt, S. C.; Laloy, J.; Dogne, J. M.; Feller, G.; Mespouille, L.; Mottet, D.; Piel, G. PEGylated and Functionalized Aliphatic Polycarbonate Polyplex Nanoparticles for Intravenous Administration of HDAC5 siRNA in Cancer Therapy. *ACS Appl. Mater. Interfaces* **2017**, *9*, 2181−2195.
(15) Zhang, Y.; Buhrman, J. S.; Liu, Y.; Rayahin, J. E.; Gemeinhart, R. A. Reducible Micelleplexes are Stable Systems for Anti-miRNA Delivery in Cerebrospinal Fluid. *Mol. Pharmaceutics* **2016**, *13*, 1791−1799.
(16) Perez, A. P.; Cosaka, M. L.; Romero, E. L.; Morilla, M. J. Uptake and intracellular traffic of siRNA dendriplexes in glioblastoma cells and macrophages. *Int. J. Nanomed.* **2011**, *6*, 2715−2728.
(17) Salzano, G.; Costa, D. F.; Sarisozen, C.; Luther, E.; Mattheolabakis, G.; Dhargalkar, P. P.; Torchilin, V. P. Mixed Nanosized Polymeric Micelles as Promoter of Doxorubicin and miRNA-34a Co-Delivery Triggered by Dual Stimuli in Tumor Tissue. *Small* **2016**, *12*, 4837−4848.
(18) Mittal, A.; Chitkara, D.; Behrman, S. W.; Mahato, R. I. Efficacy of gemcitabine conjugated and miRNA-205 complexed micelles for treatment of advanced pancreatic cancer. *Biomaterials* **2014**, *35*, 7077−7087.
(19) Kumar, V.; Mondal, G.; Slavik, P.; Rachagani, S.; Batra, S. K.; Mahato, R. I. Codelivery of small molecule hedgehog inhibitor and miRNA for treating pancreatic cancer. *Mol. Pharmaceutics* **2015**, *12*, 1289−1298.
(20) Kumari, P.; Muddineti, O. S.; Rompicharla, S. V.; Ghanta, P.; B, B. N. A. K.; Ghosh, B.; Biswas, S. Cholesterol-conjugated poly(D, L-lactide)-based micelles as a nanocarrier system for effective delivery of curcumin in cancer therapy. *Drug Delivery* **2017**, *24*, 209−223.
(21) Cheng, L. C.; Jiang, Y.; Xie, Y.; Qiu, L. L.; Yang, Q.; Lu, H. Y. Novel amphiphilic folic acid-cholesterol-chitosan micelles for paclitaxel delivery. *Oncotarget* **2017**, *8*, 3315−3326.
(22) Yu, J. M.; Li, W. D.; Lu, L.; Zhou, X. Y.; Wang, D. Y.; Li, H. M.; Xu, X. Y.; Chen, J. Preparation and characterization of galactosylated glycol chitosan micelles and its potential use for hepatoma-targeting delivery of doxorubicin. *J. Mater. Sci.: Mater. Med.* **2014**, *25*, 691−701.
(23) Yu, J.; Xie, X.; Zheng, M.; Yu, L.; Zhang, L.; Zhao, J.; Jiang, D.; Che, X. Fabrication and characterization of nuclear localization signal-conjugated glycol chitosan micelles for improving the nuclear delivery of doxorubicin. *Int. J. Nanomed.* **2012**, *7*, 5079−5090.
(24) Huang, X.; Liao, W.; Zhang, G.; Kang, S.; Zhang, C. Y. pH-sensitive micelles self-assembled from polymer brush (PAE-g-cholesterol)-b-PEG-b-(PAE-g-cholesterol) for anticancer drug delivery and controlled release. *Int. J. Nanomed.* **2017**, *12*, 2215−2226.
(25) Szymanowski, F.; Hugo, A. A.; Alves, P.; Simoes, P. N.; Gomez-Zavaglia, A.; Perez, P. F. Endocytosis and intracellular traffic of cholesterol-PDMAEMA liposome complexes in human epithelial-like cells. *Colloids Surf., B* **2017**, *156*, 38−43.
(26) Frere, A.; Kawalec, M.; Tempelaar, S.; Peixoto, P.; Hendrick, E.; Peulen, O.; Evrard, B.; Dubois, P.; Mespouille, L.; Mottet, D.; Piel, G. Impact of the structure of biocompatible aliphatic polycarbonates on siRNA transfection ability. *Biomacromolecules* **2015**, *16*, 769−779.
(27) Danquah, M.; Fujiwara, T.; Mahato, R. I. Self-assembling methoxypoly(ethylene glycol)-b-poly(carbonate-co-L-lactide) block copolymers for drug delivery. *Biomaterials* **2010**, *31*, 2358−2370.
(28) Wu, D.; Zheng, Y.; Hu, X.; Fan, Z.; Jing, X. Anti-tumor activity of folate targeted biodegradable polymer-paclitaxel conjugate micelles on EMT-6 breast cancer model. *Mater. Sci. Eng., C* **2015**, *53*, 68−75.
(29) Navarro, G.; Pan, J.; Torchilin, V. P. Micelle-like nanoparticles as carriers for DNA and siRNA. *Mol. Pharmaceutics* **2015**, *12*, 301−313.
(30) Lundy, B. B.; Convertine, A.; Miteva, M.; Stayton, P. S. Neutral polymeric micelles for RNA delivery. *Bioconjugate Chem.* **2013**, *24*, 398−407.
(31) Dhanya, C.; Jeyaraman, J.; Janeesh, P.; Shukla, A.; Sivakumar, S.; Abraham, A. Bio-distribution and in vivo/in vitro toxicity profile of PEGylated polymer capsules encapsulating LaVO 4: Tb 3 nanoparticles for bioimaging applications. *RSC Adv.* **2016**, *6*, 55125−55134.
(32) Sun, P.; Huang, W.; Jin, M.; Wang, Q.; Fan, B.; Kang, L.; Gao, Z. Chitosan-based nanoparticles for survivin targeted siRNA delivery in breast tumor therapy and preventing its metastasis. *Int. J. Nanomed.* **2016**, *11*, 4931−4945.
(33) Ran, R.; Liu, Y.; Gao, H.; Kuang, Q.; Zhang, Q.; Tang, J.; Fu, H.; Zhang, Z.; He, Q. PEGylated hyaluronic acid-modified liposomal delivery system with anti-gamma-glutamylcyclotransferase siRNA for drug-resistant MCF-7 breast cancer therapy. *J. Pharm. Sci.* **2015**, *104*, 476−484.
(34) Dunn, K. W.; Kamocka, M. M.; McDonald, J. H. A practical guide to evaluating colocalization in biological microscopy. *Am. J. Physiol. Cell. Physiol.* **2011**, *300*, C723−42.
(35) Abraham, T.; Allan, S. E.; Levings, M. K. Deconvolution and chromatic aberration corrections in quantifying colocalization of a transcription factor in three-dimensional cellular space. *Micron* **2010**, *41*, 633−640.
(36) Villalta, J. I.; Galli, S.; Iacaruso, M. F.; Antico Arciuch, V. G.; Poderoso, J. J.; Jares-Erijman, E. A.; Pietrasanta, L. I. New algorithm to determine true colocalization in combination with image restoration and time-lapse confocal microscopy to MAP kinases in mitochondria. *PLoS One* **2011**, *6*, e19031.
(37) Wang, L.; Zhang, X.; Cui, G.; Chan, J. Y.; Wang, L.; Li, C.; Shan, L.; Xu, C.; Zhang, Q.; Wang, Y.; Di, L.; Lee, S. M. A novel agent exerts antitumor activity in breast cancer cells by targeting mitochondrial complex II. *Oncotarget* **2016**, *7*, 32054−32064.
(38) Bao, L.; Hazari, S.; Mehra, S.; Kaushal, D.; Moroz, K.; Dash, S. Increased expression of P-glycoprotein and doxorubicin chemoresistance of metastatic breast cancer is regulated by miR-298. *Am. J. Pathol.* **2012**, *180*, 2490−2503.
(39) Khuu, C.; Jevnaker, A. M.; Bryne, M.; Osmundsen, H. An investigation into anti-proliferative effects of microRNAs encoded by the miR-106a-363 cluster on human carcinoma cells and keratinocytes using microarray profiling of miRNA transcriptomes. *Front. Genet.* **2014**, *5*, 246.
(40) Misso, G.; Di Martino, M. T.; De Rosa, G.; Farooqi, A. A.; Lombardi, A.; Campani, V.; Zarone, M. R.; Gulla, A.; Tagliaferri, P.; Tassone, P.; Caraglia, M. Mir-34: a new weapon against cancer? *Mol. Ther.−Nucleic Acids* **2014**, *3*, e195.
(41) Salva, E.; Turan, S. O.; Akbuga, J. The development of ternary nanoplexes for efficient small interfering RNA delivery. *Biol. Pharm. Bull.* **2013**, *36*, 1907−1914.
(42) Wu, Y.; Crawford, M.; Yu, B.; Mao, Y.; Nana-Sinkam, S. P.; Lee, L. J. MicroRNA delivery by cationic lipoplexes for lung cancer therapy. *Mol. Pharmaceutics* **2011**, *8*, 1381−1389.
(43) Zhang, Y.; Liu, Y.; Sen, S.; Kral, P.; Gemeinhart, R. A. Charged group surface accessibility determines micelleplexes formation and cellular interaction. *Nanoscale* **2015**, *7*, 7559−7564.
(44) Conti, D. S.; Brewer, D.; Grashik, J.; Avasarala, S.; da Rocha, S. R. Poly(amidoamine) dendrimer nanocarriers and their aerosol formulations for siRNA delivery to the lung epithelium. *Mol. Pharmaceutics* **2014**, *11*, 1808−1822.
(45) Dominska, M.; Dykxhoorn, D. M. Breaking down the barriers: siRNA delivery and endosome escape. *J. Cell Sci.* **2010**, *123*, 1183−1189.
(46) Zhu, C.; Jung, S.; Luo, S.; Meng, F.; Zhu, X.; Park, T. G.; Zhong, Z. Co-delivery of siRNA and paclitaxel into cancer cells by biodegradable cationic micelles based on PDMAEMA-PCL-PDMAEMA triblock copolymers. *Biomaterials* **2010**, *31*, 2408−2416.
(47) Putnam, D.; Gentry, C. A.; Pack, D. W.; Langer, R. Polymer-based gene delivery with low cytotoxicity by a unique balance of side-chain termini. *Proc. Natl. Acad. Sci. U. S. A.* **2001**, *98*, 1200−1205.
(48) Nelson, C. E.; Kintzing, J. R.; Hanna, A.; Shannon, J. M.; Gupta, M. K.; Duvall, C. L. Balancing cationic and hydrophobic content of PEGylated siRNA polyplexes enhances endosome escape, stability, blood circulation time, and bioactivity in vivo. *ACS Nano* **2013**, *7*, 8870−8880.
(49) Xue, H. Y.; Liu, S.; Wong, H. L. Nanotoxicity: a key obstacle to clinical translation of siRNA-based nanomedicine. *Nanomedicine (London, U. K.)* **2014**, *9*, 295−312.

DOI: 10.1021/acs.molpharmaceut.8b00228
Mol. Pharmaceutics 2018, 15, 239−2402

AAPS PharmSciTech (2020) 21:280
DOI: 10.1208/s12249-020-01812-y

Research Article

Folate-Targeted Cholesterol-Grafted Lipo-Polymeric Nanoparticles for Chemotherapeutic Agent Delivery

Saurabh Sharma,[1] Sudeep Sudesh Pukale,[1] Deepak K. Sahel,[1] Devesh S. Agarwal,[2] Manu Dalela,[3] Sujata Mohanty,[3] Rajeev Sakhuja,[2] Anupama Mittal,[1] and Deepak Chitkara[1,4]

Received 21 July 2020; accepted 2 September 2020

Abstract. Docetaxel (DTX), an FDA approved chemotherapeutic agent, is used as a first-line treatment for triple-negative breast cancer (TNBC). Its poor aqueous solubility, rapid metabolism, short half-life, and effective targeting to the cancer cells limits its optimal therapeutic use. Herein, we report folate targeted amphiphilic lipopolymer grafted with cholesterol conjugated carbonate and DL-lactide prepared by microwave assisted ring opening polymerization, for the efficient actively targeted delivery of DTX. The DTX-loaded folate-targeted lipopolymeric nanoparticles (F-DTX-LPNs) prepared by the emulsion solvent evaporation method exhibited a smaller size of ~115.17 nm with a PDI of 0.205 and encapsulation efficiency of >80%. Further, these lipopolymeric nanoparticles (F-DTX-LPNs) showed a good on-bench stability and sustained DTX release for 7 days. Cell-based assays in MDA-MB-231 cells revealed a significant enhancement in the intracellular uptake of folate-targeted lipopolymeric nanoparticles compared to non-targeted nanoparticles. Further, methyl beta-cyclodextrin (Mβ-CD) completely inhibited the uptake of these nanoparticles in the cells, indicating a lipid raft-mediated uptake mechanism. The developed F-DTX-LPNs showed improved cytotoxicity, apoptosis, and significant fold-change in expression levels of Bcl-2, BAX and Ki-67 as compared to non-targeted DTX-LPNs and free DTX. Further, F-DTX-LPNs showed an improved *in vivo* pharmacokinetic profile in *Sprague Dawley* rats as compared to the free DTX. The bio-imaging of *ex vivo* tissues demonstrated that the DiR loaded folate targeted LPNs exhibited intense signals after 24 h because of slow release of DiR dye from the nanoparticles.

KEY WORDS: Docetaxel; Targeting; Folate; Breast cancer; Lipopolymers; Nanoparticles.

INTRODUCTION

Among the currently available chemotherapeutics, docetaxel (DTX; a 'Taxane' derivative) is a highly potent FDA approved small molecule used as a first-line treatment for triple-negative breast cancer (TNBC). It acts by stabilizing tubulin heterodimer, resulting in impaired mitosis and inhibition of cellular proliferation in the cancer cells (1,2). However, DTX has poor aqueous solubility and undergoes rapid metabolism in the biological environment resulting into lower plasma half-life (3,4). Taxotere® is a commercially available product of docetaxel; however, its administration is associated with several undesirable side effects, including hypersensitivity reactions, fluid retention, neurotoxicity, musculoskeletal toxicity, and neutropenia (5). There is also a risk of development of drug resistance due to its efflux by P-glycoprotein (P-gp) (6). Also, the product has a stability issue as it should be used within 8 h post-dilution with the infusion fluid as it gets precipitated. Further, the presence of a higher amount of surfactant and ethanol necessitates the use of special tubing materials of infusion bag assembly to prevent the problem of leaching of plastic components. Thus, high cost is also a major pitfall of the available product.

Over the past few decades, nanotechnology has made major contributions in cancer treatment with several nanocarriers being explored and translated to the clinic, including liposomes (Doxil® and Myocet®) (7), albumin-bound paclitaxel nanoparticle (Abraxane®) and polymeric micelles (Genexol® PM) (8). Further, several nanotechnology based systems are in the clinical and preclinical investigation to enable the delivery of hydrophobic drugs while largely

[1] Department of Pharmacy, Birla Institute of Technology and Science (BITS)-Pilani, Pilani Campus, Vidya Vihar, Pilani, 333 031, Rajasthan, India.
[2] Department of Chemistry, Birla Institute of Technology and Science (BITS)-Pilani, Pilani Campus, Vidya Vihar, Pilani, 333 031, Rajasthan, India.
[3] Stem Cell Facility, DBT-Centre of Excellence for Stem Cell Research, All India Institute of Medical Sciences (AIIMS), New Delhi, 110029, India.
[4] To whom correspondence should be addressed. (e-mail: deepak.chitkara@pilani.bits-pilani.ac.in)

Published online: 09 October 2020

mitigating the toxicity of chemotherapeutic agents as well as the excipients (9–11). There have been several attempts to design novel formulations of docetaxel as well to overcome its side effects along with improvement in drug delivery to the target site. These carrier systems aim to provide *in vitro* and *in vivo* stability, prolonged drug release profile, high intracellular uptake, improved pharmacokinetic profile, enhanced permeability and retention (EPR) at the tumor site, and target specificity to tumor cells (12). Tao et al. prepared the functionalized aptamer-based DTX loaded nanoparticles by simple surface modification method that showed efficient drug targeting to the tumor site with an effective and safe treatment as compared to Taxotere and nanoparticles without surface modification (13). In another study, Bowerman et al. reported the PLGA based nanoparticles by using modern technology (PRINT), which can encapsulate DTX, actively transport it to the tumor site, and showed to be effective in a taxane resistant triple-negative breast cancer (14).

Among different materials used for preparing nanoparticles, biodegradable polymers including polyesters and polycarbonates, have gained enormous interest owing to the advantages, such as biodegradability and biocompatibility, amenability to surface modification, tailor-made properties to suit delivery requirements, *etc.* Danquah et al. reported the PEGylated polyester and polycarbonate-based amphiphilic diblock copolymer for controlled delivery of hydrophobic non-steroidal anti androgen, bicalutamide for treating prostate cancer that showed an improvement in the drug loading of the hydrophobic drug by incorporating the carbonate moiety as compared to PEG-b-PLLA (15). In another study, Bariwal et al. reported the efficient loading of a novel tubulin destabilizing agent (QW-296) in m-PEG-b-P(CB-co-LA) nanoparticles for treating metastatic melanoma (16). The nanoparticles showed improved QW-296 solubility, effective tumor growth inhibition, and prolong survival rate of mice bearing metastatic lung melanoma. Further, modification of the polycarbonate backbone has been carried out to improve the delivery of small hydrophobic molecules. Feng Li et al. have reported amphiphilic polycarbonate-based lipopolymers grafted with dodecanol for improved loading of a hydrophobic model drug, embelin. In other reports, drugs have been conjugated to the polycarbonate backbone to improve their delivery (17). Chitkara et al. reported self-assembling gemcitabine conjugated PEGylated polycarbonate copolymeric micelles with lower particle size, controlled drug release profile, enhanced drug loading and reduction in plasma metabolism along with enhancement in antitumor activity in a pancreatic cancer xenograft model in NSG mice (18).

We have previously reported the modifications of polycarbonate backbone with morpholine, cholesterol, and cationic chain to improve the delivery of miRNA-34a, wherein we have grafted the polycarbonate block of the amphiphilic copolymer by EDC/HOBT coupling (19). Studies have reported the use of monomers with desired side chains, followed by ring-opening polymerization to prepare the grafted polycarbonate copolymers. Nederberg et al. reported metal-free or organocatalyst assisted ROP of cyclic esters (lactide), lactones, and cyclic silyl ethers (hexamethyltrisiloxane and carbosilanes) yielding polymers of predictable molecular weights with narrow polydispersity index having potential biomedical applications (20). In another study, passively targeted cholesterol grafted copolymer provided a rigid fused ring structure that has improved the encapsulation efficiency of the rigid hydrophobic small anticancer molecule (21).

To develop a safe and effective delivery system for DTX, herein, we report novel biodegradable folate-conjugated lipopolymers consisting of cholesterol grafted hydrophobic polycarbonate, polylactide and hydrophilic polyethylene glycol block. Cholesterol modified cyclic carbonate monomer was synthesized using a multi-step approach followed by microwave-assisted ring-opening polymerization with DL-lactide in the presence of methoxy poly(ethylene glycol) afforded the copolymers. For actively targeting, folate was appended onto the PEG block. DTX was loaded in the lipopolymeric nanoparticles followed by a thorough characterization for size, surface morphology, entrapment efficiency, on-bench stability, and *in vitro* DTX release. Cell-based assays, including intracellular uptake mechanism, cytotoxicity, apoptosis, and gene expression were performed in MDA-MB-231 breast cancer cells. *In vivo* pharmacokinetics was performed in *Sprague Dawley* rats after intravenous administration of lipopolymeric nanoformulation with a dose of 10 mg/kg. Further, to explore the potential *in vivo* application of this targeted nano system, *ex vivo* tissue distribution of DiR loaded folate conjugated lipopolymeric nanoparticles was conducted in *Swiss albino* mice.

MATERIALS AND METHODS

Materials

2-bromoethylamine hydrobromide (99%), bis(hydroxymethyl) propionic acid, tin(II) 2-ethylhexanoate ($Sn(Oct)_2$), methoxypoly(ethylene glycol) (m-PEG, 5000 Da), cholesteryl chloroformate (98%), and propidium iodide were procured from Sigma Aldrich (St. Louis, MO) and were used as received. Maleimide poly(ethylene glycol)-hydroxyl (mal-PEG-OH, 5000 Da) was procured from Xi'an Ruixi Biological Technology Co., Ltd. (Ruixibio), Shaanxi Province, China. DL-lactide was purchased from TCI Chemicals (India) Pvt. Ltd. Docetaxel was provided by Fresenius Kabi as a kind gift, Bad Homburg, Germany. Fetal Bovine Serum (FBS), Dulbecco's Modified Eagle Medium (DMEM), TrypLE and Annexin V Apoptosis Detection Kit FITC were obtained from ThermoFisher Scientific (MA, USA). 3-(4,5-dimethylthiazol-2-yl)-2,5-diphenyltetrazolium bromide (MTT) was procured from Sisco Research Laboratories (Mumbai, India). All other chemicals and reagents were of analytical grade and purchased from local vendors.

Methods

Characterization of Intermediates, Monomer and Lipopolymers

The synthesis schemes are shown in fig. 1, 2 and 3. All the intermediates, monomers and lipopolymers were characterized by ^{1}H and ^{13}C NMR spectroscopy (AVANCE II Bruker NMR Using TOPSPIN) at 400 and 100 MHz, respectively. For Be-Chol, Chol-MPA and MTC-Chol,

samples were prepared in deuterated chloroform ($CDCl_3$), while deuterated dimethyl sulphoxide (DMSO-d_6) was used for folate-SH monomer, mal-PEG-b-p(MTC-Chol-co-LA) lipopolymer and folate-PEG-b-p(MTC-Chol-co-LA). HRMS of the intermediates determined by High Resolution Mass Spectrometry (6545 Q-TOF LC/MS), Agilent equipped with an auto-sampler in ESI^+ mode. *Synthesis of Cholester-3-yl (2-bromoethyl)carbamate (Be-Chol, 3).* Cholesteryl chloroformate (13.02 g, 29.1 mM, 1equiv.) (**1**) and triethylamine (8.64 mL) were added to a solution of 2-bromoethylamine hydrobromide (6.27 g, 31.8 mM, 1.1 equiv.) (**2**) in 100 mL of chloroform in a dry round-bottom flask, under nitrogen atmosphere. The reaction mixture was stirred for 30 min. on a dry ice bath/acetone, followed by stirring at room temperature for 12 h. After completion of the reaction, chloroform was evaporated and the crude mixture was dissolved in dichloromethane (DCM). The crude mixture was washed first with 0.1 N HCl solution (saturated with brine), followed by sodium bicarbonate solution (saturated with brine). The organic layer was collected, dried over anhydrous sodium sulphate and evaporated to obtain a solid product that was subsequently recrystallized from ethanol, and thereafter from acetone to obtain pure Be-Chol (**3**) as a white solid (22). Yield: 81% (10.34 g). Figure 4 showed ^1H NMR (400 MHz, $CDCl_3$) δ 5.42–5.36 (m, 1H), 5.09 (t, J = 6.1 Hz, 1H, NH), 4.60–4.45 (m, 1H), 3.66–3.55 (m, 2H), 3.49 (t, J = 5.8 Hz, 2H), 2.42–2.25 (m, 2H), 2.10–1.74 (m, 6H), 1.66–1.25 (m, 12H), 1.25–1.05 (m, 8H), 1.03 (s, 3H), 0.93 (d, J = 6.5 Hz, 3H), 0.89 (d, J = 1.9 Hz, 3H), 0.87 (d, J = 1.9 Hz, 3H), 0.69 (s, 3H); ^{13}C NMR (100 MHz, $CDCl_3$) δ 155.9 ($C{=}O_{Carbamte}$), 139.7, 122.6, 74.7, 56.7, 56.1, 50.1, 42.6, 42.3, 39.7, 39.5, 38.5, 37, 36.6, 36.2, 35.8, 32.8, 31.9, 31.9, 28.3, 28.1, 28.0, 24.3, 23.8, 22.9, 22.6, 21.0, 19.3, 18.7, 11.9.

Synthesis of (Cholester-3-yloxy)carbonyl)amino)ethyl 3-hydroxy-2-(hydroxymethyl)-2-methylpropanoate (Chol-MPA, 5). A mixture containing 2-bis(hydroxymethyl) propionic acid (4.5 g, 31.3 mM, 1.1 equiv.) (**4**) and potassium hydroxide (2.2 g, 30.3 mM, 1.1 equiv.) in dimethylformamide (DMF; 200 mL) was heated to 100°C for 2 h. Thereafter, *N*-(2-bromoethyl) carbamoyl cholesterol (Be-Chol, **3**) (16 g, 1.12 equiv.) was added to the reaction mixture and stirred for another 18 h at 100°C. After 24 h, the mixture was dissolved in ethyl acetate and washed with saturated brine solution and distilled water. The organic layer was separated, dried using anhydrous sodium sulphate and evaporated to afford crude Chol-MPA, which was further purified by column chromatography using silica gel as an adsorbent using gradient phase ratio of ethyl acetate-hexane as the mobile phase to furnish pure Chol-MPA (**5**) as a yellowish oily semi-solid (23). Yield: 85% (12.45 g). Fig. 5 showed ^1H NMR (400 MHz, $CDCl_3$) δ5.44–5.31 (m, 2H), 4.56–4.46 (m, 1H), 4.28 (t, J = 5.0 Hz, 2H), 3.91 (d, J = 11.4 Hz, 2H), 3.74 (d, J = 11.5 Hz, 2H), 3.48 (q, J = 5.5 Hz, 2H), 3.42–3.30 (m, 2H), 2.42–2.24 (m, 2H), 2.11–1.74 (m, 7H), 1.65–1.40 (m, 8H), 1.39–1.10 (m, 11H), 1.08 (s, 3H), 1.01 (s, 3H), 0.92 (d, J = 6.5 Hz, 3H), 0.88 (d, J = 1.9 Hz, 3H), 0.87 (d, J = 1.9 Hz, 3H), 0.68 (s, 3H).; ^{13}C NMR (100 MHz, $CDCl_3$) δ 175.7 ($C{=}O_{Ester}$), 156.7 ($C{=}O_{Carbamte}$), 139.7, 122.6, 74.7, 71.8, 68.3, 4.2, 56.7, 56.1, 50.0, 49.5, 42.3, 39.7, 39.5, 38.5, 37.3, 37.3, 37.0, 36.5, 36.2, 35.8, 31.9, 31.9, 28.2, 28.1, 28.0, 24.3, 23.8, 22.8, 22.6, 21.0, 19.3, 18.7, 17.1, 11.9; HRMS (ESI-TOF) m/z: $[M+Na]^+$ calculated for $C_{35}H_{59}NO_6Na$ 612.4235; Found 612.4229.

Synthesis of (Cholester-3-yl)oxy)carbonyl)amino)ethyl 5-methyl-2-oxo-1,3-dioxane-5-carboxylate (MTC-Chol, 6). Chol-MPA (10 g) (**5**) was added to 200 mL of anhydrous DCM in a round-bottom flask. This was followed by the addition of pyridine (8.0 g) to it. The reaction mixture was then cooled using a dry ice/acetone bath. Thereafter, triphosgene (2.74 g dissolved in DCM) was added drop wise into the reaction mixture in 1 h, which was followed by continuous stirring for another 2 h at room temperature. After this, the reaction was quenched by adding saturated aqueous ammonium chloride solution (100 mL), and the organic layer was separated, washed twice with a mixture of 0.1 N HCl (saturated with brine) and sodium bicarbonate (saturated with brine) (23). The organic layer was dried over anhydrous sodium sulphate and concentrated to obtain crude MTC-Chol, which was further purified using column chromatography using ethyl acetate:-hexane as the mobile phase. The fractions containing pure MTC-Chol (**6**) were dried under vacuum to afford pure MTC-Chol as a white solid. Yield: 67% (6.7 g); Fig. 6 showed ^1H NMR (400 MHz, $CDCl_3$) δ 5.41–5.36 (m, 1H), 4.95 (t, J = 6.2 Hz, 1H), 4.70 (d, J = 10.9 Hz, 2H), 4.59–4.44 (m, 1H), 4.30 (t, J = 5.1 Hz, 2H), 4.23 (d, J = 10.9 Hz, 2H), 3.48 (q, J = 5.6 Hz, 2H), 2.42–2.25 (m, 2H), 2.10–1.93 (m, 2H), 1.92–1.39 (m, 12H), 1.35 (s, 6H), 1.28–1.03 (m, 9H), 1.02 (s, 3H), 0.93 (d, J = 6.5 Hz, 3H), 0.89 (d, J = 1.8 Hz, 3H), 0.87 (d, J = 1.8 Hz, 3H), 0.69 (s, 3H); ^{13}C NMR (100 MHz, $CDCl_3$) δ 175.7 ($C{=}O_{Ester}$), 156.2 ($C{=}O_{Carbamte}$), 147.6 (C=O), 139.7, 122.6, 74.8, 73.0, 68.9, 65.3, 56.7, 56.1, 50.0, 42.3, 39.7, 39.5, 38.5, 37.0, 36.6, 36.2, 35.8, 31.9, 31.9, 28.2, 28.1, 28.0, 24.3, 23.8, 22.8, 22.6, 21.0, 19.3, 18.7, 17.4, 11.9; HRMS (ESI-TOF) m/z: $[M+Na]^+$ calculated for $C_{36}H_{57}NO_7Na$ 638.4027; Found 638.4031.

Microwave-Assisted Synthesis of Maleimide-Terminated PEGylated Lipopolymer (Mal-PEG-b-P(MTC-Chol-Co-LA, 9). m-PEG or maleimide PEG (mal-PEG-OH) (Mn,5000 Da; 0.216 g) (**8**) was taken in a 10 mL microwave specific vial and kept at 120°C for 5 min. in a Microwave chamber (Monowave 400, Anton Parr). After 5 min., MTC-Chol monomer (0.636 g) (**6**) and DL-lactide (0.148 g) (**7**) and stannous 2-ethyl hexanoate ($Sn(Oct)_2$; 10 mol% of m-PEG or mal-PEG-OH) solution in anhydrous toluene were subsequently added. The reaction mixture was irradiated under microwave at 150°C for 1 h to obtain m-PEG-b-p(MTC-Chol-co-LA) or mal-PEG-b-p(MTC-Chol-co-LA) *via* ring-opening polymerization (ROP). The crude lipopolymer was purified by precipitation method, wherein it was dissolved in chloroform followed by precipitation with an excess amount of cold diethyl ether. Purification was performed twice, and the lipopolymer thus obtained was dried under vacuum. Figure 8 showed ^1H NMR (400 MHz, DMSO-d_6) of mal-PEG-b-p(MTC-Chol-co-LA) lipopolymer showed the characteristic peaks at δ7.2 (-C<u>H</u>=C<u>H</u>-) of mal-PEG, δ5.45 to 5.05 (-CH_2-C=C<u>H</u>-CH_2- and -CO-C<u>H</u>(CH_3)-O-CO-) of cholesterol and DL-lactide, δ4.65 to 4.40 (-COO-C<u>H_2</u>-CH(CH_3)-C<u>H_2</u>-O-), δ3.85–3.5 (-C<u>H_2</u>C<u>H_2</u>-O) of mal-PEG,

δ2.45–0.55 (protons from cholesterol and CH_3 in the carbonate monomer and DL-lactide) (Fig. 8A). Similarly the above ring opening polymerization of methoxy polyethylene glycol (m-PEG, **14**) was carried using varying ratios of MTC-Chol and DL-lactide to afford a series of lipopolymers, m-PEG-b-P(MTC-$Chol_{11}$-co-LA_5) (**15**), m-PEG-b-P(MTC-$Chol_{15}$-co-LA_{15}) (**16**), m-PEG-b-P(MTC-$Chol_{11}$-co-LA_{27}) (**17**), m-PEG-b-P(MTC-$Chol_{25}$-co-LA_{30}) (**18**) (Fig. 3).

Synthesis of Folate-Thiol (Folate-SH, 12). N-hyrodxysuccinimide derivative of folic acid (FA-NHS 1.02 g, (**10**)) and triethylamine (0.2 mL) were dissolved in anhydrous DMSO (10 mL), followed by the addition of cysteamine hydrochloride (**11**) (0.059 g, 0.8 mmol). The reaction was stirred for 48 h at room temperature under dark conditions. After this, the mixture was diluted with diethyl ether to precipitate our crude product, which was filtered and washed with excess diethyl ether to afford pure folate-SH (**12**) as an orange solid (24). Yield: 56% (0.625 g); Fig. 7 showed ^{1}H NMR (400 MHz, DMSO-d_6) δ8.64 (J = Hz, -CO-NH-, 1H), δ7.61, 6.64 (benzyl protons of folate, 4H), 4.48 (-NH-CH(COOH)-CH_2-, 2H), 4.36 (-CH_2-NH-, 2H), 3.76 (-NH-CH_2-CH_2-SH, 2H), 2.91(-CH_2-CH_2-SH, 2H), 2.69 (-CH_2-CH_2-CO-NH-, 2H); ^{13}C NMR (100 MHz, $CDCl_3$) δ174.4 (CH_2-CO-NH-), 167.1 (-NH-CH(COOH)), 151.7 (-C=N-). 129.4, 128.1, 121.4, 111.73 (aromatic C=C of benzyl).

Synthesis of Folate-PEG-b-P(MTC-Chol-Co-LA) Lipopolymer (13). To a solution of mal-PEG-b-p(MTC-Chol-co-LA) lipopolymer (200 mg) (**9**) in DMSO (2 mL), folate-SH (10 mg dissolved in DMSO) (**12**) and triethylamine (20 μL) were added, and the reaction mixture was stirred for 24 h at room temperature. After this, the reaction mixture was dialyzed using a SnakeSkin™ dialysis membrane (molecular weight cut-off 3500 Da, ThermoFisher Scientific) against purified water for 48 h and lyophilized to obtain to obtain folate-PEG-b-p(MTC-Chol-co-LA) lipopolymer (**13**). Figure 8B showed ^{1}H NMR (400 MHz, DMSO-d_6) of fol-PEG-b-p(MTC-Chol-co-LA) lipopolymer showed the characteristic peaks at δ6.9, 7.5 and 8.67 for the corresponding to folate moiety, δ7.2 (-CH=CH-) of mal-PEG, δ5.45 to 5.05 (-CH_2-C=CH-CH_2- and -CO-CH(CH_3)-O-CO-) of cholesterol and DL-lactide, δ4.65 to 4.40 (-COO-CH_2-CH(CH_3)-CH_2-O-), δ3.85–3.5 (-CH_2CH_2-O) of mal-PEG, δ2.45–0.55 (protons from cholesterol and CH_3 in the carbonate monomer and DL-lactide) (Fig. 8B).

Preparation of DTX Loaded Folate Conjugated Lipopolymeric Nanoparticles (F-DTX-LPNs). Single emulsion-solvent evaporation method was adopted for the preparation of DTX loaded lipopolymeric nanoparticles. Briefly, a solution of DTX (5 mg) and folate-PEG-b-p(MTC-Chol-co-LA) lipopolymer (95 mg) in DCM (400 μL) was added to 3 mL of purified water containing tween 80 (1% *w/v*) and sonicated using a probe sonicator (Sonics Vibra cell™, Newtown, CT, USA) at 25% amplitude for 3 min. to form a o/w emulsion. It was then kept on stirring overnight at RT to remove DCM, resulting into formation of nanoparticles that were subsequently centrifuged at 5000 rpm for 5 min. to remove unentrapped drug or larger particles as a pellet. The supernatant containing DTX loaded nanoparticles was collected and analyzed for particle size and ζ- potential using Malvern Zetasizer. The DTX content in the nanoparticles was analyzed by RP-HPLC analytical method. Briefly, a Shimadzu HPLC system coupled with a photodiode array (PDA) detector was used for analysis, and chromatographic separation was achieved on an Inertsil ODS 3 V C18 column (5 μm, 4.6 × 250 mm) with a mobile phase consisting of acetonitrile and purified water in the ratio of 70:30. Flow rate, injection volume, and analytical wavelength were kept as 1 mL/min., 20 μL, and 227 nm, respectively. The drug entrapment efficiency was determined by taking 100 μL of nanoparticle suspension and diluted with 900 μL acetonitrile followed by heating on water batch at 60°C till clear solution is observed followed by bath sonication for 5 min. to extract the DTX. The samples were centrifuged at 17500 rpm for 10 min., filtered, and analyzed using the developed HPLC method. Morphological characterization of DTX loaded nanoparticles was determined using Field Emission Scanning Electron Microscopy (FESEM) (FEI, ApreoLoVac). On-bench stability of DTX-loaded nanoparticles was determined for 5 days by observing any changes in its particle size, polydispersity index (PDI), and ζ-potential.

In vitro DTX Release from Lipopolymeric Nanoparticles. DTX release from the DTX loaded nanoparticles was determined using a dialysis bag method. Briefly, dialysis bag (3.5 KDa cut-off; SnakeSkin™ Dialysis Tubing, ThermoFischer Scientific) containing the free drug or drug-loaded nanoparticles F-DTX-LPNs was placed in 30 mL of phosphate buffer saline (100 mM; pH 7.4) containing tween 80 (1% *w/v*), sodium azide (0.2% w/v) and ethanol (2% *v*/v) to maintain the sink condition. Sodium azide (0.2% w/v) was also added to the release media as a preservative to prevent the microbial growth in the release media during the study. Studies were performed at 37°C/100 rpm in an incubator. Release samples (2 mL) were taken at regular time intervals, *i.e.*, 0.25, 0.5, 1, 2, 4, 8, 12 (time, h), 1, 2, 3, 4, 5, 6 and 7 (time, days) and replaced with the equal quantity of fresh release media at each time point. The amount of DTX in the release samples was determined by RP-HPLC method as given above, and cumulative release was plotted against time.

In vitro Cell-Based Assays

All the in vitro cell culture assays were performed in MDA-MB-231 cell line. The cells were acquired from National Centre for Cell Science, Pune, India and cultured in Dulbecco's Modified Eagle's Medium (DMEM) supplemented with 10% of fetal bovine serum (FBS; HyClone, Logan, UT) and 1% antibiotics (100 U/mL penicillin/streptomycin) and incubated under humid environment at 37°C/ 5% CO_2.

In vitro Cellular Uptake Studies and Pathway Mediated Endocytosis

To evaluate the potential of lipopolymeric nanoparticles for intracellular delivery of loaded cargo, *in vitro* cellular uptake studies were conducted on MDA-MB-231 cells. A

hydrophobic fluorescent dye (coumarin-6; C6) was loaded in the nanoparticles as a hydrophobic model drug to enable visualization of their uptake in the cells. Briefly, MDA-MB-231 cells were seeded in a 6-well plate with cell density of 1×10^5 cells/well and allowed to grow for overnight. Prior to treatment, cells were washed three times with PBS (10 mM, pH 7.4) and fresh serum-free DMEM media was added followed by incubation for 1 h. Further, folate-targeted and non-targeted C6 loaded nanoparticles, and blank nanoparticles were added to the respective wells and further incubated for 4 h. After 4 h incubation, cells were washed with chilled PBS, fixed with 2% paraformaldehyde (PFA 2% *v*/v) for 5–10 min., counterstained with DAPI (to stain nucleus; 300 nM) and observed under a fluorescence microscope (Vert.A1, ZEISS, Oberkochen, Germany).

To further understand the uptake mechanism of the folate-targeted nanoparticles (F-C6-LPNs) in MDA-MB-231 cells (1×10^5cells/well), four endocytic inhibitors *i.e.*, methyl β-cyclodextrin (Mβ-CD), nystatin (mycostatin), chlorpromazine (CPZ) and amiloride.HCl (AM) were used. Briefly, cells were seeded in 6-well cell culture plates and allowed to adhere for 24 h. Next, cells were washed with PBS (twice), and media was replaced with fresh serum-free DMEM followed by treatment with methyl β-CD (3 mM), nystatin (27 μM), CPZ (10 μM) and AM (1 mM) for 30 min. With Endocytic inhibitors cells were incubated for 0.5 h followed by washing thrice with PBS. Further cells were treated with C6 loaded nanoparticles (F-C6-LPNs) for 4 h. Herein, cells without endocytic inhibitors treatment were taken as negative control. Uptake mechanism of nanoparticle was analyzed qualitatively and quantitatively using fluorescence microscopy and flow cytometry, respectively. For microscopic evaluation, cells were washed with PBS, fixed with para formaldehyde (4% *v*/v) for 10 min., counterstained with DAPI (for nucleus labeling; 300 nM) and observed under a fluorescence microscope (Vert.A1, ZEISS, Oberkochen, Germany). For flow cytometry analysis, cells were washed with PBS, trypsinized, redispersed in PBS and analyzed using Cytoflex (Beckman Coulter, USA) at excitation and emission wavelength of 488 and 510 nm respectively. Flow cytometry data were interpreted using CytExpert 2.1 software.

In vitro Cytotoxicity Studies

Cytotoxicity studies of folate-targeted and non-targeted lipopolymeric nanoparticles loaded with DTX were performed in MDA-MB-231 breast cancer cells. Briefly, MDA-MB-231 cells were seeded in 96-well cell culture plate (5×10^3 cells/well) and allowed to adhere for overnight followed by treatment with free DTX (in DMSO), DTX loaded folate targeted and non-targeted lipopolymeric nanoparticles at a concentration range from 1 nM to 50 nM equivalent to DTX (25,26). Untreated cells and DMSO treated cells were kept as controls. The cytotoxicity of the folate conjugated lipopolymer (folate-PEG-b-p(MTC-Chol-co-LA)) was also studied at a concentration range from 1 μg/mL- 1 mg/mL. After 48 h of treatment, media was discarded and replaced with fresh media containing 0.5 mg/ml of 3-(4,5-dimethylthiazol-2-yl)-2,5-ditetrazolium bromide (MTT) dye followed by incubation for 5 h. After 5 h, the media was removed and formed formazan crystals were dissolved in 200 μL of pure DMSO. Further, to determine the cell viability absorbance of the samples was recorded at 570 nm using microplate reader (BioTek Epoch). To correct the interference due to cellular debris, absorbance at 630 nm was subtracted from absorbance at 570 nm (19). The percentage cell viability was calculated using the formula given below:

$$\%\text{Cell viability} = (\textit{Absorbance ofsample wells}/\textit{Absorbance of control wells}) \times 100$$

Apoptosis Assay

For apoptosis assay, cells (MDA-MB-231)(1×10^6cells/well) were seeded in 6-well plate with a density of 1×10^6 cells/well and allowed to adhere overnight. Next day, the media was replaced with the fresh media containing free DTX (50 nM), DTX loaded folate-targeted and non-targeted lipopolymeric nanoparticles equivalent to 50 nM of DTX. After 48 h incubation, the cells were washed with PBS, harvested with trypsin, centrifuged at 1200 rpm/3 min. at 4°C and redispersed in annexin binding buffer followed by treatment with FITC-Annexin V and PI (ThermoFisher Scientific, USA) as per the manufacture's protocol. The apoptosis status of cells (early and late apoptosis) were quantified by flow cytometry using Cytoflex (Beckman Coulter, USA) and data were interpreted using CytExpert software (27,28).

Gene Expression Study

MDA-MB-231 cells (1×10^6 cells/well) were seeded in a 6-well cell culture plate and allowed to adhere for 24 h followed by treatment with Free DTX (50 nM) (in DMSO), DTX loaded folate-targeted and non-targeted lipopolymeric nanoparticles equivalent to 50 nM of DTX for 48 h. Next, cells were washed,trypsinized and total RNA was extracted using PureLink® RNA Mini Kit (Ambion®, ThermoFisher Scientific) according to the manufacture's protocol. RNA samples were quantified by Nanodrop (Simplinano™ spectrophotometer, biochrom, Harvard Bioscience. Inc.) and cDNA was synthesized from RNA using GeneMax™ First Strand cDNA Synthesis Kit (PUREGENE, Genetix Biotech Asia, Pvt. Ltd.) on a thermal cycler (Bio-Rad; Hercules, CA) according to the manufacturer's protocol. Gene expression was quantified using Maxima SYBR Green/ROX qPCR Master Mix (2X) assay kit (Thermo Fisher Scientific Baltics UAB, Vilnius, Lithuania). Real-time PCR primers were designed for Bcl-2, BAX, ki67, SIRT1 and GAPDH gene were used as given below (29).

Bcl-2: Forward sequence- 5'-gtccaagaatgcaaagcaca −3'.
Reverse sequence- 5'-ccggttatcgtaccctgttc-3',
BAX: Forward sequence- 5'-gctggacattggacttcctc-3'.
Reverse sequence- 5'-ctcagcccatcttcttccag-3'.
ki67: Forward sequence-5'-tctgacctgacagacctcaaga-3'.
Reverse sequence- 5'-gtgtgtgttggggtgtttattg-3'.
SIRT1: Forward sequence- 5'-gaacatagacacgctggaac-3'.
Reverse sequence- 5'-ctaggacatcgaggaactacc-3'.

GAPDH: Forward sequence- 5'-tggcttgtgctgtaagatcg-3'. Reverse sequence- 5'-aatctccactttgccactgc-3'.

Pharmacokinetic Studies in Sprague Dawley (SD) Rats

Pharmacokinetic studies were performed in *Sprague Dawley Rats* (SD rats; females; 8–10 weeks, 200–250 g). SD Rats procured from the Central Animal Facility, BITS-Pilani (Pilani, Rajasthan India). The Institutional Animal Ethics Committee (IAEC) approved the animal protocol, BITS-Pilani (IAEC/RES/23/09) and experiments were conducted as per CPCSEA guidelines. Animals were kept under regular 12 h light/dark cycle in standard ventilated cages and fed with standard diet ab libitum.

For the preparation of free DTX solution, accurately weighed amount of DTX (10 mg) was transferred in a 2 mL glass vial containing 260 mg of Tween 80 and diluted with 13% *w*/w solution of ethanol (95%) *v*/v in water (735.6 mg). The mixture was bath sonication (1 min) and vortexed (1 min) to obtain a clear solution. The F-DTX-LPNs were administered in normal saline. Animals ($N = 6$) were injected with 10 mg/kg dose of free DTX (Taxotere®) or DTX-loaded folate-targeted lipopolymeric nanoparticles (F-DTX-LPNs) *via* tail vein injection. Blood samples were collected from retro-orbital plexus into disodium EDTA containing microcentrifuge tubes for each pre-set time points (0.08, 0.25, 0.5, 1, 2, 4, 6, 8, 12, 24, 48 and 72 h) and centrifuged for 15 min at 6500 rpm. to obtain plasma. The plasma samples were subsequently stored at −80°C until further utilization. For bioanalysis of DTX, a HPLC system (Shimadzu, Kyoto, Japan) equipped with a Photo Diode Array (PDA) detector (SPD-M20A), binary pump (LC-20 AD), and autosampler (SIL-HTC, Shimadzu, Japan) was used. Chromatographic separation of DTX and paclitaxel (PTX; internal standard) from the plasma interferences was achieved using mobile phase solvent system consisting of acetonitrile and water mixture (ratio of 48:52% v/v) on Inertsil® ODS (C18) column (250 × 4.6 mm, 5 μm). Flow rate was kept at 1 mL/min. and eluents were monitored at a wavelength of 227 nm. DTX and PTX showed a retention time of 19 and 24 min., respectively and standard curves were plotted from 50 ng/mL-5000 ng/mL and the injection volume was kept at 80 μL. LC solution software version 1.22 SP1 was used for data handling and compilation. Phoenix 8.0 WinNonlin software (Pharsight Corporation, USA) was used to determined different pharmacokinetic parameters including elimination half-life $AUC_{0-\infty}$, area under curve from zero to infinity CL, clearance MRT, mean residence time C_0, drug concentration in plasma at t = 0; AUC_{0-t} $t_{1/2}$, area under curve from zero to the last time point and V_d, apparent volume of distribution. Plasma concentration-time profiles of DTX were plotted and analyzed by non-compartmental model approach using the Phoenix 8.0 WinNonlin software (Pharsight Corporation, USA) software.

In vivo Bioimaging

DiR dye was used as a fluorescent marker to examine the *in vivo* distribution of folate targeted lipopolymeric nanoparticles in swiss albino mice. All experiments were performed as per CPCSEA guidelines after approval from IAEC, BITS-Pilani (IAEC/RES/27/7). Herein, DiR dye was loaded in the lipopolymeric nanoparticle using similar method as that of F-DTX-LPNs. For biodistribution study, mice were divided into three groups ($N = 3$) and were injected with DiR loaded F-LPNs (DiR equivalent to 400 μg/kg) intravenously. At specific time points *i.e.* 30 min., 6 h, 12 h and 24 h, animals were sacrificed and whole blood was removed. Vital organs including liver, heart, kidney, lungs and spleen were isolated and washed with phosphate buffer saline (PBS) and pet dry for bioimaging analysis. DiR dye accumulation in the isolated tissues was determined by DiR signal intensity provide by *in vivo* imaging system (IVIS) Lumina XR (Perkin Elmer, UK) at excitation and emission wavelength of 745 and 788 nm, respectively (30).

Statistical Analysis

All the Data are presented as the mean ± standard deviation and difference between any two or more groups was determined by analysis of variance (ANOVA) followed by Tukey's test, wherein $p \leq 0.05$ was considered to be statistically significant.

Results

Low solubility and permeability of DTX hinder its optimal therapeutic utilization. Taxotere®, the conventional formulation of DTX, utilizes a high concentration of surfactant and ethanol to solubilize DTX for parenteral application (31). To improve its delivery, several nanotechnology-based approaches have been reported in the literature. Herein, we have designed the folate-targeted lipopolymer containing cholesterol conjugated carbonate and DL-lactide as pendant groups for efficient delivery of DTX. Initially mal-PEG-b-p(MTC-Chol-co-LA) was synthesized by ring-opening polymerization (ROP) using cyclic carbonate monomer (with cholesterol side-chain), DL-lactide and maleimide-PEG-OH as a chain initiator in presence of stannous octoate as a catalyst. This above synthesized lipopolymer was covalently linked to thiol-derivatized folate (folate-SH) to form folate-targeted lipopolymer, folate-PEG-b-p(MTC-Chol-co-LA).

MTC-Chol monomer was synthesized using a reaction scheme as shown in Fig. 1. The synthesis commenced with the preparation of *N*-(2-bromoethyl) carbamoyl cholesterol (Be-Chol, **3**) from 2-bromoethylamine hydrobromide (**2**) and cholesterylchloroformate (**1**). Be-Chol (**3**) was then reacted with 2-bis (hydroxymethyl) propionic acid (**4**) to afford cholesteryl 2,2-bis (hydroxymethyl)-5-carboxyloyloxy) ethyl carbamate (Chol-MPA, **5**), which on ring closure with triphosgene yielded MTC-Chol monomer (**6**). (21) Thereafter, microwave-assisted ring-opening polymerization of MTC-Chol (**6**) with DL-lactide (**7**) and mal-PEG-OH (**8**) as a macro initiator in the presence of $Sn(Oct)_2$ yielded maleimide-terminated PEGylated lipopolymer (mal-PEG-b-p(MTC-Chol-co-LA, **9**) (Fig. 1). Macro initiator in the presence of $Sn(Oct)_2$ yielded maleimide-terminated PEGylated lipopolymer (mal-PEG-b-p(MTC-Chol-co-LA, **9**) (Fig. 1). Subsequently, the thiol-derivative of folic acid (folate-SH, **12**) was synthesized by reacting active *N*-hydroxysuccinimide ester of folic acid (**10**) with cysteamine (**11**) in the presence of a triethyl amine to afford folate-SH product (**12**). Finally,

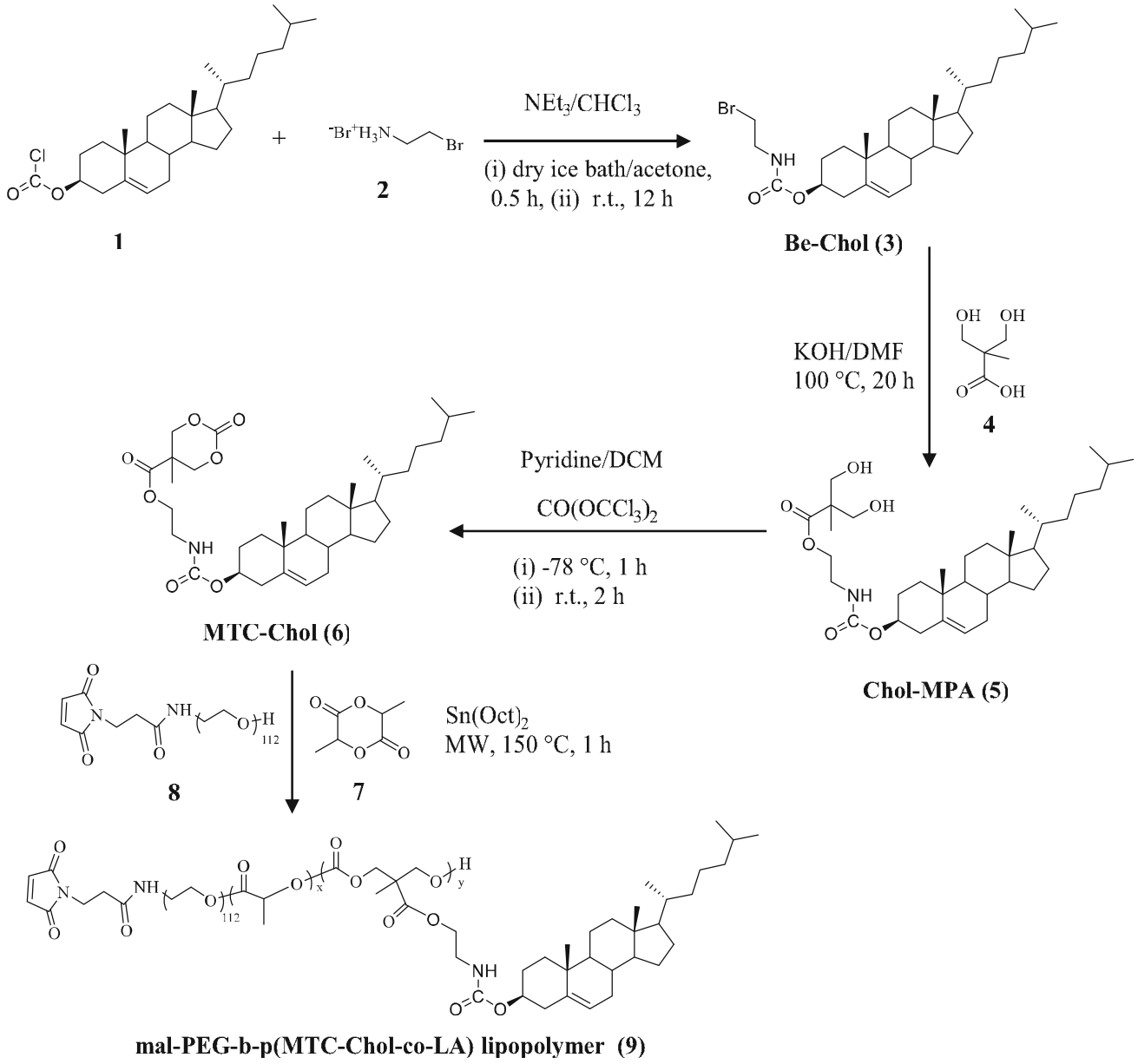

Fig. 1. Synthetic scheme of mal-PEG-b-p(MTC-Chol-co-LA) lipopolymer **(9)**

folate-SH (**12**) on reaction with mal-PEG-b-p(MTC-Chol-co-LA) lipopolymer (**9**) in DMSO at room temperature afforded folate-PEG-b-p(MTC-Chol-co-LA) lipopolymer(**13**) (Fig. 2). FA-SH; 24.24 μmol/g of Polymer.

Further, a series of lipopolymers, m-PEG-b-P(MTC-$Chol_{11}$-co-LA_5 (**14**), m-PEG-b-P(MTC-$Chol_{15}$-co-LA_{15}(**15**), m-PEG-b-P(MTC-$Chol_{11}$-co-LA_{27} (**16**) were also synthesized by varying ratios of MTC-Chol and DL-lactide with m-PEG (methoxy polyethylene glycol) (**14**) following above strategy as shown in synthetic scheme (Fig. 3).

Preparation and Characterization of DTX Loaded Folate Conjugated Lipopolymeric Nanoparticles (F-DTX-LPNs)

The emulsion solvent evaporation method was adopted to prepare DTX loaded lipopolymeric nanoparticles (DTX-LPNs). Among different lipopolymers, m-PEG-b-p(MTC-$Chol_{29}$-co-LA_{30}) showed an encapsulation efficiency of 91.2% with a particle size of 140 nm (PDI-0.164). DTX loaded nanoparticles prepared using folate-conjugated lipopolymer (F-DTX-LPNs) showed a particle size 115.17 (PDI- 0.205) nm and encapsulation efficiency of 80.14%. ζ-potential of these nanoparticles was found to be −9.13 mV (Fig. 9A). Further, FE-SEM analysis showed that the nanoparticles were spherical in shape (Fig. 9B). Nanoparticles showed good colloidal on-bench stability for at least 5 days without any significant change in the particle size, PDI, and ζ-potential (Fig. 9 C). *In vitro* drug release studies indicated that the F-DTX-LNPs exhibited a sustained drug release profile of DTX for 7 days in contrast to the free drug, that showed a complete drug release within 4 h (Fig. 9D). A DTX release from F-DTX-LPNs have not reached to 100% at the

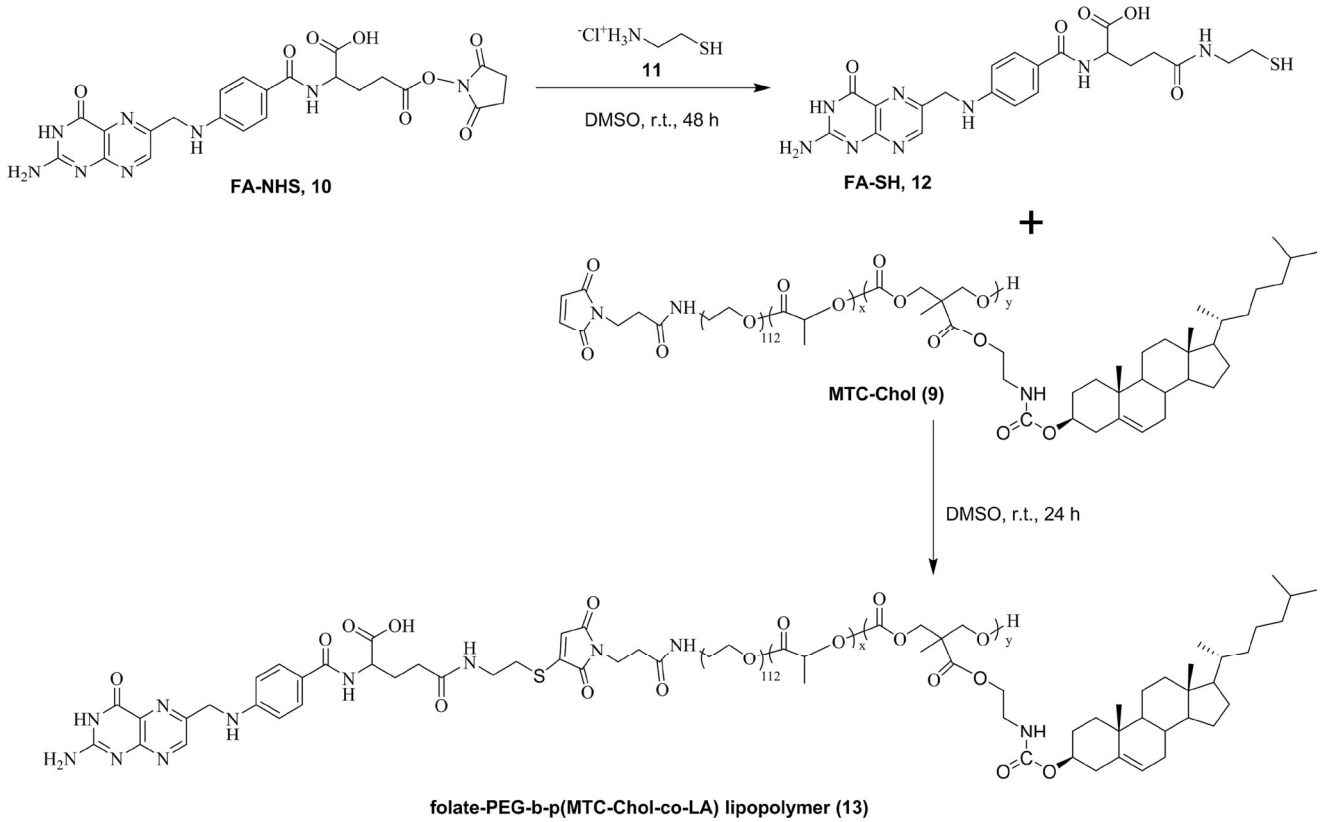

Fig. 2. Synthesis scheme of folate-PEG-b-p(MTC-Chol-co-LA) lipopolymer (**13**)

end of the 7-day drug release study and was expected to release for a more prolonged period to reach to 100%.

Cellular Uptake and Pathway Mediated Endocytosis

Cellular uptake studies were performed in MDA-MB-231 breast cancer cells. Coumarin-6 (C6) was loaded in the nanoparticles as a fluorescent hydrophobic model drug to investigate the uptake efficiency and endocytosis process. Efficient intracellular uptake was observed for both the targeted and non-targeted nanoparticles, wherein the folate-targeted nanoparticles showed higher intracellular uptake, as evident from the intense green fluorescence in the cells. Blank nanoparticles and free C6 were kept as controls that showed negligible fluorescence in the cells (Fig. 10A).

To determine the specific pathway for the endocytosis, MDA-MB-231 cells were also treated with the endocytosis pathway inhibitors before the treatment with the C6 loaded nanoparticles. It was evident from the fluorescence spectroscopy images that folate-targeted nanoparticles followed the lipid raft mediated intracellular uptake since the treatment of the cell with methyl beta-cyclodextrin (Mβ-CD) (cholesterol-depleting agent, were used to disrupt several lipid raft mediated endocytic pathways), completely inhibited the green fluorescence in the cells while the cells treated with other inhibitors such as chlorpromazine (CPZ; clathrin-dependent pathway inhibitor), nystatin (deplete cholesterol from membranes and block the formation of caveolae) and amiloride (macopinocytic pathway inhibitor) showed green fluorescence indicating the uptake of these nanoparticles

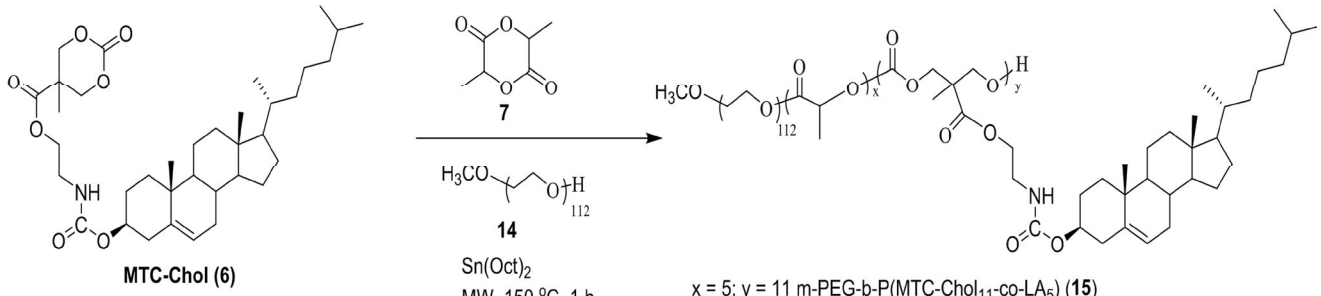

Fig. 3. Synthetic scheme of m-PEG-b-p(MTC-Chol-co-LA) lipopolymers **(15–18)**

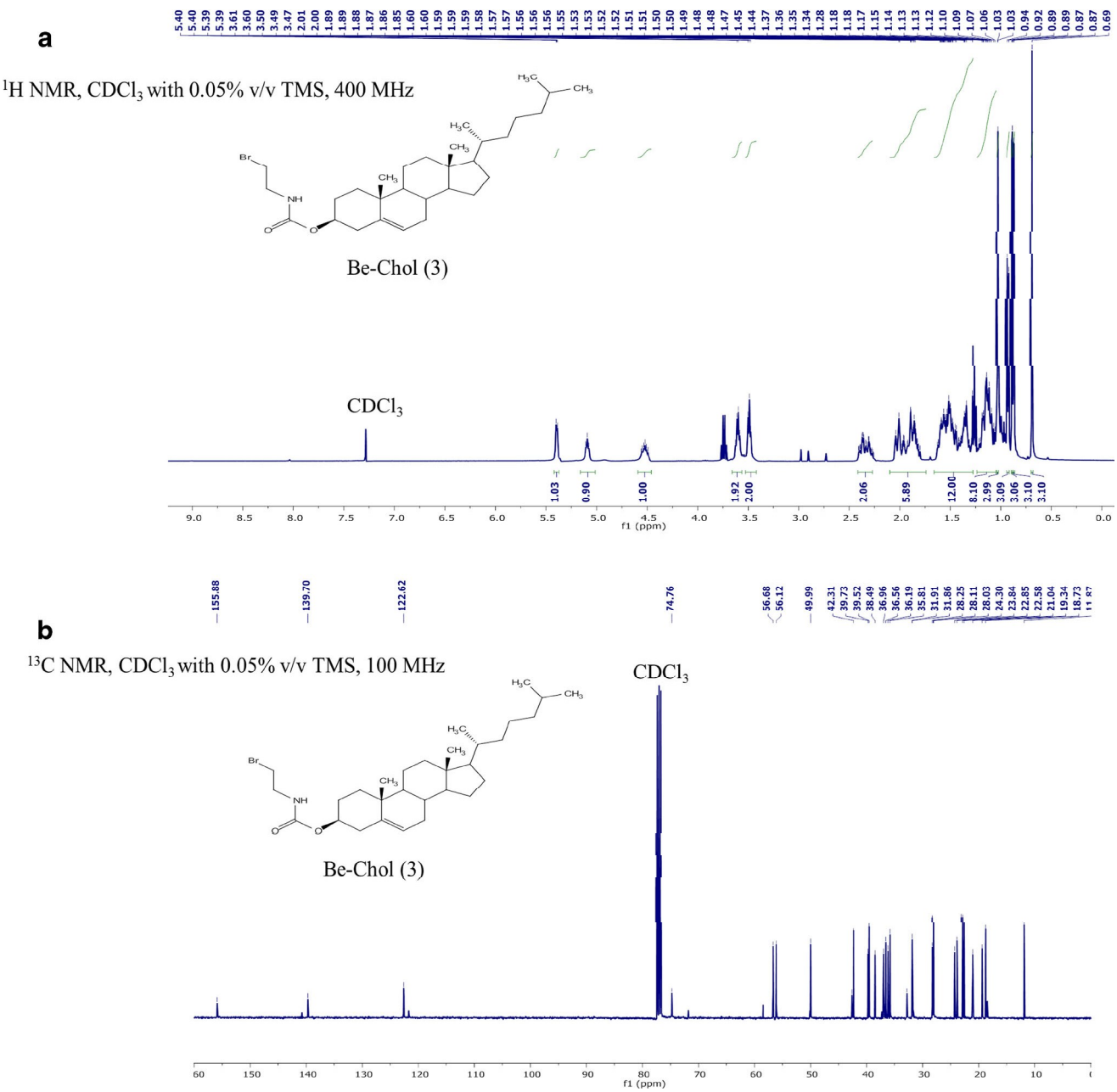

Fig. 4. **a** ^{1}H NMR and **b** ^{13}C NMR of *N*-(2-bromoethyl) carbamoyl cholesterol (Be-Chol)

(Fig. 10) (32,33). Further, the quantitative cellular uptake (%) was determined using flow cytometry where, cells treated with C6 loaded LPNs with and without inhibitor were taken as positive and negative control respectively. Figure 10B showed the uptake of C6 loaded LPNs evaluated using flow cytometry in the presence of inhibitors. The endocytic uptake data revealed that there was no effect of nystatin (Nyst), amiloride (AML) and chlorpromazine (CPZ) on the uptake of LPNs. More than 95% uptake was observed in each treatment groups except Mβ-CD treated cells. The uptake of nanoparticle got decreased to 11.77% in the presence of Mβ-CD (Fig. 10B and C). These results collectively indicated that lipid-raft mediated internalization could be the possible uptake mechanism of the developed LPNs.

In vitro Cytotoxicity, Apoptosis and Gene Expression Analysis

Cytotoxicity, apoptosis, and gene expression analysis were performed in MDA-MB-231 cells, wherein, it was observed that F-DTX-LPNs showed improved cytotoxicity, apoptosis and significant fold-change in expression levels of Bcl-2, BAX and Ki-67 as compared to DTX-LPNs and free DTX. Cell viability of 42.70% was observed with F-DTX-LPNs, while DTX-LPNs and the free DTX showed 58.14% and 66.43% cell viability at 50 nM concentration. respectively (Fig. 11A). A lower IC_{50} of 54.58 nM was observed for F-DTX-LPNs in comparison to DTX-LPNs

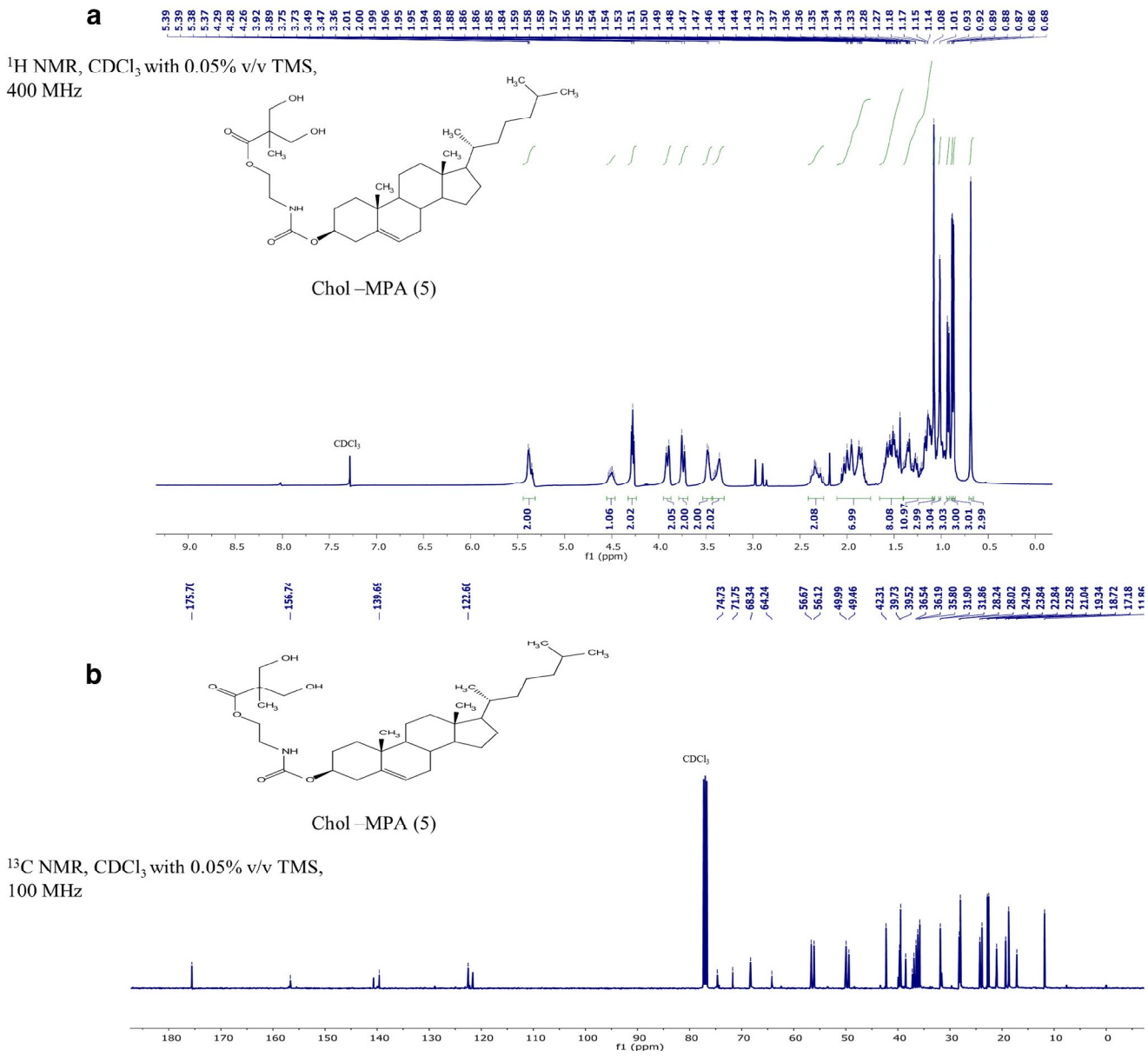

Fig. 5. **a** ^{1}H NMR and **b** ^{13}C NMR of Chol-MPA monomer

and free DTX wherein the IC_{50} were found to be 81 nM and 91.83 nM, respectively.

Blank folate-targeted nanoparticles did not show any significant change in the cell viability up to lipopolymer concentrations as high as 100 μg/ml (Fig. 11B). Flow cytometry analysis of apoptosis indicated that F-DTX-LPNs induced 82.97% apoptosis (64.13% early and 18.84% late stage) while non-targeted lipopolymeric nanoparticles induced 53.80% apoptosis (43.94% early and 9.86% late stage) and free DTX induced 39.13% apoptosis (25.79% early and 13.34% late stage). Blank folate-targeted nanoparticles did not show any apoptosis-inducing potential (Fig. 11C).

The real-time PCR analysis of Bcl-2, Ki67, BAX, and SIRT1 gene was performed to understand the impact on the downstream targets of DTX when it was delivered using folate-targeted nanoparticles. A significant down regulation in the expression of the Bcl-2 and Ki67, whereas the expression of BAX was increased after treatment with the F-DTX-LPNs as compared to the DTX-LPNs and free DTX. Further, the expression of the SIRT1 gene showed no significant difference in the cells treated with the DTX loaded nanoparticles or free DTX (Fig. 12).

In vivo Pharmacokinetics and Bioimaging

The comparative *in vivo* pharmacokinetics of DTX solution (Taxotere®) and F-DTX-LPNs was studied in *Sprague Dawley* (SD) rats at 10 mg/kg dose given intravenously. The plasma concentration profiles are shown in (Fig. 13A), and their pharmacokinetic parameters are shown in Table 2. The folate-targeted lipopolymeric nanoparticles showed a significantly lower Cmax (μg/mL) (3.20 ± 1.78 *versus* 8.29 ± 3.48) and higher $AUC_{0-\infty}$ (μg*h/L) (35,379.89 ± 8527.41 *versus* 5515.93 ± 1824.90) as compared to the free

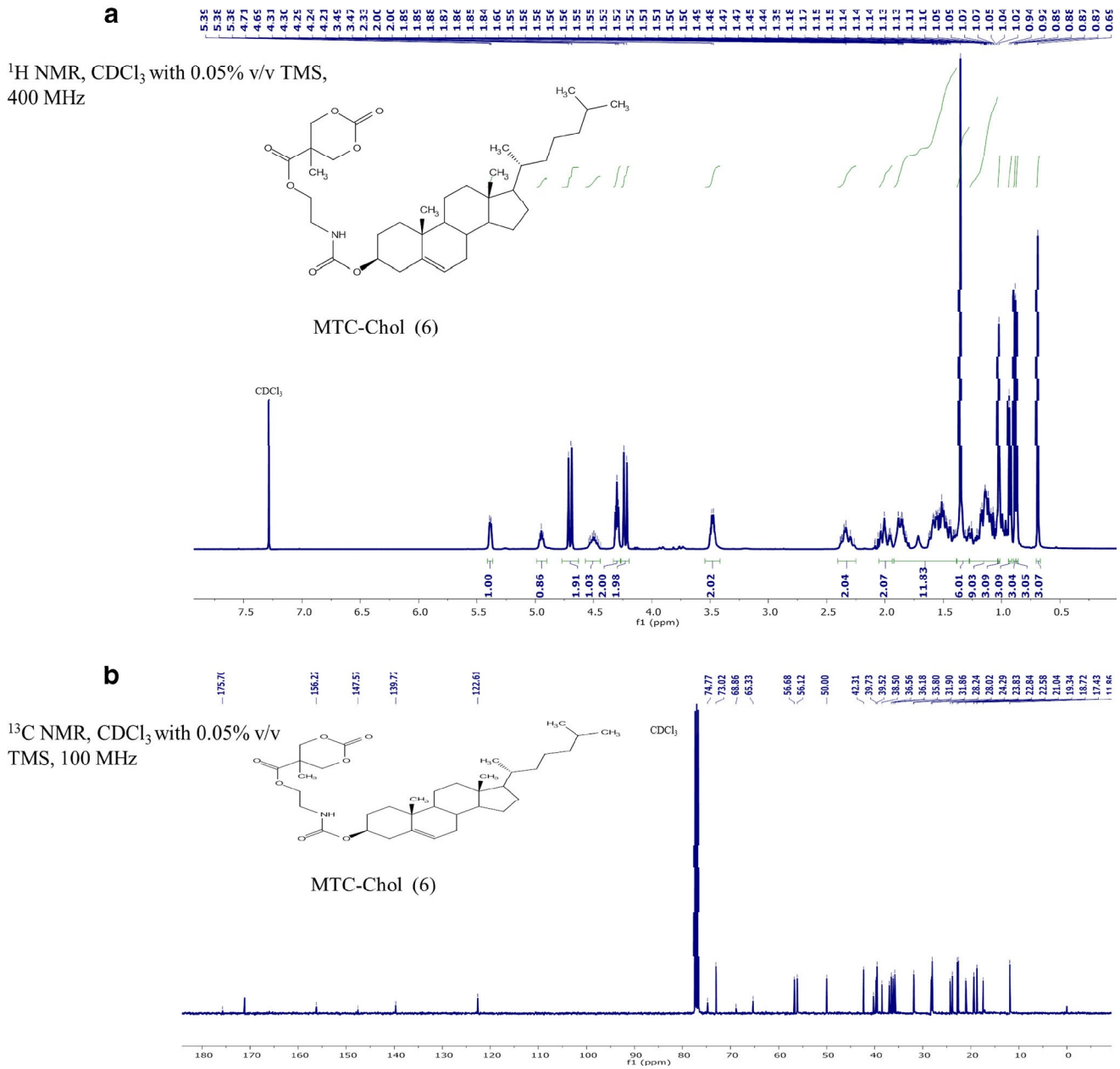

Fig. 6. **a** ^{1}H NMR and **b** ^{13}C NMR and mass spectrum of the MTC-Chol

DTX. Further, the plasma half-life ($t_{1/2}$)(h) was observed to be 14.64 ± 3.99 h for DTX delivered using folate-targeted nanoparticles (F-DTX-LPNs) as compared to 2.51 ± 2.68 h for free DTX.

Biodistribution of DiR loaded nanoparticles (F-DiR-LPNs) was examined by measuring the fluorescence of DiR dye in isolated tissues with excitation and emission wavelength at 745 nm and 788 nm, respectively at different time points. DiR dye has been reported for its unique fluorophore nature as it emits photons at highest wavelength and itself reduces the risk of auto-fluorescence due to blood and fur of the mice. Figure 13B showed that nanoparticles have biodistributed to different organs with major accumulation in the liver with respect to other organs at 6, 12 and 24 h.

DISCUSSION

Cancer is one of the major devastating illnesses with an increasing number of new cases diagnosed every year. The mortality rate has reduced in recent years due to a better understanding of the disease at the molecular level with improved diagnosis and treatment options. The use of chemotherapeutics forms a pivotal modality for treatment with Taxanes, particularly paclitaxel and docetaxel, being used as first-line treatment option in several cancers at advanced stages (34). Taxotere® is the first FDA approved marketed formulation of DTX approved for the treatment of metastatic breast cancer. Although the quality of life has improved due to aggressive treatment options in the past few years (35). However this formulation suffers from several

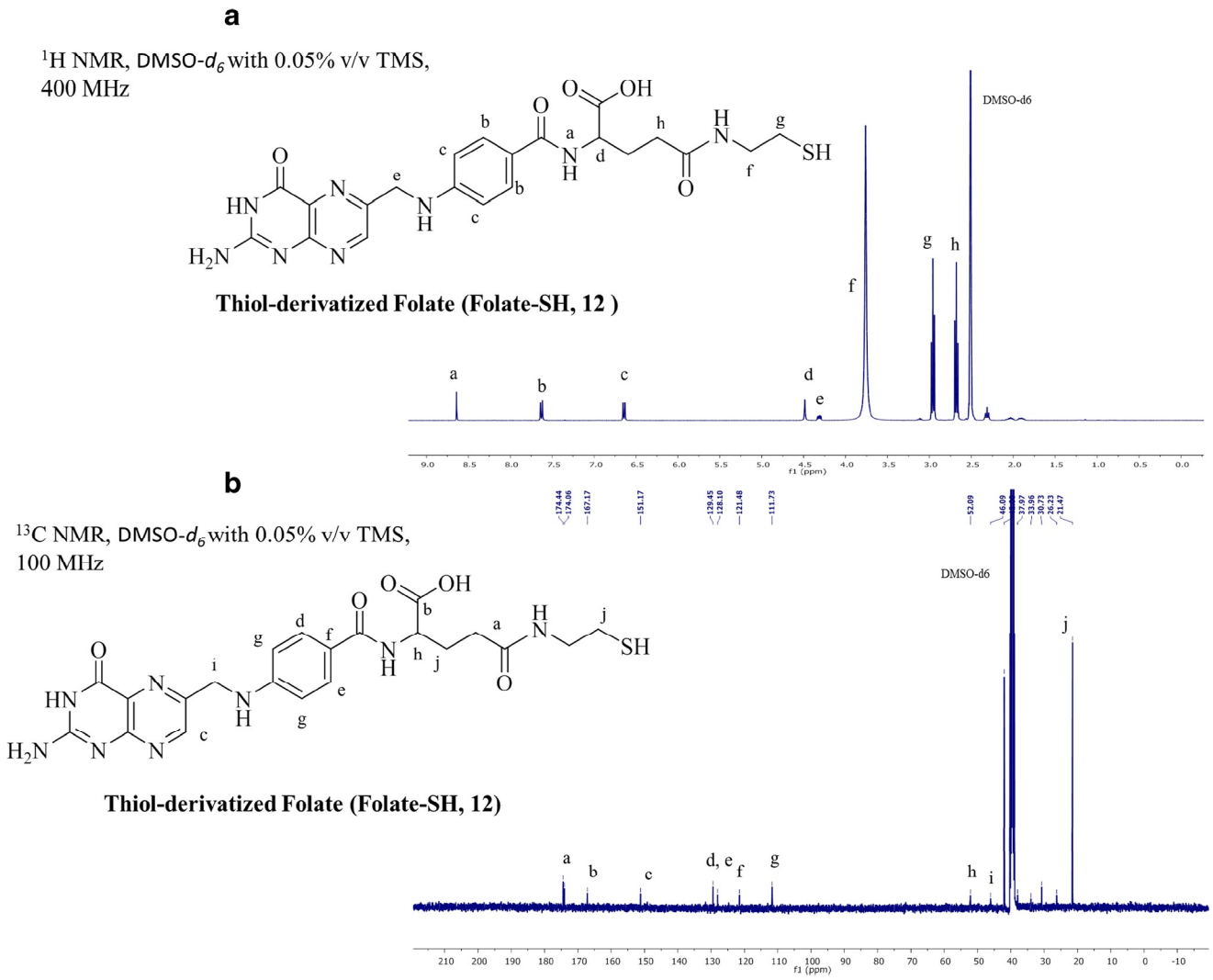

Fig. 7. **a** ^{1}H NMR and **b** ^{13}C NMR of Thiol-derivatized folate (folate-SH)

disadvantages such as non-specific biodistribution, cumulative fluid retention, acute hypersensitivity reactions, neurotoxicity, nail toxicity, nasolacrimal duct stenosis myalgia, asthenia, and febrile neutropenia. The general consensus on use of chemotherapeutic agents including DTX is that the therapeutic outcomes in patients would not improve further if new treatment strategies are not adopted. Research has been envisaged to find new methods to decrease the risks of these chemotherapeutics, along with improving the efficacy. Designing new delivery systems of DTX, in particular, the nanomedicines have provided a decisive lead, as it offers several advantages owing to their nano-size range, passive and active targeting, controlled drug release and improved pharmacokinetics resulting in a better therapeutic response and decreased toxicity.

In the current study, we have synthesized folate-targeted lipopolymers with cholesterol side chains and used the same for developing DTX loaded nanoparticles. Previously, Wang et al. reported the core-shell lipid-polymer hybrid (LPH) nanoparticles containing docetaxel and FTY720 to possess greater serum stability profile, longer shelf life, steady uptake by tumor cells and sustained intracellular drug release (36,37). In another study, it has been demonstrated by Liu et al. that docetaxel loaded folic acid conjugate nanoparticles of mixed lipid monolayer and biodegradable polymer core have greater stability, surface properties in favor of endocytic uptake, stealth effect to provide longer circulation of nanoparticles in the plasma and most effective targeting (38). Werner et al. have also prepared folate targeted biodegradable polymeric nanoparticles containing DTX that are more effective than non-targeted NPs and free drug (39).

Aliphatic polycarbonates and polyesters are an important class of biodegradable polymers and are widely explored in biomedical and pharmaceutical applications (40,41). A multi-step reaction was used to synthesize a cyclic carbonate monomer with a cholesterol side chain. In the first step, 2-bromoethylamine hydrobromide was reacted with cholesteryl chloroformate to obtain *N*-(2-bromoethyl) carbamoyl cholesterol. Cholesterol chloroformate is highly hygroscopic and susceptible to degradation. Thus, the reaction was performed under inert atmosphere and the product yield was improved by keeping the reaction at chilled condition under dry ice/acetone bath. The crude product obtained was recrystallized to obtain a pure product for next step wherein it was reacted

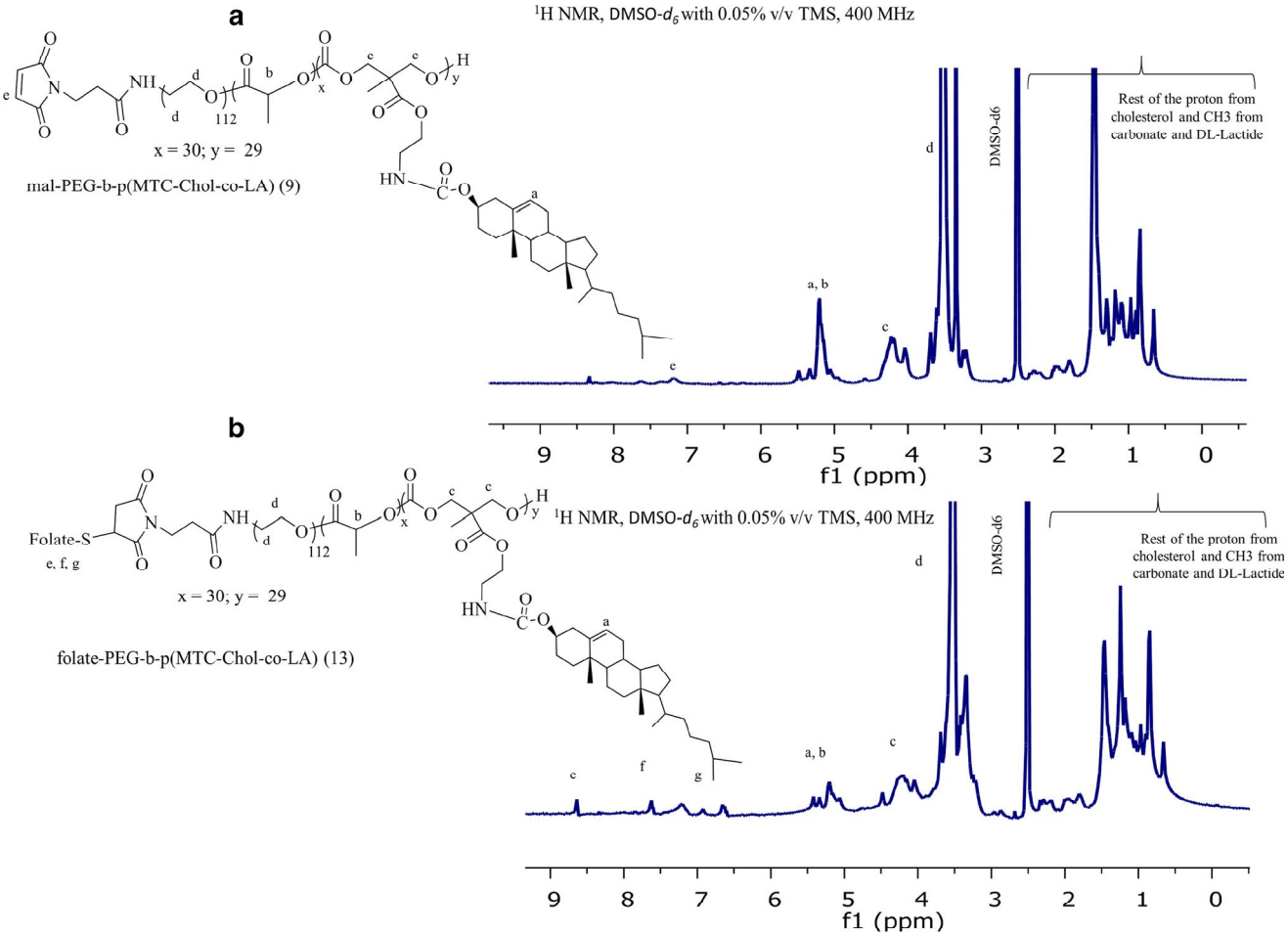

Fig. 8. ^{1}H NMR of **a** mal-PEG-b-p(MTC-Chol-co-LA) and **b** folate-PEG-b-p(MTC-Chol-co-LA) lipopolymers

with bis(hydroxymethyl) propionic acid. The product obtained was purified by column chromatography and subjected to characterization by ^{1}H NMR and ^{13}C NMR that indicated successful synthesis of the product. For cyclization, MPA-Chol was reacted with triphosgene in the presence of a strong base, pyridine, to obtain a cyclic carbonate monomer (MTC-Chol) that was further confirmed by ^{1}H NMR, ^{13}C NMR, and HRMS data indicating the successful synthesis of the monomer.

Ring-opening polymerization was adopted for the synthesis of lipopolymers wherein FDA approved and a safe organometallic catalyst, $Sn(Oct)_2$ was employed (42–44). The microwave irradiation method was adopted for the polymer synthesis as it provides shorter reaction time and higher percentage yield. It has been previously reported that microwave irradiation polymerization provides ample of benefits over conventional oil bath/plate heating method, including uniform swift heating, reduction in reaction time, immense selectivity due to induction of ionic conductivity as a result of dipolar oscillation by monowave radiations (45). Also, it has been observed that many of the time consuming polymeric reactions got completed within hours by the means of monowave irradiation. Improvement in reaction yield and product selectivity are also the major reported advantages of monowave assisted chemical reactions (46). We have synthesized series of lipopolymers with varying amounts of MTC-Chol and DL-lactide, as shown in Table 1. Further, folate conjugated lipopolymer was synthesized using maleimide terminated PEG-OH as a macroinitiator instead of m-PEG to obtain mal-PEG-b-p(MTC-Chol-co-LA). It was further reacted with the thiol derivative of folic acid to obtain folate conjugate lipopolymer. ^{1}H and ^{13}C NMR indicated the successful synthesis of the lipopolymers. Venkataraman et al. have earlier reported the polycarbonate diblock copolymers with two different units of carbonate monomer (*i.e.*, 4 and 11 units) in the hydrophobic block with a total molecular of weight 7500 Da and 11,800 Da, respectively (23). These copolymers were self-assembled to form disc-like micelles and stacked-like morphology. In our study, the molecular weight of the hydrophobic block was kept to 28,740 Da with 30, and 29 units of LA and MTC-Chol, respectively, as this will ensure efficient loading of the hydrophobic drug in the nanoparticles.

DTX loaded nanoparticles were prepared using the synthesized lipopolymers by the emulsion solvent evaporation method. It was observed that both lactic acid and cholesterol impact the encapsulation efficiency of DTX. Higher encapsulation efficiencies were observed in the lipopolymer with 30 units and 29 units of lactic acid and cholesterol, respectively. It could be attributed to the increased hydrophobicity of the lipopolymer that enabled a higher payload of the hydrophobic drug. The particle size of

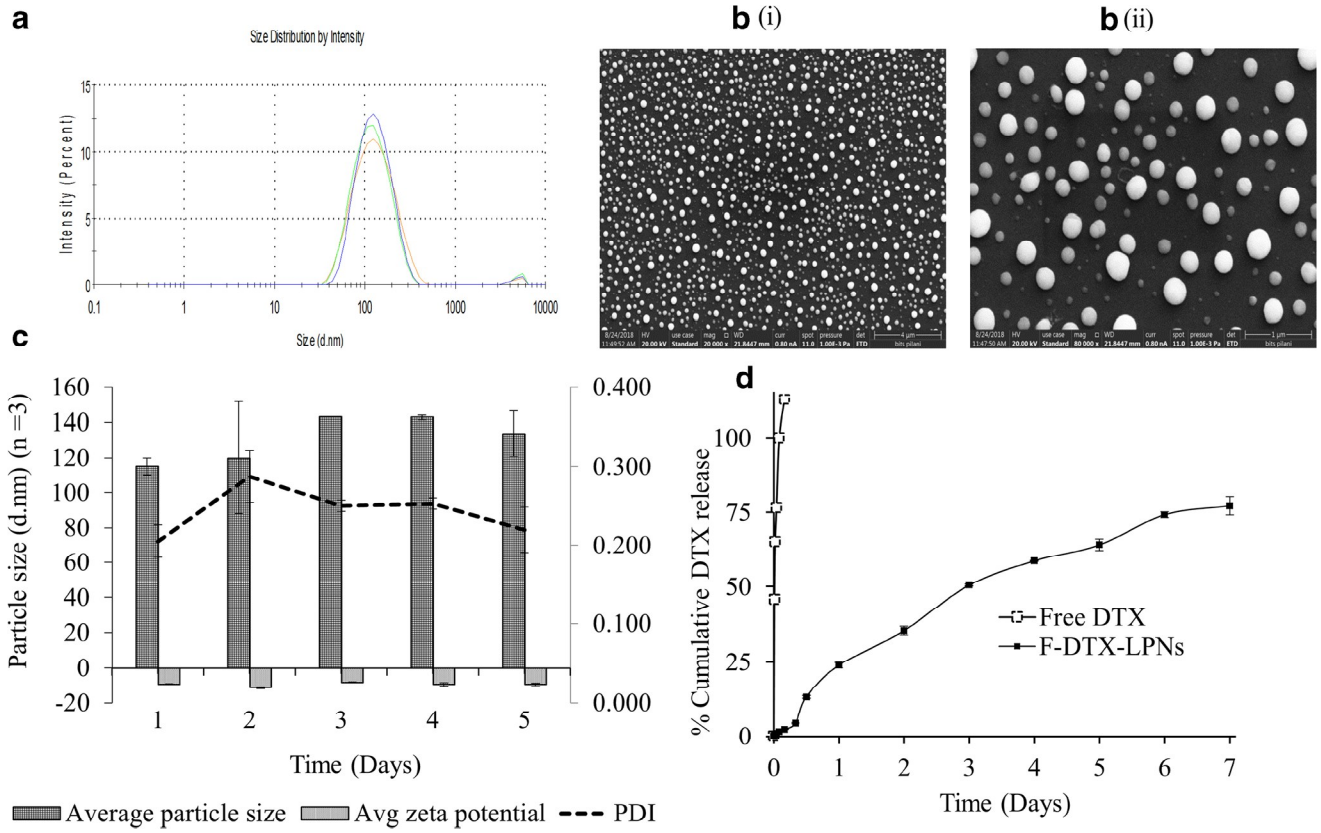

Fig. 9. **a** Characterization of of docetaxel loaded folate-PEG-b-p(MTC-Chol-co-LA) lipopolymeric nanoparticles (F-DTX-LPNs) obtained by using Malvern Zetasizer (Nano-ZS) ($n = 3$),**b** (i) and (ii) SEM image of spherical F-DTX-LPNs, **c** On-bench stability of F-DTX-LPNs for a period of five days and **d** *In-vitro* drug release from free DTX and F-DTX-LPNs. Each point represents the mean ± SD

DTX loaded nanoparticles was found to be 140 nm with a PDI of 0.164 ensuring the long circulation and targeted delivery of the nanoparticles *via* enhanced permeation and retention (EPR) effect and folate mediated active targeting respectively. Lee at al. reported the synthesis of PEG and cholesterol-containing polycarbonates based micelles for passive targeted drug delivery of highly hydrophobic molecule, paclitaxel (PTX) (21). Their optimal compositions have sub-50 nm size with a narrow size distribution, and exceptional kinetic stability and better *in vivo* profile. Further, they concluded that these types of delivery nanocarriers have an immense potential for the delivery of highly hydrophobic anticancer drugs with highly rigid molecular structure and conformation (21). In another study, DIR dye loaded micelles, and PTX loaded micelles comprising cholesterol conjugated polyoxyethylene sorbitol oleate showed 164 nm and 170 nm particle size with better accumulation at the tumor site, reduced tumor growth owing to EPR effect (47). In this study, the smaller particle size suggests that the lipopolymeric nanoparticles are having the immense potential of effective biodistribution into tumor tissues by evading immune surveillance and circulate for a prolonged period (due to EPR effect). This property makes the nanomedicines more advantageous for parenteral applications as compared to the solutions of the free drug. Further, the lower absolute value of the ζ-potential of drug-loaded nanoparticles also indicates shielding by PEG chains on the copolymer (48–50). Field-emission scanning electron microscopy showed that the nanoparticles are spherical with narrow particle size distribution that is in agreement with the size determined by the zetasizer (Fig. 9).

The *in vitro* drug release profiles of the DTX loaded folate conjugated lipopolymeric nanoparticles showed a controlled release for 7 days. The drug release behavior is dependent on the physical retention of the drug and intraparticular pores of the nanoparticles. It was observed approximately 13.25% of DTX was released in the initial 12 h. In the following 48 h, the percent cumulative release reached approximately 35.34% while at the end of 7 days the percent cumulative release reached up to 77.72% indicating a controlled and sustained drug release pattern that was due to loading of drug inside the hydrophobic core. It has been shown that the diffusion of the hydrophobic drugs could dominantly govern the drug release over a shorter period from polymeric nanoparticles. Free DTX solution, equivalent to the Taxotere® formulation prepared *in-house,* was kept as a control in the release studies that showed 100% drug release within 4 h, indicating that the dialysis membrane does not hinder the DTX release and sink conditions were maintained in the release media (51,52).

For the investigation of intracellular uptake of the nanoparticles, Coumarin-6-loaded folate-targeted and non-targeted nanoparticles were incubated with the MDA-MB-231 cells. Significantly higher green fluorescence was observed inside the cells treated with the folate-targeted nanoparticles that could be attributed to the presence of folic

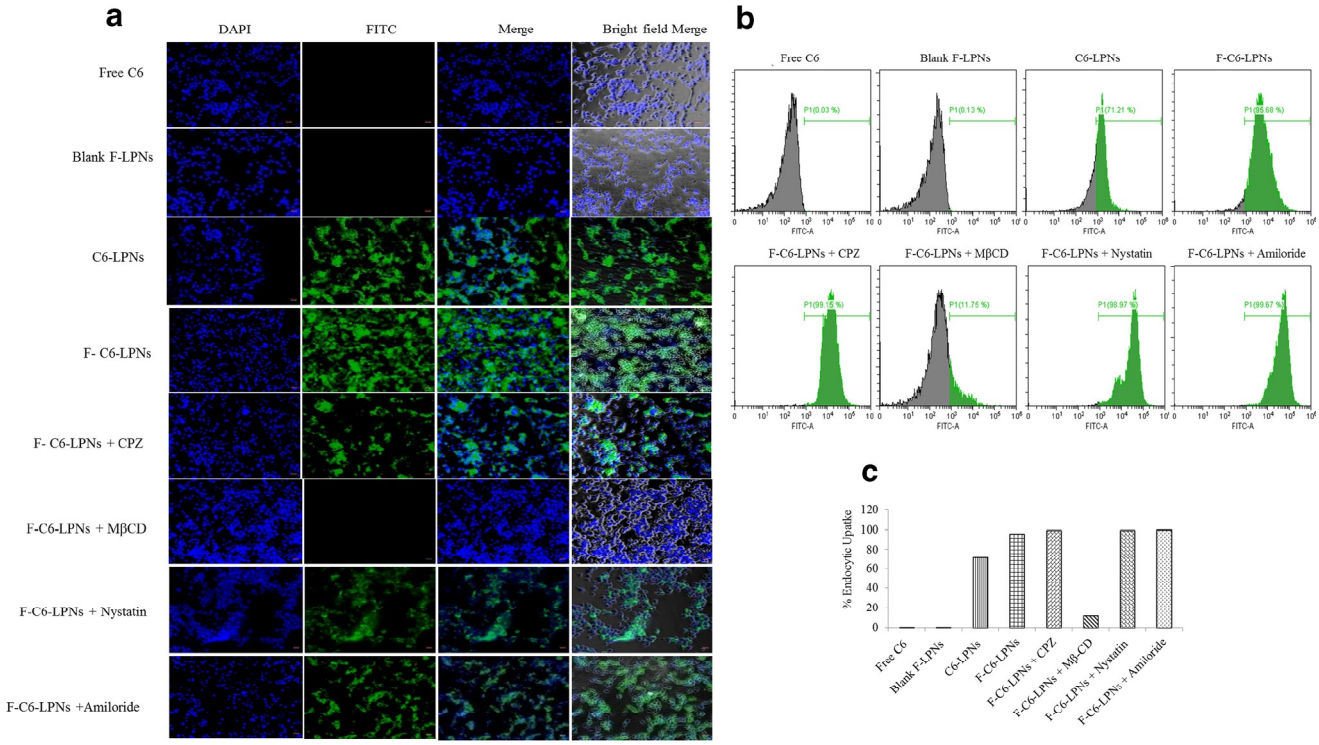

Fig. 10. **a** Fluorescence microscopic images, **b** Flow cytometry based quantitative cellular uptake (%), **c** Bar graph cellular uptake (%) of MDA-MB-231 cells treated with green fluorescent dye (Coumarin 6; C6) loaded lipopolymeric nanoparticles. Cells were treated with various endocytosis inhibitors followed by treatment with free C6 or C6 loaded targeted or non-targeted LPNs and analyzed under fluorescent microscope. Cells were counterstained with DAPI to stain the nucleus. The scale bar is 100 μm

acid on the surface of the nanoparticles enabling their binding with folate receptors on the cancer cells and ensuring receptor-mediated endocytosis. Earlier reports have also indicated that in the breast cancer cell, especially TNBC cells have higher folate receptor expression. Nahire et al. prepared the folate targeted multifunctional polymerosomes and analyzed the uptake in two cell line PANC-1 and MCF-7 cells. The endocytic data showed folate containing polymerosomes were taken up more effectively as compared to non-targeted polymerosomes. Further, the MCF-7 cells showed higher and faster uptake of folate targeted polymerosome than PANC-1 cells (53,54). In another report, the folate targeted nanoformulation showed greater internalization in MDA-MB-231 cells as compared to non-targeted formulations (55,56). Further, in our study, uptake of Coumarin6 (C6) loaded folate-targeted nanoparticles was completely inhibited by methyl β-cyclodextrin (Mβ-CD), which acts as inhibitor of lipid raft mediated intracellular uptake by affecting the signaling pathway resulting in cholesterol depletion (57). Thus it could be concluded that folate-targeted lipopolymeric nanoparticles follow the lipid raft-mediated endocytic uptake.

DTX loaded folate-targeted lipopolymeric nanoparticles showed a significantly higher cytotoxicity and apoptotic potential as compared to the non-targeted nanoparticles and free DTX that could be attributed to its higher intra-cellular uptake. Further, the blank nanoparticles did not show any cytotoxicity and apoptotic effect, suggesting the lipopolymer is biocompatible and non-toxic. Results in this study were in agreement with previous reports of folate-targeted formulation containing folate targeted formulation showing increased internalization in MDA-MB-231 cells. In this study the PTX loaded nanoparticles showed significant toxicity than free PTX (55). In another study docetaxel showed biphasic cytotoxicity curve with respect to drug concentration in MDA-MB231 cells (TNBC cells) (2). In another study at the end of 48 h, docetaxel loaded chitosan nanoparticle treated with MDA-MB-231 cells at 0.05, 0.5 and 5 μg/mL concentration of DTX showed reduction in percent cell viability from 46.09, 37.41 and 26.29% for docetaxel loaded nanoparticles and 69.98. 60.78 and 49.59% for free DTX, respectively (58).

Mitochondrial apoptosis pathway is mediated by anti-apoptotic proteins such as Bcl-2, which is up-regulated by phosphorylation that leads to breast cancer malignancy. It has been reported that DTX inhibits the Bcl-2 phosphorylation (59). On the other side, a pro-apoptotic protein BAX is activated by the linked BH3 protein responsible for induction for apoptosis and inhibition of the anti-apoptotic Bcl-2 protein. Upon activation, BAX and BAK form a pore structure in the outer membrane of mitochondria to release cytochrome-c and activate the apoptosome (60). In our study, we observed a significant down regulation of Bcl-2 and upregulation of BAX gene expression upon treatment with the folate targeted DTX loaded nanoparticles. Further, Ki-67 was observed to be down-regulated. It is an antigen nuclear protein expressed in all the phases of the cell cycle (G1, S, G2 and M phase) except G0 phase (61). The nuclear expression of this gene is related to the high tumor proliferation, direly correlated to the tumor growth size and increase in the mortality rate of TNBC patients (Fig. 7) (62).

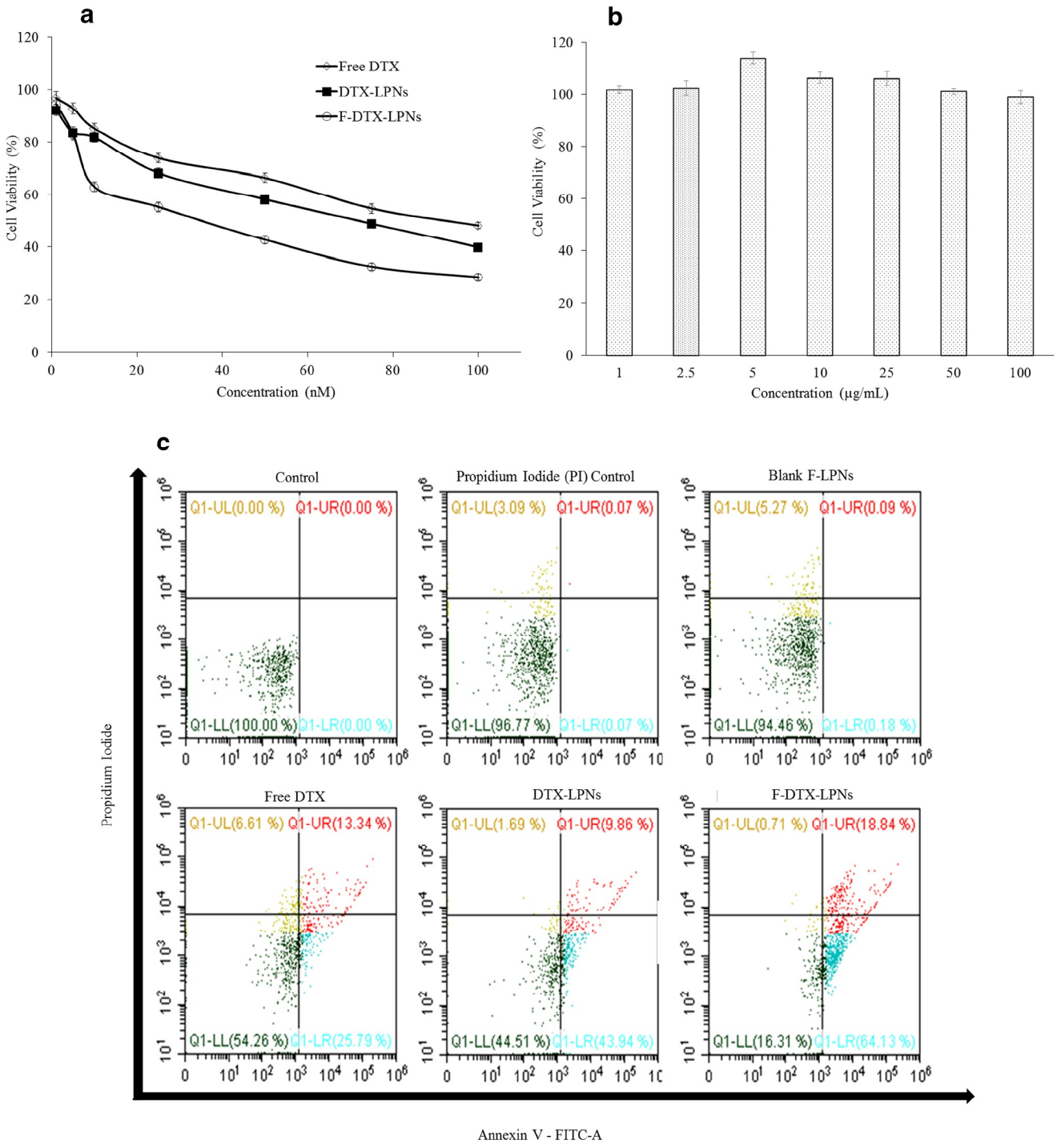

Fig. 11. *In vitro* cytotoxicity evaluation of **a** % Cell viablity *vs* Concentration curve of free DTX, DTX-LPNs and F-DTX-LPNs, and **b** blank lipopolymeric nanoparticles in MDA-MB-231 breast cells following treatment. DTX and DTX loaded LPNs were tested in the concentation range from 1 to 50 nM DTX concetration while blank lipopolymeric nanoparticles were tested in the concentration range 1–100 µg/mL (polymer concentration). Each point represents the mean ± SD. **c** Flow cytometric analysis of apoptosis in MDA-MB-231 cell line treated with free DTX, DTX-LPNs and F-DTX-LPNs at a concetration of 50 nM for 48 h. Untreated cells, propidium iodide treated cells and blank LPNs treated cells were kept as controls

In humans, DTX's pharmacokinetic profile is consistent with a three-compartment pharmacokinetic model, with half-lives for the α, β, and γ phases of 4 min, 36 min, and 11.1 h (63). The Mean pharmacokinetic parameters of docetaxel following IV injection of Taxotere formulation in rats showed a half-life of 1.173 ± 1.154 h (64). The *in vivo* pharmacokinetics of DTX from DTX loaded folate-targeted nanoparticles showed an decrease in the C_{max} and increase in the $t_{1/2}$, and AUC as compared to the DTX solution (equivalent to marketed Taxotere formulation). This could be attributed to

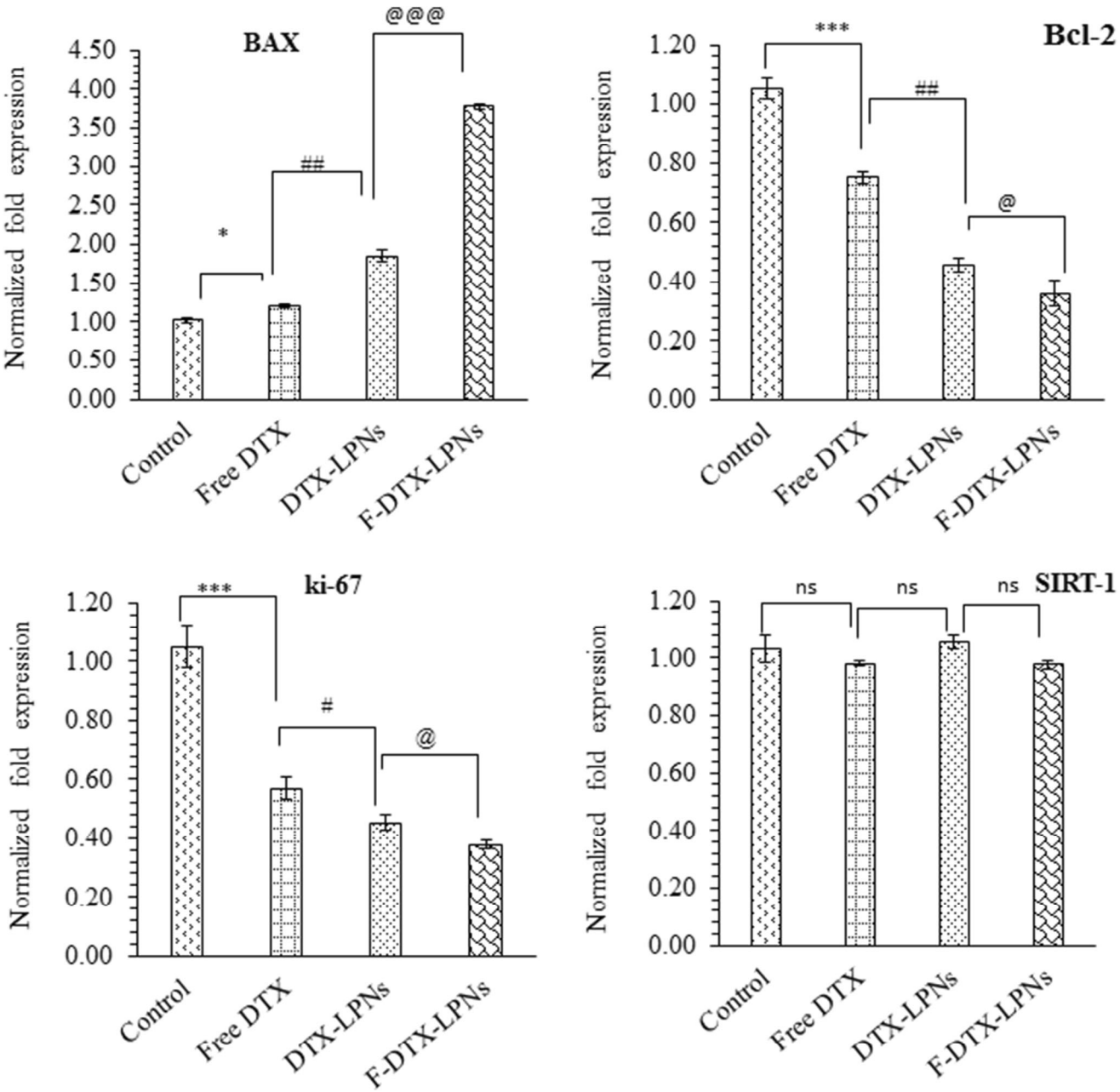

Fig. 12. Gene expression analysis of BAX, Bcl-2, Ki-67 and SIRT-1 in MDA-MB 231 cells treated with Free DTX, DTX-LPNs and F-DTX-LPNs. Each point represents the mean ± SD. Statistical analysis were performed using one way ANOVA followed by Tukey's multiple comparison test. ns: (non-significant) ***(Control *vs* Free DTX), #(Free DTX *vs* DTX-LPNs) and @(DTX-LPNs *vs* F-DTX-LPNs). (* $P < 0.05$, ## $P < 0.01$, @@@ and *** $P < 0.001$) was considered as statistically significant

the reduction of the clearance rate of the drug in the case of folate-targeted nanoparticles due to sustained release and longer circulation of lipopolymeric nanoparticles containing the hydrophobic drug entrapped in the lipophilic core of nanoparticles (65,66). It was observed that the Tmax for the free DTX and F-DTX-LPNs is almost similar in the pharmacokinetic study that could be due to the limitation of the bioanalytical method to differentiate between the DTX loaded in the nanoparticles or the free DTX that has been released from the nanoparticles. Further, it is difficult to co-relate the *in vitro* drug release profile with the *in vivo* pharmacokinetic profile owing to the difference in the release

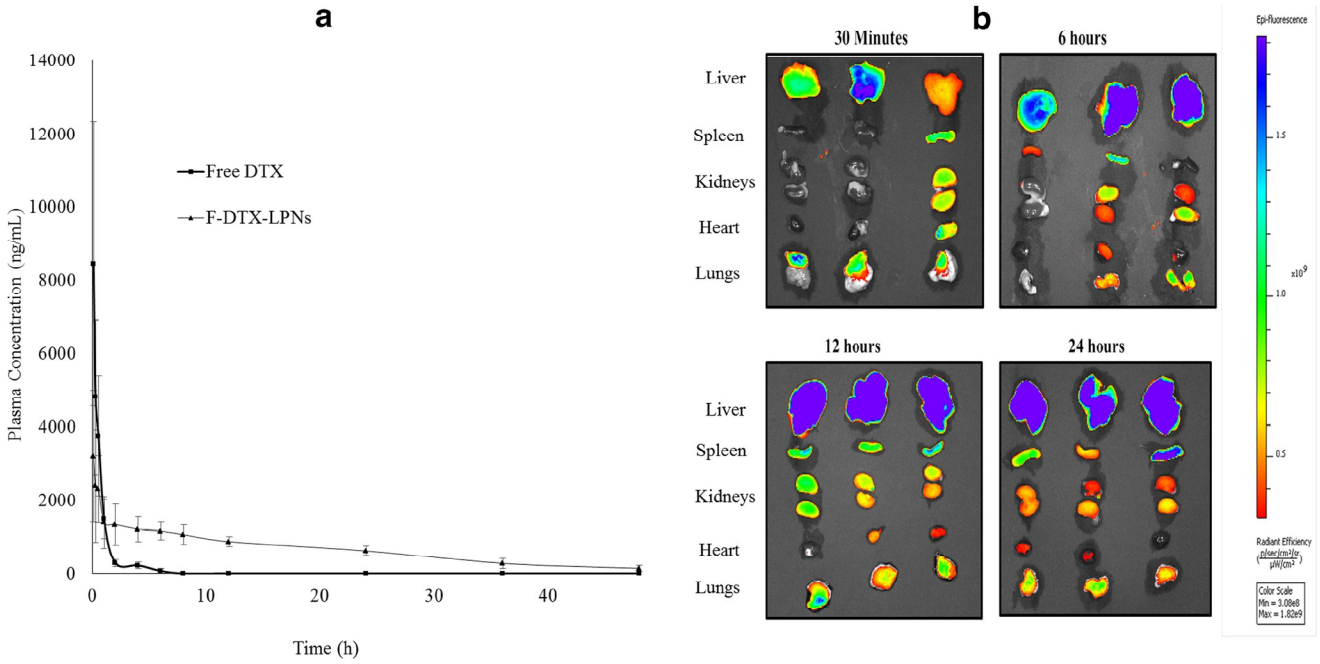

Fig. 13. Plasma concentration–time profile in SD rats after intravenous (*i.v.*) administration *via* tail vein injection of free DTX (Taxotere®) andF-DTX-LNPs at 10 mg/kg dose of DTX. Each point represents the mean ± SD ($n = 6$) and (B) *Ex-vivo* tissue distribution shown by NIRF bio-imaging of F-DiR-LPNs in mice at different time points ($n = 3$). **a** Plasma concentration–time profile of DTX in *sprague dawley*rats after intravenous injection of free DTX (Taxotere®) andF-DTX-LNPs given at a dose of 10 mg/kg (equivalent to DTX). Each point represents the mean ± SD (n = 6) and **b** *Ex vivo* tissue imaging of vital organs of *swiss albino* mice after intravenous injection of DiR dye loaded LPNs (n = 3)

of the drug in the biological milieu as compare to the release in the *in vitro* condition. Further, the hydrophilic surface of nanoparticles (due to the presence of PEG) could prevent their aggregation and prolong the systematic circulation owing to the stealth effect (67). A NIRF molecular probe DiR dye was used for *ex vivo* tissue bioimaging of folate targeted lipopolymeric nanoparticles. The unique feature of this dye is that, it does emit NIR photons, which have negligible absorbance minimizing the interference due to presence of water and hemoglobin during the bioimaging study. The DiR loaded folate conjugated lipopolymeric nanoparticles were retained for longer duration till 24 h in all tissues. We showed that fluorescence intensity of DiR loaded nanoparticles started to saturate in liver within 6 h after *i.v.* administration in mice. The intensity was stronger till 24 h after injection due to high uptake of these nanoparticles by liver as obvious due to the elimination of nanoparticles through reticulo endothelial system (RES). Moreover, the intensity was observed in all organs after 24 h due to the sustained release of DiR dye from the nanoparticles. In future, these folate targeted lipopolymeric nanoparticles have an immense potential and application in drug delivery and improving efficacy of treatment in breast cancer model.

In summary, folate-targeted lipopolymers containing cholesterol sub-units have been synthesized and used for the delivery of a hydrophobic drug molecule, docetaxel (DTX). These lipopolymers were able to efficiently load the drug and showed particle size <140 nm with a narrow size distribution, better on-bench stability, and prolonged DTX release profile. Further, folate-targeted nanoparticles showed higher intracellular uptake in MDA-MB-231 cells with improved cytotoxicity and apoptotic potential along with an improvement *in vivo* pharmacokinetic profile of drug in *Sprague Dawley* rats. *Acknowledgments and Funding Support.* The financial support from SERB-Department of Science and Technology (DST) (YSS/2014/000521) and DST-Rajasthan (S.No.

Table 1. Characterization of amphiphilic lipopolymers

				^{1}H NMR
Lipopolymers	Lactic Acid (Units)	MTC-CHOL (Units)	Ratio	Mn[a](Da)
m-PEG-b-P(MTC-Chol$_{11}$-co-LA$_5$ (15)	5	11	1:2.2	11,927
m-PEG-b-P(MTC-Chol$_{15}$-co-LA$_{15}$ (16)	15	15	1:1	15,035
m-PEG-b-P(MTC-Chol$_{11}$-co-LA$_{27}$ (17)	27	11	2.7:1	13,511
m-PEG-b-P(MTC-Chol$_{29}$-co-LA$_{30}$ (18)	30	29	1:1	24,480
mal-PEG-b-P(MTC-Chol$_{29}$-co-LA$_{30}$ (9)	30	29	1:1	24,570
fol-PEG-b-P(MTC-Chol$_{29}$-co-LA$_{30}$ (13)	30	29	1:1	24,972

[a] Average molecular weight determined by *^{1}H NMR*

Table 2. Pharmacokinetic parameters of free DTX (Taxotere®) and F-DTX-LPNs following intravenous administration at a dose of 10 mg/kg (equivalent to DTX) in *Sprague Dawley* rats. Data are presented as mean ± SD (n = 6)

Pharmacokinetic Parameters	Free DTX (Taxotere®)	F-DTX-LPNs
AUC(0-t) (μg*h/L)	5408.00 ± 1624.77	31,434.80 ± 5929.47
$AUC_{0-\infty}$ (μg*h/L)	5515.93 ± 1824.90	35,379.89 ± 8527.41
MRT(0-t) (h)	0.946 ± 0.33	14.60 ± 3.96
MRT(0-inf) (h)	1.37 ± 1.36	20.20 ± 7.69
Kel	0.48 ± 0.29	0.05 ± 0.012
t1/2kel (h)	2.51 ± 2.68	14.64 ± 3.98
Cmax (μg /mL)	8.29 ± 3.47	3.20 ± 1.78
Tmax (h)	0.108 ± 0.06	0.15 ± 0.17
Cl (mL/h/kg)	502.76 ± 178.42	83.83 ± 23.43
Vss (mL/kg)	464.30 ± 207.34	1150.78 ± 178.87

P7 (3)/VPro./RandD/2016/3228) to DC is duly acknowledged. The financial support from Council for Scientific and Industrial Research (CSIR) (File no 09/719(0087)/2018-EMR-1) for senior research fellowship (SRF) to SS is duly acknowledged. The financial support to DKS from Indian Council of Medical Research (File no. 45/66/2019-Nan/BMS) for ICMR-SRF is duly acknowledged.

COMPLIANCE WITH ETHICAL STANDARDS

Conflict of Interest There are no conflicts to declare pertaining to the data presented in this publication. The authors (DC and AM) are the founding directors of Nanobrid Innovations Private Limited, India, that is involved in the development of nanotechnology-based products. They have a business and/or financial interest in the operations of the company. The same could be disclosed on request.

REFERENCES

1. Dumontet C, Jordan MA. Microtubule-binding agents: a dynamic field of cancer therapeutics. Nat Rev Drug Discov. 2010;9(10):790–803.
2. Hernández-Vargas H, Palacios J, Moreno-Bueno G. Molecular profiling of docetaxel cytotoxicity in breast cancer cells: uncoupling of aberrant mitosis and apoptosis. Oncogene. 2007;26(20):2902–13.
3. Feng L, Mumper RJ. A critical review of lipid-based nanoparticles for taxane delivery. Cancer Lett. 2013;334(2):157–75.
4. Ekladious I, Colson YL, Grinstaff MW. Polymer–drug conjugate therapeutics: advances, insights and prospects. Nat Rev Drug Discov. 2019;18(4):273–94.
5. Ho MY, Mackey JR. Presentation and management of docetaxel-related adverse effects in patients with breast cancer. Cancer Manag Res. 2014;6(1):253-9.
6. Choudhury H, Gorain B, Pandey M, Kumbhar SA, Tekade RK, Iyer AK, et al. Recent advances in TPGS-based nanoparticles of docetaxel for improved chemotherapy. Int J Pharm. 2017;529(1–2):506–22.
7. Rafiyath SM, Rasul M, Lee B, Wei G, Lamba G, Liu D. Comparison of safety and toxicity of liposomal doxorubicin vs. conventional anthracyclines: a meta-analysis. Experimental Hematology & Oncology. 2012;1(1):10.
8. Witters LM, Santala SM, Engle L, Chinchilli V, Lipton A. Decreased response to paclitaxel versus docetaxel in HER-2/neu transfected human breast cancer cells. Am J Clin Oncol. 2003;26(1):50–4.
9. Shi J, Kantoff PW, Wooster R, Farokhzad OC. Cancer nanomedicine: progress, challenges and opportunities. Nat Rev Cancer. 2017;17(1):20-37.
10. Singh AP, Biswas A, Shukla A, Maiti P. Targeted therapy in chronic diseases using nanomaterial-based drug delivery vehicles. Signal Transduction and Targeted Ther. 2019;4(1):1–21.
11. Patra JK, Das G, Fraceto LF, Campos EV, del Pilar Rodriguez-Torres M, Acosta-Torres LS, et al. Nano based drug delivery systems: recent developments and future prospects. J Nanobiotechnology. 2018;16(1):71.
12. Ernsting MJ, Murakami M, Undzys E, Aman A, Press B, Li SD. A docetaxel-carboxymethylcellulose nanoparticle outperforms the approved taxane nanoformulation, Abraxane, in mouse tumor models with significant control of metastases. J Control Release. 2012;162(3):575–81.
13. Tao W, Zeng X, Wu J, Zhu X, Yu X, Zhang X, et al. Polydopamine-based surface modification of novel nanoparticle-aptamer bioconjugates for in vivo breast cancer targeting and enhanced therapeutic effects. Theranostics. 2016;6(4):470-84.
14. Bowerman CJ, Byrne JD, Chu KS, Schorzman AN, Keeler AW, Sherwood CA, et al. Docetaxel-loaded PLGA nanoparticles improve efficacy in taxane-resistant triple-negative breast cancer. Nano Lett. 2017;17(1):242–8.
15. Danquah M, Fujiwara T, Mahato RI. Self-assembling methoxypoly (ethylene glycol)-b-poly (carbonate-co-L-lactide) block copolymers for drug delivery. Biomaterials. 2010;31(8):2358–70.
16. Bariwal J, Kumar V, Chen H, Bhattarai RS, Peng Y, Li W, et al. Nanoparticulate delivery of potent microtubule inhibitor for metastatic melanoma treatment. J Control Release. 2019;309:231–43.
17. Li F, Danquah M, Mahato RI. Synthesis and characterization of amphiphilic lipopolymers for micellar drug delivery. Biomacromolecules. 2010;11(10):2610–20.
18. Chitkara D, Mittal A, Behrman SW, Kumar N, Mahato RI. Self-assembling, amphiphilic polymer–gemcitabine conjugate shows enhanced antitumor efficacy against human pancreatic adenocarcinoma. Bioconjug Chem. 2013;24(7):1161–73.
19. Sharma S, Mazumdar S, Italiya KS, Date T, Mahato RI, Mittal A, et al. Cholesterol and Morpholine grafted cationic Amphiphilic copolymers for miRNA-34a delivery. Mol Pharm. 2018;15(6):2391–402.
20. Nederberg F, Lohmeijer BG, Leibfarth F, Pratt RC, Choi J, Dove AP, et al. Organocatalytic ring opening polymerization of trimethylene carbonate. Biomacromolecules. 2007;8(1):153–60.
21. Lee AL, Venkataraman S, Sirat SB, Gao S, Hedrick JL, Yang YY. The use of cholesterol-containing biodegradable block copolymers to exploit hydrophobic interactions for the delivery of anticancer drugs. Biomaterials. 2012;33(6):1921–8.
22. Wang Y, Gao S, Ye WH, Yoon HS, Yang YY. Co-delivery of drugs and DNA from cationic core-shell nanoparticles self-assembled from a biodegradable copolymer. Nat Mater. 2006;5(10):791–6.
23. Venkataraman S, Lee AL, Maune HT, Hedrick JL, Prabhu VM, Yang YY. Formation of disk- and stacked-disk-like self-assembled morphologies from cholesterol-functionalized amphiphilic polycarbonate diblock copolymers. Macromolecules. 2013;46(12):4839–46.
24. Atkinson SF, Bettinger T, Seymour LW, Behr J-P, Ward CM. Conjugation of folate via gelonin carbohydrate residues retains ribosomal-inactivating properties of the toxin and permits targeting to folate receptor positive cells. J Biol Chem. 2001;276(30):27930–5.

25. Roy A, Murakami M, Ernsting MJ, Hoang B, Undzys E, Li S-D. Carboxymethylcellulose-based and docetaxel-loaded nanoparticles circumvent P-glycoprotein-mediated multidrug resistance. Mol Pharm. 2014;11(8):2592–9.
26. Abou-El-Naga AM, Mutawa G, El-Sherbiny IM, Mousa SA. Activation of polymeric nanoparticle intracellular targeting overcomes chemodrug resistance in human primary patient breast cancer cells. Int J Nanomedicine. 2018;13:8153-64.
27. Mazumdar S, Italiya KS, Sharma S, Chitkara D, Mittal A. Effective cellular internalization, cell cycle arrest and improved pharmacokinetics of Tamoxifen by cholesterol based lipopolymeric nanoparticles. Int J Pharm. 2018;543(1–2):96–106.
28. Italiya KS, Mazumdar S, Sharma S, Chitkara D, Mahato RI, Mittal A. Self-assembling lisofylline-fatty acid conjugate for effective treatment of diabetes mellitus. Nanomedicine. 2019;15(1):175–87.
29. Soe ZC, Kwon JB, Thapa RK, Ou W, Nguyen HT, Gautam M, et al. Transferrin-conjugated polymeric nanoparticle for receptor-mediated delivery of doxorubicin in doxorubicin-resistant breast cancer cells. Pharmaceutics. 2019;11(2):1-17.
30. Tan T, Hu H, Wang H, Li J, Wang Z, Wang J, et al. Bioinspired lipoproteins-mediated photothermia remodels tumor stroma to improve cancer cell accessibility of second nanoparticles. Nat Commun. 2019;10(1):1–17.
31. Gad SF, Park J, Park JE, Fetih GN, Tous SS, Lee W, et al. Enhancing docetaxel delivery to multidrug-resistant cancer cells with albumin-coated nanocrystals. Mol Pharm. 2018:1-45.
32. Zhang L, Yang X, Lv Y, Xin X, Qin C, Han X, et al. Cytosolic co-delivery of miRNA-34a and docetaxel with core-shell nanocarriers via caveolae-mediated pathway for the treatment of metastatic breast cancer. Sci Rep. 2017;7:46186.
33. Li Y, Gao L, Tan X, Li F, Zhao M, Peng S. Lipid rafts-mediated endocytosis and physiology-based cell membrane traffic models of doxorubicin liposomes. Biochimica et Biophysica Acta (BBA)-Biomembranes. 2016;1858(8):1801–11.
34. Harbeck N, Penault-Llorca F, Cortes J, Gnant M, Houssami N, Poortmans P, Ruddy K, Tsang J, Cardoso F. Breast cancer (Primer). Nat Rev Disease Primers. 2019;5(66):1-31.
35. Mustacchi G, De Laurentiis M. The role of taxanes in triple-negative breast cancer: literature review [Corrigendum]. Drug Des Devel Ther. 2015;9:5669-70.
36. Mandal B, Bhattacharjee H, Mittal N, Sah H, Balabathula P, Thoma LA, et al. Core–shell-type lipid–polymer hybrid nanoparticles as a drug delivery platform. Nanomedicine. 2013;9(4):474–91.
37. Wang Q, Alshaker H, Böhler T, Srivats S, Chao Y, Cooper C, et al. Core shell lipid-polymer hybrid nanoparticles with combined docetaxel and molecular targeted therapy for the treatment of metastatic prostate cancer. Sci Rep. 2017;7(1):1–8.
38. Liu Y, Li K, Pan J, Liu B, Feng S-S. Folic acid conjugated nanoparticles of mixed lipid monolayer shell and biodegradable polymer core for targeted delivery of Docetaxel. Biomaterials. 2010;31(2):330–8.
39. Werner ME, Copp JA, Karve S, Cummings ND, Sukumar R, Li C, et al. Folate-targeted polymeric nanoparticle formulation of docetaxel is an effective molecularly targeted radiosensitizer with efficacy dependent on the timing of radiotherapy. ACS Nano. 2011;5(11):8990–8.
40. Dai Y, Zhang X. Recent development of functional aliphatic polycarbonates for the construction of amphiphilic polymers. Polym Chem. 2017;8(48):7429–37.
41. Washington KE, Kularatne RN, Karmegam V, Biewer MC, Stefan MC. Recent advances in aliphatic polyesters for drug delivery applications. Wiley Interdisciplinary Reviews: Nanomedicine and Nanobiotechnology. 2017;9(4):e1446.
42. Howe P, Watts P. Tin and inorganic tin compounds: world health organization; 2005.
43. Hege CS, Schiller SM. Non-toxic catalysts for ring-opening polymerizations of biodegradable polymers at room temperature for biohybrid materials. Green Chem. 2014;16(3):1410–6.
44. Sobczak M. Ring-opening polymerization of cyclic esters in the presence of choline/SnOct 2 catalytic system. Polym Bull. 2012;68(9):2219–28.
45. Wiesbrock F, Hoogenboom R, Schubert US. Microwave-assisted polymer synthesis: state-of-the-art and future perspectives. Macromol Rapid Commun. 2004;25(20):1739–64.
46. Dudley GB, Richert R, Stiegman A. On the existence of and mechanism for microwave-specific reaction rate enhancement. Chem Sci. 2015;6(4):2144–52.
47. Tian Y, Mi G, Chen Q, Chaurasiya B, Li Y, Shi D, et al. Acid-induced activated cell-penetrating peptide-modified cholesterol-conjugated Polyoxyethylene sorbitol Oleate mixed micelles for pH-triggered drug release and efficient brain tumor targeting based on a charge reversal mechanism. ACS Appl Mater Interfaces. 2018;10(50):43411–28.
48. Chen J, Wu Q, Luo L, Wang Y, Zhong Y, Dai H-B, et al. Dual tumor-targeted poly (lactic-co-glycolic acid)–polyethylene glycol–folic acid nanoparticles: a novel biodegradable nanocarrier for secure and efficient antitumor drug delivery. Int J Nanomedicine. 2017;12:5745–60.
49. Nie J, Cheng W, Peng Y, Liu G, Chen Y, Wang X, et al. Co-delivery of docetaxel and bortezomib based on a targeting nanoplatform for enhancing cancer chemotherapy effects. Drug Deliv. 2017;24(1):1124–38.
50. Gong X, Zheng Y, He G, Chen K, Zeng X, Chen Z. Multifunctional nanoplatform based on star-shaped copolymer for liver cancer targeting therapy. Drug Deliv. 2019;26(1):595–603.
51. Han M, Li Z, Bi D, Guo Y, Kuang H, Wang X. Novel folate-targeted docetaxel-loaded nanoparticles for tumour targeting: in vitro and in vivo evaluation. RSC Adv. 2016;6(69):64306–14.
52. Wang XS, Kong DJ, Lin TY, Li XC, Izumiya Y, Ding XZ, et al. A versatile nanoplatform for synergistic combination therapy to treat human esophageal cancer. Acta Pharmacol Sin. 2017;38(6):931–42.
53. Marshalek JP, Sheeran PS, Ingram P, Dayton PA, Witte RS, Matsunaga TO. Intracellular delivery and ultrasonic activation of folate receptor-targeted phase-change contrast agents in breast cancer cells in vitro. J Control Release. 2016;243:69–77.
54. Nahire R, Haldar MK, Paul S, Ambre AH, Meghnani V, Layek B, et al. Multifunctional polymersomes for cytosolic delivery of gemcitabine and doxorubicin to cancer cells. Biomaterials. 2014;35(24):6482–97.
55. Kumar P, Huo P, Liu B. Formulation strategies for Folate-targeted liposomes and their biomedical applications. Pharmaceutics. 2019;11(8):381.
56. Mukhopadhyay R, Sen R, Paul B, Kazi J, Ganguly S, Debnath MC. Gemcitabine co-encapsulated with Curcumin in Folate decorated PLGA nanoparticles; a novel approach to treat breast adenocarcinoma. Pharm Res. 2020;37(3):1–9.
57. Malnar M, Kosicek M, Lisica A, Posavec M, Krolo A, Njavro J, et al. Cholesterol-depletion corrects APP and BACE1 misstrafficking in NPC1-deficient cells. Biochimica et Biophysica Acta (BBA)-Molecular Basis of Disease. 2012;1822(8):1270–83.
58. Jain A, Thakur K, Kush P, Jain UK. Docetaxel loaded chitosan nanoparticles: formulation, characterization and cytotoxicity studies. Int J Biol Macromol. 2014;69:546–53.
59. Singh SK, Banerjee S, Acosta EP, Lillard JW, Singh R. Resveratrol induces cell cycle arrest and apoptosis with docetaxel in prostate cancer cells via a p53/p21WAF1/CIP1 and p27KIP1 pathway. Oncotarget. 2017;8(10):17216-28.
60. Zinkel S, Gross A, Yang E. BCL2 family in DNA damage and cell cycle control. Cell Death Differ. 2006;13(8):1351–9.
61. Sun X, Kaufman PD. Ki-67: more than a proliferation marker. Chromosoma. 2018;127(2):175–86.
62. Martin TA, Ye L, Sanders AJ, Lane J, Jiang WG. Cancer invasion and metastasis: molecular and cellular perspective. In Madame Curie Bioscience Database [Internet]. Landes Bioscience. 2013.
63. Sanofi US. TAXOTERE®(docetaxel) Injection concentrate, Intravenous infusion (IV) Prescribing Information. 2010.

64. Park JH, Kim YJ, Kwon KE, Lee SG, Lee BK, Lee HJ. Effects of formulation on pharmacokinetics of docetaxel in rats. J Pharm Invest. 2012;42(1):51–5.
65. Yang C, Wu T, Qi Y, Zhang Z. Recent advances in the application of vitamin E TPGS for drug delivery. Theranostics. 2018;8(2):464-85.
66. Yoo JW, Irvine DJ, Discher DE, Mitragotri S. Bio-inspired, bioengineered and biomimetic drug delivery carriers. Nat Rev Drug Discov. 2011;10(7):521–35.
67. Blanco E, Shen H, Ferrari M. Principles of nanoparticle design for overcoming biological barriers to drug delivery. Nat Biotechnol. 2015;33(9):941-51.

CHAPTER 6

CONCLUSIONS AND FUTURE PROSPECTS

- Conclusions
- Future prospects

6.1. Conclusions

Several strategies have been adopted to improve the therapeutic outcome in the treatment of breast cancer, particularly TNBC. Apart from surgery and radiation therapy, chemotherapeutic plays a pivotal role wherein taxane's, including PTX and DTX, have been widely prescribed for breast cancer treatment. Ample of limitations originates with chemotherapy *viz.* toxicity, short half-life, poor tissue-specific delivery and chemo-resistance. To further enhance the delivery, nanotherapeutic approaches have been utilized that could deliver the drug efficiently to the target tumor site. Apart from that, the combination of a chemotherapeutic agent with small oligonucleotides such as microRNA has opened up a new avenue in the area of cancer therapeutics. However, most of the conventional chemotherapeutics and miRNA treatment were unable to meet the clinical therapeutic demands because of the delivery hurdles. Upon consideration of entire challenges provided by these molecules, nano-carrier mediated delivery platforms have been evolved, including polymeric systems that showed several advantages such as biodegradability, biocompatibility, ease of surface modification, functionalization, stability, efficient complexation, sustained release, etc.

In the present work, we have designed the non-viral polymeric vectors for delivering the DTX and miR-34a combination for the treatment of breast cancer. The following are the specific conclusion that could be drawn for the work outlined in different chapters.

The bioanalytical method for the analysis of DTX was developed using RP-HPLC coupled with a photodiode array detector. A protein precipitation method was adopted for the extraction of DTX from the biological samples. The method was developed and validated as per the USFDA

guidelines and the results showed that the method could be applicable for accurate and precise quantitation of DTX in the plasma samples.

For the effective delivery of miR-34a, we have prepared a series of cationic amphiphilic copolymers grafted with cholesterol (chol), N,N-dimethyldipropylenetriamine (cation chain) and 4-(2-aminoethyl)morpholine (Morph). The synthesized cationic functionalized copolymer forms an ionic complex with miR-34a at low N/P ratios (~2/1) to form nanoplexes of size ~108 nm and a zeta potential ~ +39 mV. The endocytic transfection and co-localization in the breast cancer cell line suggested that the nanoplexes effectively deliver the green fluorescent-labeled siRNA into the cytoplasm within two hours, escaped from the lysosomal environment and release into the cytoplasm. The developed miR-34a nanoplexes enhance the cytotoxicity in 4T1 and MCF-7 cells with 28% and 34% cancer cell viability and effective induction of apoptosis. Further, cationic miR-34a nanoformulation was found to have immense potential for future application as a delivery vehicle in the treatment of breast cancer.

Folate targeted lipopolymeric nanoparticles loaded with DTX (F-DTX-LPNs) were prepared that demonstrated experimental evidence in the treatment of breast cancer. Maleimide-PEG-b-p(MTC-Chol-co-LA) lipopolymers were successfully synthesized using microwave-assisted ring-opening polymerization of MTC-Chol (cyclic carbonate), DL-lactide (cyclic ester) and mal-PEG-OH (macro-initiator) in the presence of $Sn(Oct)_2$ which was further conjugated with thiol modified folate to yield folate conjugated lipopolymer. Also, a series of mPEG-b-p(MTC-Chol-co-LA) lipopolymers were prepared and the effect of varying the composition on the formulation was determined. The F-DTX-LPNs showed a particle size <200 nm with a narrow polydispersity index, high encapsulation efficiency > 80 % and good on-bench stability. *In vitro* drug release and pharmacokinetic studies indicated that the F-DTX-LNPs exhibited a sustained drug release profile

of DTX up to a week in contrast to the Taxotere® formulation. The time-dependent *ex vivo* tissue distribution profile of DIR dye loaded nano-carrier showed the accumulation of nanoparticles for a longer duration, which supports the hypothesis of sustained-release profiles of the developed nano-carrier.

Research evidence of the synergistic application of miRNA with anticancer molecules attracted our focus on the co-delivery of miR-34a and DTX for the treatment of breast cancer. We prepare an actively targeted hybrid nanoplexes for the co-delivery of DTX and miR-34a. The nanoplexes exhibited an average particle size of < 150 nm with efficient complexation with miR-34a and high entrapment efficiency of DTX (94.8%) with a sustained *in vitro* release profile. Further, nanoplexes demonstrated significantly high transfection efficiency in 4T1 and MCF-7 following a lipid-raft and clathrin-mediated endocytic uptake pathway. These nanoplexes showed improved cytotoxicity and apoptosis along with significant fold-change in expression levels of various apoptotic, antiapoptotic and cell proliferating genes. Further, an improved *in vivo* pharmacokinetics of fluorescent-labeled siRNA and DTX was observed in *Swiss albino* mice. Furthermore, these cationic nanoplexes demonstrated *in vivo* safety profile in *swiss albino* mice.

6.2. Future prospects

In the present work, we have developed nano-carriers for delivering hydrophobic molecules (such as DTX) and RNAi therapeutics (such as miR-34a) as well as for their simultaneous delivery. There are several aspects of the developed formulations that could be studied in the future to enable their clinical translation.

- These combination therapeutics could be tested for resistant cancers as this combination could harness the advantage of targeting several oncogenic pathways that could reverse the chemo-resistance.
- Although pharmacokinetics and biodistribution studies were performed in animal models, however, to have a better understanding, these studies could be conducted in xenograft tumor models.
- Although efficacy assessment is performed in cell-based assays using cytotoxicity, apoptosis, gene expression, etc., further assessment of developed formulations in xenograft tumor models could provide an insight into the improved efficacy of the combination when delivered using developed carriers.
- Apart from the DTX and miR-34a, other hydrophobic drugs and miRNA therapeutics could also be delivered using the designed nano-carriers.
- These nano-carriers could also be modified with other pendant groups on the hydrophobic polycarbonate block such as imidazole, guanidine, etc. that could potentially improve the delivery of these therapeutics.